Wavelets Based Solutions of Integral and Integro-Differential Equations

Thesis Submitted for the Award of the Degree of

DOCTOR OF PHILOSOPHY (Ph.D.)

in

Mathematics

By

Sabiha Bakhtawar

Registration Number: 12015214

Supervised By

Dr. Ratesh Kumar (11755)

Associate Professor

Department of Mathematics

School of Chemical Engineering and Physical Sciences

LOVELY PROFESSIONAL UNIVERSITY, PUNJAB

2024

DECLARATION

I, hereby declared that the presented work in the thesis entitled **"*Wavelets Based Solutions of Integral and Integro-Differential Equations*"** in fulfilment of degree of **Doctor of Philosophy (Ph. D.)** is outcome of research work carried out by me under the supervision of **Dr. Ratesh Kumar (11755)**, working as Associate Professor, in the Department of Mathematics, School of Chemical Engineering and Physical Sciences, Lovely Professional University, Punjab, India. In keeping with general practice of reporting scientific observations, due acknowledgements have been made whenever work described here has been based on findings of other investigator. This work has not been submitted in part or full to any other University or Institute for the award of any degree.

Signature of Scholar

Name of the scholar: Sabiha Bakhtawar

Registration No.: 12015214

Department / School: Department of Mathematics / School of Chemical Engineering and Physical Sciences

Lovely Professional University

Punjab, India.

CERTIFICATE

This is to certify that the work reported in the Ph. D. thesis entitled "***Wavelets Based Solutions of Integral and Integro-Differential Equations***" submitted in fulfillment of the requirement for the reward of degree of **Doctor of Philosophy (Ph.D.)** in the Department of Mathematics, School of Chemical Engineering and Physical Sciences, is a research work carried out by **Sabiha Bakhtawar**, **12015214**, is bonafide record of her original work carried out under my supervision and that no part of thesis has been submitted for any other degree, diploma or equivalent course.

Signature of Supervisor

Name of the Supervisor: Dr. Ratesh Kumar

Designation: Associate Professor

Department / School: Department of Mathematics / School of Chemical Engineering and Physical Sciences

University: Lovely Professional University Punjab, India.

Dedicated

To

Almighty

Allah

and

My Family

ABSTRACT

Integral and integro-differential equations are mathematical equations that involve both differentiation and integration operations. These equations are widely used in various fields of science and engineering to model a wide range of phenomena, including physical processes, population dynamics, fluid mechanics, and signal processing. They provide a powerful mathematical framework for describing systems with memory, non-local interactions, and dynamic behaviour. Integral equations involve an unknown function that appears under an integral sign. The solution to an integral equation is typically sought in terms of the unknown function itself, rather than its derivatives. These equations often arise in problems involving boundary value conditions, where the integral represents the influence of the unknown function over a given domain. Integro-differential equations combine both differential and integral terms. They are a generalization of ordinary differential equations, where the unknown function depends on its derivatives as well as on its integrals. Integro-differential equations are encountered in problems that involve memory effects or non-local interactions, where the value of the unknown function at a given point depends not only on its derivatives but also on its history over a certain interval. The solution of integral and integro-differential equations is crucial for several reasons. Integral and integro-differential equations provide a flexible and powerful framework for modelling complex phenomena that cannot be adequately described by ordinary differential equations. They capture memory effects, non-local interactions, and dynamics that depend on both local and global properties of the system. Many real-world problems in physics, engineering, biology, finance, and other fields can be formulated as integral or integro-differential equations. Solving these equations enables us to understand and predict the behaviour of the systems under study. Integral and integro-differential equations often lack closed-form analytical solutions, especially for complex systems. Solving these equations analytically is often infeasible or highly challenging. Therefore, numerical methods play a crucial role in obtaining approximate solutions that are accurate and computationally efficient. Various numerical techniques have been developed to solve integral and integro-differential equations. These include finite difference methods, finite element methods, spectral methods, and wavelet-based methods. Each technique

has its advantages and limitations, making it important to explore and develop new methods to improve the accuracy, efficiency, and robustness of the numerical solutions. Wavelet methods offer several advantages over other numerical methods when it comes to solving integral and integro-differential equations. Wavelet methods utilize the concept of multiresolution analysis, which allows for the representation of a function at different levels of detail. This property enables the capture of both local and global features of the function efficiently. It is particularly useful when dealing with signals or functions that exhibit localized phenomena or sharp transitions. Wavelet methods provide an adaptive representation of functions. This adaptivity leads to efficient compression and sparsity, reducing the computational complexity compared to other methods that use a fixed basis representation. Wavelets have compact support, which means that they are nonzero only in a finite interval. This property allows for efficient localization of features and reduces the computational burden by focusing computations on the regions of interest. It also leads to better handling of boundary conditions compared to methods that use global basis functions. Wavelet bases are orthogonal, which simplifies the computation of expansions, integrals, and inner products. Orthogonal wavelet bases enable accurate and efficient numerical approximations, as they provide good stability and convergence properties. Wavelet methods are well-suited for handling functions with singularities or discontinuities. The compact support and adaptivity of wavelets allow for effective representation and approximation of functions with localized singularities. This makes wavelet methods particularly useful when dealing with problems of singular behaviour. Numerous wavelets exhibiting different characteristics have been documented in the literature for the examination of diverse forms of data, signals, images, and solution analysis. However, among the available options, the Haar wavelet stands out as the mathematically simplest, computationally efficient, conceptually simple, and memory-friendly wavelet. It is recognized as the oldest orthonormal wavelet with compact support in the literature. The Haar wavelet possesses a basic rectangular pulse pair with an explicit expression that allows for seamless integration of any desired number of times without constraints. The distinctive properties of Haar wavelets, combined with their simple explicit expression, have motivated their application in Haar wavelet bases with spectral methods for solving various integral and integro-differential equations encountered in

scientific and technological domains. Within wavelet techniques, enhancing the dilation factor of the wavelet family contributes to increased solution accuracy. While dyadic wavelets, where the dilation factor operates as powers of 2, dominate the literature, this thesis introduces novel Haar scale 3 (non-dyadic) wavelet-based numerical methods. These methods, employing dilation factors that operate as powers of 3, are developed for the analysis of linear and nonlinear integral and integro-differential equations of diverse types. The objective of this thesis is to investigate the effectiveness and efficiency of Haar wavelet methods in solving integral and integro-differential equations. This thesis focuses on the advancement of algorithms utilizing Haar Scale 3 Wavelets, in combination with established numerical techniques including the Collocation method, Quasilinearization process, and Thomas algorithm. These algorithms are designed to effectively solve a variety of significant integral and integro-differential equations. This thesis is structured into six chapters, each of which is outlined below, providing a concise overview of the content and key points covered in each chapter.

Chapter 1- Chapter 1 of this thesis focuses on providing an introduction to the topic, covers important mathematical concepts related to integrals, integro-differential equations, and wavelets, which serve as foundational knowledge for the subsequent chapters. Additionally, the chapter includes a literature review. The chapter also includes the motivation of choosing wavelets, scope and objectives of the study.

Chapter 2- A novel numerical technique called the Haar wavelet collocation method is introduced in this chapter to solve Volterra, Fredholm and mixed Volterra-Fredholm integro-differential equations. Several illustrative examples are utilized to test the method and compare its performance against exact solutions and existing methods. The results demonstrate that the proposed method outperforms other approaches, indicating its superiority and effectiveness. Therefore, the proposed scheme offers a promising alternative approach and an efficient numerical method for solving variety of integro-differential equations.

Chapter 3- This chapter contains a new Haar Wavelet collocation approach for resolving both linear and non-linear integral equations. In order to validate the method and evaluate its efficacy in comparison to exact solution and pre-existing methods,

several illustrative numerical examples are used. The outcomes show that the proposed method is superior to other methods and is more efficient. As a result, the proposed scheme provides a useful alternative method and a powerful numerical technique for solving a wide range of integral equations.

Chapter 4- This chapter explores the characteristics of Lane-Emden and Emden-Fowler type equations using Haar scale 3 wavelets. These equations are known to possess singularity at the origin, which poses a significant challenge. To address this issue, a novel approach is proposed and applied to various Lane-Emden and Emden-Fowler equations. The outcomes are presented in the form of tables and graphs, indicating the reliability of the method for solving such equations.

Chapter 5- This chapter introduces a novel hybrid method based on Haar scale 3 wavelets for solving fractional integro-differential equations. The proposed method involves approximating the solution using Haar scale 3 wavelets with a dilation factor of 3, and the domain is discretized using the collocation method. Nonlinearities in the problems are addressed through the Quasilinearization technique. To demonstrate the effectiveness of the proposed method, various fractional equations are solved. The obtained solutions are compared with exact and numerical solutions from existing literature, highlighting the superior efficiency of the proposed method in comparison to other approaches.

Chapter 6- This chapter presents the conclusions derived from the current research work and provides a comprehensive discussion on the impact of the proposed method on various types of integral and integro-differential equations. The study draws conclusions based on the findings and also suggests potential avenues for future research in this field.

Throughout the study, approximately 300 reputable research publications, books, theses, and notes were consulted and cited in the references. For all the computational work, MATLAB program have developed.

ACKNOWLEDGMENT

First and foremost, I express my deepest gratitude and thanks to the Almighty Allah for granting me the strength, wisdom, and perseverance to complete this thesis. Without His blessings and guidance, this accomplishment would not have been possible. I am truly grateful for His unwavering support throughout this journey.

I would like to extend my heartfelt appreciation to my supervisor ***Dr. Ratesh Kumar*** *for his invaluable guidance, patience, and expertise. His insightful feedback, constant encouragement, and willingness to share his knowledge have been instrumental in shaping the direction of this thesis. I am truly fortunate to have had the opportunity to work under his supervision, and I am grateful for his belief in my abilities. His own zeal for perfection, passion, unflinching courage and conviction has always inspired me to do more.*

I would like to express my sincere gratitude to Dr. K. C. Juglan, Head of the School of Chemical Engineering and Physical Sciences, Dr. Kulwinder Singh, Head of the Department of Mathematics and all other faculty members of the Department of Mathematics.

I prolong my heartfelt thanks to the esteemed Heads of Lovely Professional University, Dr. Ashok Mittal (Chancellor), Mrs. Rashmi Mittal (Pro- Chancellor), Dr. Preeti Bajaj (Vice- Chancellor), Dr. Loviraj Gupta (Executive Dean), Dr. Monica Gulati (Registrar) for their visionary leadership has created opportunities for intellectual exploration, interdisciplinary collaboration, and transformative research endeavors. I am deeply grateful to them for providing me with the platform to realize my research aspirations.

Besides these respected people, I would like to pay hearty gratitude to the rest of my end-term presentation panel members: Dr. Sanjay Mishra, Dr. Pankaj Kumar and Dr. Rakesh Yadav for their insightful comments and encouragement, and also for the hard question which incented me to widen my research from various perspectives.

I would like to acknowledge my teacher Javaid Ahmed Bandy for always inspiring me to pursue higher studies. I take this opportunity to sincerely acknowledge Dr. Javid

Iqbal, Dr. Rustam Abbas, and Mr. Tehseen Abbas for their guidance, moral support and valuable suggestions.

I am deeply indebted to my parents Mr. Abdul Rashid and Mrs. Shahnaz Akhter for their unconditional love, unwavering support, and continuous encouragement throughout my academic journey. Their sacrifices, both emotional and financial, have been instrumental in enabling me to pursue higher education. Their belief in my abilities and their constant words of motivation have been a driving force behind my success. I am forever grateful for their guidance, patience, and understanding during the challenging times, and I dedicate this thesis to them.

I would like to express my heartfelt gratitude to my loving husband Dr. Javid Shabir for his constant support, understanding, and encouragement throughout the entire process of completing this thesis. His patience, and constant words of motivation have been a source of strength during the challenging times. I am truly blessed to have him as my partner in life, and I am grateful for his presence, love, and support. I would like to extend my sincere gratitude and appreciation to my in-laws, Mr. Mohd Shabir and Mrs. Nazira Begum for their support and encouragement throughout my Ph.D. journey. Their understanding of the time and effort required to complete this thesis have been truly invaluable.

I would like to express my deepest appreciation to my seniors and friends Sufiara Yousuf, Rafia Jan, Rupali Verma, Balqees Akhter, Jaya Gupta and Sumaira Yousuf for providing encouragement, lending an empathetic ear, and cheering me on during both the triumphs and the challenges. I would like to extend my deepest appreciation to my siblings Habiba Bakhtawar and Abdul Barr. Their incredible support, encouragement and love have been a constant source of strength throughout Ph. D journey. Lastly, I would like to thank all those individuals who directly or indirectly have supported me throughout my academic journey. Though it is not possible to mention each person individually, please know that your support has played a significant role in my accomplishments.

Sabiha Bakhtawar

TABLE OF CONTANTS

LIST OF TABLES

LIST OF FIGURES

Chapter 1.
Introduction

1.1 Introduction

Integral equations (IEs) and integro-differential equations (IDEs) are important mathematical tools in various scientific fields. They represent a class of equations that involve integrals or derivatives of an unknown function, which makes their solution challenging and requires advanced mathematical techniques. These equations are encountered in many physical problems [1]. Integral equations have applications in many fields, such as economics, finance, and image processing [2]. IDEs are a combination of differential and integral equations. They involve derivatives and integrals of an unknown function and are often used to model physical phenomena that exhibit both temporal and spatial variations. Examples of such phenomena include heat conduction [3], diffusion [4], and wave propagation [5]. In physics, integral equations and integro-differential equations serve as powerful mathematical tools for modelling and understanding diverse phenomena including wave propagation [5], heat transfer [3], fluid mechanics [6], and electromagnetic fields [7]. In engineering, IEs and IDEs are used in the design and optimization of various systems, such as electrical circuits [8], mechanical systems [9], and control systems [10]. The solution of these equations can help engineers design systems that are efficient, reliable, and safe. In economics, IEs and IDEs are used to model various economic phenomena, such as economic growth, financial markets, and consumer behaviour [11]. The solution of these equations can help economists make predictions about the behaviour of these phenomena and develop policies that promote economic stability and growth. In biology, IEs and IDEs are encountered in the modelling of the behaviour of populations, ecosystems, and biological processes [12]. In neuroscience the solution of IEs can be used to model the behaviour of neurons and neural networks [13]. These equations provide a mathematical framework for modelling complex phenomena and making predictions about their behaviour.

Solving these equations is therefore crucial for developing scientific theories, designing systems, and making informed decisions in various fields of science and engineering. Integral and integro-differential equations are of great importance in mathematical modelling because they provide a framework for understanding complex phenomena in various scientific fields. They allow researchers to describe physical systems in terms of mathematical equations that can be solved numerically or analytically. The solution of IEs and IDEs can provide insight into the behaviour of physical systems and can be used to make predictions about future behaviour. The solution of these equations can be challenging because of the nonlinearities and singularities that often appear in these equations. Many researchers have developed new techniques for solving these equations, and there is ongoing research to find new applications of these equations in different fields.

1.2 Challenges and Perspectives in dealing with Integral Equations (IEs) and Integro-Differential Equations (IDEs)

Many researchers are working on introducing different numerical methods for solving problems that involve derivatives and integrals. Some integrals and derivatives cannot be determined precisely, and a few require special functions that pose a computational problem. To fully grasp the qualitative aspects of a wide variety of occurrences and processes in the natural sciences, solutions to integral equations are crucial. As a result, the investigation of these equations to find exact or approximate solutions is of the utmost significance. The solution of IEs and IDEs is essential in various scientific fields for several reasons. IEs and IDEs are often used to model physical phenomena that cannot be described by ordinary differential equations. These phenomena may exhibit spatial or temporal variations that require the use of integrals and derivatives in the equations. Numerical methods including finite element [14], finite difference [15], and boundary element methods [16], are commonly used to solve these equations. Analytical methods, such as Laplace transforms [17], [18], Green's functions [19], and perturbation theory [20], can also be used to find solutions of these equations. However, these methods exhibit low order accuracy, high cost, and are subject to certain geometric limitations. While they demonstrate excellent spatial localization, their overall accuracy is reduced. Another alternative "the Semi-analytic technique" provides

a series solution, but its convergence poses a significant challenge. The validity of the solution depends on the convergence of the series, and some methods are highly sensitive to the initial guess provided. The accuracy and efficiency of these methods heavily rely on starting with a good initial approximation. A distinct category of numerical algorithms involves “spectral methods” wherein the solution is typically discretized. This discretization involves approximating the solution using a set of infinitely differentiable basis functions. These basis functions form a series that represents an approximation of the continuous solution that remains nonvanishing throughout the entire domain. These techniques are often combined with the “method of weighted residuals”. The Spectral approaches exhibit “exponential convergence rates” when the anticipated solution is “smooth in nature”. However, their “spatial localization” suffers when dealing with “discontinuous and non-smooth solutions”. Furthermore, spectral approaches possess less impact in handling complex geometries but offer lower computational costs compared to the “Finite difference method (FDM), Finite element method (FEM), and Finite volume method (FVM)”. While “FDM, FEM, and FVM” operate on compact support, “spectral methods” work on a global support scale. Spectral methods display weaker “spatial localization for complex problems and irregular geometries” nevertheless, they are more accurate and yield fewer errors. On the Contrary “FDM, FEM, and FVM” exhibit better spatial localization but lower accuracy. Each method possesses its own set of benefits and constraints. Wavelet-based approaches offer a potential solution in this scenario by leveraging the advantages of different approaches. By employing wavelet bases to approximate the unknown solution, we can achieve both precise localization in space and time and improved accuracy. Wavelets possess numerous advantages, such as being “orthonormal” and having “compact support” for dilation and translation through “multiresolution analysis (MRA)” and are well-suited for the computational environment. They exhibit localization properties in both spatial and temporal domains, making them highly effective in addressing various scientific and technological challenges. Furthermore, wavelet-based approaches could be readily generalized to higher dimensions to handle more intricate challenges. Wavelets also integrate seamlessly with established fast and highly accurate numerical techniques, facilitating a strong connection between the two. In the literature, there are numerous wavelets available for analyzing different types of

data, signals, images, and solutions. However, the Haar wavelet stands out as the simplest in terms of mathematical formulation, computational efficiency, conceptual clarity, and memory usage. This wavelet documented in past studies, holds the distinction of being the most ancient orthonormal wavelet with a compact support. The Haar wavelet has a "simplest mathematical expression" consisting of a pair of rectangular pulses, allowing for integration without any limitations on the desired number of times. Due to the favourable characteristics of wavelets and the clear representation of the Haar wavelet, we were inspired to utilize Haar wavelet bases in conjunction with spectral methods to address a range of functional equations in scientific and technological domains.

1.3 Fundamental Terminology Employed in Integral Equations and Integro-Differential Equations

1.3.1 Integral Equations

Any equation where the unknown function is enclosed by an integral sign is known as an integral equation. Integral equation for $\xi(\varkappa)$ is given by (1.1), which is the standard form [2], [21],

$$\xi(\varkappa) = f(\varkappa) + \lambda_0 \int_{\mathscr{g}(\varkappa)}^{\hbar(\varkappa)} K(\varkappa, t)\xi(t)dt. \tag{1.1}$$

The limits of the integrals, $\mathscr{g}(\varkappa)$ and $\hbar(\varkappa)$, can take on constant, variable, or mixed values. λ_0 is a known parameter with a fixed value. $K(\varkappa, t)$ is a function that is already given containing two variables $\varkappa$ and t referred to as the nucleus or integration kernel. The unknown function $\xi(\varkappa)$ which needs to be determined exists within and outside the integral sign in most cases, although there are instances where it solely appears within the integral sign.

Classification of Integral Equations

The major classification of integral equations is based on two distinct factors. The first one is the limits of integration, whether the limits of integrals are constants or variables, and the second one is based on the linearity of unknown function. Based on these two factors integral equations are classified into various types.

Some of the more general types of integral equations are presented below [2], [21].

- ❖ Fredholm integral equations
- ❖ Nonlinear Fredholm integral equations
- ❖ Nonlinear Fredholm Hammerstein integral equations
- ❖ Volterra integral equations
- ❖ Nonlinear Volterra integral equations
- ❖ Nonlinear Volterra Hammerstein integral equations
- ❖ Volterra-Fredholm integral equations
- ❖ Nonlinear Volterra-Fredholm integral equations
- ❖ Nonlinear Volterra-Fredholm Hammerstein integral equations

1.3.1.1 Fredholm Integral Equations

Erik Ivar Fredholm (7 April 1866 - 17 August 1927), a distinguished Swedish researcher and mathematician, is widely recognized for his significant contributions to integral equations and spectral theory. His work in these areas laid the foundation for the development of vector spaces theory. Fredholm integral equations find extensive applications across various fields. Research indicates that a wide range of boundary value problems could be effectively changed into corresponding Fredholm integral equations. Equation (1.2) illustrates a typical representation of a Fredholm integral equation,

$$\varphi(\varkappa)\xi(\varkappa) = f(\varkappa) + \lambda_0 \int_{a_1}^{a_2} K(\varkappa, t)\xi(t)dt\,;\ a_1 \leq \varkappa, t \leq a_2. \qquad (1.2)$$

The limits of integration, denoted by a_1 and a_2, are constant values, and the unknown function $\xi(\varkappa)$ is present within the integral sign. The function $K(\varkappa, t)$, referred to as the integration kernel, is a known function, while λ_0 is a constant parameter. Additionally, $f(\varkappa)$ is another function with a predetermined value. Equation (1.2) demonstrates that the function $\xi(\varkappa)$ under the integral sign appears linearly, meaning its power is one. Hence, equation (1.2) is referred to as the linear Fredholm integral equation. The function $\varphi(\varkappa)$ will further divide the Fredholm integral equation into three different types depending upon the values of $\varphi(\varkappa)$.

If $\varphi(\varkappa) = 0$; then equation (1.2) reduces to,

$$f(\varkappa) = \lambda_0 \int_{a_1}^{a_2} K(\varkappa, t)\xi(t)dt\,;\ a_1 \leq \varkappa, t \leq a_2. \qquad (1.3)$$

The equation (1.3) is referred to as the Fredholm IEs of the first kind.

If $\varphi(\varkappa) = 1$; then equation (1.2) becomes as,

$$\xi(\varkappa) = f(\varkappa) + \lambda_0 \int_{a_1}^{a_2} K(\varkappa, t)\xi(t)dt\,;\ a_1 \leq \varkappa, t \leq a_2. \qquad (1.4)$$

This equation (1.4) is called the second kind of Fredholm IEs.

If $\varphi(\varkappa) \neq 0, 1$; then equation (1.2) is called the third kind of Fredholm IEs. More precisely, the only difference between the 1st kind and 2nd kind is that in the first kind of Fredholm IEs, the function $\xi(\varkappa)$ is solely present within the integral sign. Conversely, in the 2nd kind of Fredholm IEs, the function $\xi(\varkappa)$ seems inside and outside the integral sign.

1.3.1.2 Nonlinear Fredholm Integral Equations

The general representation of nonlinear Fredholm IEs is expressed as,

$$\varphi(\varkappa)\xi(\varkappa) = f(\varkappa) + \lambda_0 \int_{a_1}^{a_2} K(\varkappa, t)\mathcal{F}(\xi(t))dt\,;\ a_1 \leq \varkappa, t \leq a_2. \qquad (1.5)$$

Here a_1, a_2 are limits of integration. λ_0 is a known parameter. $\mathcal{F}(\xi(t))$is a nonlinear function of $\xi(t)$ such as the exponential function or logarithmic function or polynomial function of degree greater than one. i.e., $\mathcal{F}\big(\xi(t)\big) = \xi^n(t); where\ n > 1, \sin\big(\xi(t)\big), \cos\big(\xi(t)\big), or\ e^{\xi(t)}$ etc. $K(\varkappa, t)$is a kernel function whose value is already known.

1.3.1.3 Nonlinear Fredholm Hammerstein Integral Equations

The typical representation of a nonlinear Fredholm Hammerstein IEs is provided as,,

$$\varphi(\varkappa)\xi(\varkappa) = f(\varkappa) + \lambda_0 \int_{a_1}^{a_2} K(\varkappa, t)\mathcal{F}(t, \xi(t))dt\,;\ a_1 \leq \varkappa, t \leq a_2. \qquad (1.6)$$

1.3.1.4 Volterra Integral Equations

Vito Volterra (1860 –1940), a well-known mathematician and physicist was an Italian researcher known for his contribution to “Bio-Mathematics and integral equations”.

The concept of Volterra IEs was first given by Vito Volterra. Volterra began exploring integral equations in 1884, but his extensive research started in 1896. Du Bois-Reymond (1818 –1896) was a German researcher who chose to give the name integral equation in 1888. T. Lalescu (1882-1929), a Romanian mathematician known for his great contribution to functional equations, however, was the one who gave the name Volterra integral equation in 1908. Volterra IEs are encountered in various domains. Equation (1.7) presents a standard form of Volterra IEs, where one integral's limit instead of being constant is variable '$\varkappa$',

$$\varphi(\varkappa)\xi(\varkappa) = f(\varkappa) + \lambda_0 \int_{a_1}^{\varkappa} K(\varkappa, t)\, \xi(t)dt\,;\ a_1 \leq \varkappa, t \leq a_2. \tag{1.7}$$

It can be observed from equation (1.7) that Volterra IEs are a "special case" of Fredholm IEs in which the kernel $K(\varkappa, t)$ involved in the integral vanishes for $t > \varkappa$. This equation is called the Volterra linear IEs as the function $\xi(t)$ manifest linearly inside the integral sign as mentioned earlier in the description of Fredholm linear IEs. Volterra IEs are further divided into three main types depending on the value of $\varphi(\varkappa)$. A brief description is presented below.

If $\varphi(\varkappa) = 0$; then equation (1.7) yields

$$f(\varkappa) = \lambda_0 \int_{a_1}^{\varkappa} K(\varkappa, t)\, \xi(t)dt\,;\ a_1 \leq \varkappa, t \leq a_2. \tag{1.8}$$

The resulting equation (1.8) is called the 1st kind of Volterra IEs.

If $\varphi(\varkappa) = 1$; then equation (1.7) reduces to,

$$\xi(\varkappa) = f(\varkappa) + \lambda_0 \int_{a_1}^{\varkappa} K(\varkappa, t)\, \xi(t)dt\,;\ a_1 \leq \varkappa, t \leq a_2. \tag{1.9}$$

This equation (1.9) represents the 2nd kind of Volterra IEs.

If $\varphi(\varkappa) \neq 0, 1$; then equation (1.7) represents the 3rd kind of Volterra IEs. The main difference between 1st and 2nd kinds of Volterra IEs is the existence of unknown function $\xi(\varkappa)$ inside and outside the integral sign. When the "unknown function" is solely present under the integral sign, it corresponds to the first kind of Volterra IEs. On the contrary, if the "unknown function" exists under the integral sign and outside of it, it corresponds to the 2nd kind of Volterra IEs.

1.3.1.5 Nonlinear Volterra Integral Equations

The standard representation of nonlinear Volterra IEs is presented below in equation (1.10) in which one integral limit is a variable rather than constant as in Fredholm integral equation.

$$\varphi(\varkappa)\xi(\varkappa) = f(\varkappa) + \lambda_0 \int_{a_1}^{\varkappa} K(\varkappa, t)\, \mathcal{F}(\xi(t))dt\,;\ a_1 \leq \varkappa, t \leq a_2. \qquad (1.10)$$

Here $K(\varkappa, t)$ is the nucleus or kernel of integration and is a known function. $f(\varkappa)$ is also given in advance. $\mathcal{F}(\xi(t))$ is the nonlinear function in unknown function $\xi(t)$ like the exponential, logarithmic, inverse function, or polynomial function of degree greater than or equal to two, etc. λ_0 is a fixed constant parameter. The Volterra nonlinear integral equation is further divided into three main categories depending upon the values of $\varphi(\varkappa)$.

If $\varphi(\varkappa) = 0$; equation (1.10) becomes the first kind of Volterra nonlinear integral equation as presented in equation (1.11),

$$f(\varkappa) = \lambda_0 \int_{a_1}^{\varkappa} K(\varkappa, t)\, \mathcal{F}(\xi(t))dt\,;\ a_1 \leq \varkappa, t \leq a_2. \qquad (1.11)$$

If $\varphi(\varkappa) = 1$; then equation (1.10) becomes the 2nd kind of nonlinear Volterra IEs as written in equation (1.12),

$$\xi(\varkappa) = f(\varkappa) + \lambda_0 \int_{a_1}^{\varkappa} K(\varkappa, t)\, \mathcal{F}(\xi(t))dt\,;\ a_1 \leq \varkappa, t \leq a_2. \qquad (1.12)$$

If $\varphi(\varkappa) \neq 0, 1$; then equation (1.10) becomes the third kind of nonlinear Volterra IEs. The different kinds of Volterra IEs have different origins and applications.

1.3.1.6 Nonlinear Volterra Hammerstein Integral Equations

The standard representation of nonlinear Hammerstein Volterra IEs is given as,

$$\varphi(\varkappa)\xi(\varkappa) = f(\varkappa) + \lambda_0 \int_{a_1}^{\varkappa} K(\varkappa, t)\mathcal{F}(t, \xi(t))dt\,;\ a_1 \leq \varkappa, t \leq a_2. \qquad (1.13)$$

1.3.1.7 Volterra-Fredholm Integral Equations

The Volterra-Fredholm IEs developed as a consequence of parabolic constrained optimization problems, the quantitative modelling of the spatiotemporal evolution of

an epidemic, and a variety of certain other biological and physical models. The Volterra-Fredholm IEs are a hybrid of the Volterra integral and the Fredholm integral, which are two different integral equations. The combination of these two equations appears in a single integral equation. The integral equation of the Volterra-Fredholm type could be written in the generalized form as,

$$\xi(\varkappa) = f(\varkappa) + \lambda_0 \int_{a_1}^{\varkappa} K_1(\varkappa, t)\xi(t)dt + \lambda_1 \int_{a_1}^{a_2} K_2(\varkappa, t)\xi(t)dt\,; \quad a_1 \leq \varkappa, t \leq a_2. \tag{1.14}$$

Here $K_1(\varkappa, t)$ and $K_2(\varkappa, t)$ represents the kernel of the equation.

1.3.1.8 Nonlinear Volterra-Fredholm Integral Equations

The basic structure of the Volterra-Fredholm nonlinear IEs is,

$$\xi(\varkappa) = f(\varkappa) + \lambda_0 \int_{a_1}^{\varkappa} K_1(\varkappa, t)\, \mathcal{F}_1\big(\xi(t)\big)dt + \lambda_1 \int_{a_1}^{a_2} K_2(\varkappa, t)\, \mathcal{F}_2\big(\xi(t)\big)dt\,; a_1 \leq \varkappa, t \leq a_2. \tag{1.15}$$

1.3.1.9 Nonlinear Volterra-Fredholm Hammerstein Integral Equations

The standard representation of Volterra-Fredholm nonlinear Hammerstein IEs is,

$$\xi(\varkappa) = f(\varkappa) + \lambda_0 \int_{a_1}^{\varkappa} K_1(\varkappa, t)\, \mathcal{F}_1\big(t, \xi(t)\big)dt + \lambda_1 \int_{a_1}^{a_2} K_2(\varkappa, t)\, \mathcal{F}_2\big(t, \xi(t)\big)dt\,; a_1 \leq \varkappa, t \leq a_2. \tag{1.16}$$

1.3.2 Integro-Differential Equations (IDEs)

Vito Volterra studied population growth in early 1900, which eventually resulted in the development of a special type of equation called the IDEs [21]. In these particular kinds of equations, the "unknown function" denoted by $\xi(\varkappa)$ appears on one side of the equation as an ordinary derivative, while on the other side of the equation, it occurs under the integral sign. This kind of equation is a result of a variety of

phenomena that are encountered in the physical sciences. When transforming a differential equation to an IEs, an IDEs is easily seen as an intermediate stage. The current flowing in a closed circuit in electronic engineering problems can be easily determined by using the following integro-differential equation;

$$L\frac{dI}{dt} + RI + \frac{I}{C}\int_0^t I(\tau)d\tau = g(t)\,, I(0) = I_0,$$

where L represents inductance, R represents resistance, C denotes capacitance, and $g(t)$ means applied voltage [2]. The typical representation of an integro-differential equation is provided as;

$$\xi^{(n)}(x) = f(\varkappa) + \lambda_0 \int_{g(\varkappa)}^{\hbar(\varkappa)} K(\varkappa, t)\xi(t)dt, \tag{1.17}$$

where $\xi^{(n)}(x)$ represents the n^{th} derivative of ξ. $g(\varkappa)$, and $\hbar(\varkappa)$ are the lower and upper limits of integration. $K(\varkappa, t)$ is the nucleus of the integral. λ_0 is a constant parameter. $f(\varkappa)$ is also known function.

Classification of Integro-Differential Equations

The classification of integro-differential equation is based upon two distinct factors. The first one is the limits of integration, whether the limits of integrals are constants or variables, and the second one is based on the linearity of unknown function. Based upon these two factors, IDEs are classified into various categories. Some of the more general types of IDEs are presented below [21].

- Linear Fredholm integro-differential equations
- Nonlinear Fredholm integro-differential equations
- Nonlinear Fredholm Hammerstein integro-differential equations
- Linear Volterra integro-differential equations
- Nonlinear Volterra nonlinear integro-differential equations
- Nonlinear Volterra Hammerstein integro-differential equations
- Volterra-Fredholm integro-differential equations
- Nonlinear Volterra-Fredholm integro-differential equations
- Nonlinear Volterra-Fredholm Hammerstein integro-differential equations

1.3.2.1 Fredholm Integro-Differential Equations

Numerous scientific applications involve the 2nd kind of Fredholm IDEs. Some examples of these applications include the theory of signal processing and artificial neural network. The general structure of the Fredholm integro-differential equation is,

$$\xi^{(n)}(x) = f(\varkappa) + \lambda_0 \int_{a_1}^{a_2} K(\varkappa, t)\xi(t)dt\,;\ \xi^{(p)}(0) = b_p, 0 \le p \le n-1. \qquad (1.18)$$

The Fredholm IDEs comprise the "unknown function" $\xi(\varkappa)$ and one or more than one of its derivatives such as $\xi'(x), \xi''(x), \xi'''(x)$ ... "inside and outside the integral sign". As in Fredholm IEs, integration limits are fixed in Fredholm IDEs. The equation is called IDEs as it comprises both differential operator as well as integral operators in the single equation. Fredholm IDEs require initial conditions $\xi'(0), \xi''(0), \xi'''(0), \ldots\ \xi^{n-1}(0)$ to get particular solutions.

1.3.2.2 Nonlinear Fredholm Integro-Differential Equations

The basic structure of Fredholm nonlinear IDEs is,

$$\xi^{(n)}(x) = f(\varkappa) + \lambda_0 \int_{a_1}^{a_2} K(\varkappa, t)\mathcal{F}(\xi(t))dt\,;\ \xi^{(p)}(0) = b_p, 0 \le p \le n-1, \quad (1.19)$$

where $\xi^{(n)}(x) = \frac{d^n\xi}{dx^n}$, is n^{th} derivative of x. $\mathcal{F}(\xi(t))$ is nonlinear in $\xi(t)$.

1.3.2.3 Nonlinear Fredholm Hammerstein Integro-differential Equations

The typical representation of nonlinear Hammerstein Fredholm IEs is provided as,

$$\xi^{(n)}(x) = f(\varkappa) + \lambda_0 \int_{a_1}^{a_2} K(\varkappa, t)\mathcal{F}\big(t, \xi(t)\big)dt\,;\ \xi^{(p)}(0) = b_p, \quad 0 \le p \le n-1. \qquad (1.20)$$

1.3.2.4 Volterra Integro-Differential Equations

In the Volterra IDEs, both the "unknown function" $\xi(x)$ and one of its derivatives appear inside as well as outside the integral sign. Similar to Volterra IEs, one of the integration limits is variable. This equation is referred to as an "integro-differential" equation as it incorporates both differential and integral operators within a single

equation. For Volterra IDEs, it is crucial to provide initial conditions to determine specific solutions. The general representation of Volterra IDEs is presented as follows,

$$\xi^{(n)}(x) = f(\varkappa) + \lambda_0 \int_{a_1}^{\varkappa} K(\varkappa, t)\xi(t)dt\,;\ \xi^{(p)}(0) = b_p, 0 \le p \le n-1. \qquad (1.21)$$

1.3.2.5 Nonlinear Volterra Integro-Differential Equations

The typical representation of a 2nd kind Volterra nonlinear integro-differential equation is given as,

$$\xi^{(n)}(x) = f(\varkappa) + \lambda_0 \int_{a_1}^{\varkappa} K(\varkappa, t)\mathcal{F}(\xi(t))dt\,;\ \xi^{(p)}(0) = b_p, 0 \le p \le n-1, \qquad (1.22)$$

where $\mathcal{F}(\xi(t))$ is the nonlinear function in $(\xi(t))$ like the exponential function, logarithmic function, trigonometric function, or polynomial function having a degree greater than or equal to 2. Volterra integro-differential equations have been found to be useful in an extensive range of physical applications, including the formation of glass, neutron diffusion, wind ripple in the desert, and nano-hydrodynamics, etc.

1.3.2.6 Nonlinear Volterra Hammerstein Integro-Differential Equations

The general structure of Volterra Hammerstein nonlinear IDEs is mentioned as follows,

$$\xi^{(n)}(x) = f(\varkappa) + \lambda_0 \int_{a_1}^{x} K(\varkappa, t)\mathcal{F}\big(t, \xi(t)\big)dt\,;\ \xi^{(p)}(0) = b_p, \quad 0 \le p \le n-1. \qquad (1.23)$$

1.3.2.7 Volterra-Fredholm Integro-Differential Equations

The Volterra-Fredholm IDEs can be formulated as a unified integral equation, combining separate Volterra and Fredholm integrals along with a differential operator. Many physical and chemical phenomena lead to the emergence of Volterra-Fredholm IDEs. The general form of the Volterra-Fredholm IDEs can be expressed as follows,

$$\xi^{(n)}(x) = f(\varkappa) + \lambda_0 \int_{a_1}^{\varkappa} K_1(\varkappa, t)\xi(t)dt + \lambda_1 \int_{a_1}^{a_2} K_2(\varkappa, t)\xi(t)dt\,; \quad \xi^{(p)}(0) = b_p, 0 \le p \le n-1. \qquad (1.24)$$

Where $\xi^{(n)}(x)$ is the n^{th} derivative of x.

1.3.2.8 Nonlinear Volterra-Fredholm Integro-Differential Equations

The basic structure of Volterra-Fredholm nonlinear IDEs is,

$$\xi^{(n)}(x) = f(\varkappa) + \lambda_0 \int_{a_1}^{\varkappa} K_1(\varkappa, t)\mathcal{F}_1(\xi(t))dt + \lambda_1 \int_{a_1}^{a_2} K_2(\varkappa, t)\mathcal{F}_2(\xi(t))dt\,;\ \xi^{(p)}(0) = b_p, 0 \le p \le n-1. \tag{1.25}$$

1.3.2.9 Nonlinear Volterra-Fredholm Hammerstein Integro-Differential Equations

The general structure of Volterra-Fredholm Hammerstein nonlinear integro-differential equation is,

$$\xi^{(n)}(x) = f(\varkappa) + \lambda_0 \int_{a_1}^{\varkappa} K_1(\varkappa, t)\mathcal{F}_1\big(t, \xi(t)\big)dt + \lambda_1 \int_{a_1}^{a_2} K_2(\varkappa, t)\mathcal{F}_2\big(t, \xi(t)\big)dt\,;\ \xi^{(p)}(0) = b_p, \quad 0 \le p \le n-1. \tag{1.26}$$

1.3.3 Singular Integral Equations

Singular integral equations are those for which the integral's limits can be either infinite or the kernel $K(\varkappa, t)$ may reach infinity at certain points within the integration interval. In general, the first kind of integral equation [2], [21]

$$f(\varkappa) = \lambda_0 \int_{g(\varkappa)}^{\hbar(\varkappa)} K(\varkappa, t)\xi(t)dt\,;\ a_1 \le \varkappa, t \le a_2, \tag{1.27}$$

or the second kind of integral equation

$$\xi(\varkappa) = f(\varkappa) + \lambda_0 \int_{g(\varkappa)}^{\hbar(\varkappa)} K(\varkappa, t)\xi(t)dt\,;\ a_1 \le \varkappa, t \le a_2. \tag{1.28}$$

is said to be the singular integral equation of the first style if the lower limit of integral $g(\varkappa)$or the upper limit of integral $\hbar(\varkappa)$ becomes infinite or both $g(\varkappa), \hbar(\varkappa)$ becomes

infinite. The following are some examples of singular integral equations of the first style that are presented:

$$F(\lambda) = \int_{-\infty}^{\infty} e^{-\iota\lambda\varkappa}\xi(\varkappa)d\varkappa. \qquad \text{(Fourier transform)}$$

$$L\big(\xi(\varkappa)\big) = \int_{0}^{\infty} e^{-\lambda\varkappa}\xi(\varkappa)d\varkappa. \qquad \text{(Laplace transform)}$$

Further equations (1.27) and (1.28) are called the second style of the integral equation if the kernel $K(\varkappa, t)$ involved in the IEs becomes infinite within the domain of integration. Some examples of such kind of integral equations are:

$$\varkappa^2 = \int_0^{\varkappa} \frac{1}{\sqrt{\varkappa - t}}\xi(t)dt. \qquad \text{(Abel's integral equation)} \qquad (1.29)$$

$$\varkappa = \int_0^{\varkappa} \frac{1}{(\varkappa - t)^{\alpha}}\xi(t)dt\,, 0 < \alpha < 1. \qquad (1.30)$$

(Generalised Abel's integral equation)

$$\xi(\varkappa) = 1 + 2\sqrt{\varkappa} - \int_0^{\varkappa} \frac{1}{\sqrt{\varkappa - t}}\xi(t)dt. \qquad (1.31)$$

The integral equation similar to equation (1.31), is referred to as weakly-singular integral equations. These equations have a variety of applications in superfluidity, heat conduction, and crystal growth.

1.3.4 Homogeneity Concept

When the function $f(\varkappa)$ is replaced with zero in Volterra or Fredholm integral equations, it results in homogeneous IEs or IDEs, respectively. In contrast, if $f(\varkappa)$ is non-zero, it is referred to as a nonhomogeneous or inhomogeneous IEs or IDEs [21].

1.3.5 Solution of Integral or Integro-Differential Equations

On the interval of integration, a solution to an IEs or IDEs is a function $\xi(\varkappa)$ that may be selected in a way that it accomplishes the equation that has been presented. To put it another way, if the given solution is implemented to solve the problem on the "right side of the equation", then the result of this direct substitution should be the same as the solution on the "left side of the equation"[21].

1.4 Motivation and Scope of Using Wavelets for Solving Various Functional Equations

A “wavelet” can be described as a mathematical function that breakdown a particular function into different components. After some initial resistance, Morlet and Grossmann finally coin the term “wavelet” in the early 1980s. Since the 1980s, scientists have been paying more attention to the word “wavelet”. A description of wavelet describes as “a wave-like function with an amplitude that starts at zero, rises, and then drops back to zero.” Researchers are very curious about discovering such a function, which expands a new subject of research in applied harmonic analysis called “wavelet analysis”. In mathematics, wavelets are local orthonormal bases that are composed of small waves that break a function into many layers at various scales. Many scientific real-world problems have nonlinear mathematical modelling. Nonlinear differential and IEs can be used to model these nonlinear problems. Integral equations frequently appear in computational fluid dynamics, biological models, plasma physics, chemical kinetics, as well as in other disciplines. In the majority of situations, solving them proves to be highly challenging, particularly analytically. Presently, there’s a need to introduce a standardized method that can effectively handle both IEs and IDEs through the application of “wavelet-based algorithms” for achieving a “numerical solution”. The literature review highlights the use of the “Taylor series” for analyzing functions locally, but when researchers aimed to assess functions globally, the Taylor series proved inadequate, leading to the introduction of the “Fourier series”. However, while the Fourier series is effective for studying functions globally, it falls short when it comes to examining functions locally. Wavelets were created to overcome these restrictions. Wavelets have penetrated a variety of disciplines in science and engineering due to their advantages over numerical and other approximation approaches. Wavelet is a wave pattern with a graph that oscillates over a short distance and dumps very quickly. It is used as a mechanism to break down information, operators, or functions into different frequencies and then study each frequency component with a resolution that corresponds to its scale. Wavelets are indeed a unique family of basis functions for estimating general functions. They include important characteristics such as compact support, orthogonality, time and frequency

localization, biorthogonality, and efficient algorithms. From existing literature, we found a variety of wavelets having different characteristics such as:

- ❖ Haar wavelets
- ❖ Hermite wavelets
- ❖ Legendre wavelets
- ❖ Bernoulli wavelets
- ❖ Cosine and Sine wavelets
- ❖ Daubechies wavelets
- ❖ Spline wavelets

The Haar wavelet is the simple as well as oldest living orthonormal waveform having compact supports amongst wavelets. Haar wavelet is computationally inexpensive. In our study, we have taken under consideration only Haar wavelets.

1.5 Basic Preliminaries Related to Wavelets

"Orthonormal wavelets" are a class of contemporary functions capable of both expanding and compressing. These characteristics allow wavelet-based numerical algorithms to exhibit a qualitative improvement over other techniques. The following are a few definitions that are fundamental to comprehending wavelets:

1.5.1 The Space $L^2(\mathbb{R})$

The "space $L^2(\mathbb{R})$" is a vector space of "square-integrable function". It is expressed as;

$$L^2(\mathbb{R}) = \{\xi : \mathbb{R} \to \mathbb{C}\} : \int_{-\infty}^{\infty} |\xi(t)|^2 dt \ < \infty.$$

"For getting the finite value of unknown coefficients it is very much required that vector space should be a space of square integral function".

1.5.2 Inner Product

The inner product between two functions $\xi_1, \xi_2 \epsilon\ L^2(\mathbb{R})$ is defined by $\langle \xi_1, \xi_2 \rangle = \int_{-\infty}^{\infty} \xi_1(t)\ \xi_2(t)\ dt$, Specifically, the norm of the function ξ is determined by $\|\xi\|_2 = \langle \xi_1, \xi_2 \rangle^{\frac{1}{2}} = \left(\int_{-\infty}^{\infty} |\xi(t)|^2 dt\right)^{\frac{1}{2}}$.

1.5.3 Orthonormal function

Two functions $\xi_1, \xi_2 \epsilon\ L^2(\mathbb{R})$ are said to be orthonormal if ,

$$\langle \xi_1, \xi_2 \rangle = \begin{cases} 0; & if\ \xi_1 \neq \xi_2, \\ 1; & if\ \xi_1 = \xi_2. \end{cases}$$

This suggests that "the information conveyed by one function is unrelated to the data carried by any other function". There appears to be no duplication in the representation, which is beneficial as it eliminates the need for unnecessary computational cycles or storage due to coefficient redundancy.

1.5.4 Translation and Dilation Operator in $L^2(\mathbb{R})$

The dilation operator denoted as D_α, and the translation operator denoted as T_α, are defined for any square-integrable function $\xi(t)$ belonging to the space $L^2(\mathbb{R})$.

1) $D_\alpha \xi(t) = a^{\frac{1}{2}} \xi(at)$ for any $a > 0\ \epsilon\ \mathbb{R}$.
2) $T_b \xi(t) = \xi(t - b)$ for any $b\ \epsilon\ \mathbb{R}$.

Translation refers to "shifting the location of a function by b units", while dilation involves "spreading or compressing the function". When a value greater than 1 is used for the dilation operator $D_\alpha \xi(t)$, the function $\xi(t)$ becomes narrower, indicating compression. On the other hand, if a value between 0 and 1 is used, the function $D_\alpha \xi(t)$ becomes more spread out, implying stretching of the function $\xi(t)$.

1.5.5 Wavelets

The set of function achieved by translating and dilating a function $\psi(t)\ \epsilon\ L^2(\mathbb{R})$,

$$\psi_{\mathrm{b,a}}(t) = \frac{1}{a^{\frac{1}{2}}}\psi\left(\overline{\frac{t-b}{a}}\right), a > 0, b \in \mathbb{R},$$

Where ψ fulfills the "admissibility condition" as specified by,

$$C_\psi = \int_{-\infty}^{\infty} \frac{\left|\hat{\psi}(\omega)\right|^2}{\omega} d\omega < \infty.$$

is referred to as a "wavelet family". When we keep the "function ψ" fixed (with $a = 1, b = 0$), it is commonly known as the mother wavelet.

1.5.6 Wavelet Transformation

The definition of integral wavelet transforms (IWT) on the space $L^2(\mathbb{R})$is given by the following equation in connection to every basic wavelet,

$$W_\psi \xi(a,b) = \int_{-\infty}^{\infty} \xi(t)\psi\left(\overline{\frac{t-b}{a}}\right) dt\,;\ \xi(t) \in L^2(\mathbb{R}),$$

which quantifies the degree to which the function $\xi(t)$ is superimposed on the scaled and translated component of the wavelet. Alternately, this may be formulated as

$$W_\psi \xi(a,b) = \langle \xi, \psi_{b,a} \rangle.$$

1.5.7 Wavelet Series

A function $\psi(t)$ belonging to the space $L^2(\mathbb{R})$ is referred to as an orthonormal wavelet if the set of wavelets ψ forms an "orthonormal basis for $L^2(\mathbb{R})$" i.e.,

$$\langle \psi_{\mathrm{b,a}}, \psi_{\mathrm{d,c}} \rangle = \delta_{b,d}.\delta_{a,c},$$

where $\delta_{b,a}$ represents the Kronecker delta symbol defined as follows,

$$\delta_{b,a} = \begin{cases} 0; & if\ a \neq b, \\ 1; & if\ a = b. \end{cases}$$

The representation of each function $\xi(t)$ in the space $L^2(\mathbb{R})$ using the orthonormal wavelet family $\{\psi_{\mathrm{b,a}}(t)\}_{b,a}$ in a series form is referred to as a wavelet series, as given below,

$$\xi(t) = \sum_{b,a=0}^{\infty} C_{b,a}\psi_{\mathrm{b,a}}(t),$$

where $C_{b,a}$ represents the wavelet coefficients and values of $C_{b,a}$ are given by $C_{b,a} = \langle \xi, \psi_{\mathrm{b,a}} \rangle$. Solving a mathematical model using wavelet transforms is mathematically advantageous when working in a space where "the inner product of a function with itself corresponds to the size (norm) of the function". Due to this rationale, we will be working within the specified space referred to as $L^2(\mathbb{R})$. The Haar wavelet is the most basic wavelet that satisfies the admissibility condition. It forms an "orthonormal family with compact support" and can be described as;

1.5.8 Scale 2 Haar Function

$$\phi(t) = \begin{cases} 1; & t\,\epsilon[0,1), \\ 0; & elsewhere. \end{cases}$$

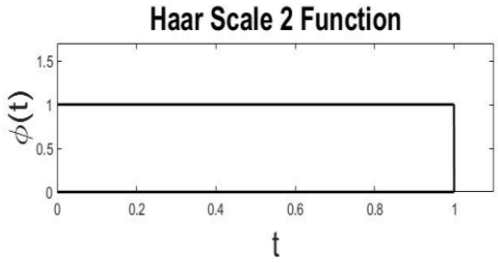

Figure 1.1: Scale 2 Haar Function

1.5.9 Scale 2 Haar Wavelet

$$\psi(t) = \begin{cases} 1; & t\,\epsilon\left[0,\frac{1}{2}\right), \\ -1; & t\,\epsilon\left[\frac{1}{2},1\right), \\ 0; & elsewhere. \end{cases}$$

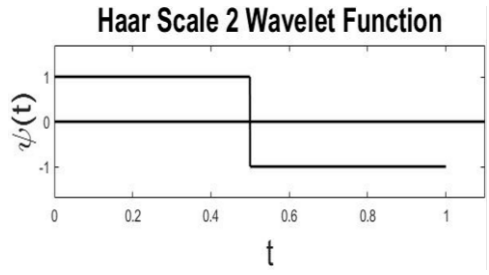

Figure 1.2: Scale 2 Haar Wavelet Function

1.5.10 Multiresolution Analysis (MRA) or Multiscale Approximation (MSA)

For the theory of wavelets to work, it is essential to understand the "multiresolution analysis (MRA)" idea, developed by "Y. Meyer and S. Mallat". A multiresolution analysis for the space of square-integrable function $L^2(\mathbb{R})$ is described as a "sequence of closed subspace $V_j \subset L^2(\mathbb{R}), j \in \mathbb{Z}$" having the below-mentioned properties;

(i) $\ldots \subset V_{-1} \subset V_0 \subset V_1 \subset \cdots$

(ii) $clos_{L^2}\left(\cup_{j \in \mathbb{Z}} V_j\right) = L^2(\mathbb{R})$,

(iii) $\cap_{j \in \mathbb{Z}} V_j = \{0\}$,

(iv) $if\ \xi(x) \in V_j$ if and only if $\xi\left(2^{-j}x\right) \in V_0$. This indicates that the spaces are essentially "rescaled versions of the central space V_0".

(v) $\xi(x) \in V_0$ if and only if $\xi(x-m) \in V_0\ \forall\ m \in \mathbb{Z}$.

(vi) $\exists$ a scaling function $\phi \in V_0$ such that set $\{\phi(x-m)\}_{m \in \mathbb{Z}}$ constitutes an orthonormal basis within V_0, referred to as a "Riesz basis" in V_0.

Condition (i) to condition (iii) implies, elements in the subspaces V_j provide a unique approximation for any function in $L^2(\mathbb{R})$. Furthermore, as $j \to \infty$ there is a rise in the accuracy of the approximation. The invariance of the system of subspaces V_j to the translation and dilation operators are expressed by conditions (iv) and (v).

In a given Multiresolution analysis $\{V_j\}$ within $L^2(\mathbb{R})$ using the scaling function ϕ, a wavelet can be derived from a new subspace $\{W_j\}$ in $L^2(\mathbb{R})$ that fulfils the following conditions:

a) $V_{j+1} = V_j + W_j, V_j \perp W_j\ \forall\ j$ i.e., $V_{j+1} = V_j \oplus W_j$

b) $\ldots W_{-1} \perp W_0 \perp W_1 \ldots$

c) $V_j = V_0 \oplus \sum_{i=0}^{j-1} W_j \implies L^2(\mathbb{R}) = V_0 \oplus \sum_{i=0}^{j-1} W_j$ as $j \to \infty$

Hence, any square-integrable function has the possibility of being represented using the "Haar wavelet series expansion" and this representation could be employed "to solve

numerical problems". By employing the Multiresolution Analysis (MRA) with the Haar scale 2 wavelet family, we can derive the following:

1.5.11 Scale 2 Haar Wavelet Family

The family of Haar wavelets is described as

$$h_i(t) = \psi\left(2^j t - k\right) = \begin{cases} 1; & \rho_1(i) \le t < \rho_2(i), \\ -1; & \rho_2(i) \le t < \rho_3(i), \\ 0; & elsewhere. \end{cases}$$

where $i = 1, 2, 3, \dots, 2p$. $\rho_1(i) = \frac{k}{p}$, $\rho_2(i) = \frac{2k+1}{2p}$, $\rho_3(i) = \frac{k+1}{p}$, $p = 2^J, j = 0,1,2, \dots$ and $k = 0, 1,2, \dots p - 1$. Here 'i' the wavelet number and the value of 'i' is obtained from the following mathematical relation

$$i = 2^j + k + 1.$$

The function $h_1(t)$ is known as the father wavelet, the function $h_2(t)$ as the mother wavelet, and all other functions $h_3(t), h_4(t)$, ... are created by "translating and dilating the mother wavelet".

1.5.12 Haar Scale 3 Wavelet Family

"Wavelet family" is an "orthonormal subfamily" of $L^2(\mathbb{R})$. From a fixed function known as the mother wavelet, all other functions in the wavelet family are constructed via translations and dilations. In Haar scaling 2 wavelets, a single mother wavelet provides the entire wavelet family, meanwhile, in Haar scale 3 two mother wavelets construct the extended wavelet family. The structure of the wavelet family for the Haar scale 3 along with their integrals [22] is presented in this section;

Haar scaling Function

$$h_i(t) = \varphi(t) = \begin{cases} 1, & 0 \le t < 1, \\ 0, & otherwise. \end{cases} \quad for\ i = 1. \tag{1.32}$$

Symmetric Haar wavelet

$$h_i(t) = \psi^1\left(3^j t - k\right) = \frac{1}{\sqrt{2}} \begin{cases} -1; & \rho_1(i) \le t < \rho_2(i), \\ 2; & \rho_2(i) \le t < \rho_3(i), \\ -1; & \rho_3(i) \le t < \rho_4(i), \\ 0; & elsewhere. \end{cases} \quad (1.33)$$

$$for\ i = 2, 4, \dots, 3p - 1.$$

Anti-Symmetric Haar wavelet

$$h_i(t) = \psi^2\left(3^j t - k\right) = \sqrt{\frac{3}{2}} \begin{cases} 1; & \rho_1(i) \le t < \rho_2(i), \\ 0; & \rho_2(i) \le t < \rho_3(i), \\ -1; & \rho_3(i) \le t < \rho_4(i), \\ 0; & elsewhere. \end{cases} for\ i = 3, 5, \dots, 3p. \quad (1.34)$$

where $p = 3^j, j = 0,1,2, \dots\ and\ k = 0,1,2, \dots p - 1. \rho_1(i) = \frac{k}{p}, \rho_2(i) = \frac{3k+1}{3p}, \rho_3(i) = \frac{3k+2}{3p},\ \rho_4(i) = \frac{k+1}{p}$.

For this wavelet family, the wavelet number is represented by i, dilation factor is represented by j, and the translation parameter is represented by k. For the computation of wavelet number i following relations are used.

$$i - 1 = 3^j + 2k.\ \text{(For even values of wavelet number)}$$

$$i - 2 = 3^j + 2k.\ \text{(For odd values of wavelet number)}$$

The whole wavelet family would be constructed by utilizing the above-mentioned expressions for various translations and dilations of $h_2(t)$, $h_3(t)$. $h_2(t)$ and $h_3(t)$ are considered as mother wavelets, and the remaining wavelets formed from these two parent wavelets are referred to as daughter wavelets. Figure 1.1 displays the initial nine elements of the Haar wavelet family.

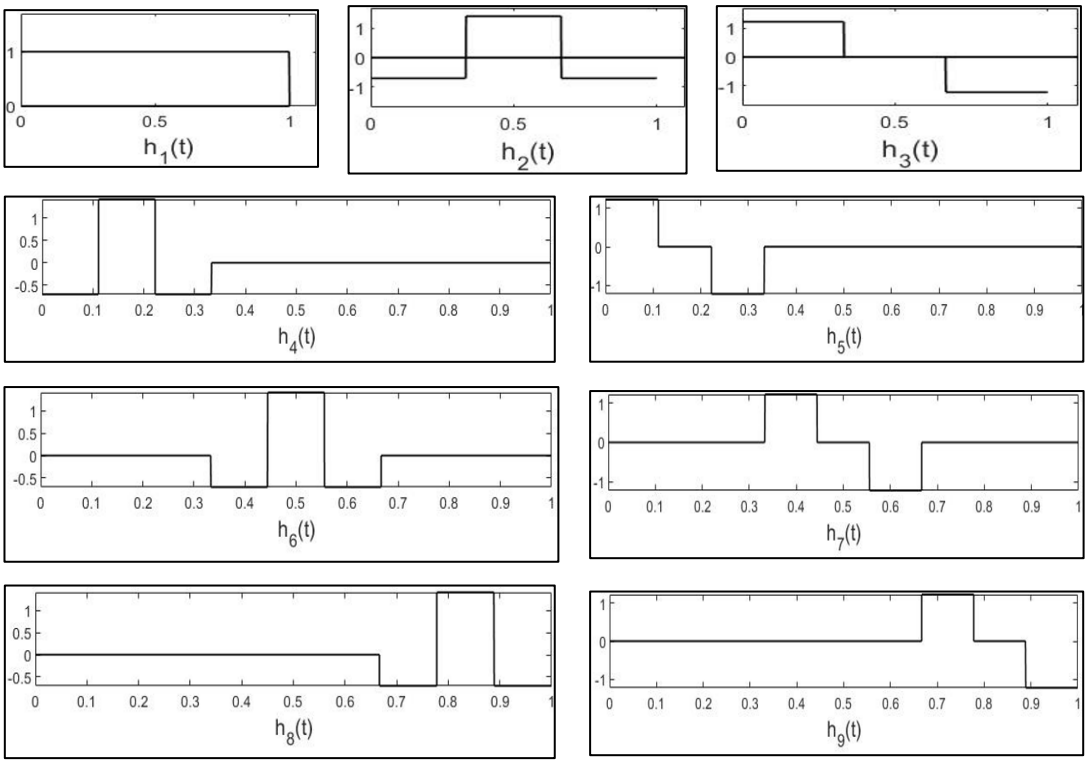

Figure 1.3: First nine members of Scale 3 Haar Wavelet family.

The primary distinction between the "Haar scale 2 wavelets" and "Haar scale 3 wavelets" lies in their construction. The Haar scale 2 wavelets are generated using a single mother wavelet, which gives rise to all the subsequent wavelets. On the other hand, the "Haar scale 3 wavelets" utilize two "mother wavelets" with distinct factors as well as different shapes to generate the wavelet family. As a result of this advantage, the Haar scale 3 wavelet accelerates the rate at which solutions converge.

Using the formula provided, one can efficiently evaluate the integrals of equations (1.32) - (1.34) over the interval $[0, 1)$ the desired number of times.

$$q_{\delta,i}(t) = \int_0^t \int_0^t \int_0^t \dots \delta \text{ times } \dots \int_0^t h_i(x)(dx)^{\delta} = \frac{1}{(\delta-1)!}\int_0^t (t-x)^{m-1} h_i(x)dx\,; \quad (1.35)$$

$$m = 1,2,3,\dots, i = 1,2,..3p.$$

Upon computing the aforementioned integrals, the resulting values are obtained as follows:

$$q_{\beta,i}(t) = \frac{t^{\beta}}{\beta!}\ for\ i = 1. \tag{1.36}$$

$q_{\beta,i}(t)'s$ for $i = 2,4,6, \ldots 3p-1$ are explained as $q_{\beta,i}(t) =$

$$\frac{1}{\sqrt{2}}\begin{cases} 0; & 0 \le t \le \alpha_1(i), \\ \frac{-1}{\beta!}(t-\alpha_1(i))^{\beta}; & \alpha_1(i) \le t \le \alpha_2(i), \\ \frac{1}{\beta!}\left[-\left(t-\alpha_1(i)\right)^{\beta} + 3(t-\alpha_2(i))^{\beta}\right]; & \alpha_2(i) \le t \le \alpha_3(i), \\ \frac{1}{\beta!}\left[-\left(t-\alpha_1(i)\right)^{\beta} + 3\left(t-\alpha_2(i)\right)^{\beta} - 3\left(t-\alpha_3(i)\right)^{\beta}\right]; & \alpha_3(i) \le t \le \alpha_4(i), \\ \frac{1}{\beta!}\left[-\left(t-\alpha_1(i)\right)^{\beta} + 3\left(t-\alpha_2(i)\right)^{\beta} - 3\left(t-\alpha_3(i)\right)^{\beta} + \left(t-\alpha_4(i)\right)^{\beta}\right]; \alpha_4(i) \le t \le 1. \end{cases} \tag{1.37}$$

$q_{\beta,i}(t)'s$ for $i = 3,5,7, \ldots 3p$ are given below $q_{\beta,i}(t) =$

$$\sqrt{\frac{3}{2}}\begin{cases} 0; & 0 \le t \le \alpha_1(i), \\ \frac{1}{\beta!}(t-\alpha_1(i))^{\beta}; & \alpha_1(i) \le t \le \alpha_2(i), \\ \frac{1}{\beta!}\left[\left(t-\alpha_1(i)\right)^{\beta} - (t-\alpha_2(i))^{\beta}\right]; & \alpha_2(i) \le t \le \alpha_3(i), \\ \frac{1}{\beta!}\left[\left(t-\alpha_1(i)\right)^{\beta} - \left(t-\alpha_2(i)\right)^{\beta} - \left(t-\alpha_3(i)\right)^{\beta}\right]; & \alpha_3(i) \le t \le \alpha_4(i), \\ \frac{1}{\beta!}\left[\left(t-\alpha_1(i)\right)^{\beta} - \left(t-\alpha_2(i)\right)^{\beta} - \left(t-\alpha_3(i)\right)^{\beta} + \left(t-\alpha_4(i)\right)^{\beta}\right]; \alpha_4(i) \le t \le 1. \end{cases} \tag{1.38}$$

Figure 1.4 illustrates their corresponding first integrals.

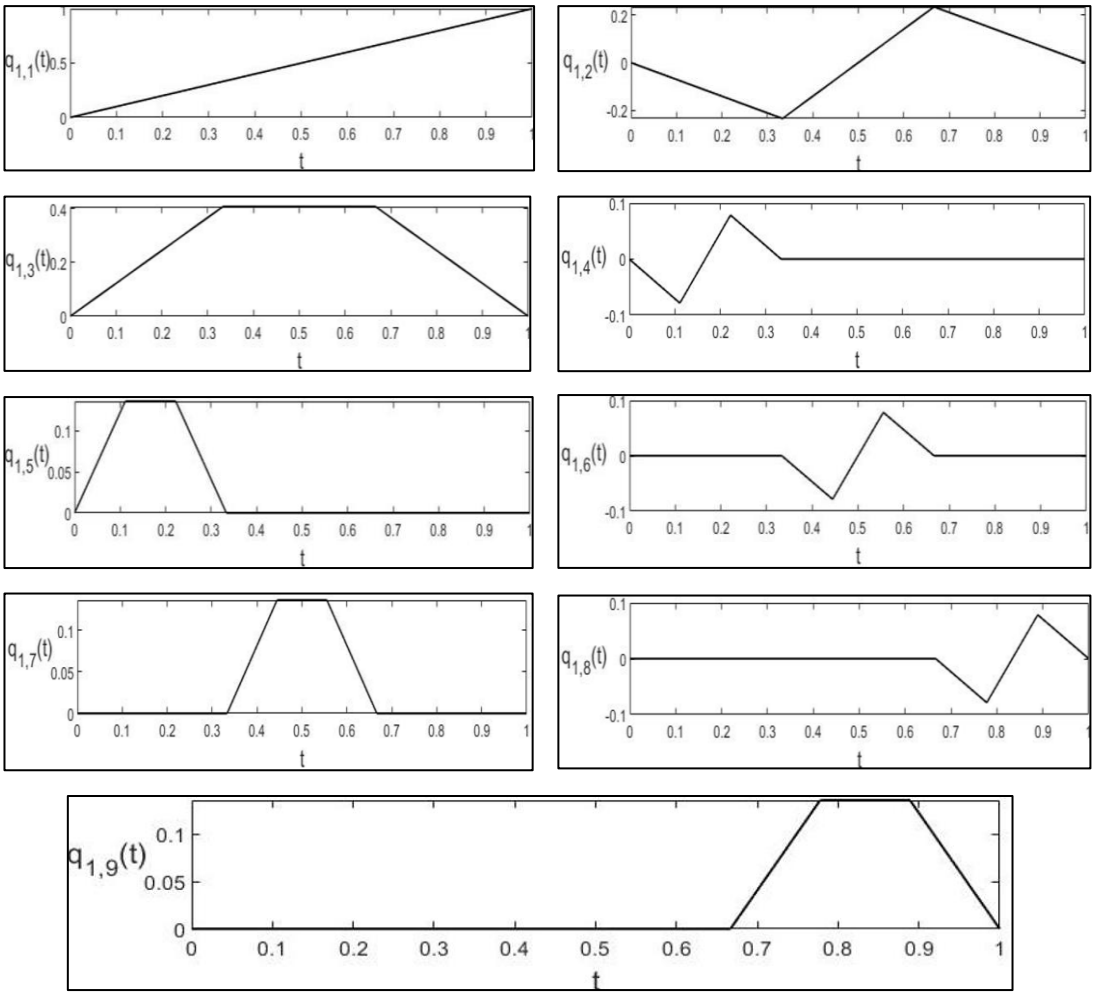

Figure 1.4: Integrals of first nine members of Scale 3 Haar Wavelet family.

1.6 Collocation Technique

The Haar wavelet collocation technique has been extensively examined in order to get a better understanding of physical occurrences described by functional equations. The collocation technique, which is a type of weighted residual technique, is an effective discretization strategy for solving functional equations. The initial proposal for it was made by “Kantorovich in 1934”. After 3 years, “Frazer R. A.” and others suggested it in 1937, with the same objectives in mind. A “weighted truncated series expansion of the basis functions” is implemented in the collocation technique to find the solution at various “points of the domain” also termed as “collocation points”. The “weight functions” are employed to assure a close satisfaction of the differential equation through the “truncated series expansion of basis functions”. Hence, an effective “approximate solution” to the functional equations with minimal residual requires

appropriate values for the weight functions. In our thesis work, the fundamental concept underlying the application of the "collocation method" is to identify the optimal weight that ensures the "residual becomes zero at the collocation points". Within this technique, the weight function serves as the Haar wavelet coefficient that will be calculated during the Haar wavelet collocation technique, and the "unknown function" is estimated by a "truncated series of Haar wavelet basis functions". The following is a brief explanation of the Haar wavelet collocation technique.

Consider a one-dimensional differential equation,

$$\mathbb{L}\xi(s) = \varphi(s); \forall\, s \,\epsilon\, [a, b], \tag{1.39}$$

Subject to the boundary constraints

$$\xi(a) = \alpha_1\,; \xi(b) = \alpha_2. \tag{1.40}$$

Here, φ represents a continuous real-valued function of s over the interval $[a, b]$, while $\mathbb{L}$ denotes the linear differential operator, which could have either constant or variable coefficients. By considering a set of Haar wavelet family $\{h_i\}_i$ and using the fact that Haar wavelets form a complete orthonormal basis in $l_2([a, b])$, ∃ some finite set Δ s.t.,

$$l_2([a, b]) = span\{h_i; i\, \epsilon\Delta\}. \tag{1.41}$$

Let H be any subspace of $l_2([a, b])$ where we want to "express the solution to the desired problem". Thus, for each finite set Δ_1;

$$H = span\{h_i; i\, \epsilon\Delta\}. \tag{1.42}$$

The Haar wavelet family will now be used to make an approximation of the unknown functions,

$$\xi(s) = \sum_{i=1}^{n} a_i h_i(s)\,; \forall\, s \,\epsilon\, [a, b], \tag{1.43}$$

where $a_i's$ represent the "wavelet coefficients" that have to be calculated in the process. Hence, by applying $\mathbb{L}$ into the previous equation, we find

$$\mathbb{L}\xi(s) = \sum_{i=1}^{n} a_i \mathbb{L}h_i(s)\,; \forall\, s \,\epsilon\, [a, b]. \tag{1.44}$$

The differential operator $\mathbb{L}$ will incorporate "boundary conditions". Upon utilizing equation (1.43) and incorporating the boundary conditions, equation (1.44) transforms into

$$\sum_{i=1}^{n} a_i \mathbb{L}h_i(s) = \varphi(s);\ \ \forall\, s \,\epsilon\, [a, b], \tag{1.45}$$

The preceding equation will need to be discretized using the "n" collocation points $\{s_i\}_{i=1}^{n}$.

While choosing the collocation points, one must use extreme caution in order to prevent the development of algebraic equations that are singular in nature. The composition of Haar wavelets is discontinuous. As a result, the following method is implemented to avoid having the collocation point coincide with the discontinuity point. Initially, a formula is used to determine where on the curve or surface the grid points will be placed, which is given as;

$$\overline{s_l} = \frac{l}{n};\ \ l = 0, 1, 2, 3, \ldots n; n = 2^j \ or\ 3^j, j = 0, 1, 2, \ldots \tag{1.46}$$

After that, the following equation is utilized to ascertain the "collocation points".

$$s_l = \frac{\overline{s_{l-1}} + \overline{s_l}}{2} = \frac{l}{n};\ \ l = 0, 1, 2, 3, \ldots n. \tag{1.47}$$

Now, Eq. (1.45) becomes as

$$\sum_{i=1}^{n} a_i \mathbb{L}h_i(s_l) = \varphi(s_l);\quad l = 0, 1, 2, 3, \ldots n. \tag{1.48}$$

This set of "n" equations can be readily transformed into the matrix form.

$$\begin{bmatrix} \mathbb{L}h_1(s_1) & \mathbb{L}h_2(s_1) & \ldots. & \mathbb{L}h_{n-1}(s_1) & \mathbb{L}h_n(s_1) \\ \mathbb{L}h_1(s_2) & \mathbb{L}h_2(s_2) & \ldots. & \mathbb{L}h_{n-1}(s_2) & \mathbb{L}h_n(s_2) \\ \mathbb{L}h_1(s_3) & \mathbb{L}h_2(s_3) & \ldots. & \mathbb{L}h_{n-1}(s_3) & \mathbb{L}h_n(s_3) \\ \vdots & \vdots & \ldots. & \vdots & \vdots \\ \vdots & \vdots & \ldots. & \vdots & \vdots \\ \mathbb{L}h_1(s_{n-2}) & \mathbb{L}h_2(s_{n-2}) & \ldots. & \mathbb{L}h_{n-1}(s_{n-2}) & \mathbb{L}h_n(s_{n-2}) \\ \mathbb{L}h_1(s_{n-1}) & \mathbb{L}h_2(s_{n-1}) & \ldots. & \mathbb{L}h_{n-1}(s_{n-1}) & \mathbb{L}h_n(s_{n-1}) \\ \mathbb{L}h_1(s_n) & \mathbb{L}h_2(s_n) & \ldots. & \mathbb{L}h_{n-1}(s_n) & \mathbb{L}h_n(s_n) \end{bmatrix} \begin{bmatrix} a_1 \\ a_2 \\ a_3 \\ \vdots \\ \vdots \\ a_{n-2} \\ a_{n-1} \\ a_n \end{bmatrix} = \begin{bmatrix} \varphi(s_1) \\ \varphi(s_2) \\ \varphi(s_3) \\ \vdots \\ \vdots \\ \varphi(s_{n-2}) \\ \varphi(s_{n-1}) \\ \varphi(s_n) \end{bmatrix}$$

By resolving the aforementioned set of equations, the "wavelet coefficients $a_i's$" can be computed with relatively little effort. By putting the wavelet coefficients "$a_i's$" in the Eq. (1.43) yields a uniquely represented "approximation solution" of the equation in "solution space H" as

$$\xi(s) = \sum_{i=1}^{n} a_i h_i(s)\,; \forall\, s \,\epsilon\, [a, b]. \tag{1.49}$$

1.7 The Quasilinearization Approach

In 1965, Bellman [23] and Kalaba [24] first proposed the idea of the Quasilinearization approach for solving nonlinear functional equations. In the Quasilinearization approach, the "nonlinear functional equation" is solved recursively via a sequence of "linear equations" rather than being solved explicitly. The main benefit of this method is that if it converges, it exhibits quadratic convergence toward the solution of the parent functional equation. The Quasilinearization approach is basically the generalization of Newton-Raphson method. The key motivation for using this approach is that numerous non-linear functional equations cannot be solved analytically, irrespective of the fact that solving these equations is a requirement of the problem. In this work, the Quasilinearization technique is used with "Scale 3 Haar wavelets" for approximating the solution of a variety of functional equations. To understand the procedure and working rule of the Quasilinearization technique, consider a nonlinear ordinary differential equation of second order,

$$\xi''(s) = \varphi(\xi(s), s) \;\; \forall\, s \,\epsilon\, [a, b], \tag{1.50}$$

having the boundary conditions

$$\xi(a) = \alpha_1 \,\&\, \xi(b) = \alpha_2, \tag{1.51}$$

where $\varphi(\xi(s), s)$ is nonlinear in s and ξ. Now, consider an initial approximation for $\xi(s)$ as $\xi_0(s) = \xi(a) = \alpha_1$, then by using the Taylor expansion (up to first two terms) of $\varphi(\xi(s), s)$ about $\xi_0(s)$.

$$\varphi(\xi(s), s) \approx \varphi(\xi_0(s), s) + \big(\xi(s) - \xi_0(s)\big)\varphi_\xi(\xi_0(s), s), \tag{1.52}$$

By using equation (1.52) in equation (1.50),

$$\xi''(s) \approx \varphi(\xi_0(s), s) + \big(\xi(s) - \xi_0(s)\big)\varphi_\xi(\xi_0(s), s), \tag{1.53}$$

Solving the equation (1.53) for $\xi(s)$, the next approximation $\xi_1(s)$ would be obtained. By applying the Taylor expansion on $\varphi(\xi(s), s)$ about $\xi_1(s)$ as explained

$$\begin{aligned} \varphi(\xi(s), s) &\approx \varphi(\xi_1(s), s) + \big(\xi(s) - \xi_1(s)\big)\varphi_\xi(\xi_1(s), s), \\ \xi''(s) &\approx \varphi(\xi_1(s), s) + \big(\xi(s) - \xi_1(s)\big)\varphi_\xi(\xi_1(s), s). \end{aligned} \tag{1.54}$$

Solving the equation (1.54) for $\xi(s)$, next approximation $\xi_2(s)$ would be obtained. In order to obtain the desired efficiency, Continuing the preceding technique and employing the following "recurrence relation" as a generalisation of the above technique,

$${\xi''}_{m+1}(s) \approx \varphi(\xi_m(s), s) + \big(\xi_{m+1}(s) - \xi_m(s)\big)\varphi_\xi(\xi_m(s), s), \tag{1.55}$$

having boundary conditions

$$\xi_m(a) = \alpha_1 \; and \; \xi_m(b) = \alpha_2. \tag{1.56}$$

Again, considering a differential equation (non-linear) of the form

$$\xi''(s) = \varphi(\xi'(s), \xi(s), s) \;\; \forall \, s \in [a, b], \tag{1.57}$$

where $\varphi(\xi'(s), \xi(s), s)$ is nonlinear in s, ξ, and ξ'. Repeating the preceding technique, we have attained a recurrence relation of the form

$$\begin{aligned} {\xi''}_{m+1}(s) \approx \; & \varphi\big({\xi'}_m(s), \xi_m(s), s\big) \\ & + \big(\xi_{m+1}(s) - \xi_m(s)\big)\varphi_\xi\big({\xi'}_m(s), \xi_m(s), s\big) \\ & \big({\xi'}_{m+1}(s) - {\xi'}_m(s)\big)\, {\varphi'}_\xi\big({\xi'}_m(s), \xi_m(s), s\big). \end{aligned} \tag{1.58}$$

The Quasilinearization technique is generalised for "higher-order non-linear functional equation". The obtained "recurrence relation" is given as follows

$$\begin{aligned} \mathbb{L}^n \, \xi_{m+1}(s) \approx \; & \varphi\big({\xi^{n-1}}_m(s), {\xi^{n-2}}_m(s), {\xi^{n-3}}_m(s), \dots, {\xi'}_m(s), \xi_m(s), s\big) \\ & + \sum_{j=0}^{n-1} ({\xi^j}_{m+1}(s) \\ & - {\xi^j}_m(s))\, {\varphi^j}_\xi\big({\xi^{n-1}}_m(s), {\xi^{n-2}}_m(s), \dots, {\xi'}_m(s), \xi_m(s), s\big). \end{aligned} \tag{1.59}$$

Here φ is the nonlinear function in ${\xi^{n-1}}_m(s)$, ${\xi^{n-2}}_m(s)$, ${\xi^{n-3}}_m(s)$, …, ${\xi'}_m(s)$, $\xi_m(s)$, and s. $\mathbb{L}^n$ is nth order, linear differential operator. In order to calculate $\xi_{m+1}(s)$, the value of $\xi_m(s)$ is already known at each step. The Quasilinearization algorithm commences with an initial approximation $\xi_0(s)$ and proceeds to generate a sequence of

convergent functions, ultimately leading to the “solution of the nonlinear functional equation”.

1.8 Review of Literature

The wavelets were introduced for the first time in the work of Alfred Haar (11 October, 1885-16 March 1993), a Hungarian mathematician in 1909 [25]. The “Haar wavelet” is a function that is constant within specific intervals and changes abruptly at the boundaries of these intervals whose primary characteristic is its compact wavelet support. Due to the fact that it is not continuously differentiable, it was not explored extensively during that period. In the 1980s, S. Mallat [26] with Y. Meyer [27] contributed to the field of wavelet analysis by introducing multiresolution analysis. This provided field with the greatest potential for development. The notable benefit of multiresolution analysis was that it empowered other mathematicians to “mathematically construct their own family of wavelets”. Y. Meyer utilized findings from multiresolution analysis to develop his wavelets, which possessed continuous differentiability but lacked compact support. A few years later, Ingrid Daubechies drew inspiration from the work of Mallat and Meyer [28], [29] and introduced “a new set of wavelet bases” that was both “orthonormal and possessed compact support”. These wavelets served as the cornerstone for various applications of wavelet analysis. Since its inception, the study of wavelets has been viewed as purely intellectual. However, extensive research into the field has resulted in the creation of a powerful scientific mathematical technique with broad useful applications. In the Daubechies family of wavelets, wavelets were typically categorized based on the number of vanishing moments they exhibited. By imposing the requirement of vanishing moments, a system of simultaneous algebraic equations, both linear and nonlinear, was derived for the coefficients. Statistical results for coefficients were acquired by resolving the corresponding equations. This method has addressed the requirement of researchers for a clear explanation of wavelet construction and is now widely used. As a consequence, various wavelet-based families such as Symlet wavelets, Coiflet wavelets, etc., were developed. The continuity, differentiability, and compactness criteria were achieved by all these wavelets. They found widespread use in fields like signal processing and image processing, along with significant applications in areas of numerical analysis. A major

drawback among these wavelets seemed to be that they lacked an “explicit form of expression” and hence could not be employed conveniently for “discretization” despite of being their attractive characteristics. It was essential to produce the wavelets with the aid of filter coefficients. Hence, it was difficult to do analytical differentiation and integration upon those wavelets. Because of this, the process became incredibly difficult whenever the integration of a set of “nonlinear functions” were needed in an application. Then, a novel idea called “connection coefficients” was established to discover the procedure for finding different types of integrals. However, finding out these “connection coefficients” was a very tiring process that had to be done for every integral individually. Aside from that, the approach could only be used for a few basic kinds of nonlinearities in the equations. Now, several pessimistic predictions have been made because getting the solutions by using wavelets was so hard. When it came to addressing mathematical problems, numerous researchers believed that the wavelet technique gave no advantages when compared to more conventional techniques. Strang and Nguyen penned “***The competition with other methods is severe. We do not necessarily predict that wavelets will win***”. It offered a great boost to explore alternative possibilities to break out of this impasse. Once again, mathematicians began contemplating the entire range of wavelet families that had been developed up to that point. Chen and Hsiao [30] addressed the drawback of the Haar wavelet in 1997, which lacked differentiability at points of discontinuity. Despite “approximating the solution function” using the “Haar wavelet series” they utilized the “Haar wavelet series” to approximate “the highest order derivative present in the problem”. Integrating the highest order derivative resulted in the production of all other derivatives as well as the solution function itself. The integration matrices for the Haar wavelet functions were introduced for solving the lumped and distributed parameters. The proposed method was fast and accurate and in comparison to the Fourier method the proposed method was computer oriented and was suitable for analyzing those systems that involve abruptly varying functions. This method has been demonstrated to be quite reliable and researchers are currently employing it in the process of solving mathematical models that are governed by various functional equations. Ülo Lepik [31] extended the work of Chen and Hsiao [30] in 2001, by analyzing the linear vibration of a system with one or two degrees of freedom by applying wavelet transformations. Using the three distinct

wavelet transformations, he discovered that the obtained results were qualitatively similar for vibrations with a single degree of freedom but different for vibrations with two degrees of freedom, where the Haar wavelets and Mexican hat shows different results than the Morlet wavelet. Lepik and Tamme in 2004, [32] studied the performance of solutions for linear IEs by using Haar wavelet. Integral equations of various types were examined, including Volterra and Fredholm equations, integro-differential equations, and several others. The convergence rate was determined to be $O(M^{-2})$ for the Volterra and Fredholm equations, and the solution achieved by utilizing Haar wavelets seems to be more successful than standard methods with the same step size. In 2005, Maleknejad and Mirzaee [33] used "Rationalized Haar functions" for obtaining the solution of Fredholm 2nd kind of IEs, and the result obtained by using Rationalized Haar wavelets had a high degree of accuracy. In 2005, U. Lepik [34] devised a new approach that relies on the Haar wavelet to contrast the "Chen and Hsiao method (CHM) with the segmentation and approximation technique using piecewise constant approximation method" for solving a variety of differential equations. He determined that the wavelet matrices "H" as well as the matrices of their integrals have become increasingly sparse, making the process highly efficient, and hence technically very simple, in the work of Chen and Hsiao. However, the instability becomes a hindrance while attempting to approximate higher-order derivatives. In 2006, Lepik [35] developed an algorithm to tackle integral equations. The proposed numerical method was suitable for solving Volterra IEs and IDEs. The algorithm also works for boundary value problems in ordinary differential equations. He obtained that the solutions exhibited high accuracy even with a limited no. of "collocation points" and error decreases rapidly with the increasing number of collocation points. He further noticed that if the collocation points were doubled, the error decreased four times. In 2006, Ordokhani [36] introduced a method for finding the solution of mixed "Volterra Fredholm Hammerstein IEs" by using "Rationalized Haar wavelets". The operational matrices involved in the proposed method contain many zeroes and due to this feature, Haar transforms faster than Walsh and block-pulse functions. The proposed algorithm was computationally attractive and less time-consuming. U. Lepik [37] employed the Haar wavelet methodology in 2007, to tackle the "evolution equation" having nonlinearity. When applied to the Sine Gordon and Burger equations, the technique

proved to be competitive with other classical techniques. The computation complexity and efficiency of the procedure both were determined to be extremely reasonable. The boundary condition is handled automatically during the solution process, making this method appropriate for the boundary value problems. In 2007, Lepik and Tamme [38] formulated a numerical technique for solving nonlinear Fredholm IEs using Haar wavelet. The key advantages of the method were sparse representation, fast transformation as well as the ability to implementation of the fast algorithm. Due to these advantages, the algorithm was highly accurate even for the smaller number of calculation points and error decreases rapidly with the increasing number of collocation points. The error functions were reduced by nearly four times when the number of collocation points was doubled. In 2007, Babolian and Shahsavaran [39] introduced an algorithm for solving the nonlinear IEs (Volterra IEs and Fredholm IEs) of 2^{nd} kind. The technique was based on "Haar wavelets" and problems were solved by using the "collocation technique". To solve Volterra IEs he applied the features of Block Pulse functions. If the nonlinear term involved in the equation was non-exponential the results obtained were more accurate in comparison to exponential functions. In 2007, U. Lepik [40] presented a brief review of the application of the Haar wavelet transform, in which he covered a variety of differential equations and integral equations. In 2007, Reihani and Abadi [41] resolved the 2^{nd} kind of IEs using the double rationalized Haar functions, associated integration and product matrices, and Newton-Cotes nodes. Because of the large number of zeros in rationalized Haar matrices and operational matrices of integration, the Haar transform appears numerically more interesting than other square functions like the Walsh and block-pulse functions. The effectiveness of this approach is illustrated by examples that achieve the desired outcomes. In 2008, Chang and Piau [42] constructed basic operational Matrices of Haar Wavelets to resolve the differential equations. He then successfully carried out all of the computations using the matrix representation of wavelet transform along with their integrals, which made the process easier. U. Lepik [43] created an innovative approach of non-uniform Haar wavelets in 2008 to resolve differential and integral equations. Furthermore, he demonstrated that the utilization of the "Haar wavelet method" with a "non-uniform mesh" applies to problems where there are sudden or rapid alterations in the solution. Babolian and Shahsavaran [44] in 2009, handled the "non-linearity" in their technique

to determine the solution of nonlinear Fredholm IEs and established the convergence of the Haar wavelets technique through error analysis, an extremely significant problem at the time. In 2009, Lepik [45] presented a "computational technique" for finding the approximate numerical solutions of fractional Fredholm IEs and fractional Volterra IEs. In his study, he used the Caputo derivative for fractional derivatives. He solved some nonfractional equations by the proposed method. The method was also applicable for solving first kind linear IEs as well as weakly singular IEs and IDEs. The key features of the proposed method were its small computational cost and its simplicity. In 2010, Hariharan and Kannan [46] developed a wavelet-based approach. The primary goal of this research was to use the Haar wavelet approach on a set of widely used complex parabolic equations in various scientific fields. The effectiveness of the "Haar wavelet approach" for solving nonlinear functional equations was also demonstrated. The author claims that other non-linear parabolic equations can also be resolved using the same technique. The presented scheme appears to be easily extended, with some modifications to solve the system of equations involving other physical, chemical, or biological processes, like diffusion, nonlinear convection, reaction, and dispersion reaction. In 2010, Siraj-ul-Islam, Aziz, and Haqq [47] discussed the comparative study of Haar wavelet and hybrid functions. He presented a numerical technique based on hybrid functions and uniform Haar wavelet for finding the approximate solution of definite integrals. In his study, he applied the wavelet-based algorithm to single integrals, double integrals, triple integrals as well as improper integrals and the results obtained in his work were more accurate and showed the efficiency of the proposed work. In 2010, G. Hariharan [48] used the Haar wavelets technique to address a "physical model" involving "deflection in a beam having a finite length" driven via a fourth-order differential equation with the corresponding boundary and initial constraints. The technique used to solve this model involved developing a generalised operation matrix and the matrices of their integral, and the findings compared to the precise solution that was reported in past studies. The results demonstrated that the Haar wavelet method uses less CPU time and provides better outcomes with smaller degrees of freedom than the alternative methods. In 2010, Siraj-ul-Islam and his co-workers [49] designed a numerical technique by using a uniform Haar wavelet to solve a large class of boundary value problems. A majority of the difficulties associated with

Neumann's boundary conditions in numerical techniques were handled automatically. One significant benefit of the Haar wavelet-based approach was its ease of use and generalizability across a wide range of boundary conditions. To ensure the method's wide application and reliability, a convergence analysis was provided. In 2011, Fazal-i-Haq and his co-workers [50] used a uniform Haar wavelet for the approximation of nonlinear BVP having 3rd order. Unlike other approaches, the method provided there required no conversion from BVPs to IVPs or vice versa to obtain approximate solutions. The Haar wavelets efficacy was evaluated by comparing it with well-known methods like the finite difference method, spline-based methods, etc. A higher Haar wavelet level provides more precise solutions. The simplicity and effectiveness of the approach were its primary benefits. As a means of verifying the efficacy of the suggested strategy, a convergence analysis was provided in addition to a numerical approach for generating multi-point BVPs and IVPs. In 2011, Fazal-i-Haq [51] extended their work for resolving 4th order BVPs via Haar wavelets. Parameterized BVPs and BVPs associated with two-dimensional channels with porous walls were taken into consideration. In 2011, Babolian, Bazm, and lima [52] approximated the solution of 2-D IEs using rationalized Haar (RH) functions. The author used the bivariate collocation approach in combination with "Newton-Cotes nodes" that transformed the problem into a set of "algebraic equations". Several test problems were given to illustrate the effectiveness and precision of the suggested method. Two key benefits of the approach under consideration seem to be (1) the ease through which integrals can be computed and (2) even though the associated matrices may have computational complexity, they typically have many zero entries. This helps to keep the computational effort within attainable limits. He applied the algorithm to some test problems and the results obtained show that the rate of convergence was O (m^{-2}). In 2011, Hashemiparast, Sabzevari, and Fallahgoul [53] introduced a new method called rationalized Haar s-functions for approximating the solution of "linear and non-linear" Volterra IEs of the second kind. This new technique was the refinement of the rationalized Haar function. Calculations involved in the method were simpler because IEs involved in the method were converted to a system of equations that contains an identity matrix. In 2011, Saeedi et.al, [54] solved fractional integration by applying Haar wavelet operational matrix. In the proposed method, fractional IEs with weakly

singular kernels were reduced to a system of algebraic equations. The proposed method was applied to different examples and the obtained findings were reasonable. In 2011, Shahsavaran [55] applied the Haar wavelet based numerical method on the properties of "block pulse functions" for calculating the approximate solution of Volterra IEs of 2nd kind having "weakly singular kernels". The findings revealed that the proposed method was simple and requires less computation. In 2011, Ü Lepik [56] employed two-dimensional Haar wavelets to successfully resolve problems with partial differential equations. In 2012, Ülo Lepik [57] used the "Haar wavelet" technique on the "physical model of elastic beam buckling" and developed an approach for a wide variety of buckling situations, including cracking simulation, beams with a flexible cross-section, beam vibrations on an elastic foundation, and so on. Using Haar wavelets, the author demonstrated their several benefits, including: "good accuracy for a limited no. of nodal points, use of common programming for resolving the many problems, handling of singularities in intermediate boundary constraints, simplicity for implementation". By using a variety of examples, the author also demonstrated that the technique is extendable to problems with a higher degree of complexity. In 2012, V. Mishra et al., [58] introduced an algorithm based on "Haar wavelet". The algorithm was presented to decrease the complexity in the formulation of the operational matrices based on wavelets. Calculating the derivatives of the Haar wavelet operational matrices is quite useful. He applied the collocation technique along with Haar wavelet for approximating the solution of differential equations, IEs, as well as IDEs. The proposed algorithm provides better results in comparison to the Wavelet-Galerkin method which was computationally complicated. The author applied the algorithm to different test problems and results show that relatively better solutions were obtained for small values of resolution and for higher values of resolution better solutions were expected. In 2012, Berwal et. al., [59] described the Haar wavelet method as a solution to the Wave-like equation. An evaluation is conducted, comparing the precise solution to the wave-like equation with its approximate solution which was obtained using MATLAB. The precision of the Haar wavelet solution was demonstrated through this computation. The presented approach was not only easy to apply, but it also provides an implicit form for approximating solutions. The author further claims that the BVPs are also easily solved using this technique. Hence, the proposed approach was highly reliable, easy to

implement, efficient to execute, cheap to compute, and versatile. In 2012, Ziari et al., [60] created an innovative technique for solving 2nd order linear fuzzy Fredholm IEs using fuzzy Haar wavelet (FFIE-2). The estimated level of error for the proposed technique was also provided. In conclusion, illustrative numerical examples were provided to determine the precision and effectiveness of the suggested method. In 2012, Dehghan and Birgani [61] solved linear Volterra and Fredholm IEs by applying a new version of the Haar wavelet called the M-Haar wavelet. This new method was based on the collocation technique. In his study, he applied the new hybrid method to some numerical examples found from the existing literature for which the exact solutions were known and he obtained error estimates corresponding to both methods Haar wavelet as well as M- Haar wavelets and by using error functions accuracy was estimated. He proved that the results obtained by using the M-Haar wavelet were more accurate than the Haar wavelet. In 2013, Aziz and Siraj-ul-Islam [62] presented two different computational techniques for finding the solution of "Volterra IEs of the second kind and Fredholm IEs of the second kind". In his work, he derived formulae for the computation of the Haar coefficient without solving any system of equations and applied the formulae in the presented numerical technique. Compared to other methods he claimed that for the computation of integrals involved this method did not require any intermediate numerical technique. In 2013, Harpreet Kaur and co-workers [63] solved the complex "Blasius equation" across uniform collocation points by utilizing a quasi-linearization method in combination with the Haar wavelet. The "Blasius equation" is a very significant part of "fluid mechanics", and researchers have been looking for a solution that has a lot of potential. The author indicates that using "the Quasi-linearization technique" in combination with "the Haar wavelet approach" does not demand any iteration on the chosen "collocation points" and hence provides the Quasilinearization approach of treating with nonlinearity incredibly simple and clear. In 2013, N. Berwal and D. Panchal [64] demonstrated that the "Haar wavelet method" is effective by implementing it to solve the LCR equations. A "Haar wavelet" technique for "fractional Klein-Gordon equations" was created by Hariharan [65] in 2013. The author constructed the "wavelet operational matrices" as well as the "operational matrices comprising fractional integrals". In implementing these operational matrices to Klein-Gordon equations having fractional order, a set of

systems of equations has been produced. Then, the set of equations is converted into a "matrix system" and then solved to obtain the "coefficients of the Haar wavelet". The authors claim that their method is superior to existing approaches because it is simple, efficient, and can be easily adapted to a wide range of differential and integral equations. And unlike Daubechies wavelets, they do not have to endure the effort of figuring out the correction coefficients. In 2013, Kaur, Mittal, and Mishra [66] solved the nonlinear Volterra integral population model by using Haar wavelets which were based on operational matrices. Based upon the collocation technique and Quasilinearization method the proposed scheme was established. The author applied the algorithm to some test problems and found that the results obtained were excellent by applying the Haar wavelet collocation technique with the Quasilinearization method. In 2013, Saeedi [67] solved the nonlinear Fractional IDEs having fractional order by a unique approach based on the Haar wavelet and the advantages of block pulse functions. By using Haar wavelet along with block pulse functions he derived operational matrices and with this, he used "the operational matrix of fractional integration" for converting the nonlinear Fredholm IDEs to a set of "algebraic equations". The presented algorithm did not require any integration and because of this computational burden became less. In 2013, Siraj-ul-Islam et al., [68] extended the numerical method which was proposed earlier in their study to approximate the solution of Volterra and Fredholm IDEs of 2^{nd} kind. In the present work, the author proposed two numerical methods for finding the solutions of nonlinear Volterra and Fredholm IDEs. In his study, the author replaced Newton's method with Brayden's method for finding solutions to nonlinear IEs. The key feature of the proposed work was that it didn't require any numerical integration. By applying Haar wavelet approximation the integrand was approximated and after that exact solution was performed. He tested the numerical method on many test problems and found that the results obtained were more accurate only for a few nodal points. In 2013, Fayyaz and Azram [69] extended the "use of Haar wavelets" to solve the 3^{rd} order nonlinear IDEs. For approximating the kernel involved in integro-differential equations, he used a 2-dimensional Haar wavelet basis. The presented algorithm was tested on four different test problems, it provides better results with high accuracy. In 2014, Aziz, Siraj-ul-Islam, and Khan [70] solved the 2-Dimensional nonlinear First and Second kinds of Volterra IEs, Fredholm IEs as well as

Volterra-Fredholm IEs. This algorithm was the extension of the earlier work, in which the author solved the one-dimensional IEs. The key feature of the proposed work was that it didn't require computation of numerical integration and due to this, the results obtained were very accurate. The algorithm was applied to several test problems existing in the literature and the results obtained were compared with some of the existing methods. In 2014, Siraj-ul-Islam, Aziz, and Al-Fahad [71] presented a novel technique for approximating the solutions of IEs and IDEs of first as well as higher order. The proposed algorithm was a modification of the earlier work. The author claims that the new approach was much better than the existing technique because of its high accuracy and efficiency and the algorithm would be applicable for any type of nonlinear Volterra and Fredholm IEs and IDEs having initial and boundary conditions. In 2014, Saeed and Rehman [72] used the Haar wavelet-Quasilinearization method for estimating a solution to the Heat Convection-Radiation equations. The author initially used the Quasilinearization method to linearize the nonlinear heat transport equation. Upon incorporating the nodal points in the resulting algebraic equations, the resulting system can be solved by estimating the "dependent variable" as well as "their derivatives" through the "truncated series of Haar wavelet" resulting yields to a matrix system. The proposed approach is employed to examine the thermal performance in a lumped system composed of a slab constructed of a media with varying heat capacity, as well as the cooling profile of a lumper system. According to the author's promises in the manuscript, Haar wavelet-Quasilinearization yields excellent results compared to other techniques and approximately coincides with the true solution. In 2014, Arora, Brar, and Kumar [73] applied the methods of Haar Wavelet Matrices to obtain numerical results for differential equations. In 2014, Mittal et al., [74] devised a "Haar wavelet-based approach" to study processes driven by the nonlinear coupled Burgers' equation. The set of nonlinear coupled Burger PDE was converted into a new system of ODE using the Haar wavelets and Collocation approach. The resulting ODE is resolved using the Runge Kutta method. The stability of the system has been additionally provided by the author. The author claims that the approach gives quite satisfactory results when applied to test problems and could be generalized to solve additional "higher-order differential systems of the equation". In 2014, Shiralashetti et al., [75] presented a novel Haar wavelet collocation algorithm to solve nonlinear IEs

and IDEs numerically. With the use of illustrative numerical problems, the strategy was strongly shown to be effective. The presented approach performed well and was simple to implement. An error evaluation was conducted and the results demonstrate that with increasing resolution, the approximation solution improves in precision. In 2014, Hassan and Alaidarous [76] modified the "Haar wavelet" algorithm for the approximation of a system of IEs. In 2014, Santanu Saha Ray [77] explored two of the most effective methods for solving problems with fractional differential equations. He analysed Fractional Fisher-type equations and compared the findings obtained using the Haar wavelet approach and the Optimal Homotopy Asymptotic technique. The author asserted that any approach may be utilized successfully and confidently when solving equations of this type. For a fixed set of grid points, the obtained results using the optimum "Homotopy Asymptotic technique" were preferable to those obtained using "the Haar wavelet method". Yet, increasing the no. of nodal points in the Haar wavelet approach improves its precision. Kumar and pandit [78] in 2015, resolved the "Fokker Planck equations" that explain the motion of particles by implementing a technique that was based on the Haar wavelet approach. The equation involved all variables as well as constant coefficients. In 2015, Erfanian, Gachpazan, and Beiglo [79] presented an algorithm based on a rationalized Haar wavelet along with a matrix operator. He used "the Banach Fixed Point theorem" for the convergence of the proposed work. To calculate the wavelet coefficient this technique did not require the computation of a linear system; due to this advantage, the method was very efficient compared to the conventional Haar wavelet methods. In 2015, Shiralashetti and Deshi [80] tackled multi-term differential equations having nonintegral order using the collocation approach with Haar wavelet bases. Further, they discovered that HWCM has the following characteristics: "quite efficient, easy to implement, and capable of approximating the solution efficiently when compared to alternative methods". In 2015 Oruç and his co-workers [81] established a novel "hybrid method" for investigating the solution of the improved "Burger's equation". Non-linearities within the equation were treated with a Quasilinearization technique, while the temporal component was discretized and addressed via finite differencing. The author claims the devised method is entirely consistent, rapid, and computationally cost-effective, based on testing it on three experimental problems. In 2015, Fallahpour, Khodabin, and

Maleknejad [82] solved the 2-dimensional Stochastic Volterra IEs by using " the Haar wavelet" approximation. In this work, the author approximated the kernel function involved in the IEs by applying the Haar wavelet hence this method was fundamentally different from the existing method in the literature and the results obtained were very accurate. The application of the Haar wavelet method was expanded by S.C. Shiralashetti et al. [83] in 2015 for the examination of models that are driven by singular differential equations. In comparison to other approaches like the "Variational Iteration Method (VIM) and Adomian decomposition Method (ADM)," the authors demonstrate that HWCM is an effective numerical technique for solving "singular differential equations". In 2016, Shiralashetti, Kantli, and Deshi [84] established a Haar wavelet-based collocation technique with the aim to handle differential equations having nonlinearity in them. They were being developed mostly in the discipline of hydrodynamics with varying constraints. By applying HWCM to a variety of hydrodynamic equations involving varying boundary conditions, the author concluded that it provided a solid ground for its application in addressing problems of this type due to its simplicity and rapid convergence. Inderdeep Singh and Sheo Kumar [85] introduced an efficient Haar wavelet approach for numerically solving a set of first-kind nonlinear Volterra IEs in 2015. The method that was provided involved changing nonlinear Volterra IEs of the 1^{st} kind into linear Volterra IEs of the 2^{nd} kind. To determine the effectiveness and precision of the approach that was discussed, numerical examples were provided. Additionally, there has been a comparison to previous numerical approaches. The author concluded that the Haar wavelet method was superior in terms of precision, ease of use, and processing speed. In 2017, M. Erfanian and coworkers [86] invented a technique for solving IDEs of mixed "Volterra–Fredholm type" by employing rationalized "Haar wavelet bases". This allowed researchers to circumvent the requirement for numerical integration, which would otherwise have been required for such a technique. The author of the work asserts that the presented method was more efficient and saves time by omitting the intermediate step of transforming the IDEs into a difference equation. Najeeb Alam Khan et al., [87] in 2017, provided an approach for addressing the 4^{th} order Emden-Fowler equations having initial constraints using the Haar wavelet numerical technique (HWCM). "Differential equations" were converted into a set of "nonlinear or linear equations"

using the proposed technique. This led to the determination of the value of the Haar coefficients, which was followed by the acquisition of the solution throughout the entire domain [0, 1]. To evaluate the precision of the results, the nonlinear fourth-order test problems were analyzed at varying Haar levels. When compared to non-perturbative techniques that are reported in the literature, the presented method seems to be more interesting due to its simplicity and its ability to provide desirable results. Shah and Abass [88] in 2017, expanded the applicability of the "Haar wavelet" approach to include "singularly perturbed BVP" in one dimension. The authors applied Haar Wavelet series approximations to turn "singularly perturbed BVP" into a set of difference equations after which they employed the collocation method to get a set of linear equations. Authors performed experiments on five standard problems using the technique that was provided, and they concluded that the suggested technique is simple to apply on a computer, produces excellent performance when compared to other methods already in existence, and has the potential to be applied to more difficult and complex situations involving singularly perturbed equations. Two-dimensional Haar wavelets were used by Somayeh Arbabi et al. [89] to solve systems of "partial differential equations" in 2017. It was demonstrated that the approach converges and is stable. It was reported that the results generated by using the method on the numerical examples had a very excellent agreement with the actual solution. Imran Aziz et al. [90] developed a new technique in 2017 for solving elliptic three-dimensional partial differential equations having Dirichlet boundary constraints utilizing three-dimensional Haar wavelets. The author conducted extensive research and analysis on a large number of test problems to show the method's precision and wide range of applicability. In 2017, Inderdeep Singh and Sheo Kumar [91] applied 1D and 2D Haar wavelets to solve "Harry Dym (HD), BBMB, and higher-dimensional diffusion equations" and they compared their findings to those obtained using alternative approaches. The author concludes that the given method surpasses the others. Zakieh [92] expanded the use of the "2D Haar wavelet method" in 2017 to resolve the complex "age-structured population model" driven via a partial differential equation having boundary constraints as integral equations. To improve computational performance, the author of this work transformed the actual problem into an algebraic system. In 2017 Umer Saeed [93] employed the "Haar wavelet Quasilinearization method" to solve a set of functional

equations that are nonlinear and have fractional order. Furthermore, they compared their outcomes to those obtained using other methods, such as the Homotopy perturbation method and the variational iteration technique, and concluded that the proposed technique improves numerical precision in comparison with the previous two. In the same year, Prakash et al., [94] broadened the implementation of "Haar wavelets" for the resolution of a complex fractional differential equation-governed SEIR epidemic model. The model includes a dynamic population, making it difficult or impossible to solve analytically in some cases. The problem is becoming more and more challenging when the associated model is nonlinear and fractional. According to the author of this paper, the technique is performing exceptionally well in its attempt to solve the aforementioned biological models of a wide range of infectious diseases. In 2017, Ram Jiwari et al. [95] came up with a method to study the MHD Falkner-Skan flow across permeability. By applying a "Lie algebra of infinitesimal generators" the authors were capable of transforming a sequence of "2D partial differential problems" into a set of linear as well as nonlinear "ordinary differential problems" that are suitable to solve via the Haar wavelet Quasilinearization approach. S. C. Shiralashetti, et al. [96] employed an adaptive grid in 2017 by inserting grid points that seem to be the "midpoints of the nodal points" that were employed in the standard nodal pattern used mostly for Haar Wavelets. The parabolic type of PDEs was solved using the novel adaptive grid Haar wavelet methodology in conjunction with the collocation method, and the results demonstrate that the proposed technique yields higher precision compared to conventional HWCM and FDM. R. C. Mittal et al. [97] introduced a novel method in 2017, that makes use of "Haar scale 3 wavelets". The "Haar Scale 2 wavelets" were upgraded and hybridized in this version of the wavelets. Shock-wave sensitivity analysis for Burger's equations was performed using the new method. Time was discretized using a forward finite difference technique, whereas space was discretized using scale 3 wavelets for the derivatives, and non-linearities were dealt with by employing the Quasilinearization approach. Six examples were used to evaluate the suggested technique. The author asserted that the technique's performance was preferable to that of competing classical approaches and that it could be used across an extremely broad family of ODEs, PDEs, and integral equations. Foadian et al. [98] in 2017, reported that the set of equations generated by implementing Haar wavelets

together with the collocation approach and Quasilinearization on the nonlinear "coupled reaction-diffusion equations (RDEs)" is extremely sensitive to the "wavelets coefficients" as well as the matrices on the "opposite side of the equation". Using a "Tikhonov regularisation (TR) technique" they were able to establish a robust mathematical formulation for RDEs with appropriate boundary and initial constraints despite the system of linear equations being in ill condition. Moreover, the author asserted that the proposed methods outperform "the radial basis function (RBF) and finite difference method (FDM)" in terms of speed, stability, and accuracy. In 2017, Babaaghaie and Maleknejad [99] extended the use of the "Haar wavelet" with a collocation approach for resolving 2D IDEs of Volterra kind. The approximation was made to a "non-linear kernel" that is a function of "partial derivatives of arbitrary order". To generate a nonlinear system, the Haar wavelet was used to substitute the kernel approximation into the initial equation. To find a solution to the nonlinear system, the 2D Volterra IDEs were simplified into a more-simple equation involving partial derivatives. The basic equation was solved, and an approximate solution was determined. Shiralashetti et al. [100] in 2017, applied the "Haar wavelet collocation approach" for resolving the complex mixed "Volterra-Fredholm-Hammerstein IEs". The IEs provided in the manuscript were differentiated using the Standardized Leibnitz rule, transforming them into differential equations that could be solved by using the Haar wavelet technique. The outcomes were considered appropriate, with an error of the order 10^{-13}, after being examined for the exact solution. In 2017, Fathizadeh, Ezzati, and Maleknejad [101] provided a numerical technique for resolving the Abel integral equations and the fractional population growth model. This technique used the rational Haar wavelet as its basis. The author exploited characteristics of fractional calculus to solve singular integral equations by treating Abel integral equations as fractional integral equations. The Riemann-Liouville interpretation of fractional integration was offered. To approximate the numerical solution to the generalized Abel IEs, the matrix was employed. The presented strategy relied on the collocational approach. From the findings, the author asserts, the methodology may be a viable option for addressing the fractional IDEs. In 2018, Maarjus Kirs et al. [102] investigated functionally graded material beams by applying the differential quadrature method (DQM), finite difference method (FDM), and Haar wavelet method (HWM).

The effectiveness of each of the three approaches was considered before making the final choice. It was determined that HWM performed better than FDM, while the precision of DQM was found to be significantly higher than both HWM and FDM. As a result of its characteristics, HWM may also prove to be a more effective method for the examination of nanostructures. Randhir et al., [103] developed an effective computational approach to resolving the Lane-Emden equation having Neumann, Dirichlet, as well as Neumann Robin types of boundary constraints. The approach relies on the Haar wavelet. In the fields of applied mathematics and astrophysics, the "Lane-Emden type equation" has been utilized as a model for a variety of different phenomena. Comparisons were made between the analytical results obtained by the current approach including those generated through other techniques, including the VIM, the ADM [51], the TCM [33], and the true solution. The author states that the provided technique has tremendous advantages in addressing singular boundary value problems due to its ease of implementation and excellent accuracy. In 2018, Singh et al., [104] expanded the applicability of the "Haar wavelet Quasilinearization method" to address doubly singular problems with boundary conditions. The author claims that the suggested technique yields excellent performance to previous methods when applied to a wide range of physical systems regulated by the doubly singular difference equation. In the same year, Ahsan et al. [105] utilized two distinct "Haar wavelet collocation approaches" to address the issue of instabilities in inverse heat transfer. The author uses conversion to turn a "non-homogeneous PDE" into the "homogeneous form" during the 1st scheme (HWCM1), and the conventional "Haar wavelet collocation technique" in the 2nd scheme (HWCM2). HWCM1 was found to be more effective than HWCM2 in solving unsteady inverse heat problems. The author additionally asserted that HWCM1 applies to a broad range of nonlinear inverse PDEs. In 2018, Amit K. Verma and Diksha Tiwari [106] approximated the singular lane-Emden type equation via a coupling of Quasiliniearization and Haar wavelets (HWQA), The authors acknowledged that HWQA might efficiently preserve the solution incredibly close to the singularity. In 2018, J. Majak et al., [107] created an innovative higher order Haar wavelet technique that can be implemented to analyze differential and IDEs. As an application to FGM Structures, the technique was verified by testing its performance on a few differential

equations and IDEs. It was discovered that the new technique has a better degree of convergence and a lower order of inaccuracy, which means it can be employed with fewer modifications for a wide variety of functional equations. In 2018, Sirajul Haq et al. [108] employed Haar scale 2 wavelets to solve higher-dimensional Sobolev equations and BBMB equations. Where a finite differencing strategy was used to discretize the time component and a "2D Haar Wavelets collocation technique" was used to discretize the space component. The Sobolev and BBMB equations were used to evaluate the method, and the findings were compared to those obtained using a "modified weak Galerkin finite element approach". The author asserted that the current approach outperformed the "modified weak Galerkin finite element approach". In 2018, Mittal, et al., [109] devised a "Scale-3 Haar wavelet-based technique" for solving ordinary fractional dynamic systems. Several test problems were used to validate the method and compare it to Haar wavelets of scale 2. A faster convergence rate was seen with the "Scale-3 Haar wavelet-based technique" compared to the Scale-2 Haar wavelet-based technique. In 2019, M. Erfanian and A. Mansoori [110] employed Haar wavelet rationalized basis functions to handle 2^{nd} order Nonlinear IDEs. The convergence of the suggested method was also shown using the Banach theorem for fixed points. In addition, the author presented a continuous integral operator that may be applied to the Banach space. The demonstration of the approach's reliability and usefulness was provided by the resolution of a variety of examples. In 2019, Oruç et al., [111] improved the application of the finite difference approach and the 2D Haar wavelet to solve the "time-fractional reaction-sub diffusion problem". The current approach was validated by applying it to two distinct equations, after which it was compared with the alternating direction implicit method as well as the meshless-based method. The author concluded that the procedure is equally effective and simple to utilize. Ahsan et al. [112] in 2019, used the "Haar wavelet-finite technique" in conjunction with the Quasilinearization approach to study the "Schrodinger equation" and they found that the method accurately models the fundamentals of the phenomena described by the "Schrodinger equation". Extending it to the high dimension Schrodinger equation will incur significant computing expenses. But, to succeed in an irregular domain, you must possess certain supporting techniques. In 2019, the 2D Haar wavelet was adopted by Sidra Saleem et al. [113] to solve higher-dimensional parabolic

partial differential equations having nonlinearity. The Kronecker tensor product was then employed to determine the required coefficients after the differential model was transformed into a 4d array system. These coefficients contributed essentially to formulating the correct solution. After applying the method to five different problems, it was shown to be effective enough to solve higher-dimensional versions of these equations. In 2019, Rationalized Haar functions and the collocation approach were employed by Aditya Kaushik et al. [114] to resolve a variety of differential equations and IEs, and the authors asserted that their solution was superior in terms of efficiency, accuracy, competitiveness, and computing cost. In 2021, using Haar wavelets, Vaibhav et al., [115] developed an approach for numerically approximating problems with fractional initial and boundary values. In comparison to the Haar wavelet approaches that can be found in the existing literature, in which an approximation of the "fractional derivative of the function is made using the Haar basis" he made an approximation of the function as well as its conventional derivatives through using Haar basis functions. Furthermore, error constraints were obtained for the estimation of fractional integrals as well as fractional derivatives. The suggested technique also became successful in solving a problem involving a neural network that was characterized by a set of "nonlinear fractional differential equations". The numerical findings demonstrated that the computational strategy that was suggested was an appropriate technique. Irfan Awana et al. [116] expanded the use of a collocation algorithm that relies on Haar wavelets to study the Pennes heat conduction transfer model in 2020. The findings were analyzed and compared with an accurate solution of Pennes' bioheat transfer model that would have been available in the literature. It was determined that the current method worked effectively for all these particular circumstances as well. In 2019, Randhir Singh et al., [117] suggested using the Haar wavelet collocation technique to numerically solve the boundary-constrained Lane-Emden problem. The singular behaviour at the origin was fixed by transforming "the Lane-Emden problem into an integral equation". The integral problem was transformed into a set of "algebraic equations in the unknown expansion coefficients using the Haar wavelet collocation technique" and Newton's iterative procedure was used to find numerical solutions. In addition to that, both the convergence and error analyses of the method were shown. To show the reliability and versatility of the strategy, six specific examples

were given. Existing numerical and precise solutions were used as benchmarks for comparison with the numerical results. It was determined that the Haar wavelet was effective, quick, versatile, and user-friendly. Mohammadi et al. [118] in 2019, used the "Haar wavelet collocation-Picard approach" to investigate the "Emden-Fowler type equations" having non-integral order, and they compared their findings to those obtained using the "Homotopy perturbation method" and the "Adomian decomposition method". The author draws the conclusion that the suggested technique is simpler and more successful than "HPM and ADM" in solving such types of equations. In 2019, M. Fallahpour, M. Khodabin, and K. Maleknejad [119] solved the 2D-stochastic Volterra IEs with the aid of a 2D-Haar wavelet. In 2019, S. C. Shiralashetti and L. Lamani [120] solved the multidimensional stochastic IEs by using the Haar Wavelet method. In 2019, M. Erfanian and H. Zeidabadi [121] presented an algorithm for finding the solution of Fredholm IDEs in a complex plane with the aid of properties of rationalized Haar wavelets. In 2019, R. C. Mittal and Sapna Pandit [122] designed a new wavelet-based method for solving 2^{nd} order ODEs with singular coefficients and nonlinearities. The author asserts that the developed scheme outperformed the well-established methods of cubic splines, quadratic splines, and scale-2 Haar wavelets when applied to a set of standard problems. It was demonstrated that compared to the scale-2 Haar wavelet approach, the scale-3 Haar wavelet approach converged more quickly. To address the difficulty of solving Volterra and Volterra-Fredholm FrIDE problems, Amin et al., [123] designed the Haar wavelet collocation approach in 2021. Using the Haar method, the original set of equations is converted into a set of linear "algebraic equations". After deriving the system, the problem was solved using the Gauss elimination approach. To ensure the "validity and applicability" of the suggested technique, numerous test problems were collected from the relevant research. There was a comparison made between the maximum absolute error as well as the exact solution. Calculations were done to determine the maximum and mean absolute and square root errors for each possible combination of nodal points. The results confirmed the effectiveness of the Haar approach in resolving those problems. Convergence rates were also estimated experimentally for different numbers of collocation points, with an approximate value of 2. In 2020, Meisam Montazer et al., [124] introduced a non-uniform Haar wavelet-based computational approach for resolving linear integral equations of Volterra

kind (LIEV). After following the strategy that was suggested, the LIEV was simplified into a linear algebraic equation system that could be computed using the conventional way. The key benefit of adopting nonuniform Haar wavelets was the flexibility in calculating time. To numerically solve the Fractional Volterra Model (FVM) of intraspecific population dynamics, Rohul Amin et al., [125] devised the collocation technique based on Haar wavelet. In the suggested method, the "fractional derivative" would be examined in the "Caputo sense" and the approximation expressions for the unknown function would be derived by integration using Haar wavelets, and both of these are used in the nonlinear model. The method of residual correction was explored in considerable depth; its goal is to decrease the inaccuracy of the analytical solution by calculating the error. The computing performance of the suggested technique was demonstrated by an example using the residual correction approach. The numerical findings validated the approach's ease of use, precision, efficiency, and reliability. In 2020, Using the application of the p-Laplacian operators, KumSong Jong et al., [126] derived an approximation to the solution to the m-point fractional differential equations having boundary constraints and demonstrated the convergence of the suggested simulation analysis. To accomplish this goal, the operational matrix of fractional integration was coupled with the discretization approach and the fixed-point iterative approach before being used in the development of the mathematical model. The precision of the computation of fractional integrals of Haar wavelet functions was the basis for this conjunction. To demonstrate how the work could be applied, two examples were provided. In 2020, Amin et al., [127] devised a method for solving linear integral equations involving delay terms using the Haar wavelet collocation approach. The estimates that were produced for such equations are first subjected to some transformation. Then, the author uses an algebraic transformation to turn those approximations into actual equations. The resultant algebraic system was then evaluated using the Thomas algorithm. To test the appropriateness of the suggested method and ensure that it converges on the true solution, examples were collected from the relevant published research. In the same year, Amin et al., [128] extended this work to nonlinear delay IEs. In 2020, Thabet Abdeljawad and his co-workers [129] extended the use of "the Haar wavelet collocation procedure" for addressing the system of differential equations having non-integral

order. In order to numerically solve the nonlinear cubic Schrodinger equations of both 1D and 2D subject to initial and Dirichlet boundary constraints, the Haar wavelet collocation approach was employed by Nosheen Pervaiz and Imran Aziz [130] in 2020. Specifically, the researcher utilized the Haar wavelet collocation approach to calculate the spatial derivatives and the Crank-Nicolson technique to evaluate the time derivatives. The accuracy of the suggested technique was determined by implementing it to several test problems. The numerical findings obtained from such problems indicate that the suggested approach is reliable. The use of the "Haar wavelet technique" in the study of electromagnetic problems was expanded by Arun Kumar and colleagues [131] in the year 2020. The author evaluated the performance of the Haar wavelet technique for four "electromagnetic problems" relating to transmission lines, uniform plane waves in lossy dielectrics, the telegrapher's equation, and EM waves travelling through diverse media. Following the completion of the comparison study, the author came to the conclusion that the Haar wavelet techniques were significantly faster than the conventional analytical approaches. Applying Haar wavelet operational matrices, Shiralashetti et al., [132] constructed an efficient computational approach based on Haar wavelets. To demonstrate the efficacy and generalizability of the suggested approach, he took into account the partial differential equations having nonlinearity in them. The precision of the approach has been demonstrated through numerical simulation implementation. The author asserts that the suggested technique provides highly practical, effective results and is applicable across many disciplines in science and engineering. The Haar wavelet approach and Tikhonov regularisation were utilized by Saedeh Foadian et al. [133] in 2020 to provide an approximation to the time-delayed Burgers-Fisher problem. The author concludes that the method can be readily applied to a computer environment with minimal computational expense and space requirements. In 2020, Kamal Shah et al., [134] analysed a model of Coronavirus-19 disease qualitatively and numerically. It was shown that the examined model exists for Caputo fractional derivative by employing Banach's fixed point and Schauder's theorems. In addition, Broyden's methodology and the Haar collocation techniques were employed for numerical simulations. Moreover, the authors concluded that the Haar wavelet approach could be a robust resource for managing mathematical models of contagious diseases. Implementation of the "Haar wavelet technique" to the

examination of the fractional Fisher equation was expanded by Ghader Ahmadnezhad and colleagues [135] in the year 2020. Since the fractional Fisher's equation seems to be non-linear, the suggested solution employs the Iteration Picard methodology to deal with it. The resulting differential system was converted into a set of difference equations using Haar wavelets, and then the matrix method was employed to determine the solutions. The findings were then contrasted with the results achieved using other techniques that relied on an exact solution. The findings obtained were compared to the true solution and found to be consistent. Randhir Singh et al. [136] 2020 applied the Haar wavelet Quasilinearization technique to further explore Emden-Fowler type equations. After comparing the results to those obtained using the finite difference approach and the cubic spline method, it was determined that the acquired results were in excellent accordance with the precise solution, making the method the clear choice. In 2020, Meisam Montazer [137] invented an approach to quantitatively analyze stochastic Volterra IEs using wavelets that aren't uniform. Collocation points were used to determine the "non-uniform Haar wavelet coefficients". In addition, numerical instances are provided to illustrate the precision and efficacy of the suggested approach. In 2021, Hualing Wu et al., [138] resolved a class of delay IEs involving heterogeneous data transfer using the Haar collocation technique. While attempting to approximate a function whose value was unknown, Haar functions are taken into account. After implementing the "Haar collocation method" to a system of delay IEs, which involves making collocation point substitutions, we produce a linear system of equations. Using the software MATLAB, an approach was constructed to solve the problem of the desired system. This system was solved using the Gauss elimination technique. Ultimately, the result at collocation points was found by employing those coefficients. In 2021, using the fractional Brownian motion and also the Hurst parameter $H \epsilon \left(\frac{1}{2}, 1\right)$, Xiaoxia Wen and Jin Huang [139] devised the Haar wavelet method for resolving the stochastic Ito Volterra IEs. Utilizing "the operational matrix and stochastic operational matrix of the Haar wavelets basis" this method transformed the solution of the problem under study into the resolution of a system of algebraic equations. We also examined the method's convergence and established an error estimate for it. To examine the usefulness and efficacy of the current approach, numerous examples were

provided. To compute solutions to nonlinear Fredholm IEs and Fredholm IDEs in the interval $[0, t_f]$, the Leibnitz-Haar wavelet collocation technique was established by Swaidan et al., [140] in the year 2021. The fundamental idea was to change the IEs into a "higher-order differential equation" that includes the initial conditions. The Leibniz rule was utilized to perform the transformation. The required Haar coefficients were computed by first transforming the differential equation into a system of algebraic equations using the collocation points of the Haar wavelet as well as its operational matrix. In 2021, Khajehnasiri et al., [141] extended the use of "Haar wavelets" for the solution of the system of 2D-partial Volterra IEs having non-integral order and containing nonlinearity. In 2021, Alqarni et al., [142] extended the Haar wavelets for solving 3rd order IDEs having boundary constraints. The study describes the HWC technique for solving linear as well as nonlinear IDEs. The IDEs were transformed into corresponding equations. However, the linear system is resolved by using the Gauss technique and also the nonlinear system is resolved by using the Broyden technique. In 2021, Amin et al. [143] expanded the well-known numerical method known as HWC for pantograph delay IDEs having fractional order. Fixed point theory was utilized to investigate analyses for IDEs. By employing the process on distinct numerical examples, the aforementioned theory ensures the "existence and uniqueness of solutions" to the problem under consideration. The author asserts that the applicable numerical method was effective and reliable, and suggests that its precision could be enhanced by raising the no. of "collocation points". In 2022, Amin et al., [144] created HWCT to address fractional nonlinear IEs. As the initial constraints are automatically considered when constructing the formulation of the approximate solution, the HWCT appears to be highly useful for solving fractional nonlinear IEs. Several examples were given to determine the versatility and reliability of the suggested method. Approximating an unknown function is a common application of the Haar functions. After carrying out the required nodal points substitutions and using the HWCT, a set of nonlinear equations was produced. To solve the resultant problem, Broyden's technique was applied. The result at nodal points was determined using coefficients. The suggested HWCT has prospective applications for systems of nonlinear as well as linear fractional IDEs of variable order. In 2022, Muhammad Ahsan et al., [145] presented a finite-difference and "Haar wavelet collocation technique" in order to solve an ill-posed

inverse nonlinear "Cauchy problem" with a source that was dependent on the "space variable. To estimate the $\frac{\partial u}{\partial t}$ component, a 1st-order finite-difference method was used, and two separate Haar series were employed to estimate the $\frac{\partial^2 u}{\partial x^2}$ component as well as the source term. The non-linear system was linearized using a direct approach. Contrary to other numerical approaches, the newly proposed method produces a well-conditioned set of algebraic equations, hence no regularisation strategy was needed. The suggested technique generated consistent outcomes that converged to the correct solution. The correctness, "well-conditioning" of the system of equations, and "simple applicability" of the technique to nonlinear as well as linear problems have all been verified using numerical experiments. For the objective of investigating the natural frequencies of a tapered Timoshenko beam, Marmar Mehrparvar et al., [146] created a new approach that relies on the Haar wavelet technique. 6th and 4th order convergent findings for the clamped-pinned and clamped-clamped boundary constraints, respectively, were provided. The findings were determined to have a significant degree of agreement with the outcomes that were predicted by the Ritz approach. Amin et al., [147] extended the computational "Haar collocation methodology" for the resolution of fractional IDEs of linear type with variable order. The Caputo concept had been employed to define variable order fractional derivatives. Using the Haar method that was introduced, the given problem was represented as a set of algebraic equations. The Gauss elimination approach was used to solve the system and get the intended outcomes. To illustrate the convergence of the Haar collocation methodology, several instances were provided. Calculations were made to determine the variety of errors for each of the distinct collocation points. The findings provide conclusive evidence that the Haar method was an effective means of resolving the problems in consideration. In 2022, Marasi and Derakhshan [148] established a "computational approach" for solving the variable order Caputo-Prabhakar fractional IDEs that was based on the "Haar wavelet collocation algorithm". In 2022, Shiralashetti and Lamani [149] utilized the Haar wavelets for stochastic differential equations. In 2022, Amin and his co-workers [150] established a numerical approach for solving fractional IEs of the Volterra-Fredholm type. Haar wavelet collocation approach established the basis for the suggested method. The author demonstrated the "existence and uniqueness" of a

solution under specified conditions. It should be noted that some *Hyers-Ulam* type stability results were also provided. The Haar technique was employed to convert the original problem into an algebraic system, which was subsequently solved with a Gauss elimination procedure to obtain the desired outcomes. The procedure was demonstrated numerically using examples from the literature. Based on the outcomes, it was clear that the HWCT was a reliable means of addressing FIEs. In 2023, Jiraporn and his coworkers [151] investigated the Fractional Order Integro-Differential Equations (FOIDE) of the Fredholm type, highlighting their significance in image and signal processing. The study uniquely addresses the Mittage-Leffler-type derivative, specifically utilizing the Haar wavelet (HW) method. The non-singular and non-local nature of this derivative is leveraged for computational advantages. The paper establishes existence theory using the fixed point theorem, outlining sufficient conditions for uniqueness. A numerical scheme based on the HW method is proposed and applied to demonstrate applicability through various examples. In 2023, Amer Darweesh et al., [152] introduced the "Haar wavelet method" to obtain approximate solutions for linear fractional Fredholm integro-differential equations within coupled systems. Emphasizing the Caputo sense for fractional derivatives, the approach involves transforming these systems into sets of algebraic equations for easier resolution. Additionally, a refined technique called the "Laplace Haar wavelet method" incorporates the Laplace transform operator to further enhance accuracy and reduce computational time. The effectiveness, accuracy, and practicality of these methods are substantiated through illustrative examples presented in the paper, validating their validity and efficiency. In the same year, Muhammad Ahsan et al., [153] introduced the Higher-order Haar wavelet collocation method (HHWCM) as an enhancement to the Haar wavelet collocation method (HWCM). The study aims to improve precision and convergence order. HHWCM is applied to solve nonlinear ordinary differential equations under various conditions, including initial, boundary, periodic, two-point, integral, and multi-point integral boundary conditions. The paper includes essential theorems on HHWCM convergence, compares it with recent works like HWCM, and tests its efficacy on various types of differential equations.

1.9 Research Gap

The following research gap has been found as a result of an exclusive literature survey.

1. From the existing literature, it has been observed that some work has been done to finding the numerical solution of IEs and IDEs by using spectral or semi-analytical techniques, there is a good scope to analyze the behaviour of phenomenon governed by these equations using wavelets.
2. There is ample evidence supporting the presence of "Haar scale 3 wavelets" in the field of electronics engineering. However, only a limited number of algorithms have been devised that utilize Haar scale 3 wavelets, specifically for solving differential equations. The potential application of Haar scale 3 wavelets in solving integral and integro-differential equations remains unexplored.
3. While hybrid methods combining wavelets with variational, approximation, or semi-analytic techniques have been documented in the literature, there remains significant potential for the development of a novel hybrid approach. This approach would integrate wavelets with one or more of the aforementioned methods to create an innovative hybrid methodology.
4. There is vast potential for utilizing hybrid methods based on Haar Scale 3 wavelets to solve linear as well as nonlinear IEs and IDEs.

1.10 Research Objectives

1. To explore the possibility of coupling the wavelet method with other legacy methods by varying the dilation factor.
2. To investigate the applicability of wavelet method for Integro-Differential Equations.
3. To investigate the applicability of wavelet method for Integral equations.
4. To adapt the purposed techniques for solving physical models that are important in science and technology.

1.11 Research Methodology

The methodology to be used while solving a problem will consist of the following five phases

Phase 1. Formulation of the Hybrid Method

The Hybrid Method will be developed by combining the "wavelet method" with other existing methodologies or by modifying the "dilation factor".

Phase 2. Algorithm for finding the solution to the problem

An Algorithm will be developed to implement the Hybrid method obtained in phase (1)

Phase 3. Solution of the problem

The developed algorithm/ MATLAB program will be implemented on the problem to solve the problem numerically.

Phase 4. Discussion and Interpretation

The results obtained will be explained and discussed analytically or graphically by comparing it with "numerical solution or analytical solution" present in the literature survey.

Phase 5. Conclusion of the problem

Outcomes of the problem will be highlighted by giving its relevance and applications in the field or by highlighting the advantages of the methods over the other methods available in the literature for solving the same type of problem.

Chapter 2.

Numerical Solution of Integro-Differential Equations by using Scale 3 Haar Wavelets Collocation Algorithm

2.1 Introduction

Integro-differential equations (IDEs) are mathematical equations that involve both derivatives and integrals. The study of integro-differential equations has been a topic of significant interest to researchers for several decades, and they are widely used in various applications. These equations arise in a variety of applications, including physics [3], engineering [8], [9], biology [12], and economics [11]. The application of IDEs in science and engineering has been vast and diverse. In physics, they have been used to model the behaviour of fluids, electromagnetic fields, and the motion of particles in space. In engineering, integro-differential equations have been applied in the design of control systems, the analysis of heat transfer, and the study of mechanical systems. In chemistry, they have been used to model chemical reactions and the diffusion of particles in liquids and gases. One of the most significant applications of integrodifferential equations has been in the field of population dynamics. These equations have been used to model the growth and decline of populations over time, and have been instrumental in the development of models for the spread of diseases and the conservation of natural resources. Integrodifferential equations have also found applications in economics, where they have been used to model the behaviour of financial markets and the interactions between consumers and producers. They have been used to analyse the dynamics of stock prices, interest rates, and exchange rates, and to develop models for predicting economic trends and forecasting future developments. Their broad applications have led to the development of numerous techniques and methods for solving and analysing these equations. As research in these fields continues to advance, integrodifferential equations will undoubtedly continue to be an essential tool for scientists and engineers seeking to understand and control the behaviour of complex systems. The solution of IDEs is essential in many scientific and engineering fields as they provide a way to model complex phenomena and processes

that cannot be described by “ordinary differential equations or partial differential equations”. One of the primary reasons for the need to solve IDEs is to model complex systems that involve interactions between various components. Another reason for the need to solve IDEs is to analyse the behaviour of systems over time. In addition to modelling complex phenomena and analysing the behaviour of systems over time, the solution of IDEs is also essential in the development of numerical methods for solving partial differential equations. Many numerical methods such as: “finite element methods and boundary element methods” rely on the solution of IDEs to accurately model the behaviour of complex systems. One of the most significant advantages of integrodifferential equations is that they can provide a more accurate description of real-world phenomena that involve memory or history dependence. In many cases, a system's current state depends not only on its current inputs and past states but also on the entire history of the system's behaviour [21], [154], [155]. Integro-differential equations have several types, including Volterra and Fredholm IDEs. IDEs can be solved using a variety of techniques, including numerical methods and analytical solutions. Analytical solutions are often challenging to obtain due to the complex nature of the equations, and numerical methods are typically required to obtain approximate solutions. The choice of method depends on the specific problem and the accuracy required. In the recent past, many research groups have studied IDES for their solution using variant techniques. In 2000, A. Avudainayagam and C. Vani [156] solved the integro-differential equations by using the wavelet Galerkin approach. In this approach, the most commonly used bases like Fourier and Legendre for solving the IDEs were replaced by wavelet bases, and a new connection coefficient having four dimensions appeared in this technique. Thereafter, the author introduced a method for estimating the connection coefficient. The presented technique was applied to two different IDEs, which proved that the results obtained by using wavelet bases were relatively more accurate. In 2001, A.M. Wazwaz [157] demonstrated the results of higher-order IDEs having BVP by utilizing the “modified Adomain decomposition method”. Reports show that the results obtained through the utility of this method were accurate, reliable, and efficient. The Taylor collocation method was first introduced by A. Karamete et al. [158] in 2002 as an approach for estimating the solution of linear IDEs. This technique involves transforming the IDEs into a system of linear equations that consists of

unknown coefficients. These unknown coefficients in Taylor expansion were then calculated by using this method. This algorithm also worked for differential as well as integral equations. In 2003, Salah M. El-Sayed and his co-workers [159] presented a comparison between the wavelet-Galerkin method and Adomain decomposition approach for approximating the solution of IDEs. The results obtained demonstrated that Adomain decomposition approach was relatively more computer-friendly. In 2004, M.T. Rashed [160] solved the Volterra and Fredholm types of IDEs by using Chebyshev and Lagrange interpolation. In 2005, A. Arikoglu and I. Ozkol [161] applied the differential transform method to approximate the solution of IDEs. In this work, the authors presented some important results with their proofs for the transformation of integrals. In order to validate the method, a few test problems from the existing literature were solved which proved the accuracy of the algorithm. In 2007, H. Danfu et.al. [162] used the CAS wavelet for solving IDEs. In this wavelet method, IDEs were transformed into a system of linear algebraic equations with the aid of a wavelet operational matrix. The unknown coefficients were calculated by using the properties of the Sinc function. In 2011, A. Saadatmandi and M. Dehghan [163] presented a new algorithm for finding the solution to IDEs. In this algorithm, IDEs were converted to algebraic equations by using the hybrid of Legendre approximation with the Gaussian integration method. For checking the rationality and applicability, some test problems from existing literature were analysed. In this work, the results obtained by the proposed algorithm were compared with the results that were calculated by utilizing the differential transform method and Adomain decomposition method. In 2012, Manafianheris [164] employed a modified Laplace Adomain decomposition approach to address integro-differential equations. Similarly, in the same year, Yeganah et al. [165] introduced the sinc-collocation method as a solution for nonlinear integro-differential equations with a boundary value problem. This technique proved to be highly efficient in approximating solutions, particularly when dealing with singularities at the endpoints. In 2017, Kashkaria et.al., [166] described a “stochastic computational intelligence algorithm” for solving IDES of “The volterra-Fredholm type”. In 2018, Rohaninasab, Maleknejad, and Ezzat [167] developed a technique for addressing “higher order linear Volterra-Fredholm IDES under mixed conditions”. To solve these equations, the Legendre collocation spectral method was used. In 2020, Chen and his

coworkers [168] used the Galerkin approach for IDES of Fredholm type having boundary conditions. In recent years, wavelets have been used for solving a variety of functional equations because of their simplicity, orthogonality, and compact support. In 2021, Faheem et.al., [169] solved neutral delay differential equations (NDDE) by using the Gegenbaur wavelet and Bernoulli wavelet. The author claims that the results obtained by using these two wavelets are more reliable than the existing results in past studies. In the same year, Faheem and his co-workers [170] solved the NDDE by using four different wavelets namely, Laguerre wavelet, Legendre wavelet, Chebyshev wavelet, and Hermite wavelet. In 2022, Faheem et. al., [171] designed a method for solving "partial differential equations" by using "Hermite wavelet". Among all the wavelets, Haar wavelets are a relatively huge and promising technique in applied mathematics. It has been used in a wide range of scientific applications, many researchers have successfully applied the Haar wavelet collocation points approach (HWCP) for solving linear and nonlinear differential equations and very limited literature is available for the solution of IDEs. The solutions of IDEs have yet not been analyzed using Haar scale 3 wavelets. This encouraged us to utilize Haar scale 3 wavelets in order to derive the solution for IDEs. The organization of this chapter is as follows: In section 2.2, we outline the Haar scale 3 wavelet collocation approach (HWCA). Section 2.3 deals with a few numerical experiments from the previously published reports to establish the validation and convergence of HWCA. The summary of this chapter is briefly described in section 2.4.

2.2 Haar scale 3 wavelet collocation approach (HWCA)

2.2.1 Approximation of functions and their integrals

This section deals with the formulation of the numerical algorithm for solving the variety of linear and nonlinear IDEs of first and higher orders. Haar scale 3 wavelet collocation approach is introduced for the interval $[0, 1]$.

Theorem 2.2.1: If $\xi(x)$ is any square-integrable function defined on the interval $[c_1, c_2]$ such that $\xi(x) = \sum_{i=1}^{3p} a_i \psi_i(x)$, then the integral of $\psi_i(x)$ over the interval $[c_1, c_2]$ is given as,

$$\int_{c_1}^{c_2} \xi(x)dx = \frac{c_2 - c_1}{3p} \sum_{m=1}^{3p} \xi(x_m) = \frac{c_2 - c_1}{3p} \sum_{m=1}^{3p} \xi\left(c_1 + (c_2 - c_1)\frac{m - 0.5}{3p}\right). \quad (2.1)$$

Proof: Consider the integral

$$\int_{c_1}^{c_2} \xi(x)dx,$$

over the interval $[c_1, c_2]$. By employing the characteristics of Haar scale 3 wavelets [22], [172], $\xi(x)$ can be expressed as

$$\begin{aligned} \xi(x) &= \sum_{i=1}^{\infty} a_i \psi_i(x) \\ &= a_1\psi_1(x) + \sum_{even\ i} a_i \phi^1\left(3^j x - k\right) + \sum_{odd\ i} a_i \phi^2\left(3^j x - k\right), \end{aligned} \quad (2.2)$$

where '$a_i's$' are unknown wavelet coefficients, which will be calculated by the presented algorithm. Now, we will consider only finite $3p$ terms for computation.

$$\xi(x) \approx x_{3p} = \sum_{i=1}^{3p} a_i \psi_i(x). \quad (2.3)$$

In the Haar wavelet collocation approach, collocation points for the interval $[c_1, c_2]$ is given by the relation

$$x_m = c_1 + (c_2 - c_1)\frac{m - 0.5}{3p}. \quad (2.4)$$

The equation (2.3) can be written as

$$\xi(x_m) = \sum_{i=1}^{3p} a_i \psi_i(x_m)\,; m = 1, 2, , \dots, 3p. \quad (2.5)$$

Lemma 2.2.1

The approximate value of the integral

$$\int_{c_1}^{c_2} \xi(x)dx \approx a_1(c_2 - c_1). \quad (2.6)$$

Proof of Lemma 2.2.1: As we know,

$$\int_{c_1}^{c_2} \psi_i(x)dx = 0, \qquad for\ i = 2, 3, 4, \dots \quad (2.7)$$

and

$$\int_{c_1}^{c_2} \psi_1(x)dx = c_2 - c_1, \tag{2.8}$$

Integrating equation (2.3) and then by using equation (2.7) and (2.8), we get

$$\int_{c_1}^{c_2} \xi(x)dx \approx \sum_{i=1}^{3p} a_i \int_{c_1}^{c_2} \psi_i(x)dx = a_1(c_2 - c_1). \tag{2.9}$$

Hence proved.

Lemma 2.2.1 indicates that when utilizing Haar wavelet approximation for computing definite integrals, only a single coefficient is required.

Lemma 2.2.2

Value of 'a_1' for the system of equation (2.5) is given as

$$a_1 = \frac{1}{3p} \sum_{m=1}^{3p} \xi(x_m)\,;\ \ p = 3^j \ and\ j = 0, 1, 2, \ldots \tag{2.10}$$

Proof of lemma 2.2.2: For the proof of this lemma, we apply the "Principle of Mathematical Induction" on 'j'.

Step 1: For $j = 0, p = 1$, and so, $m = 1, 2, 3$, and thus the system of equations in this case is

$$\xi(x_1) = a_1\psi_1(x_1) + a_2\psi_2(x_1) + a_3\psi_3(x_1),$$
$$\xi(x_2) = a_1\psi_1(x_2) + a_2\psi_2(x_2) + a_3\psi_3(x_2),$$
$$\xi(x_3) = a_1\psi_1(x_3) + a_2\psi_2(x_3) + a_3\psi_3(x_3),$$

By solving these three equations we obtain the value of 'a_1' which is given as

$$a_1 = \frac{1}{3}[\xi(x_1) + \xi(x_2) + \xi(x_3)].$$

Thus for $j = 0$ the result is true.

Step 2: Let's assume that the result holds for $j = n - 1$.

Step 3: Now, we have to prove that the result is true for $j = n$.

For $j = n, p = 3^n$ and thus we have 3^{n+1} system of linear equations having 3^{n+1} variables. From this system of equations, by adding three consecutive equations, we obtained a new set of 3^n equations containing 3^n variables. Now by replacing $3a_1$ by

$a_1{}'$ and $\xi(x_{3m-2}) + \xi(x_{3m-1}) + \xi(x_{3m})$ by $g(x_m)$ in this system, we obtained a system similar to (2.5), and then by applying the induction hypothesis, we get

$$a_1' = \frac{1}{3.3^{n-1}} \sum_{m=1}^{3.3^{n-1}} g(x_m),$$

Putting back the valuve og $g(x_m)$ and $a_1{}'$, we get

$$a_1 = \frac{1}{3.3^{n}} \sum_{m=1}^{3.3^{n}} \xi(x_m). \tag{2.11}$$

Hence, our result is true for $j = n$. Thus, by "the Principle of Mathematical Induction" this result is true $\forall\, j = 0, 1, 2, 3, \ldots$. By using equation (2.11) in equation (2.9), and by putting the collocation points, we obtained the Quadrature based formula (2.1),

$$\int_{c_1}^{c_2} \xi(x)dx = \frac{c_2 - c_1}{3p} \sum_{m=1}^{3p} \xi\left(c_1 + (c_2 - c_1)\frac{m - 0.5}{3p}\right).$$

2.2.2 Method of Solution

Now consider 2^{nd} order linear integro-differential equation

$$\xi''(x) + m(x)\xi'(x) + n(x)\xi(x) = \mu_1 \int_m^n W_1(x,t)\xi(t)dt + \mu_2 \int_m^x W_2(x,t)\xi(t)dt + g(x), \tag{2.12}$$

with initial conditions

$$\xi(0) = \theta \;\; and \;\; \xi'^{(0)} = \sigma.$$

Here 'm' and 'n' are functions of 'x'. '$W_1(x,t)$' and '$W_2(x,t)$' are kernels of integration. $\mu_1,\ \mu_2,\ \theta,$ and σ are real constants. $g(x)$ is a known function which is already given.

When $W_1(x,t) = 0$, equation (2.12) becomes Volterra IDE, and when $W_2(x,t) = 0$ equation (2.12) becomes as Fredholm IDE.

Now, let

$$\xi''(x) = \sum_{i=1}^{3p} a_i \psi_i(x), \tag{2.13}$$

Integrating equation (2.13) on both sides from 0 to x, we get

$$\xi'(x) - \xi'(0) = \sum_{i=1}^{3p} a_i L_{i,1}(x)\,; where\ L_{i,1}(x) = \int_0^x \psi_i(x)dx, \tag{2.14}$$

By simplifying equation (2.14) and using the initial conditions, it becomes as

$$\xi'(x) = \sigma + \sum_{i=1}^{3p} a_i L_{i,1}(x), \tag{2.15}$$

Again, integrating equation (2.15) from 0 to x and by using initial conditions, it becomes as

$$\xi(x) - \xi(0) = \sigma\, x + \sum_{i=1}^{3p} a_i L_{i,2}(x)\,; where\ L_{i,2}(x) = \int_0^x L_{i,1}(x)dx,$$

$$\xi(x) = \theta + \sigma\, x + \sum_{i=1}^{3p} a_i L_{i,2}(x). \tag{2.16}$$

Equation (2.16) is the approximate solution for equation (2.12). Substituting equation (2.13), (2.15), and (2.16) in equation (2.12), we get

$$\begin{aligned}
&\sum_{i=1}^{3p} a_i \psi_i(x) + m(x)\left[\sigma + \sum_{i=1}^{3p} a_i L_{i,1}(x)\right] + n(x)\left[\theta + \sigma\, x + \sum_{i=1}^{3p} a_i L_{i,2}(x)\right] \\
&\qquad = \mu_1 \int_m^n W_1(x,t)\left[\theta + \sigma\, t + \sum_{i=1}^{3p} a_i L_{i,2}(xt)\right] dt \\
&\qquad + \mu_2 \int_m^x W_1(x,t)\left[\theta + \sigma\, t + \sum_{i=1}^{3p} a_i L_{i,2}(xt)\right] dt + g(x), \\
\Rightarrow &\sum_{i=1}^{3p} a_i \psi_i(x) + m(x) \sum_{i=1}^{3p} a_i L_{i,1}(x) + n(x) \sum_{i=1}^{3p} a_i L_{i,2}(x) \\
&\qquad - \mu_1 \int_m^n W_1(x,t) \sum_{i=1}^{3p} a_i L_{i,2}(t)\, dt \\
&\qquad - \mu_2 \int_m^z W_2(x,t) \sum_{i=1}^{3p} a_i L_{i,2}(t)\, dt \\
&\qquad = -\sigma\, m(x) - \theta\, n(x) - \sigma\, x\, n(x) \\
&\qquad + \mu_1 \int_m^n W_1(x,t)(\theta + \sigma\, t)dt + \mu_2 \int_m^z W_2(x,t)(\theta + \sigma\, t)dt \\
&\qquad + g(x),
\end{aligned} \tag{2.17}$$

$$\Rightarrow \sum_{i=1}^{3p} a_i \left[\psi_i(x) + m(x)L_{i,1}(x) + n(x)L_{i,2}(x) - \mu_1 \int_m^n W_1(x,t)L_{i,2}(t)dt \right.$$
$$\left. - \mu_2 \int_m^z W_2(x,t)L_{i,2}(t)dt \right]$$
$$= -\sigma\, m(x) - \theta\, n(x) - \sigma\, x\, n(x)$$
$$+ \mu_1 \int_m^n W_1(x,t)(\theta + \sigma\, t)dt + \mu_2 \int_m^z W_2(x,t)(\theta + \sigma\, t)dt$$
$$+ g(x).$$

By applying the result of theorem 2.2.1 for calculating the integrals and putting the collocation points, we get

$$\sum_{i=1}^{3p} a_i \left[\psi_i(x_m) + m(x_m)L_{i,1}(x_m) + n(x_m)L_{i,2}(x_m) - \mu_1 Q_{i,2}^1(x_m) \right.$$
$$\left. - \mu_2 Q_{i,2}^2(x_m) \right] \qquad (2.18)$$
$$= -\sigma\, m(x_m) - \theta\, n(x_m) - \sigma\, x_m\, n(x_m) + \mu_1 W^1(x_m)$$
$$+ \mu_2 W^2(x_m) + g(x_m),$$

where

$$Q_{i,2}^1(x_m) = \left(\frac{n-m}{3p}\right) \sum_{s=1}^{3p} W_1(x_m, t_s)L_{i,2}(t_s),$$

$$Q_{i,2}^2(x_m) = \left(\frac{x_m - m}{3p}\right) \sum_{s=1}^{3p} W_2(x_m, t_s)L_{i,2}(t_s),$$

$$W^1(x_m) = \left(\frac{n-m}{3p}\right) \sum_{s=1}^{3p} W_1(x_m, t_s)(\theta + \sigma t_s),$$

$$W^2(x_m) = \left(\frac{x_m - m}{3p}\right) \sum_{s=1}^{3p} W_2(x_m, t_s)(\theta + \sigma t_s).$$

After putting the collocation points, a system of $3p \times 3p$ algebraic equations has been obtained which can easily be reduced to the matrix form of the type

$$AH = W$$

Any iterative method could be utilized to determine the solution to these equations. For the solution this linear system, the Gauss elimination method has been implemented.

By solving these algebraic equations, the unknown Haar coefficient has been obtained. Finally, by substituting these Haar coefficients $a_i's$ in equation (2.16) solution at collocation points has been obtained.

2.3 Numerical Examples and Analysis of Errors

In this particular segment, the presented algorithm has been put to the test on twelve distinct problems to assess its suitability and precision. The outcomes derived from employing this approach are then compared to the previously documented results found in the existing literature. The M_{cp}, maximum absolute, l_2, E_{max} and l_∞ errors have been calculated for checking the accuracy of the presented algorithm, by using the MATLAB software. If ξ_{ap} is the "approximate solution" and ξ_{ex} is the "exact solution" at collocation points x_m then M_{cp}, l_2, E_{max}, l_∞, and absolute errors are calculated by using the following mathematical expressions:

$$M_{cp} - error = \sqrt{\frac{1}{3N}\sum_{i=1}^{3p}\left|\xi_{ex}(x_m) - \xi_{ap}(x_m)\right|^2},$$

$$l_2 - error = \frac{\sqrt{\sum_{i=1}^{3p}\left|\xi_{ex}(x_m) - \xi_{ap}(x_m)\right|^2}}{\sum_{i=1}^{3p}|\xi_{ex}(x_m)|^2},\ E_{max} - error = \sqrt{\sum_{i=1}^{3p}\left|\xi_{ex}(x_m) - \xi_{ap}(x_m)\right|^2},$$

$$l_\infty - error = \max\left|\xi_{ex}(x_m) - \xi_{ap}(x_m)\right|,\ \text{Absolute error} = \left|\xi_{ex}(x_m) - \xi_{ap}(x_m)\right|.$$

Example 2.1: Consider the 1st order Volterra IDE [173], [174].

$$\begin{cases} \xi'(x) = 1 - 2\,x\,sin(x) + \int_0^x \xi(t)\,dt, \\ \xi(0) = 0. \end{cases} \tag{2.19}$$

The exact solution found from the literature is $\xi(x) = x\cos(x)$ [173],[174], and the solution obtained by using the presented technique is $\xi(x) = \sum_{i=1}^{3p} a_i L_{i,1}(x)$.

The integro-differential equation of Volterra type given in Example 2.1 is solved by utilizing the proposed Haar scale 3 wavelet collocation approach (HWCA). The results obtained by using HWCA are tabulated in Table 2.1, which demonstrates the comparison among the "approximated solution and exact solution" for the level of resolution 1. The observations from Table 2.1 can be readily noticed that HWCA gives more accurate results even for the small number of collocation points. $l_2 - error$ and $l_\infty - error$ for the level of resolution 2 are 4.20E-04 and 2.79E-04 respectively.

Table 2.1: Computation of Exact Solution (ES) and Approximated Solution (AS) for Example 2.1.

x	ES [173],[174]	AS	Value of Absolute Error
0.05555556	0.05546984	0.05529813	1.72E-04
0.16666667	0.16435721	0.16384454	5.13E-04
0.27777778	0.26712977	0.26628349	8.46E-04
0.38888889	0.35985091	0.35868307	1.17E-03
0.50000000	0.43879128	0.43731840	1.47E-03
0.61111111	0.50050672	0.49874944	1.76E-03
0.72222222	0.54191119	0.53989379	2.02E-03
0.83333333	0.56034354	0.55809342	2.25E-03
0.94444444	0.55362678	0.55117387	2.45E-03

Table 2.2 and Figure 2.1 indicates that "the approximate solution converges to the exact one". Better accuracy can be achieved by increasing the no. of "collocation points". Figure 2.2 shows the graphical view of the absolute value of error for the level of resolution 2. The outcomes achieved through the utilization of HWCA are contrasted with the current approaches, as demonstrated in Table 2.2. clearly explains that HWCA is working more effectively than other approaches.

Table 2.2: Computation of multiple errors for Example 2.1.

j	$l_2 - error$	$l_\infty - error$	$E_{max} - error$	$E_{max} - error$ by using the Haar method [174]	$E_{max} - error$ by using the Legendre method [174]
0	3.43E-02	2.06E-02	2.51E-02	----------	---------
1	3.79E-03	2.45E-03	4.77E-03	----------	---------
2	4.20E-04	2.79E-04	9.17E-04	1.37e-02	1.21e-03
3	4.67E-05	3.12E-05	1.77E-04	3.49e-03	3.10e-04
4	5.19E-06	3.47E-06	3.40E-05	8.81e-04	7.82e-05
5	5.77E-07	3.86E-07	6.54E-06	2.20e-04	1.96e-05

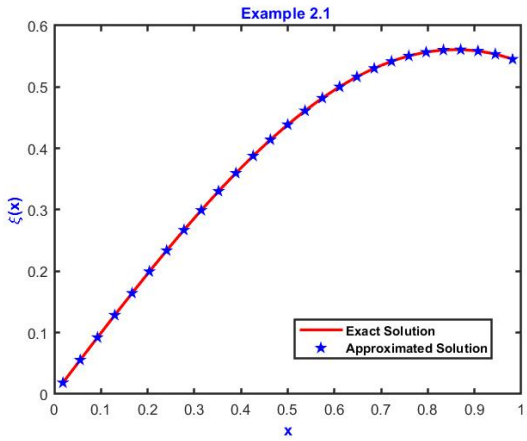

Figure 2.1: Visual analysis of exact solution and approximate solution for Example 2.1.

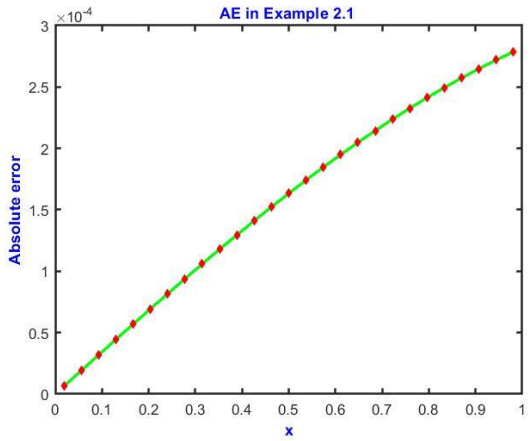

Figure 2.2: Graphical view of AE for Example 2.1.

Example 2.2: Consider the 2nd order Volterra IDEs [175].

$$\begin{cases} \xi''(x) + \xi'(x) + \xi(x) + \int_0^x e^{-(x-t)}\xi'(t)\,dt = \dfrac{\sin(x) + 3\cos(x) - e^{-x}}{2}, \\ \xi(0) = 0, \xi'(0) = 1. \end{cases} \quad (2.20)$$

The ES found from the literature is $\xi(x) = \sin(x)$ [175].

Table 2.3: Computation of Exact solution (ES) and Approximated solution (AS) for Example 2.2.

x	ES [175]	AS	Value of Absolute Error
0.055555556	0.055526982	0.055527019	3.66002E-08
0.166666667	0.165896133	0.165896515	3.82617E-07
0.277777778	0.274219289	0.274220704	1.41501E-06
0.388888889	0.379160504	0.379163801	3.29666E-06
0.500000000	0.479425539	0.479431513	5.97396E-06
0.611111111	0.573777826	0.573787045	9.21847E-06
0.722222222	0.661053722	0.661066390	1.26682E-05
0.833333333	0.740176853	0.740192721	1.58675E-05
0.944444444	0.810171396	0.810189700	1.83041E-05

Table 2.4: Computation of errors for Example 2.2.

j	$l_2 - error$	$l_2 - error$ in [175]	$l_\infty - error$	$l_\infty - error$ in [175]
0	1.68E-04	4.58E-03 ($K = 16$)	1.40E-04	3.08E-03 ($K = 16$)
1	1.90E-05	5.59E-06 ($K = 20$)	1.83E-05	3.35E-06 ($K = 20$)
2	2.11E-06	3.70E-09 ($K = 24$)	2.10E-06	2.01E-09 ($K = 24$)
3	2.35E-07	4.20E-12 ($K = 28$)	2.36E-07	2.20E-12 ($K = 28$)
4	2.61E-08	2.41E-12 ($K = 30$)	2.63E-08	9.33E-13 ($K = 30$
5	2.90E-09	-----	2.92E-09	----
6	3.22E-10	-----	3.25E-10	----

In Example 2.2, the Volterra type IDE having exponential kernel is solved through the Haar scale 3 wavelet collocation approach (HWCA). The obtained results are presented in Table 2.3, which presents a contrast between the precise solution and the estimated solution for resolution level 1. The table shows that the HWCA method produces more accurate results, even with a small number of collocation points. The $l_2 - error$ and $l_\infty - error$ for resolution level 2 are 2.11E-06 and 2.10E-06 respectively.

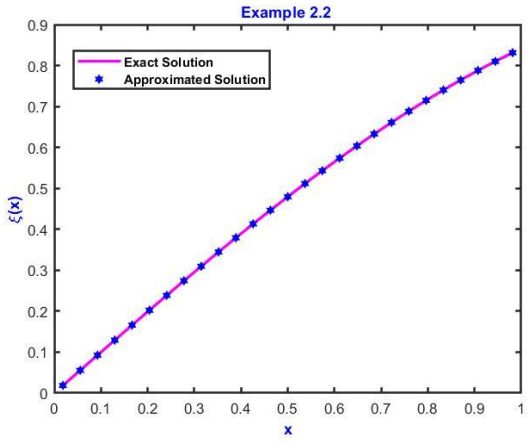

Figure 2.3: Visual analysis of exact solution and approximate solution for Example 2.2.

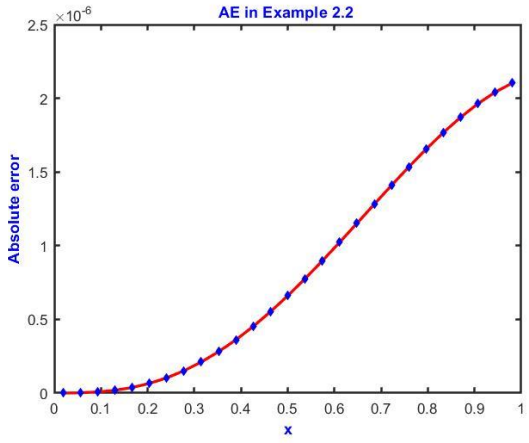

Figure 2.4: Graphical view of AE for Example 2.2.

Table 2.4 and Figure 2.3 depict that the approximated solution converges toward the exact solution. Increasing the number of collocation points can result in better accuracy. Figure 2.4 displays the absolute value of error for resolution level 2. Table 2.4

represents the comparison between the obtained findings and the existing findings, which demonstrates that HWCA is a more effective approach compared to other methods.

Example 2.3: Consider the Volterra IDE of 3rd order [176], [177].

$$\begin{cases} \xi'''(x) - x\xi''(x) = \frac{4}{7}x^9 - \frac{8}{5}x^7 + 6x^2 - x^6 - 6 + 4\int_0^x x^2t^3\xi(t)dt\,, \\ \xi(0) = 0\,, \xi'(0) = 2\,, \xi''(0) = 0. \end{cases} \quad (2.21)$$

The ES for this problem is $\xi(x) = 1 + 2x - x^3$ [176] , [177] and the AS is $\xi(x) = 1 + 2x + \sum_{i=1}^{3p} a_i L_{i,3}(x)$.

The third order integro-differential equation of Volterra kind is solved by using the proposed approach. For Example, 2.3, the solution attained by applying the proposed technique is almost equal to the precise solution giving the absolute error zero. The results that have been achieved are illustrated in Table 2.5, which presents a comparison of the actual solution and the approximate solution for level 1 of resolution.

Table 2.5: Computation of Exact solution (ES) and Approximated solution (AS) for Example 2.3.

x	ES [176] , [177]	AS	Value of Absolute Error
0.055555556	1.110939643	1.110939643	0
0.166666667	1.328703704	1.328703704	0
0.277777778	1.534122085	1.534122085	0
0.388888889	1.718964335	1.718964335	0
0.500000000	1.875000000	1.875000000	0
0.611111111	1.993998628	1.993998628	2.22045E-16
0.722222222	2.067729767	2.067729767	0
0.833333333	2.087962963	2.087962963	0
0.944444444	2.046467764	2.046467764	0

The results obtained with the HWCA method are more precise, as seen in the table, even when using only a few collocation points. For resolution level 0, the values of all the errors are 0. Table 2.6 and Figure 2.5 illustrate the convergence of the estimated solution toward the precise solution. The maximum absolute error for resolution level 2 is 10^{-16} as shown in Figure 2.6. By comparing the findings with those of other methods, as shown in Table 2.6, it becomes evident that HWCA is the stronger approach.

Table 2.6: Computation of errors for Example 2.3.

j	$l_2 - error$	$E_{max} - error$	$M_{cp} - error$	$M_{cp} - error$ [177]	$l_\infty - error$	$l_\infty - error$ [177]
0	0	0	0	2.68E-05	0	5.36E-05
1	4.15E-17	2.22E-16	7.40E-17	7.65E-06	2.22E-16	2.08E-05
2	8.31E-17	7.69E-16	1.48E-16	1.98E-06	4.44E-16	6.70E-06
3	5.18E-17	8.31E-16	9.23E-17	5.01E-07	4.44E-16	1.91E-06
4	4.80E-17	1.33E-15	8.55E-17	1.25E-07	4.44E-16	5.12E-07
5	3.03E-17	1.46E-15	5.39E-17	3.14E-08	4.44E-16	1.32E-07

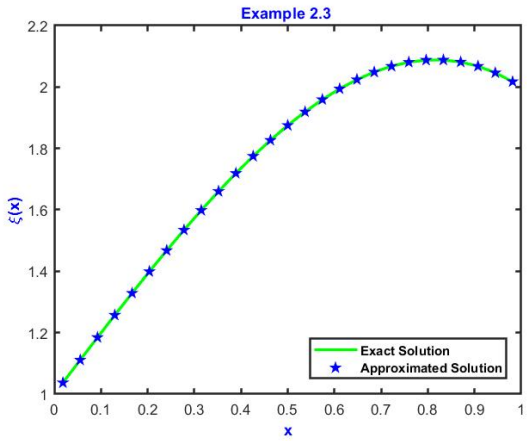

Figure 2.5: Visual analysis of exact solution and approximate solution for Example 2.3.

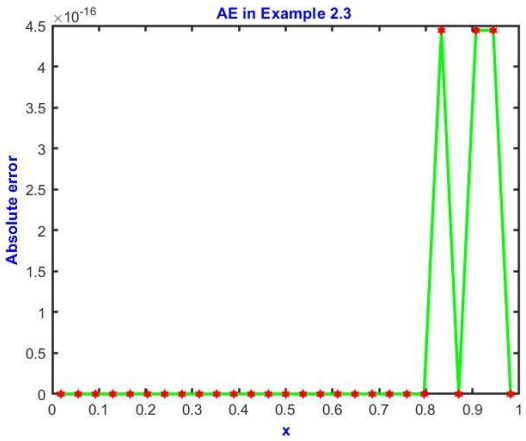

Figure 2.6: Graphical view of AE for Example 2.3.

Example 2.4: Consider the Fredholm IDE of 3rd order [177], [178].

$$\begin{cases} \xi'''(x) = 1 - e + e^x + \int_0^1 \xi(t)dt\,, \\ \xi(0) = \xi'(0) = \xi''(0) = 1. \end{cases} \tag{2.22}$$

The ES for this problem is $\xi(x) = e^x$ [177], [178] and the AS is $\xi(x) = 1 + x + \frac{x^2}{2} + \sum_{i=1}^{3p} a_i L_{i,3}(x)$.

Example 2.4 involves solving a 3rd order Fredholm type IDE via Haar scale 3 wavelet collocation approach (HWCA). The resulting outcomes are presented in Table 2.7, which reveals a comparison between the "exact solution and the approximated solution" for the resolution level 1.

Table 2.7: Computation of Exact Solution (ES) and Approximated Solution (AS) for Example 2.4.

x	ES [177], [178]	AS	Value of Absolute Error
0.055555556	1.057127745	1.057128982	1.23713E-06
0.166666667	1.181360413	1.181374950	1.45375E-05
0.277777778	1.320192788	1.320234909	4.21202E-05
0.388888889	1.475340615	1.475425767	8.51512E-05
0.500000000	1.648721271	1.648866171	1.44900E-04
0.611111111	1.842477459	1.842700212	2.22752E-04
0.722222222	2.059003694	2.059323918	3.20223E-04
0.833333333	2.300975891	2.301414864	4.38973E-04
0.944444444	2.571384435	2.571965258	5.80823E-04

The table 2.8 suggests that the HWCA method produces more accurate results, despite the small number of "collocation points". The errors (l_2 and l_3) for resolution level 2 are 1.76E-05 and 1.63E-04 respectively. Additionally, Table 2.8 and Figure 2.7 show that the approximated solution converges toward the exact solution. Increasing the no. of "collocation points" can lead to greater accuracy. Furthermore, Figure 2.8 provides

a visual representation of the absolute value of error for resolution level 2. Lastly, Table 2.8 compares the obtained results with the existing methods, demonstrating that the "HWCA method is more effective than other methods".

Table 2.8: Computation of errors for Example 2.4.

j	$l_2 - error$	$E_{max} - error$	$M_{cp} - error$	$M_{cp} - error$ [177]	$l_\infty - error$	$l_\infty - error$ [177]
0	1.35E-03	4.14E-03	2.39E-03	1.10E-03	3.94E-03	1.95E-03
1	1.58E-04	8.44E-04	2.81E-04	2.83E-04	5.81E-04	5.62E-04
2	1.76E-05	1.63E-04	3.15E-05	7.13E-05	7.04E-05	1.50E-04
3	1.96E-06	3.15E-05	3.50E-06	1.78E-05	8.05E-06	3.88E-05
4	2.17E-07	6.06E-06	3.89E-07	4.46E-06	9.03E-07	9.87E-06
5	2.42E-08	1.17E-06	4.32E-08	1.11E-06	1.01E-07	2.48E-06

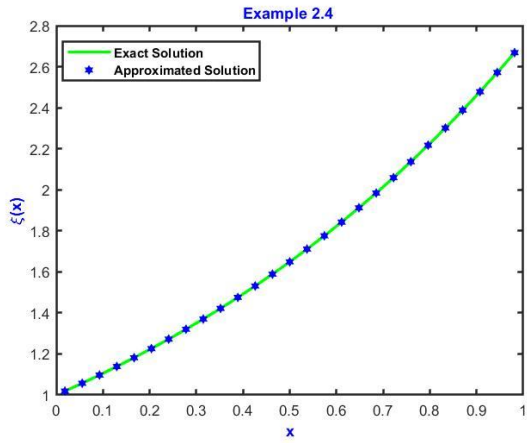

Figure 2.7: Visual analysis of exact solution and approximate solution for Example 2.4.

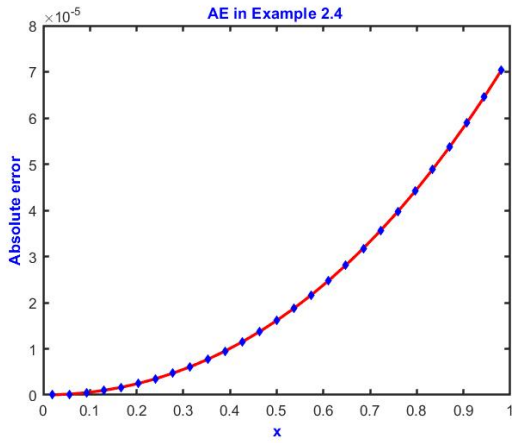

Figure 2.8: Graphical view of AE for example 2.4.

Example 2.5: Consider the Fredholm IDE of 4^{th} order [178].

$$\begin{cases} \xi^{iv}(x) = \frac{1}{4} + (1 - 2ln2)x - \frac{6}{(1+x)^4} + \int_0^1 (x-t)\xi(t)dt\,, \\ \xi(0) = 0,\ \xi'(0) = 1, \xi''(0) = -1, \xi'''(0) = 2. \end{cases} \tag{2.23}$$

The ES obtained from the literature is $\xi(x) = \ln(x+1)$ [178] and the AS is $\xi(x) = x - \frac{x^2}{2} + \frac{x^3}{3} + \sum_{i=1}^{3p} a_i L_{i,4}(x)$.

In Example 2.5, the "Haar scale 3 wavelet collocation approach (HWCA)" is utilized to solve a fourth order Fredholm type integro-differential equation having a difference kernel.

Table 2.9: Computation of Exact solution (ES) and Approximated solution (AS)for Example 2.5.

x	ES [178]	AS	Absolute Error (AE)	AE by using Power series [178]	AE by using Chebyshev series [178]
0.00	0.002055	0.002055	2.94E-14	0	2.70E-08
0.10	0.096058	0.096058	5.46E-09	6.01E-07	3.32E-07
0.20	0.185403	0.185403	4.27E-08	9.14E-06	4.23E-07
0.30	0.264262	0.264262	1.34E-07	6.21E-05	5.25E-06
0.40	0.337354	0.337354	3.02E-07	4.52E-05	2.37E-06
0.50	0.405465	0.405466	5.66E-07	3.36E-05	3.98E-05
0.60	0.471802	0.471803	9.64E-07	2.73E-05	2.17E-05
0.70	0.531596	0.531598	1.48E-06	1.64E-05	1.73E-05
0.80	0.588015	0.588017	2.15E-06	4.30E-04	1.27E-05
0.90	0.643585	0.643588	3.02E-06	2.01E-04	1.11E-05
0.99	0.692118	0.692122	4.00E-06	1.16E-04	3.17E-04

The outcomes obtained are presented in Table 2.9, which provides a comparison between the "exact and approximated solutions" for different points of the domain. The results indicate that the HWCA method yields more accurate results. The $l_2 - error, l_3 - error, M_{cp} - error,$ and $E_{cp} - error$ for resolution level 3 are

3.241298E-05, 1.265906E-04, 1.406562E-05, and 3.564459E-05 respectively. Furthermore, Table 2.10 and Figure 2.9 demonstrate the convergence of the approximated solution towards the exact one. Increasing the number of collocation points can result in greater accuracy. In addition, Figure 2.10 provides a graphical representation of the absolute value of error for resolution level 2. A comparison is also provided in Table 2.9.

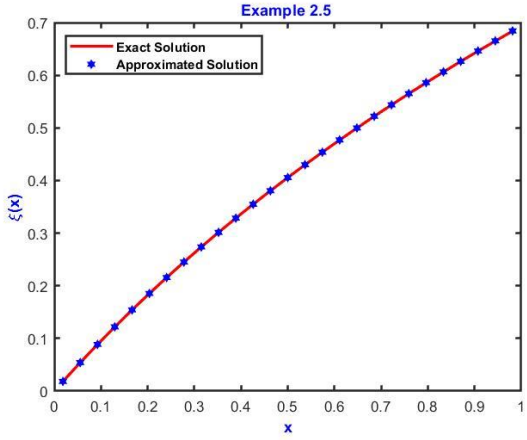

Figure 2.9: Visual analysis of exact solution and approximate solution for Example 2.5.

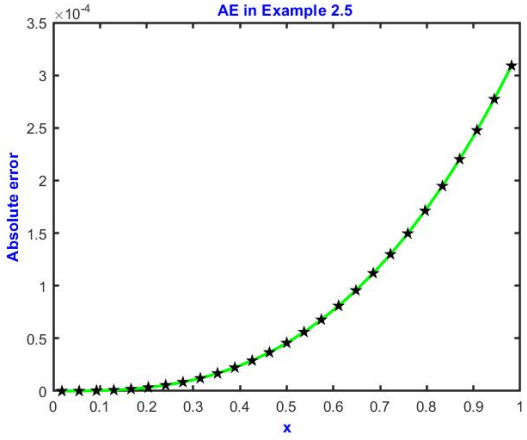

Figure 2.10: Graphical view of AE for Example 2.5.

Table 2.10: Computation of errors for Example 2.5.

j	$l_2 - error$	$E_{max} - error$	$M_{cp} - error$	$l_\infty - error$
2	2.908011E-04	6.556580E-04	1.261814E-04	3.090407E-04
3	3.241298E-05	1.265906E-04	1.406562E-05	3.564459E-05
4	3.602701E-06	2.437114E-05	1.563410E-06	4.007867E-06

Example 2.6: Consider the 8th order IDE of Fredholm type [179] ,[180].

$$\begin{cases} \xi^{8}(x) = -8e^{x} + x^{2} + \xi(x) + \int_{0}^{1} x^{2}\xi'(t)dt\,, \\ \xi(0) = 1, \xi'(0) = 0, \xi''(0) = -1 \;\; \xi'''(0) = -2, \xi^{(4)}(0) = -3, \\ \xi^{(5)}(0) = -4, \xi^{(6)}(0) = -5, \xi^{(7)}(0) = -6. \end{cases} \tag{2.24}$$

The ES obtained from literature is $\xi(x) = (1-x)e^x$ [179] ,[180] and the AS is $\xi(x) = 1 - \frac{x^2}{2} - \frac{x^3}{3} - \frac{x^4}{8} - \frac{x^5}{30} - \frac{x^6}{144} - \frac{x^7}{840} + \sum_{i=1}^{3p} a_i L_{i,8}(x)$.

The 8th order IDE of Fredholm type is solved with the aid of proposed algorithm. Table 2.11 and Figure 2.11 present a comparison among the solution obtained by the proposed method and that of ES for Example 2.6. Table 2.12 presents the calculation of $l_2 - error, l_\infty - error,$ and $E_{max} - error$ for various values of j. It is evident that as the value of j increases, the error decreases. Figure 2.12 displays the graph representing the absolute error for a resolution level of 2. Based on the observation that the estimated solution closely resembles the precise solution, as shown in Figure 2.11, it can be speculated that the suggested technique converges on the exact solution. Increasing the resolution level j can enhance the accuracy of the obtained results.

Table 2.11: Computation of Exact solution (ES) and Approximated solution (AS) for Example 2.6.

x	ES [179] ,[180]	AS	Absolute Error
0.055555556	0.998398426	0.998398426	1.11E-14
0.166666667	0.984467011	0.984467011	4.50E-12
0.277777778	0.953472569	0.953472569	1.91E-10
0.388888889	0.901597043	0.901597041	2.10E-09
0.500000000	0.824360635	0.824360623	1.23E-08
0.611111111	0.716519012	0.716518963	4.90E-08
0.722222222	0.571945471	0.571945319	1.52E-07
0.833333333	0.383495982	0.383495595	3.87E-07
0.944444444	0.142854691	0.142853848	8.43E-07

Table 2.12: Computation of errors for Example 2.6.

j	$l_2 - error$	$l_\infty - error$	$E_{max} - error$
0	2.94E-06	3.94E-06	3.95E-06
1	4.06E-07	8.43E-07	9.41E-07
2	9.13E-08	2.88E-07	3.67E-07

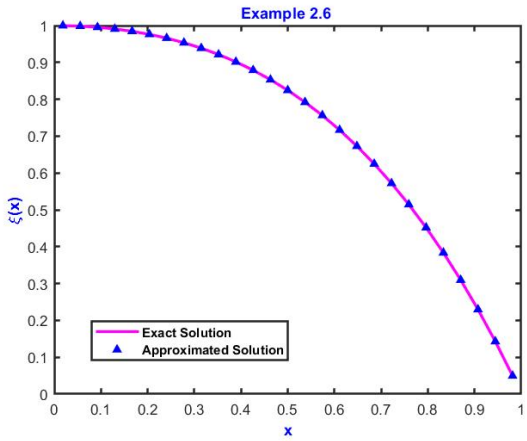

Figure 2.11: Visual analysis of exact solution and approximate solution for Example 2.6.

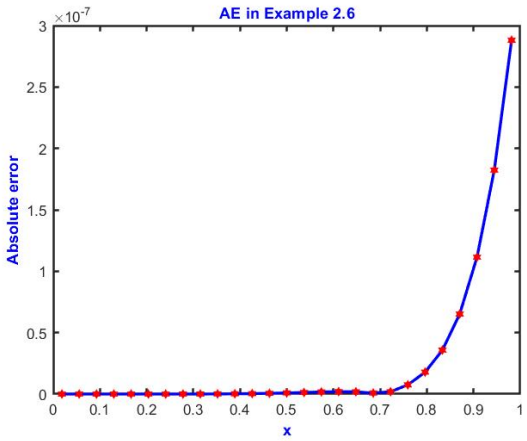

Figure 2.12: Graphical view of AE for Example 2.6.

Example 2.7: Consider the 2nd order IDE of nonlinear Fredholm type [181].

$$\begin{cases} \xi''(x) = e^x + \frac{1}{4}(e^2 - 2)x + \frac{1}{2}\int_0^1 x(t - [\xi(t)]^2)dt\,, \\ \xi(0) = \xi'(0) = 1. \end{cases} \tag{2.25}$$

The ES obtained from the literature is $\xi(x) = e^x$ [181] and the AS is $\xi(x) = 1 + x + \frac{x^2}{2} + \frac{x^3}{6} + \sum_{i=1}^{3p} a_i L_{i,4}(x)$.

Table 2.13: Computation of Exact Solution (ES) and Approximated solution (AS) for Example 2.7.

x	ES [181]	AS	Value of Absolute Error
0.055555556	1.057127745	1.057127763	1.82236E-08
0.166666667	1.181360413	1.181361197	7.83813E-07
0.277777778	1.320192788	1.320196563	3.77495E-06
0.388888889	1.475340615	1.475351195	1.05797E-05
0.500000000	1.648721271	1.648744161	2.28900E-05
0.611111111	1.842477459	1.842519973	4.25135E-05
0.722222222	2.059003694	2.059075082	7.13876E-05
0.833333333	2.300975891	2.301087485	1.11594E-04
0.944444444	2.571384435	2.571549812	1.65377E-04

The nonlinear IDE of Fredholm type is solved in Example 2.7 with the aid of presented technique. The "Quasilinearization technique" is employed to address the nonlinearity present in the problem. The approximated solution obtained by using NHWA for Example 2.7 is compared with true solution in Table 2.13 and Figure 2.13, and it can be examined from table and graph that the obtained findings by using the presented algorithm are strongly in accordance with true solution. Further with increasing the values of 'j' the error gets decreased as presented in Table 2.14, ensuring the convergence of the algorithm. Moreover, the values of $l_\infty - error$ and $M_{cp} - error$ by using this algorithm are less than in comparison with "Scale 2 Haar wavelet" as shown in Table 2.14, demonstrate that the present algorithm produces better results than other methods which attributes to the effectiveness and reliability of the algorithm. The absolute value of error for $j = 2$ is 10^{-4}, the graph for which is shown in Figure 2.14.

Table 2.14: Computation of errors for Example 2.7.

j	$l_2 - error$	$l_\infty - error$	$l_\infty - error$ [181]	$E_{max} - error$	$M_{cp} - error$	$M_{cp} - error$ in [181]
0	3.347E-04	1.006E-03	7.0423E-03	1.026E-03	3.422E-04	4.3062E-03
1	4.062E-05	1.653E-04	1.9468E-03	2.176E-04	4.188E-05	1.0794E-03
2	4.556E-06	2.074E-05	5.1227E-04	4.231E-05	4.701E-06	2.7005E-04
3	5.068E-07	2.397E-06	1.3141E-04	8.152E-06	5.229E-07	6.7524E-05
4	5.632E-08	2.698E-07	3.3281E-05	1.569E-06	5.811E-08	1.6881E-05
5	6.257E-09	3.011E-08	8.3724E-06	3.019E-07	6.457E-09	4.2197E-06
6	6.953E-10	3.351E-09	2.0983E-06	5.811E-08	7.175E-10	1.0544E-06

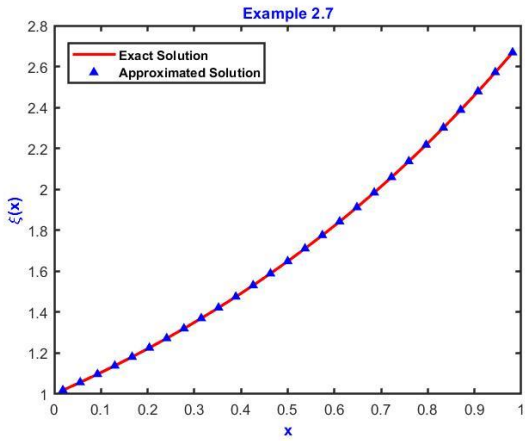

Figure 2.13: Visual analysis of exact solution and approximate solution for Example 2.7.

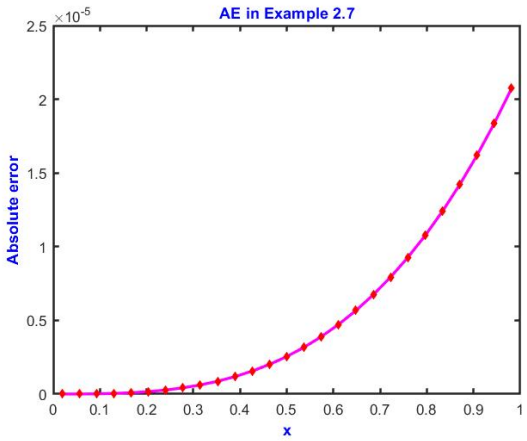

Figure 2.14: Graphical view of AE for Example 2.7.

Example 2.8: Consider the 2nd order IDE of nonlinear Volterra type [181].

$$\begin{cases} \xi''(x) = \sinh(x) + \frac{1}{2}(x - \cosh(x)\sinh(x)) + \int_0^x [\xi(t)]^2 dt, \\ \xi(0) = 0,\ \xi'(0) = 1. \end{cases} \tag{2.26}$$

The ES obtained from literature is $\xi(x) = \sinh(x)$ [181] and the AS is $\xi(x) = x + \sum_{i=1}^{3p} a_i L_{i,3}(x)$.

Table 2.15: Computation of Exact Solution (ES) and Approximated solution (AS) for Example 2.8.

x	ES [181]	AS	Value of Absolute Error
0.055555556	0.055584138	0.055584178	3.97028E-08
0.166666667	0.167439344	0.167439816	4.72403E-07
0.277777778	0.281363830	0.281365799	1.96947E-06
0.388888889	0.398765519	0.398770775	5.25596E-06
0.500000000	0.521095305	0.521106387	1.10819E-05
0.611111111	0.649864989	0.649885225	2.02359E-05
0.722222222	0.786665954	0.786699517	3.35629E-05
0.833333333	0.933188841	0.933240829	5.19875E-05
0.944444444	1.091244435	1.091320980	7.65451E-05

Example 2.8 involves the resolution of a nonlinear Volterra type integro-differential equation. To tackle the nonlinearity, the Quasilinearization method is employed. This technique involves a series of linear approximations that converge to the nonlinear solution. Through the use of this method, the solution to the nonlinear equation is obtained. Table 2.15 and Figure 2.15 compare the approximated solution obtained by applying NHWA to Example 2.8 with the actual solution. The results indicate that the presented algorithm produces accurate approximations for various resolutions. The algorithm's convergence is also evident from the reduction in error as the values of j increases, as demonstrated in Table 2.16. Furthermore, the values of $l_\infty - error$ and $M_{cp} - error$ are lower than those of the traditional Haar wavelet method as shown in Table 2.16. Figure 2.16 presents the graph of absolute error.

Table 2.16: Computation of errors for Example 2.8.

j	$l_2 - error$	$l_\infty - error$	$l_\infty - error$ in [181]	$E_{max} - error$	$M_{cp} - error$	$M_{cp} - error$ [181]
0	4.703E-04	4.953E-04	4.783E-03	5.088E-04	1.696E-04	3.102E-03
1	5.304E-05	7.654E-05	1.285E-03	1.012E-04	1.948E-05	7.801E-04
2	5.905E-06	9.543E-06	3.326E-04	1.956E-05	2.173E-06	1.953E-04
3	6.563E-07	1.102E-06	8.459E-05	3.766E-06	2.416E-07	4.886E-05
4	7.292E-08	1.240E-07	2.138E-05	7.249E-07	2.685E-08	1.222E-05
5	8.102E-09	1.384E-08	5.431E-06	1.395E-07	2.983E-09	3.067E-06
6	9.003E-10	1.540E-09	1.425E-06	2.685E-08	3.314E-10	7.776E-07

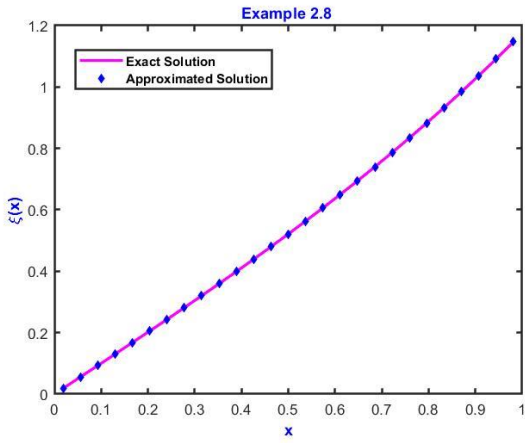

Figure 2.15: Visual analysis of exact solution and approximate solution for Example 2.8.

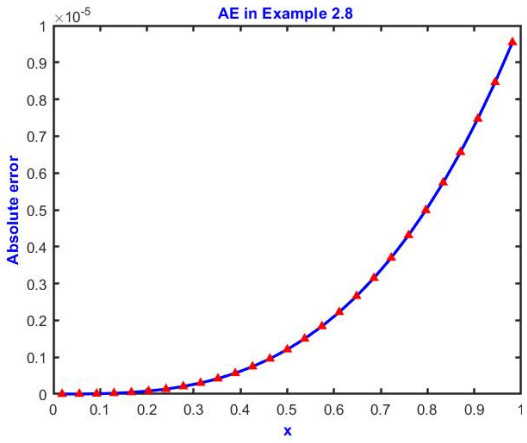

Figure 2.16: Graphical view of AE for Example 2.8.

Example 2.9: Consider the 2nd order IDE of nonlinear mixed Volterra Fredholm type [181].

$$\begin{cases} \xi''(x) + [\xi(x)]^2 = \mathrm{e}^{2x} + \frac{5}{4}e^x + \frac{1}{2}e - \frac{3}{2} - \frac{1}{4}\int_0^x \xi(t)dt - \frac{1}{2}\int_0^1 \xi(t)dt, \\ \xi(0) = \xi'(0) = 1. \end{cases} \quad (2.27)$$

The ES obtained from the literature is $\xi(x) = \mathrm{e}^x$ [181] and the AS is $\xi(x) = 1 + x + \sum_{i=1}^{3p} a_i L_{i,2}(x)$.

Example 2.9 deals with the solution of a mixed Volterra-Fredholm type nonlinear IDE. The Quasilinearization method is utilized to address the nonlinearity in Example 2.9. This approach entails a sequence of linear approximations that converge towards the nonlinear solution, ultimately leading to the solution of the "nonlinear equation". The accuracy of the presented algorithm is evaluated by comparing the approximated solution obtained through NHWA with the actual solution in Table 2.17 and Figure 2.17, indicating precise approximations for varying resolutions. The convergence of the algorithm is evident from the decreasing error with increasing values of j, as shown in Table 2.18. Moreover, the algorithm's performance is superior to that of the traditional "Haar wavelet method" as demonstrated by the $l_\infty - error$ and $M_{cp} - error$ values in Table 2.18. The graph of absolute error is shown in Figure 2.18.

Table 2.17: Computation of Exact solution (ES) and Approximated solution (AS) for Example 2.9.

x	ES [181]	AS	Value of Absolute Error
0.055555556	1.057127745	1.057186380	5.86353E-05
0.166666667	1.181360413	1.181535353	1.74940E-04
0.277777778	1.320192788	1.320483471	2.90683E-04
0.388888889	1.475340615	1.475742911	4.02295E-04
0.500000000	1.648721271	1.649226745	5.05474E-04
0.611111111	1.842477459	1.843072726	5.95267E-04
0.722222222	2.059003694	2.059669945	6.66251E-04
0.833333333	2.300975891	2.301688745	7.12855E-04
0.944444444	2.571384435	2.572114267	7.29832E-04

Table 2.18: Computation of errors for Example 2.9.

j	$l_2 - error$	$l_\infty - error$	$l_\infty - error$ in [181]	$E_{max} - error$	$M_{cp} - error$	$M_{cp} - error$ [181]
0	2.600E-03	6.349E-03	4.015E-03	7.975E-03	2.658E-03	2.805E-03
1	2.877E-04	7.298E-04	1.030E-03	1.541E-03	2.965E-04	7.041E-04
2	3.195E-05	8.120E-05	2.603E-04	2.967E-04	3.296E-05	1.766E-04
3	3.550E-06	9.023E-06	6.671E-05	5.710E-05	3.663E-06	4.467E-05
4	3.944E-07	1.002E-06	1.831E-05	1.099E-05	4.070E-07	1.169E-05
5	4.383E-08	1.114E-07	6.260E-06	2.115E-06	4.522E-08	3.485E-06
6	4.870E-09	1.237E-08	3.270E-06	4.070E-07	5.025E-09	1.488E-06

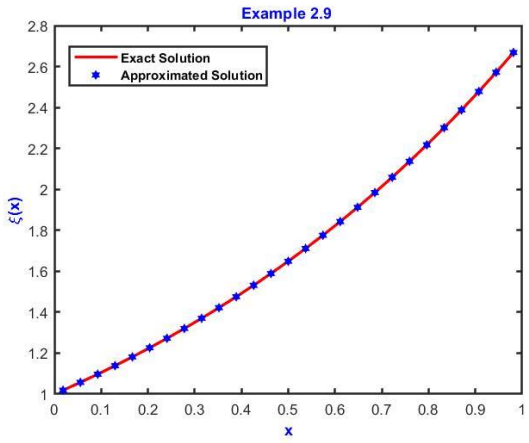

Figure 2.17: Visual analysis of exact solution and approximate solution for Example 2.9.

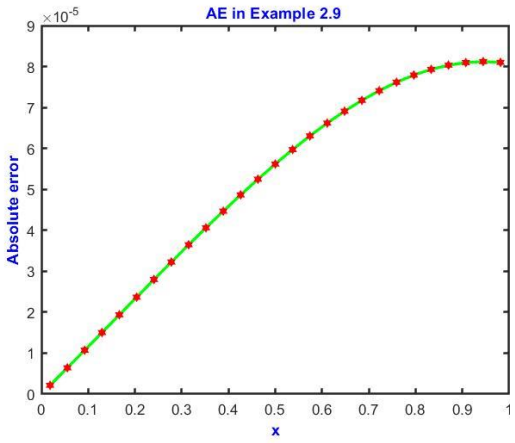

Figure 2.18: Graphical view of AE for Example 2.9.

Example 2.10: Consider the 2nd order IDE of nonlinear Fredholm type [182].

$$\begin{cases} \xi''(x) = e^x - 1 + \int_0^1 e^{-4t}[\xi(t)]^2[\xi'(t)]^2 dt\,, \\ \xi(0) = \xi'(0) = 1. \end{cases} \tag{2.28}$$

The ES obtained from the literature is $\xi(x) = \mathrm{e}^x$ [182] and the AS is $\xi(x) = 1 + x + \frac{x^2}{2} + \sum_{i=1}^{3p} a_i L_{i,3}(x)$.

In this specific example, the Leibnitz rule, which is introduced and explained in chapter 1 of the thesis, is applied in order to transform the IDE into the relevant differential equation. After the differential equation has been found, it is easily resolved by employing the NHWA. In Table 2.19 and Figure 2.19, the approximated solution obtained by using NHWA for Example 2.10 is compared with the actual solution, and it can be seen from the table and graph that the obtained findings using the presented algorithm are in strong agreement with the actual solution. As shown in Table 2.20, as the value of j increases, the error decreases, ensuring the convergence of the algorithm. Moreover, the values of $l_\infty - error$ using this algorithm are less than when compared to the method used by Siraj-ul-islam et al., [182] as shown in Table 2.20. This demonstrates that the present algorithm produces better results than other methods, which contributes to the algorithm's efficacy. Figure 2.20 illustrates the graph for absolute error.

Table 2.19: Computation of Exact solution (ES) and Approximated solution (AS) for Example 2.10.

x	ES [182]	AS	Value of Absolute Error
0.055555556	1.057127745	1.057128976	1.23123E-06
0.166666667	1.181360413	1.181374791	1.43780E-05
0.277777778	1.320192788	1.320234170	4.13817E-05
0.388888889	1.475340615	1.475423740	8.31248E-05
0.500000000	1.648721271	1.648861864	1.40593E-04
0.611111111	1.842477459	1.842692349	2.14890E-04
0.722222222	2.059003694	2.059310939	3.07245E-04
0.833333333	2.300975891	2.301394926	4.19035E-04
0.944444444	2.571384435	2.571936233	5.51798E-04

Table 2.20: Computation of errors for Example 2.10.

j	$l_2 - error$	$l_\infty - error$	$l_\infty - error$ in [182]	$E_{max} - error$	$M_{cp} - error$
0	1.293E-03	3.762E-03	1.32E-01	3.966E-03	1.322E-03
1	1.504E-04	5.517E-04	2.89E-02	8.057E-04	1.550E-04
2	1.679E-05	6.678E-05	7.76E-03	1.559E-04	1.733E-05
3	1.867E-06	7.630E-06	2.04E-03	3.003E-05	1.926E-06
4	2.075E-07	8.557E-07	5.23E-04	5.781E-06	2.141E-07
5	2.305E-08	9.537E-08	1.33E-04	1.112E-06	2.379E-08
6	2.561E-09	1.060E-08	3.34E-05	2.141E-07	2.643E-09

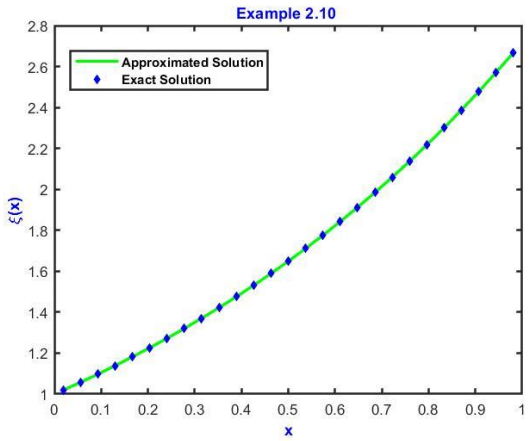

Figure 2.19: Visual analysis of exact solution and approximate solution for Example 2.10.

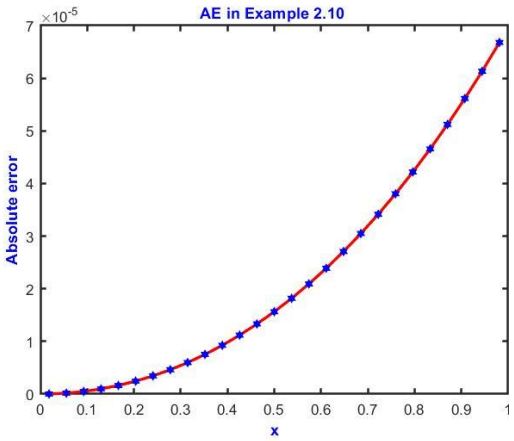

Figure 2.20: Graphical view of AE for Example 2.10.

Example 2.11: Consider the 4th order IDE of nonlinear Volterra type [182].

$$\begin{cases} \xi^{(iv)}(x) = 1 + \int_0^x e^{-t}[\xi(t)]^2 dt, \\ \xi(0) = \xi'(0) = \xi''(0) = \xi'''(0) = 1. \end{cases} \tag{2.29}$$

The ES obtained from literature is $\xi(x) = \mathrm{e}^x$ [182] and the AS is $\xi(x) = 1 + x + \frac{x^2}{2} + \frac{x^3}{6} + \frac{x^4}{24} + \sum_{i=1}^{3p} a_i L_{i,5}(x)$.

Example 2.11 involves the resolution of a fourth-order nonlinear Volterra-type integral-differential equation (IDE) with the aid of NHWA. To handle the nonlinearity, Quasilinearization is employed, followed by the application of the Leibniz rule to convert the IDE to a corresponding differential equation. The obtained differential equation is then solved using NHWA. For the purpose of providing a more comprehensive understanding of the accuracy of the results, the method which has been proposed yields results that are shown in the form of graphs and tables. Both Figure 2.21 and Table 2.21 show the clear significant agreement that can be observed among the exact and estimate solutions. Table 2.22 presents a comparison of obtained findings using the present approach with those obtained using alternative approaches described in the most recent research. The absolute error value at $j = 2$ is 10^{-6}, as depicted in Figure 2.22. Additionally, various errors are computed and displayed in Table 2.22,

demonstrating a reduction in error with an increase in the dilation factor, providing evidence of the method's convergence.

Table 2.21: Computation of Exact solution (ES) and Approximated solution (AS) for Example 2.11.

x	ES [182]	AS	Value of Absolute Error
0.055555556	1.057127745	1.057127745	2.10782E-10
0.166666667	1.181360413	1.181360444	3.12776E-04
0.277777778	1.320192788	1.320193045	2.56800E-07
0.388888889	1.475340615	1.475341627	1.01138E-06
0.500000000	1.648721271	1.648724082	2.81175E-06
0.611111111	1.842477459	1.842483828	6.36896E-06
0.722222222	2.059003694	2.059016296	1.26021E-05
0.833333333	2.300975891	2.300998545	2.26537E-05
0.944444444	2.571384435	2.571422342	3.79070E-05

Table 2.22: Computation of errors for Example 2.11.

j	$l_2 - error$	$l_\infty - error$	$l_\infty - error$ in [182]	$E_{max} - error$	$M_{cp} - error$
0	6.663E-05	2.029E-04	1.13E-04	2.043E-04	6.813E-05
1	8.673E-06	3.790E-05	3.83E-05	4.645E-05	8.941E-06
2	9.802E-07	4.936E-06	1.01E-05	9.102E-06	1.011E-06
3	1.091E-07	5.775E-07	2.56E-06	1.755E-06	1.125E-07
4	1.212E-08	6.527E-08	6.41E-07	3.378E-07	1.251E-08
5	1.347E-09	7.293E-09	1.60E-07	6.502E-08	1.390E-09
6	1.497E-10	8.119E-10	4.01E-08	1.251E-08	1.544E-10

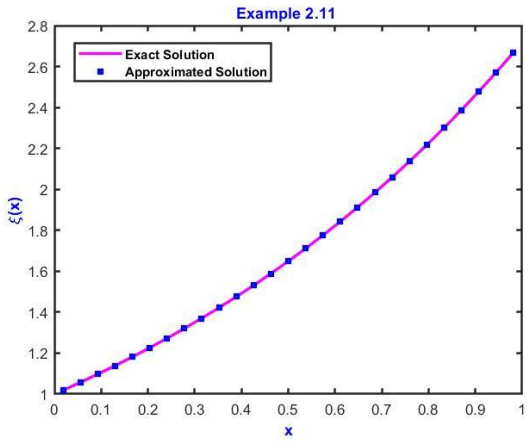

Figure 2.21: Visual analysis of exact solution and approximate solution for Example 2.11.

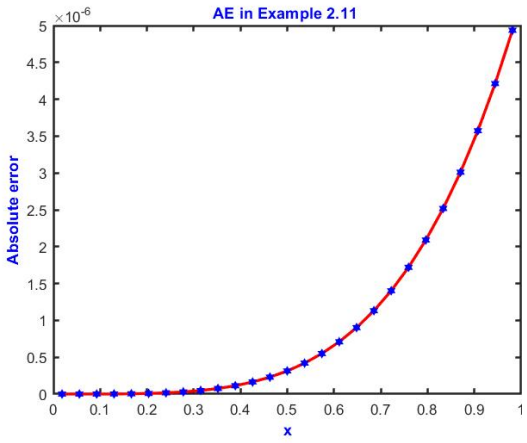

Figure 2.22: Graphical view of AE for Example 2.11.

Example 2.12: Consider the 1st order IDE of nonlinear mixed Volterra-Fredholm type [182].

$$\begin{cases} \xi'(x) + \xi(x) = f(x) + \frac{1}{4}\int_0^1 t[\xi(t)]^3 dt - \frac{1}{2}\int_0^x x[\xi(t)]^2 dt, \\ \xi(0) = 0. \end{cases} \tag{2.30}$$

where $f(x) = \frac{1}{10}x^6 + x^2 + 2x - \frac{1}{32}$. The ES obtained from literature is $\xi(x) = x^2$ [182] and the AS is $\xi(x) = x^2 + \sum_{i=1}^{3p} a_i L_{i,3}(x)$.

The last example under consideration is a first-order nonlinear mixed Volterra-Fredholm type IDE. In Example 2.12, NHWA is applied to the solution of a nonlinear IDE.

Quasilinearization is used to deal with the nonlinearity, and then the Leibniz method is used to transform the IDE into a differential equation. The resulting differential equation is solved by the NHWA method. The proposed method produces results that are displayed in the form of graphs and tables with the aim of providing a more comprehensive understanding of the accuracy of the results. The strong agreement between the exact and estimate solutions is displayed in both Figure 2.23 and Table 2.23. The findings from the current algorithm are compared to those from other methods that have been described in recent studies in Table 2.23. At $j = 0$, the absolute value of the error is 10^{-5}, as shown in Figure 2.24.

Table 2.23: Computation of Exact solution (ES) and Approximated solution (AS) for Example 2.12.

x	ES [182]	AS	Absolute Error	AE [183]	AE [184]	AE [182]
0.1	0.016803	0.016803	3.585E-08	2.6E-04	1.7E-04	1.2 E-04
0.2	0.057956	0.057954	1.159E-06	4.9E-04	2.5E-04	1.7 E-04
0.3	0.099108	0.099103	5.008E-06	7.0E-04	2.6E-04	1.5 E-04
0.4	0.181412	0.181388	2.399E-05	8.7E-04	1.9E-04	5.4 E-05
0.5	0.250000	0.249948	5.154E-05	1.0E-04	4.1E-05	1.2 E-04
0.6	0.373456	0.373339	1.172E-04	1.1E-03	2.0E-04	1.4 E-05
0.7	0.521604	0.521429	1.752E-04	9.7E-03	2.8E-04	7.3 E-05
0.8	0.634087	0.633941	1.461E-04	8.3E-04	2.8E-04	5.2 E-05
0.9	0.823388	0.823610	2.218E-04	1.8E-04	2.0E-04	4.8 E-05

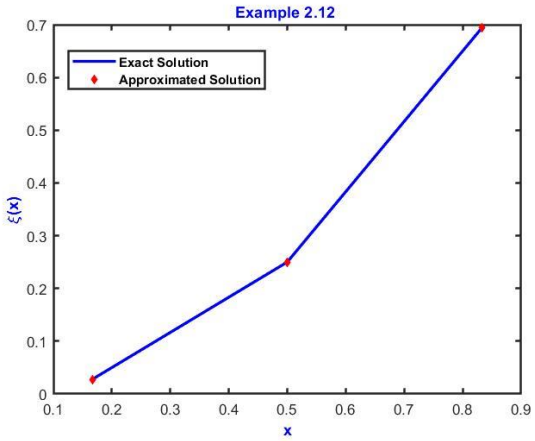

Figure 2.23: Visual analysis of exact solution and approximate solution for Example 2.12.

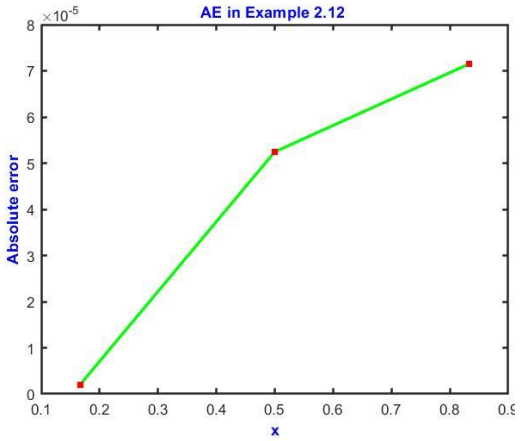

Figure 2.24: Graphical view of AE for Example 2.12.

2.4 Conclusion

A numerical algorithm has been introduced based on “Haar scale 3 wavelets” for calculating the approximate solution of Volterra IDES, Fredholm IDES, and Volterra Fredholm IDES. The integro-differential equations are converted to the corresponding linear algebraic system of equations which are then solved by “the Gauss Elimination Method”. Nonlinearity in the problem is tackled by the Quasilinearization technique. The Haar scale 3 wavelet collocation algorithm is applied to twelve different types of numerical examples found in the literature for which the exact solutions are known. The obtained results are compared with the already existing results available in the literature. From the results obtained by using HWCA, it could be observed that by increasing the number of “collocation points”, approximated solutions converge to the exact solutions. All computational tasks are performed using “MATLAB software”. The following is an overview of the primary benefits of NHWA.

1. The effectiveness and execution of NDHWCA with the use of MATLAB software can be easily achieved.

2. By increasing the dilation factor, the error becomes lesser proving the convergence of the method.

3. The proposed algorithm converges faster than the Haar scale 2 wavelets.

4. As compared to other known methods, the NDHWCA has been shown to yield better results that are more accurate.

Chapter 3.

Numerical Solution of Integral Equations by Using Scale 3 Haar Wavelets Collocation Approach

3.1 Introduction

Integral equations (IEs) are mathematical equations that involve an unknown function and an integral involving that function. They are widely used in many areas of science and engineering, including physics, engineering, mathematics, and economics, to model a wide range of phenomena. Integral equations have found applications in fields such as fluid mechanics, acoustics, signal processing, and many others. The study of integral equations is an important area of research in mathematics. Over numerous years, significant advancements have been made in the field of integral equations, with contributions from the most famous mathematicians, including Laplace, Fourier, Abel, and others. The study of nonlinear integral equations is often more challenging than that of linear integral equations, as they often do not have exact solutions and require numerical methods to solve them. Integral equations can be solved using a variety of methods, including the Galerkin method, the collocation method, and the boundary element method. These methods involve approximating the unknown function by a simpler function that can be evaluated numerically. The selection of the method relies on the specific problem and the properties of the integral equation. Integral equations have a wide range of applications in mathematics, physics, engineering, and other fields. Here are some of the most common applications of integral equations [185], [186].

Heat transfer: Integral equations are used to model the diffusion of heat in various materials, including solids and fluids. They are useful for studying problems such as heat transfer through walls and the cooling of electronic devices.

Fluid mechanics: Integral equations are used to model the flow of fluids in a wide range of applications, including aerodynamics, hydrodynamics, and oceanography.

They are particularly useful for problems involving complex geometries, where other methods may be difficult to apply.

Structural analysis: Integral equations are used to analyze the behaviour of structures, including buildings, bridges, and other engineering structures. They are useful for studying problems such as stress distribution and deformation under load.

Quantum mechanics: Integral equations are used in the study of quantum mechanics, where they are used to solve the Schrödinger equation for the wave function of a quantum system. They are particularly useful for problems involving multiple particles or complex interactions.

Financial engineering: Integral equations are used in the modelling of financial markets, where they are used to solve pricing equations for various financial instruments. They are particularly useful for problems involving stochastic processes and multiple assets.

Biology: Integral equations are used to model various biological processes, such as the spread of diseases and the growth of populations.

Signal processing: Integral equations are used in the analysis of signals, where they are used to solve various inverse problems, such as image reconstruction and deconvolution. They are particularly useful for problems involving noise and other sources of uncertainty.

3.2 Need for the Solution of Integral Equations

Integral equations are often difficult to solve analytically, particularly for complex problems involving non-linear operators or complicated geometries. In many cases, the only way to obtain a solution is through numerical methods, which involve approximating the unknown function using a discrete set of points or basis functions. Integral equations often require numerical solutions for a variety of reasons such as

Non-analytic solutions: Many integral equations do not have analytic solutions, particularly for problems involving complex geometries or non-linear operators.

Numerical methods can provide an accurate solution even when an analytic solution is not available.

High dimensionality: Integral equations often involve high-dimensional integrals, which can be difficult to evaluate analytically. Numerical methods can provide an efficient way to approximate these integrals using discrete points or basis functions.

Computational efficiency: Numerical methods can be much faster and more efficient than analytical methods for solving integral equations, particularly for problems with a large number of variables or a high degree of complexity.

Flexibility: Numerical methods are often more flexible than analytical methods, allowing for more complex geometries and boundary conditions to be modelled. This can be particularly important in engineering and scientific applications, where the accuracy of the model is critical.

Error analysis: Numerical methods can provide a way to estimate the error in the solution, which is often not possible with analytical methods. This can help to ensure that the solution is accurate and reliable.

Several researchers are currently studying the numerical techniques for solving integral equations (IEs) of both linear as well as nonlinear types. In 2002, K. Maleknejad [187] proposed the use of Legendre wavelets to solve 2nd kind of IEs. In 2004, K. Maleknejad and Y. Mahmoudi [188] developed a hybrid method that combined Taylor functions and block-pulse functions to solve the Fredholm-type IEs. In 2005, K. Maleknejad et al. [189] presented an algorithm that employed block-pulse functions to solve systems of IEs. In 2006, K. Maleknejad and F. Mirzaei [190] utilized rationalized Haar wavelets to solve linear IEs of the Fredholm type. The approach involved converting the integral equation into a system of linear algebraic equations, which was solved using iterative methods. The authors suggested that this method could be applied to approximate solutions for other problems. In 2005, Y. Mahmoudi [191] employed Legendre wavelets to solve second-order nonlinear integral equations. A Chebyshev collocation approach was introduced by A. Dascigolu and H. C. Yaslan [192] in the same year to approximate solutions for nonlinear integral equations. In 2006, S. A. Yousefi [193]

developed a numerical method for approximating solutions to Abel's integral equations. K. Maleknejad et al. [194] solved linear and nonlinear IEs of the Volterra type using orthogonal Chebyshev polynomials in 2007. K. Maleknejad [195] proposed the orthogonal triangular function (OTF) method in 2009 to solve mixed Volterra Fredholm type integral equations. The OTF method used collocation with the OTF as the basis. In 2010, A. Mohsen and M. El-Gamel [196] presented an algorithm based on sinc bases for solving integral equations of the Volterra type. This algorithm reduced the Volterra integral equation to corresponding algebraic equations by applying the properties of sinc bases. In 2011, K. Maleknejad et al. [197] introduced a novel method for approximating integral equations of Volterra type using Bernstein's approximation. The proposed technique is claimed to require less computation and provide better results than existing methods. In the same year, S. Sohrabi [198] presented a numerical method based on Chebyshev wavelets approximation (CWA) for approximating the solution of Abel's integral equations, and compared the results with the block pulse functions (BPF) method. The obtained results using CWA were observed to be more accurate than BPF. Also in 2011, A. Shahsavaran [199] approximated the solution of nonlinear IEs of mixed Fredholm Volterra type using the block pulse function (BPF) method. In the same year, K. Maleknejad and E. Najafi [200] solved IEs of the Volterra type by implementing the Quasilinearization and collocation technique. In 2011, I. Aziz et al. [201] developed a numerical algorithm, called the quadrature rule, for approximating double and triple integrals with variable limits of integration. In 2012, E. Lin and Y. Al-Jarrah [202] applied the Coiflet wavelet to the linear IEs of the Fredholm type. In the same year, Z. Chen and W. Jiang [203] implemented the Taylor expansion method for finding the approximate solution of the IEs of the Volterra Fredholm type. The proposed method was claimed to have several advantages over other existing methods and provided better results. In 2014, A. Setia [204] devised an algorithm for approximating singular integral equations of Cauchy type using Bernstein polynomials. In 2015, S. Bazm [205] constructed the Bernoulli polynomial method for solving IEs. In the same year, I. Singh and S. Kumar [206] described the Haar wavelet approach for finding the numerical solution of the nonlinear IEs of the Volterra type. In 2019, Y.H. Youssvi and R.M. Hafeez [207] implemented the hybrid of shifted Chebyshev collocation approach and Gauss Chebyshev nodes for approximating IEs of Volterra

Fredholm type. In the same year, S.H. Varmazayar and Z. Masouri [208] used the triangular function for calculating linear IEs of Fredholm type and Volterra type. In 2020, S. Amiri et al. [209] solved integral equations using a piecewise cosine basis. In 2021, F. Usta [210] constructed an algorithm for solving the integral equation of the Volterra type with fractional order using the Bernstein approximation technique. In 2022, D. Berrera et al. [211] used the Nyström method along with Gaussian quadrature for solving IEs of Fredholm type and Hammerstein integral equations. Based on a review of the available literature, it has been observed that wavelet methods have not been widely used for solving IEs, and there is a lack of research on the use of Scale 3 Haar Wavelets for this purpose. The primary objective of this study is to develop an algorithm that utilizes a non-dyadic Haar wavelet approach to approximate the solution of both linear and nonlinear Volterra and Fredholm IEs.

3.3 Scale 3 Haar Wavelet Collocation Approach

In this section, an algorithm has been designed by utilizing scale 3 Haar wavelets for approximating the solutions of a variety of IEs. The major categories of IEs addressed by the algorithm are:

Nonhomogeneous linear Volterra IEs of 2nd kind

$$\xi(x) = g(x) + \int_0^x K(x,t)\xi(t)dt. \tag{3.1}$$

Nonhomogeneous linear Fredholm IEs of 2nd kind

$$\xi(x) = g(x) + \int_0^1 K(x,t)\xi(t)dt. \tag{3.2}$$

Nonhomogeneous nonlinear Volterra IEs of 2nd kind

$$\xi(x) = g(x) + \int_0^x K(x,t)\xi(t)^n\, dt \;\; where\, n \geq 2. \tag{3.3}$$

Nonhomogeneous nonlinear Fredholm IEs of 2nd kind

$$\xi(x) = g(x) + \int_0^x K(x,t)\xi(t)^n \, dt \;\; where \; n \geq 2. \tag{3.4}$$

Nonhomogeneous mixed Volterra-Fredholm IEs of 2nd kind

$$\xi(x) = g(x) + \int_0^x K_1(x,t)\xi(t)dt + \int_0^1 K_2(x,t)\xi(t) \, dt. \tag{3.5}$$

Here $g(x)$ and the kernel function $K(x,t)$ are already given, the main aim is to calculate the unknown function $\xi(x)$. Scale 3 Haar wavelet collocation approach has been introduced for the interval $[0,1]$. The unknown function that has to be determined is approximated using "Haar scale 3 functions" and then integrals are calculated by the process of integration.

3.3.1 Approximation of solution

Utilizing the characteristics of scale 3 Haar wavelets, it is possible to represent any function belonging to the space of square integrable functions, $l_2(\mathbb{R})$ as a linear combination of Haar wavelets,

$$\begin{aligned} \xi(x) &= \sum_{i=0}^{\infty} c_i \, \psi_i(x) \\ &= c_1\psi_1(x) + \sum_{even \; i} c_i \, \phi^1\left(3^j x - k\right) + \sum_{odd \; i} c_i \, \phi^2\left(3^j x - k\right), \end{aligned} \tag{3.6}$$

where $c_i's$ are unknown wavelet coefficients, which will be calculated by the presented algorithm. By considering only finite $3p$ terms for computation,

$$\xi(x) = \xi(3p) = \sum_{i=0}^{3p} c_i \, \psi_i(x), \tag{3.7}$$

Now, for approximating the solution of equation $(3.1) - (3.5)$ consider,

$$\xi(x) = \sum_{i=0}^{3p} c_i \, \psi_i(x), \tag{3.8}$$

Integrating equation (3.8) from 0 to x, we have

$$\int_0^x \xi(x)dx = \sum_{i=0}^{3p} c_i\, L_{i,\ 1}(x);\ \ where\ L_{i,\ 1}(x) = \int_0^x \psi_i(x)dx, \qquad (3.9)$$

Again, integrating equation (3.9) from 0 to x, we have

$$\int_0^x \int_0^x \xi(x)dx\,dx = \sum_{i=0}^{3p} c_i\, L_{i,\ 2}(x):\ where\ L_{i,\ 2}(x) = \int_0^z L_{i,\ 1}(x)dx, \quad (3.10)$$

and so, it goes. By applying the substitution and inserting collocation points, a set of $N \times N$ algebraic equations can be obtained from the provided integral equations, which can be solved by any linear iterative technique. The Thomas algorithm was used to solve this linear system and obtain the undetermined Haar coefficients. By putting these coefficients in the given integral equation, a solution at the collocation points can be obtained. The procedure is explained in detail for Example 3.1.

Note: In the case of nonlinear integral equations, the Quasilinearization method is employed to linearize the nonlinear component. Then, the same approach is used to obtain the solution at various points within the domain.

3.4 Numerical Examples and Analysis of Errors

In this section, the effectiveness and precision of the proposed algorithm have been evaluated through its application to ten distinct examples. A comparison between the outcomes of this method and the results reported in previous research has been performed. In order to validate the accuracy of the proposed approach, the maximum absolute error, $M_{cp} - error$, $l_2 - error$, $E_{max} - error$, and $l_\infty - error$ has been calculated in MATLAB. The following mathematical expressions quantify various errors. Let ξ_{ap} denote the approximate solution and ξ_{ex}denote the exact solution at collocation points, then;

$$M_{cp} - error = \sqrt{\frac{1}{3N}\sum_{i=1}^{3p}\left|\xi_{ex}(x_m) - \xi_{ap}(x_m)\right|^2},$$

$$l_2 - error = \frac{\sqrt{\sum_{i=1}^{3p}\left|\xi_{ex}(x_m) - \xi_{ap}(x_m)\right|^2}}{\sum_{i=1}^{3p}|\xi_{ex}(x_m)|^2},\ E_{max} - error = \sqrt{\sum_{i=1}^{3p}\left|\xi_{ex}(x_m) - \xi_{ap}(x_m)\right|^2},$$

$$l_\infty - error = \max\left|\xi_{ex}(x_m) - \xi_{ap}(x_m)\right|, Absolute\ error = \left|\xi_{ex}(x_m) - \xi_{ap}(x_m)\right|.$$

Example 3.1: Consider Volterra IE of 2nd kind [212],

$$\xi(x) = x + \int_0^x (t - x)\xi(t)dt. \tag{3.11}$$

Let

$$\xi(x) = \sum_{i=1}^{3p} c_i\, \psi_i(x), \tag{3.12}$$

Integrating equation (3.12) from 0 to x, we have

$$\int_0^x \xi(x)dx = \sum_{i=0}^{3p} c_i\, L_{i,\ 1}(x);\ \ where\ L_{i,\ 1}(x) = \int_0^x \psi_i(x)dx, \tag{3.13}$$

Again, integrating equation (3.13) from 0 to x, we have

$$\int_0^x \int_0^x \xi(x)dx\,dx = \sum_{i=0}^{3p} c_i\, L_{i,\ 2}(x);\ \ where\ L_{i,\ 2}(x) = \int_0^z L_{i,\ 1}(x)dx, \tag{3.14}$$

Substituting equation $(3.12) - (3.14)$ in equation (3.11)

$$\sum_{i=1}^{3p} c_i\, \psi_i(x) = z - \sum_{i=0}^{3p} c_i\, L_{i,\ 2}(x),$$

$$\sum_{i=1}^{3p} c_i \left(\psi_i(x) + L_{i,\ 2}(x)\right) = z. \tag{3.15}$$

which is the required $AX = B$ form. The exact solution found from literature for Example 3.1 is $\xi(x) = sin\,(z)$ [212]. The Volterra integral equation presented in Example 3.1 has been solved by using Scale 3 Haar wavelet collocation method. The results obtained by using the presented method are tabulated in Table 3.1 which clearly explains the comparability among the exact and approximated solution for level of resolution 1. Table 3.1 depicts that NHWCA provides more accurate results for the small number of collocation points. $l_2 - error$, $l_\infty - error$, and $E_{max} - error$ for

Volterra integral equation (for the level of resolution 1) are 9.76E − 04, 7.66E − 04, and 1.53E − 03 respectively. From Table 3.2, Figure 3.1, and Figure 3.2, it can be observed that approximated solution converges to the exact solution. From Table 3.2, we can observe that by increasing the number of collocation points, accuracy of the solution gets better.

Table 3.1: Computation of Exact solution and Approximated solution for Example 3.1.

x	Exact solution [212]	Approximated solution	Absolute Error
0.055555556	0.055526982	0.055469954	5.702822970E-05
0.166666667	0.165896133	0.165726102	1.700304287E-04
0.277777778	0.274219289	0.273939402	2.798871745E-04
0.388888889	0.379160504	0.378775945	3.845589914E-04
0.500000000	0.479425539	0.478943447	4.820917123E-04
0.611111111	0.573777826	0.573207178	5.706487553E-04
0.722222222	0.661053722	0.660405180	6.485415858E-04
0.833333333	0.740176853	0.739462595	7.142578923E-04
0.944444444	0.810171396	0.809404909	7.664870378E-04

Table 3.2: Computations of different errors for Example 3.1.

j	$l_2 - error$	$l_\infty - error$	$E_{max} - error$
0	8.71E-03	6.36E-03	7.82E-03
1	9.76E-04	7.66E-04	1.53E-03
2	1.09E-04	8.68E-05	2.95E-04
3	1.21E-05	9.71E-06	5.67E-05
4	1.34E-06	1.08E-06	1.09E-05
5	1.49E-07	1.20E-07	2.10E-06
6	1.65E-08	1.33E-08	4.04E-07

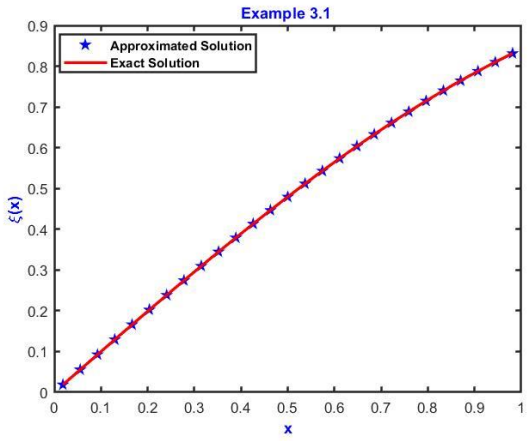

Figure 3.1: Visual analysis of exact solution and approximate solution for Example 3.1.

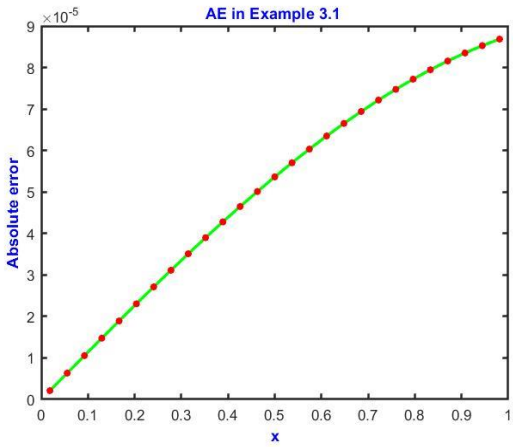

Figure 3.2: Graphical view of AE for Example 3.1.

Example 3.2: Consider the second kind of Fredholm integral equation [213],

$$\xi(x) = -2\,x^3 + 3x^2 - x\ + \int_0^1 (x^2 - x - t^2 + t)\xi(t)dt, \qquad (3.16)$$

Exact solution found from the literature for Example 3.2 is $\xi(x) = -2\,x^3 + 3x^2 - x$ [213].

Table 3.3: Computation of Exact solution and Approximated solution along with absolute error for Example 3.2 when level of resolution $j = 1$.

x	Exact solution [213]	Approximate solution	Absolute Error
0.0555555556	-0.0466392318	-0.0466392318	0
0.1666666667	-0.0925925926	-0.0925925926	2.77556E-17
0.2777777778	-0.0891632373	-0.0891632373	0
0.3888888889	-0.0528120713	-0.0528120713	6.93889E-18
0.5000000000	0.0000000000	0.0000000000	3.12066E-18
0.6111111111	0.0528120713	0.0528120713	6.93889E-18
0.7222222222	0.0891632373	0.0891632373	2.77556E-17
0.8333333333	0.0925925926	0.0925925926	0
0.9444444444	0.0466392318	0.0466392318	2.77556E-17

Table 3.4: Computations of different errors for Example 3.2.

j	$l_2 - error$	$l_\infty - error$	$E_{max} - error$	$E_{max} - error$ [214]
0	2.18463E-16	2.77556E-17	2.86E-17	----------
1	2.37160E-16	2.77556E-17	4.92E-17	1.33E-10
2	3.30185E-16	6.93889E-17	1.18E-16	3.79E-10
3	2.35656E-16	4.16334E-17	1.46E-16	3.26E-10
4	2.63632E-16	7.89299E-17	2.84E-16	4.83E-10
5	4.08185E-16	1.11022E-16	7.61E-16	----------
6	1.15566E-15	2.49800E-16	1.46E-16	----------

Example 3.2 is concerned with the resolution of a Fredholm type integral equation. Table 3.3 and Figure 3.3 shows a comparison between the approximated solution obtained by applying the presented algorithm to Example 3.2 and the actual solution. The results indicate that the presented algorithm produces highly accurate approximations for a variety of resolutions. In addition, the values of $l_2 - error$ and $l_\infty - error$ are lower than those of the existing wavelet method in the literature, as illustrated in Table 3.4. the value of absolute error for $j = 2$ is 10^{-17} which is presented graphically in Figure 3.4.

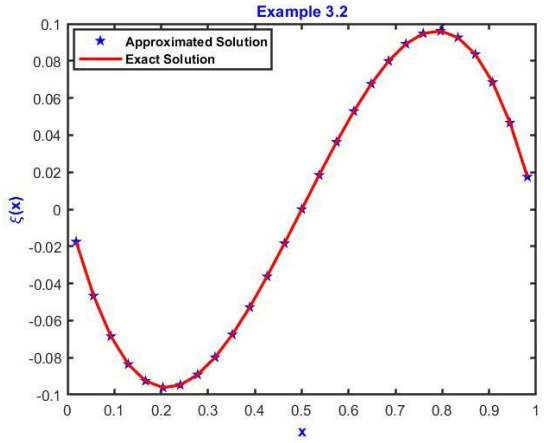

Figure 3.3: Visual analysis of exact solution and approximate solution for Example 3.2.

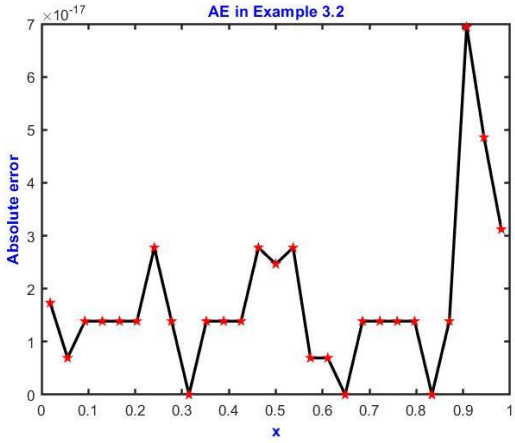

Figure 3.4: Graphical view of AE for Example 3.2.

Example 3.3: Consider a nonhomogeneous second kind of linear Volterra integral equation [213],

$$\xi(x) = x + \int_0^x \frac{1}{5}\, x\, t\, \xi(t) dt, \tag{3.17}$$

The exact solution for example 3.3 is $\xi(x) = x\, e^{\left(\frac{x^3}{15}\right)}$ [213].

Table 3.5: Computation of Exact solution and Approximated solution along with absolute error for Example 3.3 when level of resolution $j = 1$.

x	Exact solution [213]	Approximate solution	Absolute Error
0.0555555556	0.0555561906	0.0555565082	3.175456E-07
0.1666666667	0.1667181149	0.1667209790	2.864022E-06
0.2777777778	0.2781749776	0.2781830011	8.023487E-06
0.3888888889	0.3904166750	0.3904327013	1.602626E-05
0.5000000000	0.5041840761	0.5042114581	2.738196E-05
0.6111111111	0.6204802036	0.6205232131	4.300951E-05
0.7222222222	0.7405900182	0.7406544139	6.439572E-05
0.8333333333	0.8661117736	0.8662055758	9.380211E-05
0.9444444444	0.9990034913	0.9991380404	1.345490E-04

In Example 3.3, we solve a Volterra type IE having product kernels. The results of applying the suggested technique to Example 3.3 are displayed in Table 3.5 and Figure 3.5 for comparison with the exact solution. The described approach yields highly accurate estimates across a range of resolutions, as shown by the results. Table 3.6 also demonstrates that the $l_2 - error$ and $l_\infty - error$ values obtained using this method are smaller than those obtained using the current wavelet method in the literature. For $j = 6$, the value of $E_{max} - error$ is 4.92E-08 whereas the error obtained in [214] is $2.10E-03$, which clearly explains that the suggested approach fits better for such type of integral equations. For $j = 2$, the absolute value of error obtained is 10^{-5} which is displayed graphically in Figure 3.6.

Table 3.6: Computations of different errors for Example 3.3.

j	$l_2 - error$	$l_\infty - error$	$E_{max} - error$	$E_{max} - error$ [214]
0	8.6066E-04	8.3888E-04	8.74E-04	——
1	1.0310E-04	1.3455E-04	1.84E-04	1.43E-02
2	1.1554E-05	1.6836E-05	3.58E-05	2.52E-02
3	1.2851E-06	1.9457E-06	6.91E-06	1.47E-02
4	1.4280E-07	2.1903E-07	1.33E-06	7.94E-03
5	1.5867E-08	2.4443E-08	2.56E-07	4.12E-03
6	1.7630E-09	2.7198E-09	4.92E-08	2.10E-03

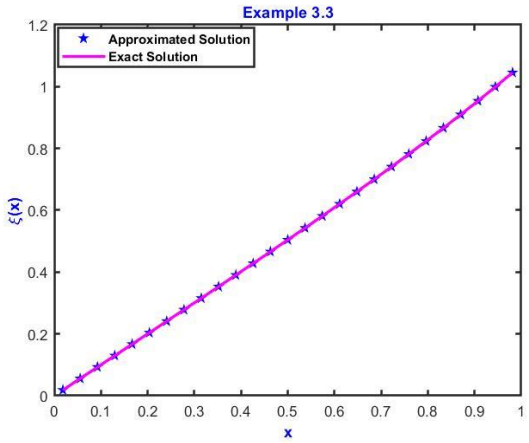

Figure 3.5: Visual analysis of exact solution and approximate solution for Example 3.3.

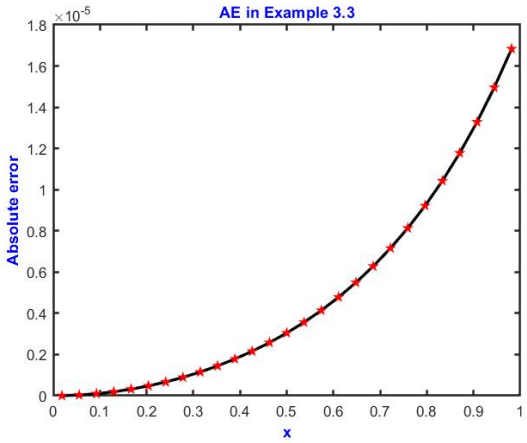

Figure 3.6: Graphical view of AE for Example 3.3.

Example 3.4: Consider a Fredholm integral equation [38], [215],

$$\xi(x) = -x^2 - \frac{x}{3}\left(2\sqrt{2} - 1\right) + 2 + \int_0^1 x\, t\, \sqrt{\xi(t)}\, dt, \tag{3.18}$$

Exact solution found from the literature is $\xi(x) = 2 - x^2$ [38], [215].

In the present study, the Leibnitz rule has been employed on the integral equation under consideration. This rule enables the transformation of the integral equation into its

corresponding differential form. Subsequently, the algorithm discussed in Chapter 2 of the thesis is employed to solve the resulting differential form.

Table 3.7: Computation of Exact solution and Approximated solution along with absolute error for Example 3.4 when level of resolution $j = 1$.

x	Exact solution [38], [215]	Approximate solution	Absolute Error
0.055555556	1.996913580	1.996913580	0
0.166666667	1.972222222	1.972222222	0
0.277777778	1.922839506	1.922839506	0
0.388888889	1.848765432	1.848765432	0
0.500000000	1.750000000	1.750000000	0
0.611111111	1.626543210	1.626543210	0
0.722222222	1.478395062	1.478395062	0
0.833333333	1.305555556	1.305555556	0
0.944444444	1.108024691	1.108024691	0

The results obtained by employing the proposed technique in Example 3.4 are presented in Table 3.7 and Figure 3.7 and are compared with the exact solution. The findings demonstrate that the proposed approach provides highly accurate estimates for various resolutions, as evidenced by the results. Additionally, Table 3.8 indicates that the error values obtained using the proposed method are smaller than those obtained using the existing wavelet method in the literature. For this particular example, the error is zero, which means that this method provides exact solutions for such types of integral equations. Table 3.8 demonstrates the superiority of the proposed approach in comparison to other numerical methods existing in the literature. The absolute value of error obtained is zero, which is graphically illustrated in Figure 3.8.

Table 3.8: Computation of absolute error with previous method for Example 3.4.

j	AE in HWM [216]	AE in HWM [38]	AE in RHWM [215]	AE by using Proposed Method
1	3.7E-03	3.3E-03	1.6E-02	0.00E+00
2	1.0E-03	2.7E-03	3.6E-02	0.00E+00
3	2.6E-04	1.1E-03	8.8E-03	0.00E+00
4	6.6E-05	3.7E-04	7.1E-03	0.00E+00
5	1.7E-05	1.1E-04	2.3E-05	0.00E+00
6	4.2E-06	3.1E-05	9.7E-07	0.00E+00

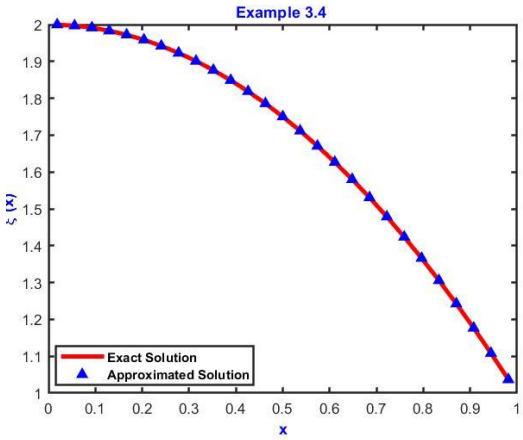

Figure 3.7: Visual analysis of exact solution and approximate solution for Example 3.4.

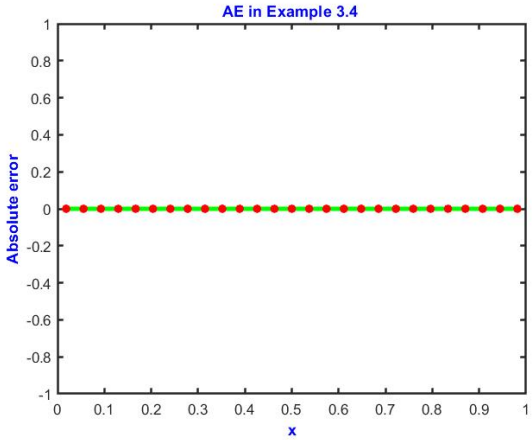

Figure 3.8: Graphical view of AE for Example 3.4.

Example 3.5: The present example involves the investigation of a mixed Volterra Fredholm type nonlinear integral equation, as described in reference [217],

$$\xi(x) = -\frac{1}{30}x^6 + \frac{1}{3}x^4 - x^2 + \frac{5}{3}x - \frac{5}{4} + \int_0^x (x-t)\xi^2(t)dt + \int_0^1 (x+t)\xi(t)dt, \tag{3.19}$$

The precise solution obtained from the existing literature is as follows $\xi(x) = x^2 - 2$ [217]. The process of approximating the integral equation under consideration involves

several steps. Firstly, the Quasilinearization technique is applied on the nonlinear component. Following this, the Leibniz rule is utilized for transforming the integral equation into its corresponding differential equation. Subsequently, the highest derivative involved in the differential equation is approximated by means of a truncated series of Haar functions. Finally, the process of integration is employed to calculate the values of all the lower-order derivatives, as elaborated in detail in Chapter 2 of the thesis.

Table 3.9: Computation of Exact solution and Approximated solution along with absolute error for Example 3.5 when level of resolution $j = 1$.

x	Exact solution [217]	Approximate solution	Absolute Error
0.055555556	-1.996913580	-1.996913580	0
0.166666667	-1.972222222	-1.972222222	0
0.277777778	-1.922839506	-1.922839506	0
0.388888889	-1.848765432	-1.848765432	0
0.500000000	-1.750000000	-1.750000000	0
0.611111111	-1.626543210	-1.626543210	0
0.722222222	-1.478395062	-1.478395062	0
0.833333333	-1.305555556	-1.305555556	0
0.944444444	-1.108024691	-1.108024691	0

The outcomes obtained through the implementation of the suggested approach to Example 3.5 are presented in Table 3.9 and Figure 3.9 and are compared with the exact solution. The results indicate that the proposed approach provides highly accurate estimates for various resolutions, as evident from the outcomes. Moreover, Table 3.10 reveals that the error values obtained using the proposed method are smaller than those obtained using the currently available wavelet methods in the literature. For this specific example, the error is zero, implying that the proposed method provides exact solutions for this type of integral equations. Hence, Table 3.10 demonstrates the superiority of the proposed approach over other existing numerical methods in the literature. The

graphical representation of the absolute error obtained is zero, which is illustrated in Figure 3.10.

Table 3.10: Comparison of absolute error with previous method for Example 3.5.

x	Error in [217]	Error by using Proposed Method
0.0	0.00000E+00	0
0.1	1.626820E-04	0
0.2	2.438211E-04	0
0.3	1.275379E-04	0
0.4	2.858734E-04	0
0.5	3.999309E-04	0
0.6	2.250428E-04	0
0.7	3.594621E-04	0
0.8	1.043774E-04	0
0.9	2.968310E-04	0

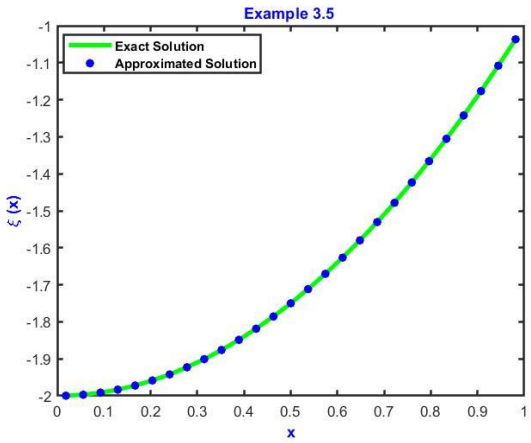

Figure 3.9: Visual analysis of exact solution and approximate solution for Example 3.5.

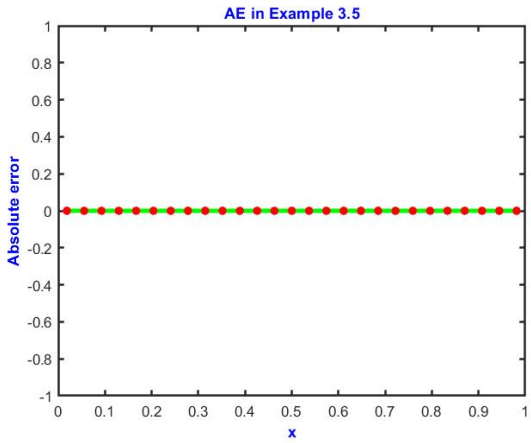

Figure 3.10: Graphical view of AE for Example 3.5.

Example 3.6: Consider a nonhomogeneous second kind of nonlinear Fredholm integral equation [218],

$$\xi(x) + \int_0^1 e^{x-2t}[\xi(t)]^3 dt = e^{x+1}, \tag{3.20}$$

The exact solution obtained from the existing literature is as follows $\xi(x) = e^x$ [218]. Example 3.6 involves the resolution of a Fredholm type nonlinear IE. The proposed technique is utilized to solve the nonlinear integral equation with an exponential kernel. The outcomes of the application are presented through tables and graphs. The nonlinearity is addressed through the use of the Quasilinearization technique.

Table 3.11: Computation of Exact solution and Approximated solution along with absolute error for Example 3.6 when level of resolution $j = 4$.

x	Exact solution [218]	Approximate solution	Absolute Error	Absolute error in [218]	Absolute error in [174]
0.10	1.10608	1.10608	2.50E-06	2.0E-03	1.4E-04
0.20	1.22593	1.22594	2.95E-06	3.3E-03	1.6 E-04
0.30	1.35320	1.35320	3.44E-06	8.7E-03	1.9 E-04
0.40	1.49367	1.49367	4.01E-06	1.E-02	2.3 E-04
0.50	1.64872	1.64873	4.65E-06	1.8E-02	2.6 E-04
0.60	1.82738	1.82738	5.42E-06	1.1E-02	3.1 E-04
0.70	2.01707	2.01708	6.27E-06	2.9E-03	3.6 E-04
0.80	2.22646	2.22646	7.23E-06	8.1E-03	4.1 E-04
0.90	2.46771	2.46772	8.37E-06	2.1E-02	4.8 E-04

Table 3.11 and Figure 3.11 present a comparison between the approximated solution obtained by applying the proposed algorithm to Example 3.6 and the actual solution. The results indicate that the presented algorithm produces highly accurate approximations for a variety of resolutions. Additionally, the comparison is also provided with the earliest method. The results indicate that the proposed method is superior for addressing such types of problems.

The values of $l_2 - error$ and $l_\infty - error$ obtained using the proposed method are lower than those obtained using the existing wavelet methods in the literature, as demonstrated in Table 3.12. Furthermore, it can be observed from Table 3.12 that increasing the dilation factor results in to decrease in the value of error that proves the convergence of the method. For $j = 2$, the value of absolute error is 10^{-4}, which is graphically presented in Figure 3.12.

Table 3.12: $l_2 - error$, $l_\infty - error$ and $E_{max} - error$ at different level of resolution for Example 3.6.

j	$l_2 - error$	$l_\infty - error$	$E_{max} - error$	$E_{max} - error$ in [174]
0	2.04361E-02	5.10241E-02	6.26838E-02	-----
1	2.23891E-03	6.48561E-03	1.19927E-02	3.0E-02
2	2.48385E-04	7.57175E-04	2.30654E-03	8.1E-03
3	2.75936E-05	8.55745E-05	4.43863E-04	2.1E-03
4	3.06590E-06	9.56294E-06	8.54208E-05	5.4E-04
5	3.40655E-07	1.06459E-06	1.64392E-05	1.3E-04
6	3.78505E-08	1.18363E-07	3.16373E-06	3.4E-05

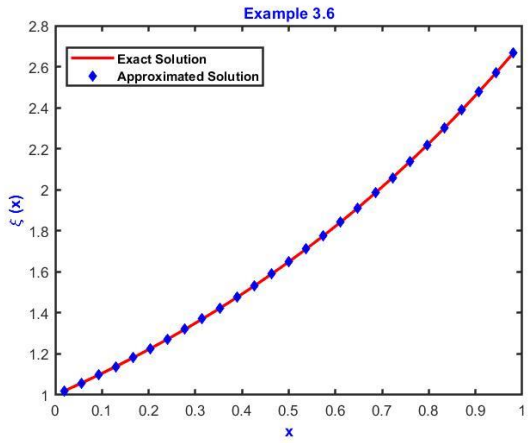

Figure 3.11: Visual analysis of exact solution and approximate solution for Example 3.6.

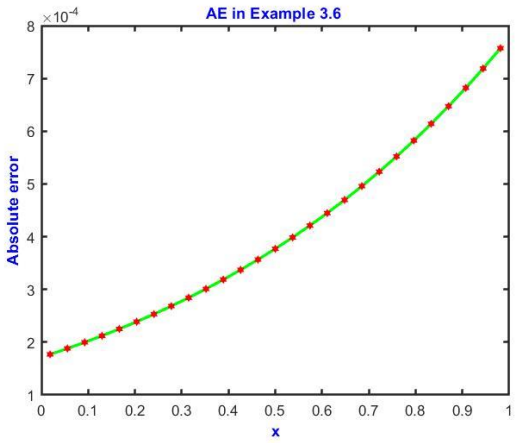

Figure 3.12: Graphical view of AE for Example 3.6.

Example 3.7: Consider Fredholm integral equation [219],

$$\xi(x) = \sin(2\pi x) + \int_0^1 (x^2 - x - t^2 + t)\xi(t)dt, \tag{3.21}$$

The exact solution is $\xi(x) = \sin(2\pi x)$ [219].

Table 3.13: Computation of Exact solution and Approximated solution along with absolute error for Example 3.7 when level of resolution $j = 1$.

x	Exact solution [219]	Approximate solution	Absolute Error
0.0555555556	0.3420201433	0.3420201433	5.5511E-17
0.1666666667	0.8660254038	0.8660254038	1.1102E-16
0.2777777778	0.9848077530	0.9848077530	0
0.3888888889	0.6427876097	0.6427876097	0
0.5000000000	0.0000000000	0.0000000000	2.0967E-17
0.6111111111	-0.6427876097	-0.6427876097	0
0.7222222222	-0.9848077530	-0.9848077530	0
0.8333333333	-0.8660254038	-0.8660254038	2.2204E-16
0.9444444444	-0.3420201433	-0.3420201433	5.5511E-17

Table 3.14: $l_2 - error$, $l_\infty - error$ and $E_{max} - error$ at different level of resolution for Example 3.7.

j	$l_2 - error$	$l_\infty - error$	$E_{max} - error$	$E_{max} - error$ [219]
0	1.3078E-16	1.1102E-16	1.60E-16	--------
1	1.2314E-16	2.2204E-16	2.61E-16	2.84E-02
2	1.7629E-16	2.2204E-16	6.48E-16	2.38E-03
3	2.6900E-16	4.4409E-16	1.71E-15	2.10E-04
4	2.3013E-16	6.6613E-16	2.54E-15	2.00E-04
5	2.7384E-16	7.7716E-16	5.23E-15	---------
6	4.2524E-16	1.2212E-15	1.41E-14	---------

In Example 3.7, we solve a Fredholm-type integral equation. We use the suggested technique and present the results in Table 3.13 and Figure 3.13 for comparison with the exact solution. The proposed approach provides highly accurate estimates across various resolutions, as demonstrated by the results. Table 3.14 shows that the error values obtained using this method are smaller than those obtained using the current wavelet method in the literature. For $j = 1$, the maximum error value $(E_{max} - error)$ is 2.61E-06, while the error obtained in [219] is 2.84E-02. This finding indicates that the suggested approach is better suited for such integral equations. For $j = 2$, the absolute error value obtained is 10^{-16} which is graphically displayed in Figure 3.14.

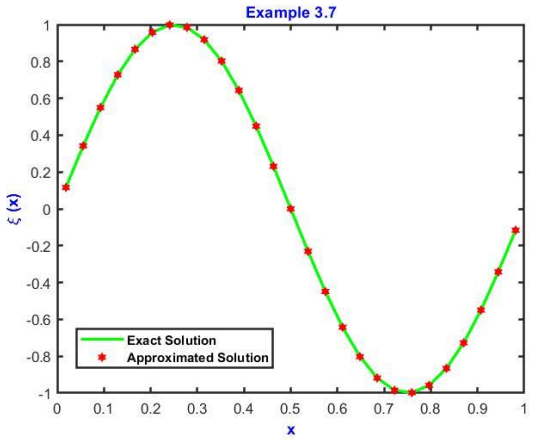

Figure 3.13: Visual analysis of exact solution and approximate solution for Example 3.7.

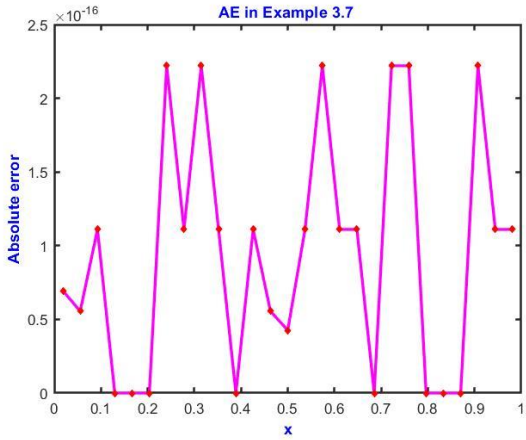

Figure 3.14: Graphical view of AE for Example 3.7.

Example 3.8: Consider Fredholm integral equation [219],

$$\xi(x) = sin(2\pi x) + \int_0^1 cosx\, \xi(t)dt, \tag{3.22}$$

Exact solution $\xi(x) = \sin(2\pi x)$ [219].

In Example 3.8, a Fredholm type integral equation is solved using the proposed collocation approach. The outcomes are presented in Table 3.15, which provides a comparison between the exact solution and the approximated solution for resolution level 1. The table suggests that despite the small number of collocation points, the presented collocation approach produces more accurate results.

Table 3.15: Computation of Exact solution and Approximated solution along with absolute error for Example 3.8 when level of resolution $j = 1$.

x	Exact solution [219]	Approximate solution	Absolute Error
0.0555555556	0.3420201433	0.3420201433	1.3878E-15
0.1666666667	0.8660254038	0.8660254038	1.3323E-15
0.2777777778	0.9848077530	0.9848077530	1.4433E-15
0.3888888889	0.6427876097	0.6427876097	1.2212E-15
0.5000000000	0.0000000000	0.0000000000	1.2534E-15
0.6111111111	-0.6427876097	-0.6427876097	1.2212E-15
0.7222222222	-0.9848077530	-0.9848077530	8.8818E-16
0.8333333333	-0.8660254038	-0.8660254038	6.6613E-16
0.9444444444	-0.3420201433	-0.3420201433	6.1062E-16

The $l_2 - error$, $l_\infty - error$ and $E_{max} - errors$ for resolution level 0 are 1.4591E-15, 1.2212E-15, and 1.79E-15 respectively, indicating a high level of accuracy. Figure 3.15 demonstrate that the approximated solution converges toward the exact solution.

Table 3.16: $l_2 - error$, $l_\infty - error$ and $E_{max} - error$ at different level of resolution for Example 3.8.

j	$l_2 - error$	$l_\infty - error$	$E_{max} - error$	$E_{max} - error$ [219]
0	1.4591E-15	1.2212E-15	1.79E-15	----------
1	1.6291E-15	1.4433E-15	3.46E-15	2.841E-02
2	1.8315E-16	3.3307E-16	6.73E-16	2.388E-03
3	4.8389E-16	6.6613E-16	3.08E-15	2.097E-04
4	3.2327E-16	6.3838E-16	3.56E-15	1.204E-04
5	7.3419E-16	1.2212E-15	1.40E-14	----------
6	4.4421E-16	8.8818E-16	1.47E-14	----------

Additionally, Figure 3.16 provides a visual representation of the absolute value of error for resolution level 2. Finally, Table 3.16 compares the obtained results with existing

methods, demonstrating that the presented method is more effective than other methods for such types of equations. Overall, these findings highlight the efficacy of the presented approach in solving Fredholm type integral equations, as it produces highly accurate results with a small number of collocation points and outperforms other methods in terms of accuracy.

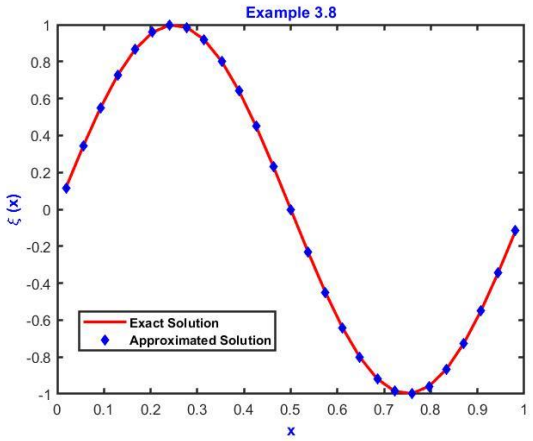

Figure 3.15: Visual analysis of exact solution and approximate solution for Example 3.8.

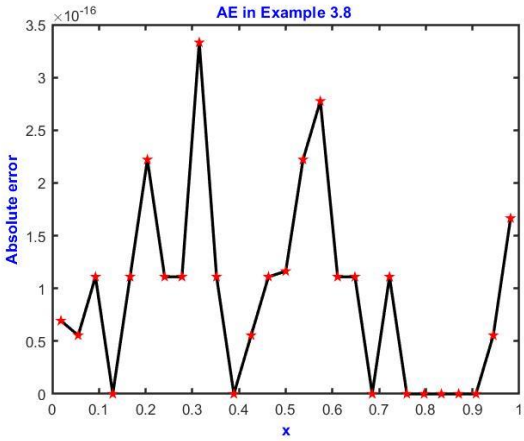

Figure 3.16: Graphical view of AE for Example 3.8.

Example 3.9: Consider the nonlinear Volterra integral equation [195]

$$\xi(x) = \frac{3}{2} - \frac{1}{2}e^{-2x} - \int_0^x \left(\xi^2(t) + \xi(t)\right)dt, \tag{3.23}$$

Exact solution $\xi(x) = e^{-x}$ [195].

The procedure for approximating the integral equation under study involves several sequential steps, each with its unique scientific rationale. Initially, the Quasilinearization technique is utilized to address the nonlinearity present in the equation. Next, the Leibniz rule is employed to transform the integral equation into its corresponding differential equation, facilitating its analysis through the mathematical techniques of calculus. Subsequently, a truncated series of Haar functions is used to approximate the highest derivative involved in the differential equation. Finally, the process of integration is employed to compute the values of all the lower-order

derivatives, providing a comprehensive understanding of the equation's behaviour. A detailed discussion of these steps can be found in Chapters 1 and 2 of the thesis.

Table 3.17: Computation of Exact solution and Approximated solution along with absolute error for Example 3.9 for $j = 6$.

x	Exact solution [195]	Approximate solution	Absolute Error	Error in [217]
0.10	0.90450649	0.90450651	1.80869E-08	1.626820E-04
0.20	0.81869332	0.81869333	1.24807E-08	2.438211E-04
0.30	0.74068274	0.74068275	8.46229E-09	1.275379E-04
0.40	0.67010553	0.67010553	5.55644E-09	2.858734E-04
0.50	0.60653066	0.60653066	3.43859E-09	3.999309E-04
0.60	0.54873636	0.54873636	1.86637E-09	2.250428E-04
0.70	0.49644909	0.49644909	6.97760E-11	3.594621E-04
0.80	0.44914409	0.44914409	1.73991E-11	1.043774E-04
0.90	0.40653248	0.40653248	8.21881E-11	2.968310E-04

Table 3.18: $l_2 - error$, $l_\infty - error$ and $E_{max} - error$ at different level of resolution for Example 3.9.

j	$l_2 - error$	$l_\infty - error$	$E_{max} - error$	$E_{max} - error$ [174]	$E_{max} - error$ [195]
0	7.785580E-03	8.584866E-03	8.785248E-03	---	---
1	8.551693E-04	1.281361E-03	1.685139E-03	2.30E-03	3.73E-03
2	9.488705E-05	1.605549E-04	3.241515E-04	1.60E-03	9.37E-04
3	1.054137E-05	1.863016E-05	6.237962E-05	4.38E-04	2.34E-04
4	1.171243E-06	2.101033E-06	1.200489E-05	1.15E-04	2.37E-03
5	1.301378E-07	2.346195E-07	2.310341E-06	2.96E-05	---
6	1.445975E-08	2.611250E-08	4.446253E-07	7.52E-06	---

Table 3.17 and Figure 3.17 illustrate a comparative analysis between the approximated solution obtained by implementing the proposed algorithm in Example 3.9 and the

actual solution. The outcomes indicate that the proposed algorithm provides highly accurate approximations for various resolutions. Furthermore, a comparison with the previous method is also presented, and the results demonstrate the superiority of the proposed method in addressing such types of problems. The values of different types of errors obtained through the proposed method are considerably lower than those obtained from the existing wavelet methods mentioned in the literature, as shown in Table 3.18. Additionally, it can be observed from Table 3.18 that increasing the dilation factor leads to a decrease in the error values, thus demonstrating the convergence of the proposed method. For $j = 2$, the absolute error value is 10^{-4}, which is graphically presented in Figure 3.18.

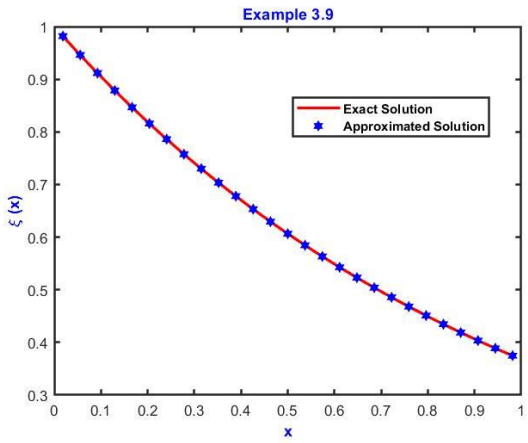

Figure 3.17: Visual analysis of exact solution and approximate solution for Example 3.9.

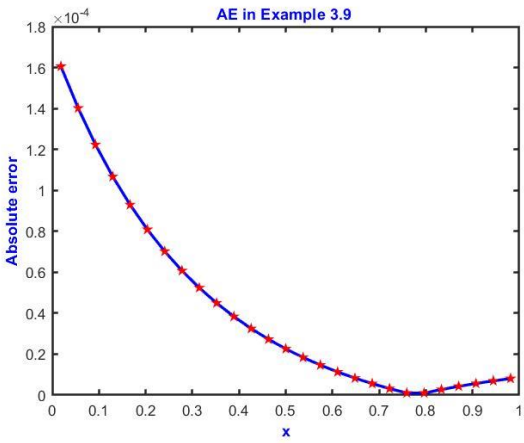

Figure 3.18: Graphical view of AE for Example 3.9.

Example 3.10: Consider the nonlinear Volterra integral equation [196],

$$\xi(x) = x - x^2 - \frac{x^5}{4} + \frac{2x^6}{5} - \frac{x^7}{6} + \int_0^x xt\left(\xi^2(t)\right)dt, \tag{3.24}$$

Exact solution $\xi(x) = x - x^2$ [196].

The last example under consideration is the nonlinear IE of Volterra type having product kernel. The method of approximating this integral equation involves several intricate steps. Initially, the Quasilinearization method is applied to linearize the nonlinear component of the equation. Afterward, the Leibniz rule is used to convert the

integral equation into a differential equation. Then, the derivative of the greatest order present in the differential equation is estimated using a truncated series of Haar functions. Finally, the process of integration is employed to compute the values of all lower-order derivatives. These steps are elaborated in detail in Chapters 1 and 2 of the thesis. The proposed algorithm is utilized to solve the integral equation under study. The comparison between the solution obtained from the proposed method and the exact solution for Example 3.10 is presented in Table 3.19 and Figure 3.19.

Table 3.19: Computation of Exact solution and Approximated solution along with absolute error for Example 3.10 for $j = 1$.

x	Exact solution [196]	Approximate solution	Absolute Error
0.0555555556	0.0524691358	0.0524692135	7.7696E-08
0.1666666667	0.1388888889	0.1388909854	2.0965E-06
0.2777777778	0.2006172840	0.2006210916	3.8076E-06
0.3888888889	0.2376543210	0.2376514058	2.9152E-06
0.5000000000	0.2500000000	0.2499728922	2.7108E-05
0.6111111111	0.2376543210	0.2375805929	7.3728E-05
0.7222222222	0.2006172840	0.2004789532	1.3833E-04
0.8333333333	0.1388888889	0.1386879989	2.0089E-04
0.9444444444	0.0524691358	0.0522500682	2.1907E-04

Table 3.20 tabulates the calculation of various errors for different dilation factors. The results indicate that as the value of j increases, the error decreases. Furthermore, Figure 3.20 illustrates the graph that represents the absolute error for a resolution level of 2. Based on the resemblance between the estimated and precise solutions, as displayed in Figure 3.19, it can be inferred that the suggested technique converges toward the exact solution. Increasing the resolution level j can lead to an improvement in the accuracy of the results obtained.

Table 3.20: $l_2 - error$ and $l_\infty - error$ at different level of resolution for Example 3.10.

j	$l_2 - error$	$l_\infty - error$	$l_\infty - error$ [219]
0	6.2288E-03	1.9642E-03	----------
1	6.1554E-04	2.1907E-04	----------
2	6.7199E-05	2.4316E-05	1.43E-03
3	7.4518E-06	2.6999E-06	7.35E-04
4	8.2779E-07	3.0004E-07	3.62E-04
5	9.1975E-08	3.3337E-08	1.79E-04
6	1.0219E-08	3.7041E-09	8.96E-05

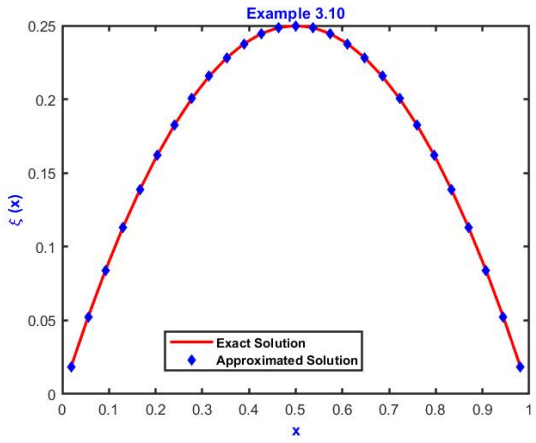

Figure 3.19: Visual analysis of exact solution and approximate solution for Example 3.10.

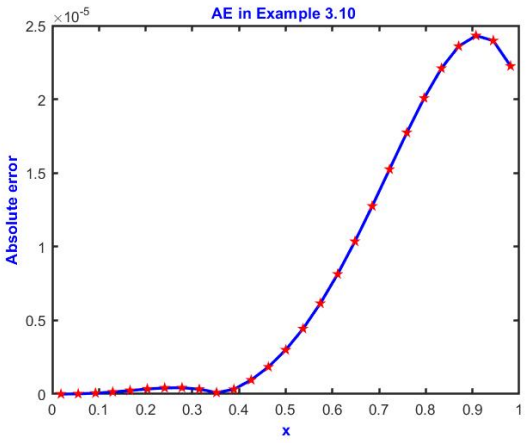

Figure 3.20: Graphical view of AE for Example 3.10.

3.5 Conclusions

In the present work, a numerical algorithm based on "Haar scale 3 (non-dyadic) wavelets" has been introduced for finding the approximate solution of Volterra IES and Fredholm IES. For linear as well as nonlinear IEs of Volterra and Fredholm type, the unknown function $\xi(x)$ is approximated by Haar scale 3 functions, and then by using the process of integration, we have obtained the expression for integrals. Nonlinearity in the problems is tackled by the Quasilinearization technique. By putting the collocation points, $N \times N$ system of equations has been obtained which is then solved by the Thomas algorithm for evaluating the unknown Haar coefficients. By substituting the value of Haar coefficients, we obtain the solution at different nodal points. The calculation of the analytical solution, approximated solution, and absolute error for different collocation points are shown in tables and graphs. The results obtained by using this method are compared with the exact solution. From the table and figures it is observed that by increasing the level of resolution, approximated solutions converge to the exact solutions. All the computational work is done by using the MATLAB software.

Chapter 4.

Numerical Solution of Lane-Emden and Emden-Fowler type Equations by using Scale 3 Haar Wavelets

4.1 Introduction

The study of stellar structures has become a major subject in stellar astrophysics since its origin. Several attempts have been made to estimate the radial profiles of the density of the star, the mass of the star, and also the pressure of the star, and the major finding of all these attempts is the Lane-Emden equation (LE-E). LE-E represents the thermal gradient of a spherical cloud of gas based on laws of basic thermodynamics as well as the mutual attraction among its particles. The polytrophic theory of stars is based on thermodynamic considerations that address the problem of energy transmission via material transfer among multiple levels of the star. These mathematical equations are fundamental to the field of stellar structure theory and have also become the subject of numerous research [173], [220]. Mathematically, LE-E is an ordinary differential equation of second order having singularity at the origin. To derive the basic model of the Lane-Emden equation, consider a spherical gas cloud as presented in Figure ⊛ [221], [222].

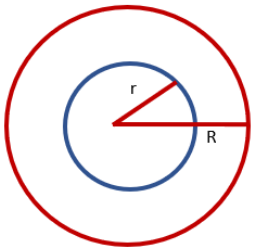

Figure ⊛: A spherical gas cloud.

Let $P(r)$ represent the sum of the pressures exerted at a radius r from the center of a spherical gas cloud. Standard gas pressure and the impact of radiation together create the total pressure,

$$P = \left(\frac{1}{3}aT^4 + \frac{RT}{v}\right),$$

In this context, a denotes the radiation constant, T signifies the absolute temperature, R symbolizes the gas constant, and ν represents the specific volume [223]. Now assume that the spherical mass is denoted by $M(r)$, the gravitational potential is denoted by ϕ, and acceleration due to gravity is denoted by g. The following is the equilibrium equation for the system configuration,

$$\frac{dP}{dr} = -\rho \frac{GM(r)}{r^2},$$

$$\frac{dM(r)}{dr} = 4\pi\rho r^2,$$

where G is the universal gravitation constant, and ρ is the density of the star at a distance r from the center of the spherical star. Eliminating the value of $M(r)$ from the above-mentioned equations gives rise to an equation. It is crucial to observe that this equation is an analogous form of the Poisson equation,

$$\frac{1}{r^2}\frac{d}{dr}\left(\frac{r^2}{\rho}\frac{dP}{dr}\right) = -4\pi G\rho.$$

The density and pressure of a degenerated electron gas are proportional to one another. The mathematical relation which describes their relation is $\rho = P^{3/5}$. Moreover, on the assumption that a relation of this kind does exist for other states of the star, we are compelled to hypothesize a relation of the type $P = K\rho^{1+\frac{1}{m}}$, where K and m are constants. By using this relation in the above-mentioned equation of hydrostatic equilibrium, we came to a conclusion,

$$\left[\frac{K(m+1)}{4\pi G}\lambda^{\frac{1}{m}-1}\right]\frac{1}{r^2}\frac{d}{dr}\left(r^2\frac{dy}{dr}\right) = -\zeta^m,$$

where λ corresponds to the central density of the star and ζ represents the non-dimensional quantity, both of which are associated with density ρ by the following expression,

$$\rho = \lambda\zeta^m(\varkappa),$$

and introduce a new parameter c and define a relation between r and c: $c = \frac{r}{\varkappa}$ and the value of $c = \left[\frac{K(m+1)}{4\pi G}\lambda^{\frac{1}{m}-1}\right]^{\frac{1}{2}}$. By substituting the value of r we obtain the basic lane-Emden equation,

$$\frac{1}{\varkappa^2}\frac{d}{d\varkappa}\left(\varkappa^2\frac{d\zeta}{d\varkappa}\right) = -\zeta^m,$$

$$\zeta''(\varkappa) + \frac{2}{\varkappa}\zeta'(\varkappa) + \zeta^m(\varkappa) = 0;\ \varkappa > 0.$$

It is also essential to establish the boundary conditions according to the following boundary constraints for hydrostatic equilibrium and normalizing consideration of the additional new variables $\varkappa$ and ζ. The consequence of $r = 0$ is,

$$r = 0 \rightarrow \varkappa = 0,$$

$$\rho = \lambda \rightarrow \zeta(0) = 1.$$

Thus further, an additional constraint must still be incorporated in to equally 120ulfil the above condition of r and $\varkappa$,

$$\zeta'(0) = 0,$$

Thus, to restate, here are the following restrictions,

$$\zeta(0) = 1, \qquad \zeta'(0) = 0.$$

The general structure of LE-E is

$$\zeta''(\varkappa) + \frac{k}{\varkappa}\zeta'(\varkappa) + f(\varkappa, \zeta(\varkappa)) = g(\varkappa);\ \varkappa \in (0,1], and\ \ k \in [0,\infty), \qquad (4.1)$$

With the initial conditions

$$\zeta(0) = \alpha_1 \text{ and } \zeta'(0) = \alpha_2. \qquad (4.2)$$

Here $g(\varkappa)$ is an analytical function while $f(\varkappa, \zeta(\varkappa))$ is a continuous real-value function. Equation (4.1) has been used to explain various problems in physical sciences and cosmology, including stellar model theory, isothermal gas sphere, physical properties of a spherical cloud of gas, modelling of the cluster of galaxies, and thermionic current theory [224]. Some of the important real-world applications of Lane-

Emden equation (4.1) are discussed in Table ⊛. Cists Jonathan Lane [225] was the first one to develop Lane-Emden equations, although Emden elaborated extensively in 1870 [226]. The Lane-Emden equation is basically a Poisson equation in astrophysics. This type of problem has received an enormous amount of attention from researchers. For further study on Lane-Emden equations, comprising their origin, modifications, and implementations, the researcher is gladly encouraged to read [225], [227].

Table ⊛: Applications of Lane-Emden equations for different values of $f(\varkappa, \zeta(\varkappa))$ in (1) by considering $g(\varkappa) = 0$ and $k = 2$.

Function type $f(\varkappa, \zeta(\varkappa))$	**Physical Applications**
$\zeta^m(\varkappa)$	This is the standard LE-E. The precise solution for this LE-E can be found in existing literature corresponding to $m = 0,\ 1, \& 5$ only and the solutions are $\frac{1-\varkappa^2}{6}$, $\frac{\sin(\varkappa)}{\varkappa}, and\ \sqrt{\frac{3}{3+\varkappa^2}}$ respectively. This equation describes the thermal gradient of a spherical cloud of gas based on laws of basic thermodynamics as well as the mutual attraction among its particles [228].
$e^{\zeta(\varkappa)}$	This LE-E is the Poisson Boltzmann equation utilised to describe isothermal gas spheres [229], [173].
$\frac{1}{e^{\zeta(\varkappa)}}$	This lane-Emden equation arises in modelling of the thermal conduction in the human head [230].
$(\zeta^2(\varkappa) - C)^{\frac{3}{2}}$	This lane-Emden equation is called the white dwarf (W-D) equation. This equation finds its application in the modelling of the gravitational potential of degenerate W-D stars.
$-\frac{\theta\zeta(\varkappa)}{\zeta(\varkappa)+k}$	The study of steady-state gas diffusion in a spherical cell with Michaelis-Menten uptake kinetics leads to the development of this equation [231].

The LE-E generally does not have solutions that can be determined by analytical techniques. In practice, several real physical and mathematical problems are often very difficult to deal with. As a result, these problems are handled by using a variety of

approximated and numerical techniques. Several researchers are working on the solution of LE-E. Wazwaz in [232] solved the LE-E types by using the Adomain decomposition method. Caglar [233] implemented the B-splines for the approximation of the singular differential equation of the LE-E type. Yousefi [234] describes the Legendre wavelets for finding the solution of the LE-E. Erturk [235] solved the LE-E in differential form by utilizing the differential transform method. Ramos [236] approximated LE-E by utilizing a series approach. The author also discusses the comparability of the homotopy perturbation method with the series approach for solving LE-E. Parand et.al., [237] used a pseudospectral algorithm for the solution of LE-E having nonlinearity in them on the semi-infinite domain. The pseudospectral algorithm was formulated by utilizing Legendre functions along with Gauss–Radau integration. In this method, nonlinear LE-E was converted to the corresponding algebraic equations which were then solved. Vanani and Aminataei [238] presented a numerical method for LE-E of the nonlinear kind. In this method, LE-E was first converted to integral equations which were then converted to the power series. The desired power series was then transformed into a Pade series approximation. Parand and his co-workers [239] approximated the LE-E by utilizing the hybrid of collocation approach along with the Hermite function. Iqbal and Javed [240] applied the optimal homotopy asymptotic algorithm on LE-E. Wazwaz et.al., [241] used the Adomain decomposition method for solving the system of LE-E by converting them into the corresponding Volterra integral equations. Taghavi and Pearce [242] applied the Tau technique for the approximation of LE-E of differential form. Yuzbasi and Sezer [243] constructed the Bessel collocation approach for the solution of LE-E of linear type. Wazwaz and Khuri [244] solved the integrodifferential form of LE-E with the aid of the variational iteration method. Asadpour et.al., [245] solved the integral form of LE-E by using the least square method.

Since it is challenging to find the analytical solution to functional equations in the majority of real-world problems. Therefore, a reliable, effective, and accurate numerical approach is needed for their solution. The utilization and importance of numerical approaches in the fields of engineering, astronomy, and mathematics have dramatically increased with the development of effective and fast computers. The popular wavelet-based approaches are used to solve a variety of models that originate

in numerous fields of scientific domains. A quantitative technique known as wavelet analysis has diverse applications in the fields of numerical analysis, image processing, quantum physics, and numerous other areas. Wavelets are modernistic orthonormal functions with the ability to dilate and translate. These characteristics allow wavelet-based numerical algorithms to exhibit a qualitative improvement over other technique. In literature, Lane-Emden equations have been solved by using numerous wavelets like, Legendre multi-wavelets [246], Bernoulli wavelet [247], Chebyshev wavelet [248], Haar scale 2 wavelets [249], Morlet wavelet [250], and Taylor wavelet [251]. Among all wavelet families with analytic expression, the Haar wavelet is the simplest. It comprises a set of piecewise constant functions. These wavelets were proposed by Hungarian mathematician Alfred Haar in 1910. However, wavelets were first used to tackle calculus problems in 1997. Haar wavelet technique has superseded the other numerical techniques because of its mathematical simplicity, high levels of efficiency, and primarily its applicability to the problems to acquire more reliable results for a small number of nodal points. The useful qualities of the Haar wavelet include its ability to be applied to conventional algorithms and its ability to be analytically integrated the desired number of times. When compared to other numerical algorithms, Haar wavelet promises simpler and faster methods of solving problems. The current study involves the implementation of scale 3 Haar wavelets to Lane-Emden and Emden-Fowler type equations of integro-differential form. The chapter is organized as in section 4.2 the conversion of the differential form of Lane-Emden equations into the Volterra integro-differential form is presented. Section 4.3 contains the scale 3 Haar wavelet (S3-HW) collocation algorithm. For the validation of the S3-HW algorithm, some applications of Lane-Emden and Emden-Fowler type equations are discussed in section 4.4. Finally, the conclusion is discussed in section 4.5 of the chapter.

4.2 Volterra Integro-Differential Representation of the Lane-Emden and Emden-Fowler type Equations

This section contains the conversion of second order ordinary differential equation of LE type to the corresponding Volterra Integro-differential equations (VIDE) or simply Volterra Integral equation as explained in [252].

Step 1: Let

$$\zeta''(\varkappa) = \upsilon(\varkappa), \tag{4.3}$$

Step 2: Integrate equation (4.3) from 0 to $\varkappa$ for the variable $\varkappa$ and then using the initial conditions (4.2),

$$\zeta'(\varkappa) = \alpha_2 + \int_0^{\varkappa} \upsilon(\varkappa)\, d\varkappa, \tag{4.4}$$

Step 3: Again, integrate equation (4.4) from 0 to $\varkappa$ for the variable $\varkappa$ and by using (4.2),

$$\zeta(\varkappa) = \alpha_1 + \alpha_2\varkappa + \int_0^{\varkappa} (\varkappa - t)\upsilon(t)\, dt, \tag{4.5}$$

Step 4: Substituting equation (4.3), (4.4), and (4.5) in equation (4.1),

$$\upsilon(\varkappa) = \mathcal{F}(\varkappa) - \int_0^{\varkappa} \Re(\varkappa, t)\upsilon(t)\, dt, \tag{4.6}$$

where $\Re(\varkappa, t)$ is the kernel function and the value of $\Re(\varkappa, t)$ is

$$\Re(\varkappa, t) = \frac{k}{\varkappa} + \mathrm{T}(\varkappa)(\varkappa - t),$$

and

$$\mathcal{F}(\varkappa) = \mathcal{g}(\varkappa) - \frac{k}{\varkappa}\alpha_2 - \mathrm{T}(\varkappa)\alpha_1 - \varkappa\mathrm{T}(\varkappa)\alpha_2.$$

Equation (4.6) is the Volterra Integral form of the LE-E (4.1) and (4.2). Now for the corresponding VIDE, differentiate equation (4.6) for the variable $\varkappa$ and by using the Leibnitz rule,

$$\upsilon'(\varkappa) + \frac{k}{\varkappa}\,\upsilon(\varkappa) = \mathcal{H}(\varkappa) - \int_0^{\varkappa} \mathbb{Q}(\varkappa, t)\upsilon(t)\, dt; \quad \upsilon(0) = \alpha_3, \tag{4.7}$$

where $\mathbb{Q}(\varkappa, t) = \frac{\partial}{\partial\varkappa}\,\Re(\varkappa, t)$ and $\mathcal{H}(\varkappa) = \mathcal{F}'(\varkappa)$. This equation (4.7) is the required VIDE of Lane-Emden equation (4.1) and (4.2).

4.3 Construction of Scale 3 Haar Wavelet Algorithm

In this section, a novel algorithm is presented for the solution of Lane-Emden equations of Volterra integro-differential form. We constructed a scale 3 Haar wavelet algorithm for the interval [0, 1]. In the proposed algorithm, the first order derivative $\upsilon'(\varkappa)$ involved in the Lane-emden equation (4.7) is approximated by scale 3 Haar functions,

and then by integrating, the value of unknown $\upsilon(\varkappa)$ is obtained. Furthermore, the integrals involved are determined by using the formula given in lemma 4.3.1.

Lemma 4.3.1: If $\upsilon(\varkappa)$ is any function belonging to the family of $l_2(R)$, the space of square-integrable function over the interval [a, b] in such a way that $\upsilon(\varkappa) = \sum_{i=1}^{3p} a_i\psi_i(\varkappa)$, then the integral of $\upsilon(\varkappa)$ on [a, b] is given as,

$$\int_a^b \upsilon(\varkappa)d\varkappa = \frac{b-a}{3p}\sum_{m=1}^{3p}\upsilon(\varkappa_m) = \frac{b-a}{3p}\sum_{m=1}^{3p}\upsilon\left(a+(b-a)\frac{m-0.5}{3p}\right). \quad (4.8)$$

Proof: See reference [34].

4.3.1 Proposed Methodology

Consider

$$\upsilon'(\varkappa) = \sum_{i=1}^{3p} a_i\psi_i(\varkappa), \quad (4.9)$$

Integrating (4.9) from 0 to $\varkappa$,

$$\upsilon(\varkappa) = \alpha_3 + \sum_{i=1}^{3p} a_i L_{i,1}(\varkappa)\,;\ \text{where } L_{i,1}(\varkappa) = \int_0^{\varkappa}\psi_i(\varkappa)d\,\varkappa, \quad (4.10)$$

Equation (4.10) is the approximate solution of the lane-Emden equation (4.1). Using (4.10) and (4.9) in (4.7),

$$\sum_{i=1}^{3p} a_i\psi_i(\varkappa) + \frac{k}{\varkappa}\left(\alpha_3 + \sum_{i=1}^{3p} a_i L_{i,1}(\varkappa)\right) = \mathcal{H}(\varkappa) - \int_0^{\varkappa}\mathbb{Q}(\varkappa,t)\left(\alpha_3 + \sum_{i=1}^{3p} a_i L_{i,1}(t)\right)dt,$$

$$\sum_{i=1}^{3p} a_i\psi_i(\varkappa) + \frac{k}{\varkappa}\left(\sum_{i=1}^{3p} a_i L_{i,1}(\varkappa)\right) + \int_0^{\varkappa}\mathbb{Q}(\varkappa,t)\sum_{i=1}^{3p} a_i L_{i,1}(t)\,dt$$

$$= \mathcal{H}(\varkappa) - \int_0^{\varkappa}\mathbb{Q}(\varkappa,t)\,\alpha_3 dt - \frac{k}{\varkappa}\alpha_3,$$

$$\sum_{i=1}^{3p} a_i[\,\psi_i(\varkappa) + \frac{k}{\varkappa} L_{i,1}(\varkappa) + \int_0^{\varkappa} \mathbb{Q}(\varkappa, t) L_{i,1}(t)dt] = \mathcal{H}(\varkappa) - \int_0^{\varkappa} \mathbb{Q}(\varkappa, t)\, \alpha_3 dt - \frac{k}{\varkappa}\alpha_3\,. \tag{4.11}$$

An $N \times N$ system of algebraic equations has been established by utilizing the lemma given in equation (4.8), for computing the integrals, and for putting the collocation points. Any iterative algorithm can be employed to determine the solutions to this system of equations. The Gauss elimination algorithm has been applied to tackle the linear problem. For the nonlinear equations, Quasilinearization is used. These algebraic equations can be solved to calculate the unknown Haar coefficient. Finally, the scale 3 Haar wavelet (S3-HW) solution at collocation points has been determined in equation (4.10) by using these Haar coefficients.

4.4 Numerical Experiments and Error Analysis

In this section, we examine several applications of Lane-Emden equations having initial or boundary conditions to analyze the efficiency and relevance of the presented algorithm. We compared the acquired results to existing numerical approaches used in the literature. Different errors have been calculated at collocation points by utilizing MATLAB software. If ξ_{ap} represents the S3-HW solution (approximate solution) and ξ_{ex} represents the true solution (exact solution), then $M_{cp} - error$, absolute error, $l_2 - error, E_{max} - error,\ and\ l_\infty - error,$ is computed by the given mathematical relation,

$$M_{cp} - error = \sqrt{\frac{1}{3N}\sum_{i=1}^{3p}\left|\xi_{ex}(x_m) - \xi_{ap}(x_m)\right|^2},$$

$$l_2 - error = \frac{\sqrt{\sum_{i=1}^{3p}\left|\xi_{ex}(x_m) - \xi_{ap}(x_m)\right|^2}}{\sum_{i=1}^{3p}|\xi_{ex}(x_m)|^2},\ E_{max} - error = \sqrt{\sum_{i=1}^{3p}\left|\xi_{ex}(x_m) - \xi_{ap}(x_m)\right|^2},$$

$$l_\infty - error = \max\left|\xi_{ex}(x_m) - \xi_{ap}(x_m)\right|, Absolute\ error = \left|\xi_{ex}(x_m) - \xi_{ap}(x_m)\right|.$$

Example 4.1: Consider the second order linear Lane-Emden differential equation of the form [232],

$$\begin{cases} \zeta''(\varkappa) + \frac{2}{\varkappa}\zeta'(\varkappa) + \zeta(\varkappa) = 6 + 12\varkappa + \varkappa^2 + \varkappa^3, \\ \zeta(0) = 0 \text{ and } \zeta'(0) = 0. \end{cases} \tag{4.12}$$

The corresponding Volterra integro-differential Lane-Emden equation is,

$$\begin{cases} \xi'(\varkappa) + \frac{2}{\varkappa}\xi'(\varkappa) = 12 + 2\varkappa + 3\varkappa^2 - \int_0^{\varkappa} \left(\frac{-2}{\varkappa^2} + 1\right) \xi(t)dt, \\ \xi(0) = 2. \end{cases} \tag{4.13}$$

The exact solution for Example 4.1 is $\zeta(\varkappa) = \varkappa^2 + \varkappa^3$ [232], and the approximated solution by using the presented algorithm is $\xi(\varkappa) = 2 + \sum_{i=1}^{3p} a_i L_{i,1}(\varkappa)$.

Table 4.1: Comparability of Exact solution with Approximated solution for Example 4.1 along with absolute error (AE).

$\varkappa$	Exact solution [232]	Approximate solution	AE	AE in differential form
0.055555555	2.333333333	2.333333333	0	1.713796E-04
0.166666666	3.000000000	3.000000000	0	3.089906E-04
0.277777777	3.666666666	3.666666666	0	7.474461E-04
0.388888888	4.333333333	4.333333333	8.88178E-16	1.115280E-03
0.500000000	5.000000000	5.000000000	0	1.460308E-03
0.611111111	5.666666666	5.666666666	8.88175E-16	1.789519E-03
0.722222222	6.333333333	6.333333333	0	2.104120E-03
0.833333333	7.000000000	7.000000000	0	2.403683E-03
0.944444444	7.666666666	7.666666666	0	2.687216E-03

Table 4.2: Computation of multiple errors for different levels of resolution for Example 4.1.

j	$l_2 - error$	$E_{max} - error$	$l_\infty - error$
0	0	0	0
1	7.91776E-17	1.25607E-15	8.88178E-16
2	0	0	0
3	9.32507E-17	4.44089E-15	8.88178E-16
4	8.63088E-17	7.11929E-15	1.77636E-15
5	8.27657E-17	1.18248E-14	1.77636E-15
6	1.07181E-16	2.65229E-14	1.77636E-15

The computation of the true solution and S3-HW solution of Example 4.1 are given in Table 4.1 for the level of resolution 1. The results shown in the table demonstrate that the method generates accurate solutions in terms of absolute error (AE) having an error of 10^{-16}. In Table 4.2, the computation of $l_2 - error, E_{max} - error, and\ l_\infty - error$ is presented. Table 4.2 illustrates that by increasing the value of j, the error becomes lesser. The comparison of S3-HW errors with that of the Adomain decomposition method and Chebyshev wavelet is given in Table 4.3.

Table 4.3: Comparison of $l_2 - error$ and $l_\infty - error$ with existing methods.

Errors	Chebyshev wavelet Method [26]	Adomain decomposition Method [10]	S3-HW method
$l_2 - error$	5.66647E−14	1.30900E−12	8.27657E-17
$l_\infty - error$	2.02061E−14	1.28586E−12	1.77636E-15

which clearly depicts that our results are better than the previous one. Furthermore, the suggested algorithm has been shown to produce high accuracy outcomes even with a small number of grid points. Figure 4.1 also shows the S3-HW solution and true solutions for level of resolution $j = 1$. The figures show that the resulting S3-HW

solution coincides well with the true solution. Figure 4.2 shows the graph of absolute error for Example 4.1 when $j = 1$.

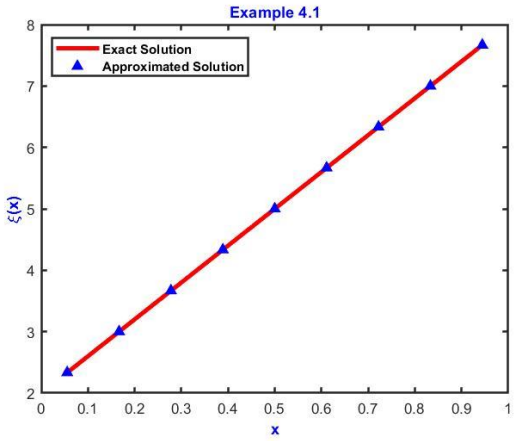

Figure 4.1: Visual analysis of exact solution and approximate solution for Example 4.1.

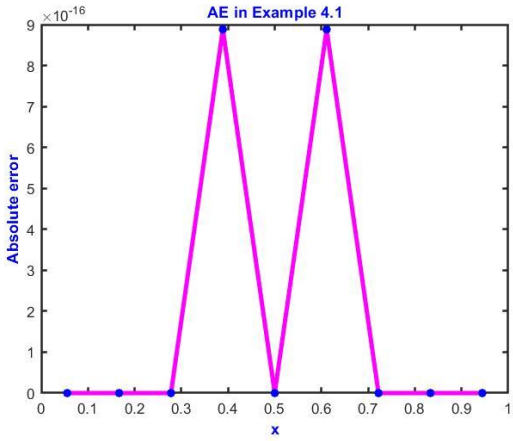

Figure 4.2: Graphical view of AE for Example 4.1.

Example 4.2: Next, we have solved the non-linear LE differential equation of the form [253],

$$\begin{cases} \zeta''(\varkappa) + \dfrac{1}{\varkappa}\zeta'(\varkappa) - \zeta^3(\varkappa) + 3\,\zeta^5(\varkappa) = 0, \\ \zeta'(0) = 0 \; and \; \zeta(1) = \dfrac{1}{\sqrt{2}}. \end{cases} \tag{4.14}$$

The corresponding Volterra integro-differential Lane-Emden equation is,

$$\begin{cases} \xi\,'(\varkappa) + \displaystyle\int_0^{\varkappa} \frac{t}{\varkappa}(3\,\xi^5(t) - \xi^3(t))\,dt = 0, \\ \xi(0) = 1. \end{cases} \tag{4.15}$$

The exact solution for Example 4.2 is $\zeta(\varkappa) = \frac{1}{\sqrt{1+\varkappa^2}}$ [253] and the approximated solution by using the presented algorithm is $\xi(\varkappa) = 1 + \sum_{i=1}^{3p} a_i L_{i,1}(\varkappa)$. This equation originates in the analysis of isothermal gas sphere equilibrium. The computation of true solution and S3-HW solution is given in Table 4.4 for Example 4.2. The results shown in table demonstrates that the method generates accurate solutions in terms of absolute error. In Table 4.5 computation of $l_2 - error, l_{max} - error, and\; l_\infty - error$ is presented. Table 4.5 illustrates that by increasing the value of j, error becomes lesser.

Table 4.4: Comparability of Exact solution with Approximated solution for Example 4.2 along with Absolute error (AE).

$\varkappa$	Exact solution [253]	Approximate solution	AE
0.055555555556	0.998460353205	0.998470899829	1.05466E-05
0.166666666667	0.986393923832	0.986400125001	6.20117E-06
0.277777777778	0.963517909630	0.963509847025	8.06260E-06
0.388888888889	0.932004671541	0.931965702446	3.89691E-05
0.500000000000	0.894427191000	0.894337637786	8.95532E-05
0.611111111111	0.853281833652	0.853124378302	1.57455E-04
0.722222222222	0.810679228400	0.810442731760	2.36497E-04
0.833333333333	0.768221279597	0.767901826959	3.19453E-04
0.944444444444	0.727013152550	0.726612960465	4.00192E-04

Table 4.5 : Computation of multiple errors for different level of resolution for Example 4.2.

j	$l_2 - error$	$E_{max} - error$	$l_\infty - error$
0	2.45168E-03	3.76885E-03	3.51118E-03
1	2.23333E-04	5.93868E-04	4.00192E-04
2	2.44184E-05	1.12448E-04	4.66187E-05
3	2.70847E-06	2.16029E-05	5.27484E-06
4	3.00884E-07	4.15668E-06	5.89792E-07
5	3.34308E-08	7.99937E-07	6.56716E-08
6	3.71453E-09	1.53948E-07	7.30203E-09

We have compared the value of absolute error for Example 4.2 obtained by using the S3-HW algorithm with that of [253] in Table 4.6. This depicts that the S3-HW algorithm is providing better results. Figure 4.3 shows the S3-HW solution and true solutions for level of resolution $j = 1$. The figures show that the resulting S3-HW

solution coincides well with the true solution. Figure 4.4 shows the graph of absolute error for Example 4.2 when $j = 1$.

Table 4.6: Comparison of absolute error for Example 4.2 at different points of the domain.

$\varkappa$	Absolute error for HWQA [253]	Absolute error for S3-HW
0	3.46100E-05	2.4900E-13
0.2	2.90983E-05	5.4250E-10
0.3	2.33723E-05	2.4290E-09
0.4	1.72621E-05	6.5520E-09
0.6	1.16388E-05	2.2080E-08
0.7	6.90631E-06	3.2627E-08
0.8	3.12139E-06	4.3902E-08
0.9	1.62325E-07	5.5151E-08

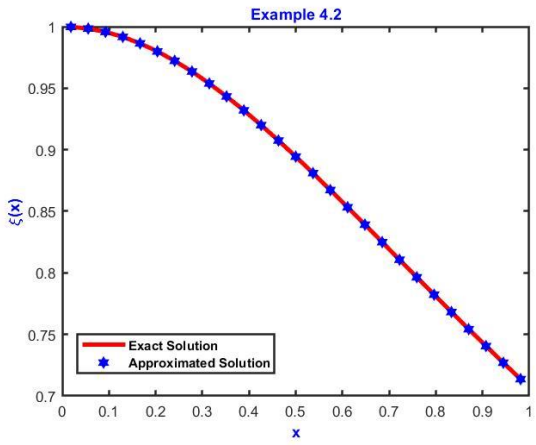

Figure 4.3: Visual analysis of exact solution and approximate solution for Example 4.2.

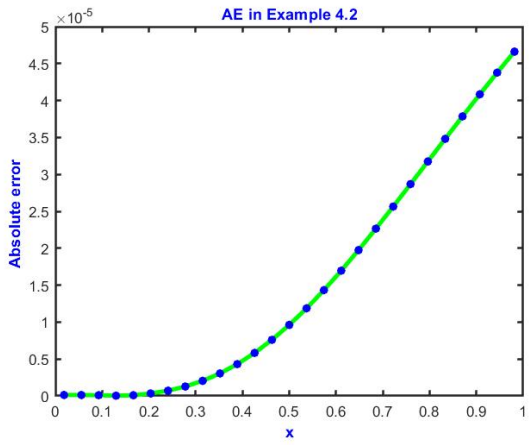

Figure 4.4: Graphical view of AE for Example 4.2.

Example 4.3: Let's consider the LE-E along with its boundary conditions [233], [243],

$$\begin{cases} \zeta''(\varkappa) + \frac{1}{\varkappa}\zeta'(\varkappa) = \left(\frac{8}{8-\varkappa^2}\right)^2, \\ \zeta'(0) = 0 \; and \; \zeta(1) = 0. \end{cases} \tag{4.16}$$

The corresponding Volterra integral Lane-Emden equation is,

$$\left\{\xi(\varkappa) + \int_0^{\varkappa} \frac{1}{\varkappa}\xi(t)\,dt - \left(\frac{8}{8-\varkappa^2}\right)^2 = 0, \right. \tag{4.17}$$

The exact solution for Example 4.3 is $\zeta(\varkappa) = 2\log\left(\frac{7}{8-\varkappa^2}\right)$ [233], [243]. The computation of true solution and S3-HW solution is given in Table 4.7 for Example 4.3. In Table 4.8 computation of $l_2 - error, E_{max} - error, and\ l_\infty - error$ is presented. Table 4.8 illustrates that by increasing the value of j, error becomes lesser. The error obtained for the Example 4.3 in [233] is 10^{-6}, in [245] the error is 10^{-8}, and by using the presented algorithm the error obtained is 10^{-9} at level of resolution 6 as shown in Table 4.9.

Table 4.7: Comparability of Exact solution with Approximated solution for Example 4.3 along with Absolute error (AE).

$\varkappa$	Exact solution [233], [243]	Approximate solution	AE
0.055555555556	0.500579076014	0.500386025849	1.93050E-04
0.166666666667	0.505238621326	0.505042573279	1.96048E-04
0.277777777778	0.514703340426	0.514501165202	2.02175E-04
0.388888888889	0.529274148817	0.529062443064	2.11706E-04
0.500000000000	0.549427679501	0.549202599104	2.25080E-04
0.611111111111	0.575849911585	0.575606964558	2.42947E-04
0.722222222222	0.609487186781	0.609220963206	2.66224E-04
0.833333333333	0.651621391086	0.651325197151	2.96194E-04
0.944444444444	0.703980101848	0.703645447854	3.34654E-04

Table 4.8: Computation of multiple errors for different levels of resolution for Example 4.3.

j	$l_2 - error$	$E_{max} - error$	$l_\infty - error$
0	3.77842E-03	3.74378E-03	2.63404E-03
1	4.26631E-04	7.35990E-04	3.34654E-04
2	4.74912E-05	1.41987E-04	3.89216E-05
3	5.27789E-06	2.73329E-05	4.39131E-06
4	5.86446E-07	5.26038E-06	4.90422E-07
5	6.51608E-08	1.01236E-06	5.45843E-08
6	7.24009E-09	1.94830E-07	6.06836E-09

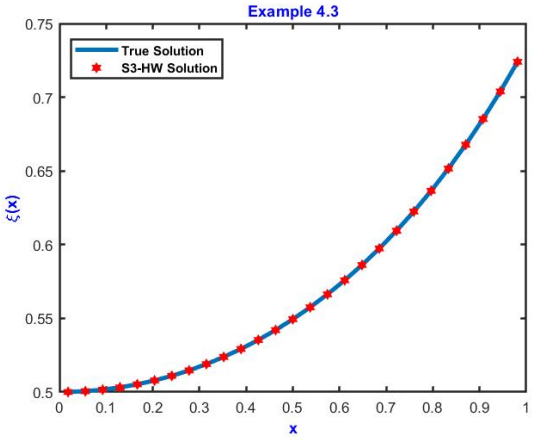

Figure 4.5: Visual analysis of exact solution and approximate solution for Example 4.3.

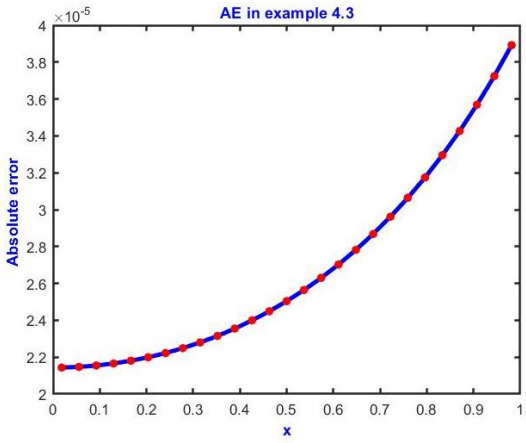

Figure 4.6: Graphical view of AE for Example 4.3.

Figure 4.5 shows the S3-HW solution and true solutions for the level of resolution $j = 1$. The figures show that the resulting S3-HW solution coincides well with the true solution. Figure 4.6 shows the graph of absolute error for Example 4.3 when $j = 1$.

Table 4.9: Comparison of Absolute error (AE) for different collocation points for Example 4.3.

$\varkappa$	AE in [233] for $\left(h=\frac{1}{20}\right)$	AE in [233] for $\left(h=\frac{1}{40}\right)$	AE in [243]	AE using HS3-W
0	2.6E-05	6.0E-06	1.6012E-06	3.26E-09
0.025	---	6.0E-06	---	3.26E-09
0.050	2.0E-05	6.0E-06	---	3.27E-09
0.075	---	6.0E-06	---	3.27E-09
0.100	2.7E-05	6.0E-06	---	3.28E-09
0.200	2.6E-05	6.0E-06	1.5665E-06	3.34E-09
0.300	2.5E-05	5.0E-06	---	3.45E-09
0.400	2.4E-05	4.0E-06	1.5577E-06	3.60E-09
0.500	2.2E-05	3.0E-06	---	3.81E-09
0.600	1.9E-05	2.0E-06	1.5524E-06	4.08E-09
0.700	1.5E-05	2.0E-06	---	4.42E-09
0.800	1.1E-05	1.0E-06	1.551E-06	4.85E-09
0.900	6.0E-05	1.0E-06	---	5.39E-09
1	0	0	1.6198E-16	---

Example 4.4: Last, consider the following LE-E. This equation finds its application in stellar structure. The equation is originating in the differential form as [254],

$$\begin{cases} \zeta''(\varkappa)+\dfrac{k}{\varkappa}\zeta'(\varkappa)+\zeta^{m}(\varkappa)=0, \\ \zeta'(0)=\alpha_1\,,\zeta(1)=\alpha_2. \end{cases} \tag{4.18}$$

having the following conditions;

$$\begin{cases} Case\ I\colon k=2,m=0,\alpha_1=0,and\ \ \alpha_2=\dfrac{1}{3!}, \\ Case\ II\colon\ k=2,m=1,\alpha_1=0,and\ \ \alpha_2=\sin 1\,, \\ Case\ III\colon\ =2,m=5,\alpha_1=0,and\ \ \alpha_2=\sqrt{\dfrac{3}{4}}. \end{cases} \tag{4.19}$$

The true solution for this Lane-Emden equation is available only for three different values of $m = 0, 1, and\ 5$ are $1 - \frac{1}{3!}\varkappa^2$, $\frac{\sin(\varkappa)}{\varkappa}$, and $\sqrt{\frac{3}{3+\varkappa^2}}$ [254] respectively. The corresponding integro-differential equation is of the form,

$$\begin{cases} \xi'(\varkappa) + \int_0^{\varkappa} \left(\frac{t}{\varkappa}\right)^k \xi^m(t)\, dt = 0, \\ \xi(0) = 1. \end{cases} \tag{4.20}$$

The computation of the true solution and S3-HW solution for case (1) of Example 4.4 corresponding to $m = 0$ is given in Table 4.10. In Table 4.11 computation of $l_2 - error, E_{max} - error, and\ l_\infty - error$ is presented. Table 4.11 illustrates that by increasing the value of j, the error becomes lesser. Figure 4.7 shows the S3-HW solution and true solutions for the level of resolution $j = 1$. The figures show that the resulting S3-HW solution coincides well with the true solution. Figure 4.8 shows the graph of absolute error for Example 4.4 when $j = 1$.

Table 4.10: Comparability of Exact solution with Approximated solution for Example 4.4 along with Absolute error (AE) for $m = 0$.

$\varkappa$	True solution [254]	S3-HW solution	AE
0.055555555556	0.999485596708	0.998971193416	5.14403E-04
0.166666666667	0.995370370370	0.994855967078	5.14403E-04
0.277777777778	0.987139917695	0.986625514403	5.14403E-04
0.388888888889	0.974794238683	0.974279835391	5.14403E-04
0.500000000000	0.958333333333	0.957818930041	5.14403E-04
0.611111111111	0.937757201646	0.937242798354	5.14403E-04
0.722222222222	0.913065843621	0.912551440329	5.14403E-04
0.833333333333	0.884259259259	0.883744855967	5.14403E-04
0.944444444444	0.851337448560	0.850823045267	5.14403E-04

Table 4.11: Computation of multiple errors for different level of resolution for Example 4.4 (when $m = 0$).

j	$l_2 - error$	$E_{max} - error$	$l_\infty - error$
0	4.88814E-03	8.01875E-03	4.62963E-03
1	5.43823E-04	1.54321E-03	5.14403E-04
2	6.04334E-05	2.96991E-04	5.71559E-05
3	6.71493E-06	5.71559E-05	6.35066E-06
4	7.46104E-07	1.09997E-05	7.05629E-07
5	8.29005E-08	2.11689E-06	7.84032E-08
6	9.21116E-09	4.07395E-07	8.71147E-09

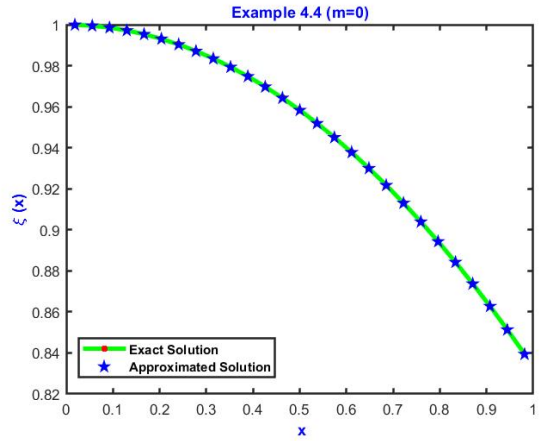

Figure 4.5: Visual analysis of exact solution and approximate solution for Example 4.4 when $m = 0$.

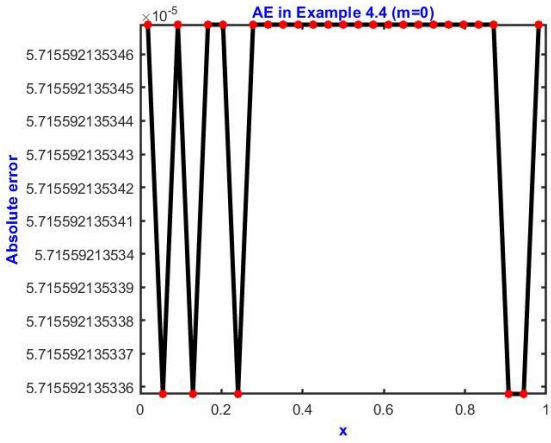

Figure 4.6: Graphical view of AE for Example 4.4 when $m = 0$.

Table 4.12: Comparability of Exact solution with Approximated solution for Example 4.4 along with Absolute error (AE) for $m = 1$.

$\varkappa$	True solution [254]	S3-HW solution	AE
0.055555555556	0.999485676085	0.998971986636	5.13689E-04
0.166666666667	0.995376796160	0.994867210111	5.09586E-04
0.277777777778	0.987189441159	0.986687755158	5.01686E-04
0.388888888889	0.974984152930	0.974494155154	4.89998E-04
0.500000000000	0.958851077208	0.958376444010	4.74633E-04
0.611111111111	0.938909170327	0.938453419119	4.55751E-04
0.722222222222	0.915305153379	0.914871603012	4.33550E-04
0.833333333333	0.888212223835	0.887803958686	4.08265E-04
0.944444444444	0.857828536959	0.857448374232	3.80163E-04

The computation of the true solution and S3-HW solution for case (2) of Example 4.4 corresponding to $m = 1$ is given in Table 4.12. In Table 4.13 computation of $l_2 - error, E_{max} - error, and\ l_\infty - error$ is presented. Table 4.13 illustrates that by increasing the value of j, the error becomes lesser. Figure 4.9 shows the S3-HW solution and true solutions for the level of resolution $j = 1$. The figures show that the resulting S3-HW solution coincides well with the true solution. Figure 4.10 shows the graph of absolute error for Example 4.4 when $j = 1$.

Table 4.13: Computation of multiple errors for different level of resolution for Example 4.4 (when $m = 1$).

j	$l_2 - error$	$l_{max} - error$	$l_\infty - error$
0	4.40116E-03	7.23062E-03	4.57220E-03
1	4.90993E-04	1.39553E-03	5.13689E-04
2	5.45922E-05	2.68719E-04	5.71471E-05
3	6.06643E-06	5.17195E-05	6.35055E-06
4	6.74057E-07	9.95356E-06	7.05627E-07
5	7.48954E-08	1.91557E-06	7.84032E-08
6	8.32171E-09	3.68651E-07	8.71146E-09

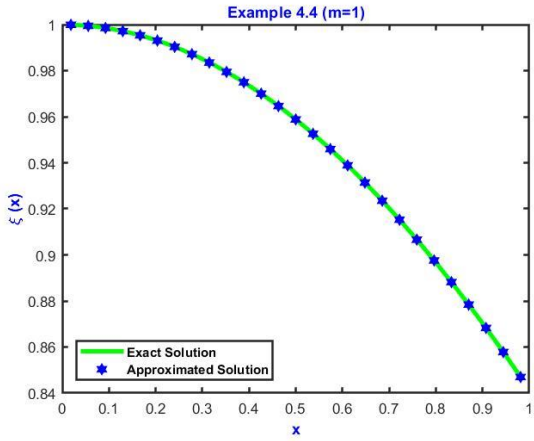

Figure 4.7: Visual analysis of exact solution and approximate solution for Example 4.4 when $m = 1$.

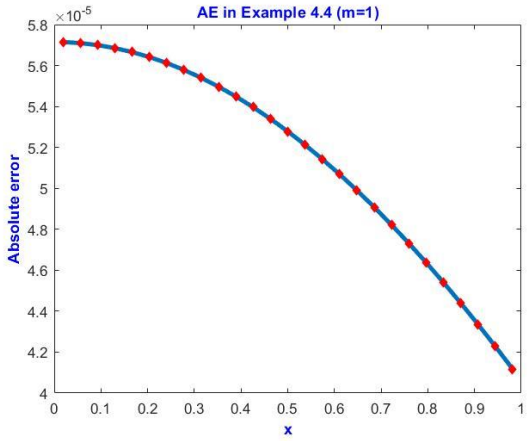

Figure 4.8: Graphical view of AE for Example 4.4 when $m = 1$.

The computation of the true solution and S3-HW solution for case (3) of Example 4.4 corresponding to $m = 5$ is given in Table 4.14. In Table 4.15 computation of $l_2 - error$ and $l_\infty - error$ is presented. We have also compared the values $l_2 - error$ and $l_\infty - error$ with that of the method presented in [255]. The value of $l_\infty - error$ and $l_2 - error$ for $j = 6$ in [255] is 8.92E-06 and 7.28E-06, while in the presented S3-HW algorithm, the errors are 1.16153E-08 and 2.93359E-08 respectively, which shows that the presented algorithm provides much better results. Table 4.15 illustrates that by increasing the value of j, error becomes lesser.

Table 4.14: Comparability of Exact solution with Approximated solution for Example 4.4 along with Absolute error (AE) for $m = 5$.

$\varkappa$	Exact solution [254]	Approximated solution	AE
0.055555555556	-0.331793425541	-0.332479068763	6.85643E-04
0.166666666667	-0.319708364572	-0.320345947060	6.37582E-04
0.277777777778	-0.296736635324	-0.297284503406	5.47868E-04
0.388888888889	-0.265048420258	-0.265476353156	4.27933E-04
0.500000000000	-0.227400928481	-0.227692828367	2.91900E-04
0.611111111111	-0.186702699731	-0.186856672356	1.53973E-04
0.722222222222	-0.145630818194	-0.145657044820	2.62266E-05
0.833333333333	-0.106368557497	-0.106285801027	8.27565E-05
0.944444444444	-0.070483367951	-0.070315068968	1.68299E-04

Table 4.15: Computation of multiple errors for different levels of resolution for Example 4.4 when $m = 5$.

j	$l_2 - error$	$l_2 - error$ [255]	$l_\infty - error$	$l_\infty - error$ [255]
0	1.66492E-02	-------	6.14990E-03	------
1	1.74408E-03	-------	6.85643E-04	-------
2	1.92617E-04	4.71E-04	7.62052E-05	1.97E-03
3	2.13876E-05	1.65E-04	8.46751E-06	4.91E-04
4	2.37623E-06	5.84E-05	9.40838E-07	1.23E-04
5	2.64023E-07	2.06E-05	1.04538E-07	3.12E-05
6	2.93359E-08	7.28E-06	1.16153E-08	8.92E-06

Table 4.16: Comparison of Absolute error (AE) for different collocation points with existing methods for Example 4.4 when $m = 5$.

$\varkappa$	Error in [251]	Error in [256]	Error in [257]	Error obtained by using the presented method
0	6.52E-06	6.32E-03	3.20E-03	1.1615E-08
0.1	6.46 E-06	6.27E-03	3.10E-03	1.1282E-08
0.2	6.30E-06	6.12E-03	2.90E-03	1.0327E-08
0.3	6.05E-06	5.87E-03	2.60E-03	8.8434E-09
0.4	5.70E-06	5.53E-03	2.20E-03	6.9841E-09
0.5	5.30E-06	5.09E-03	1.80E-03	4.9334E-09
0.6	4.84E-06	4.53E-03	1.40E-03	2.8448E-09
0.7	4.33E-06	3.82E-03	9.84E-04	8.7770E-10
0.8	3.86E-06	2.88E-03	6.07E-04	8.5490E-10
0.9	3.24E-06	1.64E-03	2.77E-04	2.2772E-09
1	1.45E-13	0	3.49E-08	3.3691E-09

In Table 4.16 we have compared the absolute error for the level of resolution 6 obtained by using the presented method with that of existing results, and this can be observed that the presented method works more efficiently.

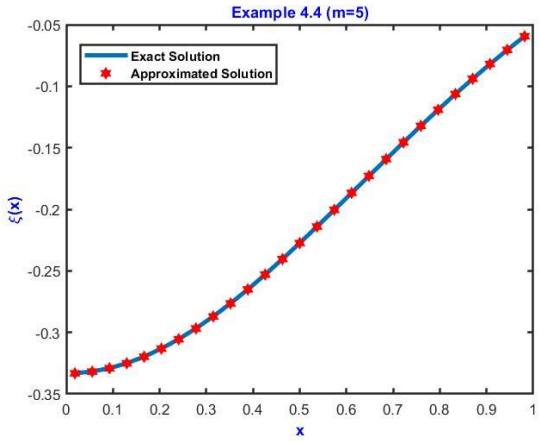

Figure 4.9: Visual analysis of exact solution and approximate solution for Example 4.4 when $m = 5$.

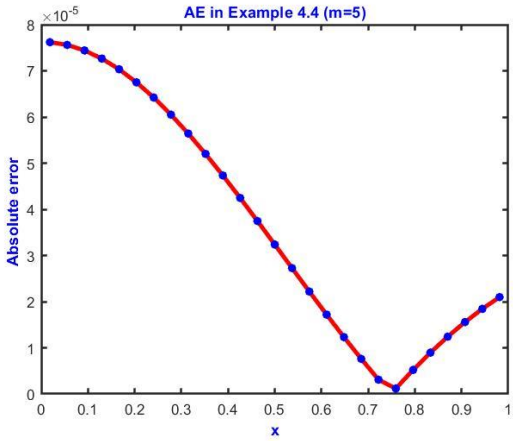

Figure 4.10: Graphical view of AE for Example 4.4 when $m = 5$.

Figure 4.11 shows the S3-HW solution and true solutions for the level of resolution $j = 1$ when $m = 5$. The figures show that the resulting S3-HW solution coincides well with the true solution. Figure 4.12 shows the graph of absolute error for Example 4.4 ($m = 5$) when $j = 1$.

Example 4.5: Consider the following Emden-fowler equation [248], [258], [232],

$$\begin{cases} \zeta''(x) + \frac{2}{x}\zeta'(x) - (4x^2 + 6)\zeta(x) = 0, & and\ 0 < x \leq 1, \\ \zeta(0) = 1, \zeta'(0) = 0. \end{cases} \tag{4.21}$$

The true solution obtained from the literature for Example 4.5 is $\zeta(x) = e^{x^2}$ [248], [258], [232]. By applying the technique mentioned above, (4.21) is converted to the Volterra integrodifferential form which is given as,

$$\begin{cases} \xi'(x) + \frac{2}{x}\xi(x) - \int_0^x \left(\frac{2}{x^2} + 12x^2 - 8tx + 6\right)\xi(t)dt = 8x, \\ \xi(0) = 2. \end{cases} \tag{4.22}$$

Table 4.17: Comparability of Exact solution with Approximated solution for Example 4.5 along with Absolute error.

x	Exact Solution [254]	Solution obtained by using NHWCA	Absolute Error
0.055555555556	2.018566217124	2.031084810106	1.251859E-02
0.166666666667	2.170575152369	2.177209062832	6.633910E-03
0.277777777778	2.493830684974	2.500874261885	7.043577E-03
0.388888888889	3.030245219289	3.039356476895	9.111258E-03
0.500000000000	3.852076250063	3.865679079825	1.360283E-02
0.611111111111	5.075649683026	5.097379736547	2.173005E-02
0.722222222222	6.884511366828	6.920284294443	3.577293E-02
0.833333333333	9.567959676644	9.627791254407	5.983158E-02
0.944444444444	13.585370204362	13.686629555573	1.012594E-01

The approximated solution obtained by using NHWCA for Example 4.5 is compared with the true solution in Table 4.17 and Figure 4.13, and it can be examined from the table and graph that the obtained findings by using the presented algorithm are strongly

under the true solution for a different level of resolution. Further with increasing the values of j the error gets decreased as presented in Table 4.18, ensuring the convergence of the algorithm. Moreover, the values of $l_2 - error$, $l_\infty - error$ by using this algorithm is less than in comparison with the Adomain decomposition method [232] and Chebyshev wavelet method [248] as shown in Table 4.19, demonstrating that the present algorithm produces better results than other methods, which attributes to the effectiveness and reliability of the algorithm. The graph for absolute error is shown in Figure 4.14.

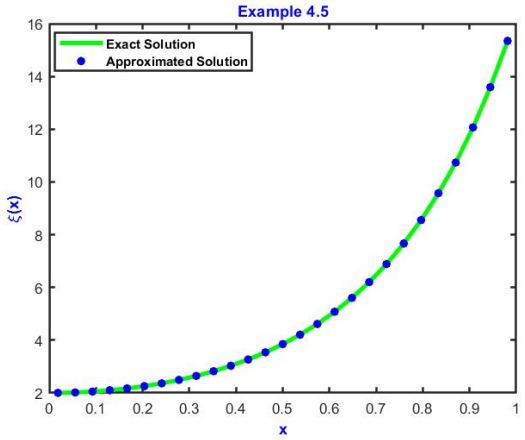

Figure 4.11: Visual analysis of exact solution and approximate solution for Example 4.5.

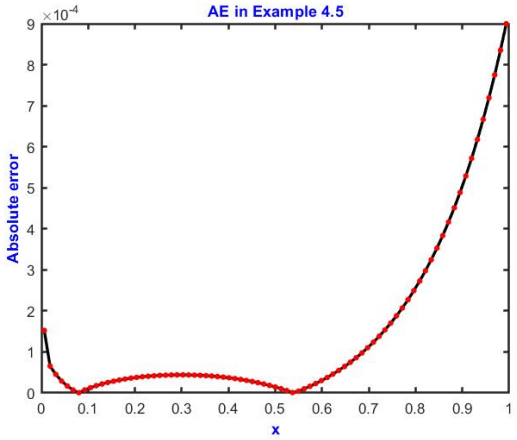

Figure 4.12: Graphical view of AE for Example 4.5.

Table 4.18: Computation of multiple errors for different level of resolution for Example 4.5.

j	$l_2 - error$	$l_\infty - error$	$E_{max} - error$
1	6.439931E-03	1.012594E-01	1.268998E-01
2	5.300090E-04	1.039881E-02	1.825504E-02
3	3.966904E-05	8.997636E-04	2.368949E-03
4	2.723184E-06	6.523842E-05	2.817027E-04
5	2.876767E-07	3.173068E-06	5.154479E-05
6	5.132399E-08	4.177646E-07	1.592802E-05

Table 4.19: Comparison of results obtained for Example 4.5 with other existing methods.

Computation of errors	Adomain decomposition method [232]	Chebyshev wavelet method [248]	Error obtained by using NHWCA
$l_2 - error$	5.59398E−06	1.05492E−07	5.132399E-08
$l_\infty - error$	5.59068E−06	1.03058E−07	4.177646E-07

Example 4.6: Consider the following Emden-fowler equation [259], [260],

$$\begin{cases} \zeta''(x) + \frac{1}{t}\zeta'(x) - \zeta(x) - (4 + x^2 - 9x - x^3) = 0, \\ \zeta(0) = 1, \zeta'(0) = 0. \end{cases} ; \ 0 < x \leq 1, \qquad (4.23)$$

The true solution obtained from the literature for Example 4.6 is $\zeta(x) = x^2 - x^3$ [259], [260]. By applying the above technique that is mentioned in section 4.2 of the article, equation (4.23) is converted to the Volterra integro-differential form which is given as,

$$\begin{cases} \xi'(x) + \frac{1}{x}\xi(x) - \int_0^x \left(\frac{1}{t^2} - 1\right)\xi(t)dt = -9 + 2x - 3x^2, \\ \xi(0) = 2. \end{cases} \qquad (4.24)$$

The numerical solution approximated by utilizing NHWCA for Example 4.6 is compared with the true solution for different collocation points in Table 4.20 and Figure 4.15. It is worth mentioning that the resulting solution and the actual values roughly coincide, which accounts for the high precision attained by the presented algorithm for a small no. of "collocation points". We have obtained the exact solution for some collocation points as shown in Table 4.20. The values of $l_2, l_{\infty,}, and\ E_{max} - error$ for different values of resolution is tabulated in Table 4.21. The absolute error obtained for the level of resolution 1 is 10^{-16} , which is presented in Figure 4.15. In Table 4.22, the behaviour of the current algorithm has been compared with reproducing kernel method [259], and the method presented in [260], and it can be observed that the error obtained by using the presented algorithm is negligible for the same collocation points.

Table 4.20: Comparability of Exact solution with Approximated solution for Example 4.6 along with absolute error.

x	Exact Solution [254]	Solution obtained by using NHWCA	Absolute Error
0.055555555556	1.666666666667	1.666666666667	2.220446E-16
0.166666666667	1.000000000000	1.000000000000	0
0.277777777778	0.333333333333	0.333333333333	2.220446E-16
0.388888888889	-0.333333333333	-0.333333333333	0
0.500000000000	-1.000000000000	-1.000000000000	0
0.611111111111	-1.666666666667	-1.666666666667	0
0.722222222222	-2.333333333333	-2.333333333333	8.881784E-16
0.833333333333	-3.000000000000	-3.000000000000	0
0.944444444444	-3.666666666667	-3.666666666667	8.881784E-16

Table 4.21: Computation of multiple errors for different levels of resolution for Example 4.6.

j	$l_2 - error$	$l_\infty - error$	$E_{max} - error$
1	2.167946E-16	8.881784E-16	1.294731E-15
2	1.449876E-16	4.440892E-16	1.505980E-15
3	2.189514E-16	8.881784E-16	3.940901E-15
4	1.780532E-16	8.881784E-16	5.551115E-15
5	4.899942E-17	2.220446E-16	2.645967E-15
6	5.124823E-17	2.220446E-16	4.793284E-15

Table 4.22: Comparison of results obtained for example 4.6 with other existing methods.

x	Absolute error for $m = 51\ in$ [259]	Absolute error for $m = 51\ in$ [260]	Absolute error for $m = 250\ in$ [260]	Absolute error for $j = 1$ by using NHWCA
0.08	4.8E-07	6.22E-06	6.02E-08	0
0.16	2.7E-06	7.28E-06	6.70E-08	0
0.32	1.3E-05	8.26E-06	7.33E-08	4.44E-16
0.48	2.9E-05	8.73E-06	7.62E-08	0
0.64	4.1E-05	8.98E-06	7.69E-08	4.44E-16
0.8	3.9E-05	9.13E-06	7.73E-08	0
0.96	1.1E-05	9.19E-06	7.81E-08	8.88E-16

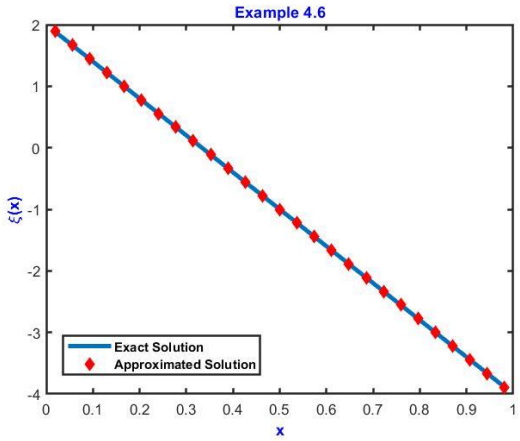

Figure 4.13: Visual analysis of exact solution and approximate solution for Example 4.6.

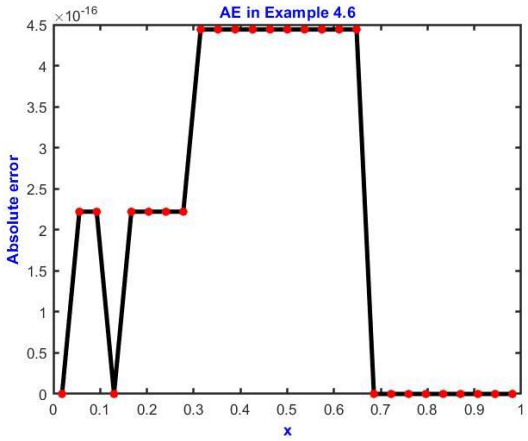

Figure 4.14: Graphical view of AE for Example 4.6.

Example 4.7: Consider the following Emden-fowler boundary value problem [256], [261],

$$\begin{cases} \zeta''(x) + \frac{1}{x}\zeta'(x) + \zeta(x) - \frac{5}{4} - \frac{x^2}{16} = 0, \\ \zeta'(0) = 0, \zeta(1) = \frac{17}{16}. \end{cases} \tag{4.25}$$

The true solution obtained from the literature for equation (6.5) is $\zeta(x) = 1 + \frac{x^2}{16}$, [256] , [261]. By applying the above technique that is mentioned in section 4.2 of the article, equation (4.25) is converted to the Volterra integro-differential form which is given as,

$$\begin{cases} \xi'(x) + \frac{1}{x}\xi(x) + \int_0^x \left(1 - \frac{1}{x^2}\right)\xi(t)dt = \frac{x}{8}, \\ \xi(0) = \frac{1}{8}. \end{cases} \tag{4.26}$$

Table 4.23: Comparability of Exact solution with Approximated solution for Example 4.7 along with absolute error.

x	Exact solution [256], [261]	Solution obtained by using NHWCA	Absolute Error
0.055555555556	0.125000000000	0.125000000000	0
0.166666666667	0.125000000000	0.125000000000	0
0.277777777778	0.125000000000	0.125000000000	0
0.388888888889	0.125000000000	0.125000000000	0
0.500000000000	0.125000000000	0.125000000000	0
0.611111111111	0.125000000000	0.125000000000	0
0.722222222222	0.125000000000	0.125000000000	0
0.833333333333	0.125000000000	0.125000000000	0
0.944444444444	0.125000000000	0.125000000000	0

For better visibility of results, the solution is depicted through tables and figures, showcasing different "collocation points" and varying "levels of resolution". The inferences derived from the algorithm employed exhibit strong consistency with the exact solution across various collocation points as shown in Table 4.23 and Figure 4.17. The values of absolute error for 0 level of resolution is shown in Figure 4.18. The comparison of presented algorithm with Variational iteration method [261], and He's variational iteration [256] is shown in Table 4.24, which clearly depicts that our results are far better than previous results. Based on the results obtained, it can be found that the presented method is more efficient and reliable than other methods.

Table 4.24: Comparison of results obtained for Example 4.7 with other existing method.

x	Error calculated in [261]	Error calculated in [256]	Error for $j = 1$ by using NHWCA
0	6.68E-02	1.42E-04	0.00000
0.1	6.62E-02	1.41E-04	0.00000
0.2	6.43E-02	1.40E-04	0.00000
0.3	6.12E-02	1.39E-04	0.00000
0.4	5.67E-02	1.36E-04	0.00000
0.5	5.09E-02	1.31E-04	0.00000
0.6	4.38E-02	1.24E-04	0.00000
0.7	3.52E-02	1.12E-04	0.00000
0.8	2.51E-02	9.15E-05	0.00000
0.9	1.34E-02	5.68E-05	0.00000
1.0	0.000000	0.000000	0.00000

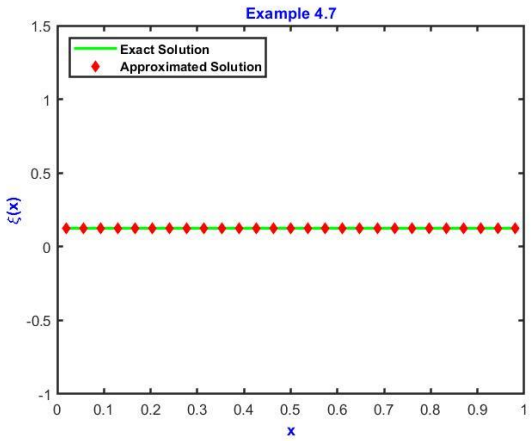

Figure 4.15: Visual analysis of exact solution and approximate solution for Example 4.7.

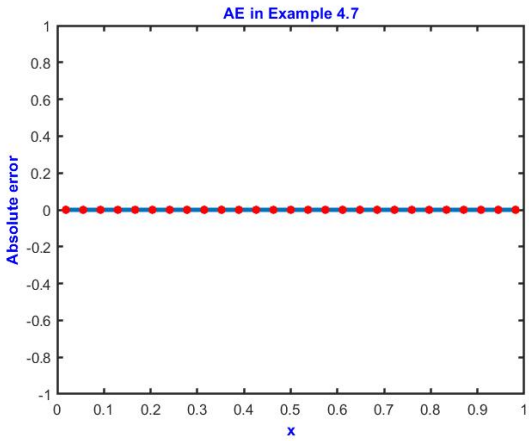

Figure 4.16: Graphical view of AE for Example 4.7.

Example 4.8: Consider the third order Emden-Fowler equation [262],

$$\begin{cases} \zeta'''(x) + \frac{4}{x}\zeta''(x) - (10 + 10x^3 + x^6)\zeta(x) = 0, \\ \zeta(0) = 1,\ \zeta'(0) = \zeta''(0) = 0. \end{cases} \tag{4.27}$$

The true solution obtained from the literature for Example 4.8 is $\xi(x) = e^{\frac{x^3}{3}}$ [262]. By applying the above technique that is mentioned in section 4.2 of the chapter, Example 4.8 is converted to the Volterra integro-differential form which is given as;

$$\begin{cases} \xi'(x) + \frac{4}{x}\xi(x) - \int_0^x \left(\frac{4}{x^2} + (15x^2 + 3x^5)(x-t)^2 + (10 + 10x^3 + x^6)(x-t) \right) \xi(t)dt \\ \qquad = 30x^2 + 6x^5, \\ \xi(0) = 2. \end{cases} \tag{4.28}$$

Table 4.25 and Figure 4.19 illustrate a comparative evaluation between the true solution and approximative numerical solution at the level of resolution 1, demonstrating the high accuracy attained by the present method. The absolute error for $j = 1$ is 10^{-3} as shown in Figure 4.19, and it can be observed that $l_2 - error$ decreases from 10^{-3} to 10^{-8} as the level of resolution increases from 1 to 6 as shown in Table

4.26, proving the convergence of NHWCA. The values of absolute error for 1 level of resolution is shown in Figure 4.20.

Table 4.25: Comparability of Exact solution with Approximated solution for Example 4.8 along with Absolute error.

x	Exact solution [262]	Solution obtained by using NHWCA	Absolute Error
0.055555555556	2.001143209901	2.002286709567	1.143500E-03
0.166666666667	2.030930946860	2.032950375058	2.019428E-03
0.277777777778	2.144325733725	2.146326065447	2.000332E-03
0.388888888889	2.402990282371	2.405840222946	2.849941E-03
0.500000000000	2.883293784666	2.888133992313	4.840208E-03
0.611111111111	3.691867450561	3.700899235735	9.031785E-03
0.722222222222	4.991200353913	5.008416122592	1.721577E-02
0.833333333333	7.042660563382	7.075299798702	3.263924E-02
0.944444444444	10.281338742829	10.342752943652	6.141420E-02

Table 4.26: Computation of multiple Errors for different level of resolution for Example 4.8.

j	$l_2 - error$	$l_\infty - error$	$E_{max} - error$
1	4.880455E-03	6.141420E-02	7.249770E-02
2	5.269308E-04	8.142502E-03	1.369918E-02
3	5.758853E-05	9.582928E-04	2.596243E-03
4	6.358071E-06	4.965373E-04	1.085166E-04
5	7.048828E-07	1.213361E-05	9.534771E-05
6	7.826138E-08	1.351010E-06	1.833590E-05

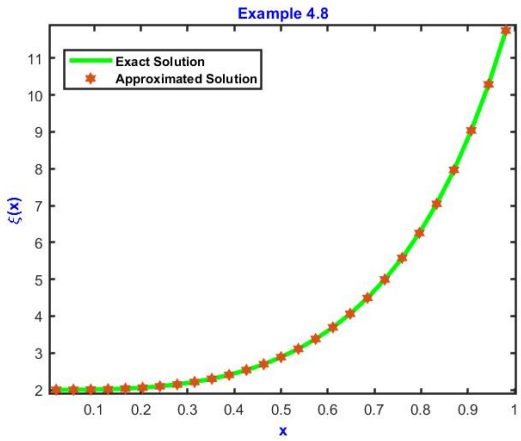

Figure 4.17: Visual analysis of exact solution and approximate solution for Example 4.8.

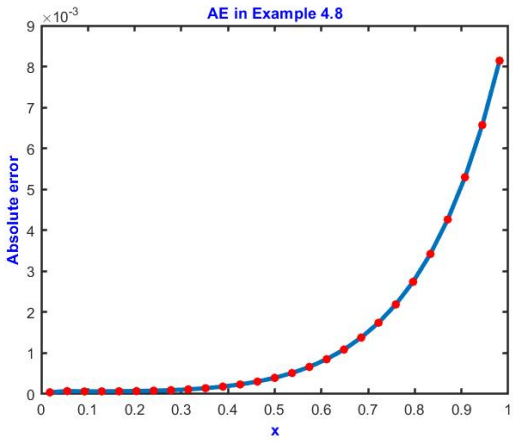

Figure 4.18: Graphical view of AE for Example 4.8.

4.5 Conclusions

In the present work, the basic Lane-Emden and Emden-Fowler type equations of differential form have been converted to the corresponding integro-differential form. These types of equations have been utilized to describe different problems in physical sciences, including diffusion of oxygen in a spherical cell, shallow membrane cap deformation, and thermal gradients in the human head. Volterra integro-differential (VID) form of "Lane-Emden type equations" reduces calculation and resolves the problem of singularity at $x = 0$. By applying the S3-HW algorithm, VID equations have been transformed into the corresponding algebraic equations. The Gauss-Elimination method is then applied to the solution of the system of algebraic equations. The quantitative result obtained by the S3-HW algorithm is compared to those acquired by the other techniques, including the Chebyshev wavelet method, Adomain decomposition method, Haar scale 2 wavelets, and also with the true solution. To demonstrate the applicability as well as the validity of the S3-HW algorithm, several applications have been presented. Tables and graphs illustrate that the presented algorithm provides less error.

Chapter 5.

Numerical Solution of Fractional Integro-Differential Equations by using Wavelets

5.1 Introduction

Fractional calculus is an area of mathematical analysis focused on extending the principles of differentiation and integration to non-integer orders. It encompasses the examination of fractional derivatives and integrals, which are mathematical operators that broaden the notion of differentiation and integration beyond whole numbers. The theory of fractional calculus has applications in a wide range of scientific and engineering fields, including physics, chemistry, engineering, economics, and biology. The origins of fractional calculus can be attributed to the contributions of renowned mathematicians like Leibniz, Euler, and Laplace during the 17th and 18th centuries. Since then, fractional calculus has undergone significant developments, with contributions from many mathematicians such as Riemann, Liouville, Grunwald, Letnikov, and Caputo. The fundamental principle of fractional calculus revolves around the notion of differentiating and integrating with non-integer orders. The fractional derivative and integral have many interesting properties that are not found in ordinary calculus. There exist numerous studies dealing with dynamical systems represented by fractional-order equations, which incorporate derivatives and integrals of arbitrary orders to describe the memory and inherent characteristics of diverse materials. In 1695, L'Hopital corresponded with Leibnitz seeking clarification on a novel notation he had introduced for the derivative of order 'n' of a linear function. L'Hopital inquired about the implications of evaluating the derivative at a half-integer value of n. Leibnitz deemed it a perplexing problem, with potentially significant consequences in the future. This marked the emergence of fractional derivatives in scientific discourse. Certain fractional differential models admit non-differentiable yet continuous solutions, exemplified by Weierstrass type functions. Ordinary or partial differential equations cannot elucidate certain characteristics of complex systems. Previously, fractional calculus was solely a mathematical concept with no discernible applications. However,

in recent times, fractional calculus has gained immense importance in various scientific and technological domains, including the fields of thermo-elasticity, fluid dynamics, viscoelastic fluids, and earthquake dynamics. Bagley and Torvik experimented to study the movement of a rigid plate immersed in a Newtonian fluid. Through their research, they discovered that the opposing force was directly related to the fractional derivative of displacement rather than velocity. The experiment also demonstrated that the fractional model provided more accurate predictions than the integer-order model for the same material. Observations in real-time and empirical data provide evidence that numerous intricate systems in nature, including phenomena like relaxation in viscoelastic materials, charge transport in amorphous semiconductors, and diffusion of pollution in the environment exhibit unconventional or abnormal dynamics. The scientific community has taken great interest in the enhanced efficiency and accuracy that fractional differential equations offer in describing anomalous system dynamics. The applications of fractional calculus are widespread and diverse. The primary domains where significant applications of fractional calculus are evident are as follows: life sciences [263], finance [264], [265], biochemistry [266], fluid mechanics [267], radio astronomy [268], geophysics [269], [270], dynamical system [271], electron emission [272], mathematical modelling [273]–[275], physical system [276], mechanics and viscoelastic material [277], [278]. As a result, several significant classical differential equations with integer-orders have been extended to the more general fractional differential equation having arbitrary orders, facilitating in-depth analyses of corresponding physical models. Several researchers are working to solve the IDEs of non-integer order due to their scientific applications in multiple branches. Some of the commonly used numerical methods are the Adomain decomposition method [279], Collocation method [280], Fractional differential transform method [281], Cosine and Sine wavelet method [282], Legendre wavelets [283], Sinc-collocation method [284], Chebyshev wavelet method [285]. In this method, a Chebyshev wavelet of the second type has been designed. Then, a computational technique is described on the Chebyshev wavelet of the second kind for tackling a class of fractional-order nonlinear FIDEs. The equation is transformed into a set of algebraic equations by applying the derived Chebyshev wavelet of the second kind operational matrix for fractional integration. The technique is demonstrated with applications, and

the obtained outcomes have been compared with those presented in the existing literature. The mixed VFIDEs having fractional order have been solved by using Genocchi polynomials operational matrices [286]. In this computational scheme, a mathematical expression is formulated by implementing the matrix method, to calculate the Genocchi coefficients of the integral kernel as well as for the integral of the product of two polynomials. Fractional IDEs having weakly singular kernels have been solved by using the compact finite difference method [287], and Taylor wavelets method [288]. Taylor wavelets are also used for resolving mixed VFIDEs [289].

Various computational methods have been developed to numerically solve various IDEs of fractional order. However, there are certain shortcomings in some numerical approaches. Most of the time, model equations comprising functional equations are generally discretized using computational methods, taking the set of a sequence of algebraic equations. Because of the considerable computational time as well as memory demand for numerical computations, the computation complexity of a large system increases in the case of direct solvers that solve the desired set of algebraic equations. Hence, introducing a simple but effective numerical approach for FIDEs continues to be an enormous task. In this work, scale 3 Haar wavelets are used for the approximation of FrIDEs. This chapter comprises different sections which are as follows: In section 5.2, certain fundamental definitions connected to fractional calculus are presented. The fundamental preliminary associated with the “scale 3 Haar wavelet” and the computing scheme are given in Section 5.3. The computational scheme is tested on various examples and is explored in section 5.4. The conclusion part is given in section 5.5 of the chapter.

5.2 Some Basic Definitions Employed in the Field of Fractional Calculus

The concept of fractional order derivative and integral is being presented by a lot of different researchers, and they are using their definitions and notations. The Caputo definition, the Grunwald-Letnikov definition, and the Riemann-Liouville definition are some of the more recent developments in the field of fractional derivatives.

5.2.1 Gamma Function

The Gamma function has deep roots in fractional calculus and is intrinsically connected to it. The gamma function (denoted by 'Γ') is a frequently used generalization of the factorial function to complex numbers in mathematics. All complex numbers, except for non-positive integers, are incorporated into the definition of the gamma function. For each integer 'n' that is positive, Γ(n) is defined as,

$$\Gamma(n) = (n-1)!\,, \tag{5.1}$$

Via the use of a convergent improper integral, the gamma function can be described as,

$$\Gamma(\alpha) = \int_0^\infty t^{\alpha-1}e^{-t}dt. \tag{5.2}$$

5.2.2 Definition

A real function $\xi(x)$, where $x > 0$ is considered to belong to the space $C_\theta, \theta \in \mathbb{R}$ if $\exists$ a number $p \in \mathbb{R}$ such that $p > \theta$ and $\xi(x) = x^p\xi_1(x)$; where $\xi_1(x) \epsilon [0, \infty)$. Furthermore, a function $\xi(x)$ is considered to belong to the space $C_k^\theta : k \in \mathbb{N} \cup \{0\}$ if and only if $\xi^{(k)} \epsilon C_\theta$.

5.2.3 Mittag-Leffler Function

In the realm of fractional calculus, the Mittag-Leffler function holds great significance as it serves as an extension of the exponential function. This function can be expressed in two distinct forms, as exemplified below;

❖ *The Mittag-Leffler function with a single parameter*

The Mittag-Leffler function with a single parameter is defined for a collection of complex numbers and a positive real number α,

$$E_\alpha = \sum_{m=0}^{\infty} \frac{x^m}{\Gamma(\alpha m + 1)};\ \alpha > 0\,, \alpha \in \mathbb{R}, s \in \mathbb{C}\,. \tag{5.3}$$

❖ *The Mittag-Leffler function with two parameters*

The Mittag-Leffler function for two parameters is defined for a collection of complex numbers along with two positive real numbers α and β,

$$E_{\alpha,\beta} = \sum_{m=0}^{\infty} \frac{x^m}{\Gamma(\alpha m + \beta)} \; ; \; \alpha, \beta > 0 \; ; \; \alpha, \beta \in \mathbb{R}, s \in \mathbb{C} \, . \tag{5.4}$$

5.2.4 Riemann-Liouville Fractional Integral Operator

The Riemann-Liouville fractional integral operator with order $\alpha > 0$ of a function $\xi(x) \in C_\theta; \theta \geq -1,$ is defined as,

$$I_s^\alpha \, \xi(x) = \frac{1}{\Gamma(\alpha)} \int_0^x (x-t)^{\alpha-1} \xi(x) dx. \tag{5.5}$$

The following is a list of several properties that the Riemann-Liouville fractional integral contains;

1. $I_x^0 \, \xi(x) = \xi(x),$
2. $\left(I_x^\alpha \, I_x^\beta \xi\right)(x) = \left(I_x^{\alpha+\beta} \xi\right)(x) = \left(I_x^\beta \, I_x^\alpha \xi\right)(x),$
3. $I_x^\alpha \, (x-\mu)^\lambda \, = \frac{\Gamma(1+\lambda)}{\Gamma(1+\lambda+\alpha)} (x-\mu)^{\lambda+\alpha}.$

The Riemann-Liouville fractional integral seems to be a linear operator, and works in the same way as the integer-order integration, which means that,

$$I_x^\alpha \left(\sum_{i=1}^m a_i \xi_i(x) \right) = \left(\sum_{i=1}^m a_i \right) I_s^\alpha \xi_i(x),$$

where $\{a_i\}_{i=1}^m$ are constants.

5.2.5 Riemann-Liouville Fractional Differential Operator

Riemann-Liouville (mathematician) introduced the fractional differential operator for positive real numbers α, a, t in the interval $[a, b]$ and is described as,

$$D_x^\alpha \xi(x) = \begin{cases} \dfrac{1}{\Gamma(m-\alpha)} \dfrac{d^m}{dt^m} \displaystyle\int_a^x \frac{\xi(t)}{(x-t)^{1+\alpha-m}} dt; \; m-1 < \alpha < m, \\ \dfrac{d^m}{dt^m} \xi(x) \; ; \qquad\qquad \alpha = m \in \mathbb{N}. \end{cases} \tag{5.6}$$

where $x \in [a, b]$ and 'α' indicates the derivative's order.

5.2.6 Caputo Fractional Differential Operator

Caputo (mathematician) introduced the fractional differential operator for positive real numbers α, a, t in the interval $[a, b]$ and is described as,

$$D_x^{\alpha}\xi(x) = \begin{cases} \dfrac{1}{\Gamma(m-\alpha)}\displaystyle\int_a^x \frac{\xi^m(t)}{(x-t)^{1+\alpha-m}}\,dt;\ m-1<\alpha<m, \\ \dfrac{d^m}{dt^m}\xi(x); \qquad\qquad \alpha = m\,\epsilon\,\mathbb{N}. \end{cases} \tag{5.7}$$

where $x\,\epsilon\,[a, b]$ and 'α' represents the derivative's order.

5.3 Scale 3 Haar wavelets and approximation of functions

Haar wavelets are rectangular waveforms made up of piecewise constant functions. Following mathematical expressions are introduced in reference [290], [291] that represent the Haar scaling function, and the mother wavelets for the scale 3 Haar wavelet family can be expressed as follows;

Haar scaling function

$$h_1(x) = \phi^0(x) = \begin{cases} 1 & x\,\epsilon\,[0,1], \\ 0 & elsewhere. \end{cases} \tag{5.8}$$

Symmetric Haar wavelet

$$h_i(x) = \phi^1\left(3^j x - k\right) = \frac{1}{\sqrt{2}}\begin{cases} -1 & x\,\epsilon\,\left[\psi_1(i),\,\psi_2(i)\right), \\ 2 & x\,\epsilon\,\left[\psi_2(i),\,\psi_3(i)\right), \\ -1 & x\,\epsilon\,\left[\psi_3(i),\,\psi_4(i)\right), \\ 0 & elsewhere, \end{cases} \tag{5.9}$$

$$for\ i = 2, 4, \ldots, 3p-1.$$

Anti-Symmetric Haar wavelet

$$h_i(x) = \phi^2\left(3^j x - k\right) = \sqrt{\frac{3}{2}}\begin{cases} 1 & x\,\epsilon\,\left[\psi_1(i),\,\psi_2(i)\right), \\ 0 & x\,\epsilon\,\left[\psi_2(i),\,\psi_3(i)\right), \\ -1 & x\,\epsilon\,\left[\psi_3(i),\,\psi_4(i)\right), \\ 0 & elsewhere, \end{cases} \tag{5.10}$$

$$for\ i = 3, 5, \ldots, 3p.$$

where $$\psi_1(i) = \frac{k}{p}, \psi_2(i) = \frac{3k+1}{3p},\ \psi_3(i) = \frac{3k+2}{3p}\ , \psi_4(i) = \frac{k+1}{p}, \tag{5.11}$$

$$p = 3^j\ , j = 0, 1, 2, \ldots\ and\ \ k = 0, 1, 2, \ldots p-1.$$

Throughout this context, 'i' symbolizes the wavelet number determined from the relations.

$$\begin{cases} i = p + 2k + 1, & (for\ i = 2,4,6, \dots) \\ i = p + 2k + 2, & (for\ i = 3,5,7, \dots) \end{cases}; \ p = 3^j.$$

Wavelet translation parameters are denoted by 'k' whereas dilation or resolution levels are indicated by 'j'. The function '$h_1(x)$' is considered the father wavelet. The functions '$h_2(x)$' and '$h_3(x)$' are termed as mother wavelets, and the functions '$h_4(x), h_5(x), \text{and } h_6(x)$' that comes from translating and stretching the mother wavelets are termed as daughter wavelets. The Haar functions $(5.8) - (5.10)$ can be integrated easily over the desired number of times with in the interval $[0, 1]$ by using the formula presented below;

$$\mathrm{P}_{\rho,i}(x) = \int_0^x \int_0^x \int_0^x \dots \rho\ times \dots \int_0^x h_i(t)(dt)^\rho\,, \tag{5.12}$$

Equivalently, by using a relation from calculus for converting the multiple integrals to single integrals, the formula becomes,

$$\mathrm{P}_{\rho,i}(x) = \frac{1}{\Gamma(\rho)} \int_0^x (x-t)^{\rho-1} h_i(t)dt, \tag{5.13}$$

where

$$\rho = 1, 2, 3, \dots \ \ and\ i = 1, 2, 3, \dots 3p.$$

Computing the above integrals generates;

$$\mathrm{P}_{\rho,i}(x) = \frac{x^\rho}{\Gamma(\rho+1)}\,, \qquad for\ i = 1. \tag{5.14}$$

$\mathrm{P}_{\rho,i}(x)'s \ \ for \ \ i = 2,4,6,8, \cdots, 3p-1,$ are given by $\mathrm{P}_{\rho,i}(x) =$

$$\sqrt{\frac{1}{2}} \begin{cases} 0 & x \in [0,\ \psi_1(i)), \\ \dfrac{-1}{\Gamma(\rho+1)}(x-\psi_1(i))^\rho & x \in [\psi_1(i),\ \psi_2(i)), \\ \dfrac{1}{\Gamma(\rho+1)}\left[-(x-\psi_1(i))^\rho + 3(x-\psi_2(i))^\rho\right] & x \in [\psi_2(i),\ \psi_3(i)), \\ \dfrac{1}{\Gamma(\rho+1)}\left[-(x-\psi_1(i))^\rho + 3\,(x-\psi_2(i))^\rho - 3\,(x-\psi_3(i))^\rho\right] & x \in [\psi_3(i),\ \psi_4(i)), \\ \dfrac{1}{\Gamma(\rho+1)}\left[-(x-\psi_1(i))^\rho + 3\,(x-\psi_2(i))^\rho - 3\,(x-\psi_3(i))^\rho + (x-\psi_4(i))^\rho\right] & x \in [\psi_4(i), 1). \end{cases} \tag{5.15}$$

$\mathrm{P}_{\rho,i}(x)'s \quad for \quad i = 3,5,7,9,\cdots,3p,$ are given by $\mathrm{P}_{\rho,i}(x) =$

$$\sqrt{\frac{3}{2}}\begin{cases} 0 & x \in [0,\ \psi_1(i)), \\ \frac{1}{\Gamma(\rho+1)}(x-\psi_1(i))^{\rho} & x \in [\psi_1(i),\ \psi_2(i)), \\ \frac{1}{\Gamma(\rho+1)}\left[(x-\psi_1(i))^{\rho} - (x-\psi_2(i))^{\rho}\right] & x \in [\psi_2(i),\ \psi_3(i)), \\ \frac{1}{\Gamma(\rho+1)}\left[(x-\psi_1(i))^{\rho} - (x-\psi_2(i))^{\rho} - (x-\psi_3(i))^{\rho}\right] & x \in [\psi_3(i), \psi_4(i)), \\ \frac{1}{\Gamma(\rho+1)}\left[(x-\psi_1(i))^{\rho} - (x-\psi_2(i))^{\rho} - (x-\psi_3(i))^{\rho} + (x-\psi_4(i))^{\rho}\right] & x \in [\psi_4(i), 1). \end{cases} \tag{5.16}$$

The relation for selecting the collocation point for the interval $[a_1, a_2]$ through using Haar scale 3 wavelet collocation algorithm is as follows;

$$x_m = a_1 + (a_2 - a_1)\frac{m - \left(\frac{1}{2}\right)}{3p};\ m = 1, 2, 3, \ldots, 3p. \tag{5.17}$$

5.3.1 Approximation of functions by scale 3 Haar wavelets

In this section, a computational scheme is discussed for approximating the solution of FrIDEs. By using the properties of scale 3 Haar wavelets, any arbitrary function $\xi(x) \in L_2(\mathbb{R})$ can be expressible as a linear combination of the basis of scale 3 Haar functions. i.e.,

$$\xi(x) = \sum_{i=0}^{\infty} a_i h_i(x) = \sum\nolimits_{even\ i} a_i \phi^1\left(3^j x - k\right) + \sum\nolimits_{odd\ i} a_i \phi^2\left(3^j x - k\right), \tag{5.18}$$

Here '$a_i's$' depicts the scale 3 Haar wavelet coefficients. The values for these coefficients are to be calculated with the aid of the presented computational scheme. A finite number of terms can be considered for computing purposes. First $3p$ are used to approximate the function $\xi(x)$,

$$\xi(x) = \sum_{i=0}^{3p} a_i h_i(x)\,; p = 3^j, j = 0,1,2, \ldots \tag{5.19}$$

5.3.2 Scale 3 Haar Wavelet computational scheme

Consider a 2nd order VFIDE of the form,

$$a(x)D''\xi(x) + b(x)D'\xi(x) + c(x)D^{\alpha}\xi(x) + d(x)\xi(x) = f(x) + \int_0^x K_1(x,t)\xi(t)dt + \int_0^1 K_2(x,t)\xi(t)dt, \tag{5.20}$$

with initial constraints

$$\xi(0) = \beta_1 \,, \xi'(0) = \beta_2. \tag{5.21}$$

Here $a(x)$, $b(x), c(x)$ and $d(x)$ are the known functions of 'x'. The following steps can be used to generate the approximate solution $\xi(x)$ for this equation.

Step 1: Estimate the derivative of the highest order involved in Eq. (5.20) by using scale 3 Haar wavelet bases,

$$D''\xi(x) = \sum_{i=0}^{3p} a_i h_i(x) = \sum\nolimits_{even\ i} a_i \phi^1\left(3^j x - k\right) + \sum\nolimits_{odd\ i} a_i \phi^2\left(3^j x - k\right), \tag{5.22}$$

where '$a_i's$' are scale 3 Haar coefficients.

Step 2: Integrate Eq. (5.22) between the limits '0' to 'x', and using the initial constraints given in Eq. (5.21), we obtain,

$$D'\xi(x) = \sum_{i=0}^{3p} a_i \mathrm{P}_{1,i}(x) + \beta_2, \tag{5.23}$$

Integrate Eq. (5.23) again between the limits '0' to 'x' and using the initial constraints,

$$\xi(x) = \sum_{i=0}^{3p} a_i \mathrm{P}_{2,i}(x) + \beta_2 x + \beta_1, \tag{5.24}$$

Step 3: Differentiate Eq. (5.24) using the Caputo derivative defined in section 5.2, to obtain the value of $D^{\alpha}\xi(x)$,

$$D^{\alpha}\xi(x) = \sum_{i=0}^{3p} a_i \mathrm{P}_{\frac{3}{2},i}(x) + D^{\alpha}(\beta_1 + \beta_2 x). \tag{5.25}$$

Step 4: Substitute Eq. $(5.22) - (5.25)$ in Eq. (5.20),

$$
\begin{aligned}
a(x)\sum_{i=0}^{3p} a_i h_i(x) + b(x)\Big(\sum_{i=0}^{3p} a_i \mathrm{P}_{1,i}(x) + \beta_2\Big) + c(x)\Big(\sum_{i=0}^{3p} a_i \mathrm{P}_{\frac{3}{2},i}(x) \\
+ D^{\alpha}(\beta_1 + \beta_2 x)\Big) + d(x)\Big(\sum_{i=0}^{3p} a_i \mathrm{P}_{2,i}(x) + \beta_2 x + \beta_1\Big) \\
= f(x) + \int_0^x K_1(x,t)\Big(\sum_{i=0}^{3p} a_i \mathrm{P}_{2,i}(t) + \beta_2 t + \beta_1\Big)dt \\
+ \int_0^1 K_2(x,t)\Big(\sum_{i=0}^{3p} a_i \mathrm{P}_{2,i}(t) + \beta_2 t + \beta_1\Big)dt,
\end{aligned}
\tag{5.26}
$$

After making the simplification,

$$
\begin{aligned}
\sum_{i=0}^{3p} a_i \Bigg[a(x)h_i(x) + b(x)\mathrm{P}_{1,i}(x) + c(x)\mathrm{P}_{\frac{3}{2},i}(x) + d(x)\mathrm{P}_{2,i}(x) \\
- \int_0^x K_1(x,t)\mathrm{P}_{2,i}(t)dt - \int_0^1 K_2(x,t)(\mathrm{P}_{2,i}(t))dt \Bigg] \\
= f(x) \\
- \{b(x)\beta_2 + c(x)D^{\alpha}(\beta_1 + \beta_2 x) + d(x)(\beta_1 + \beta_2 x)\} \\
+ \int_0^x K_1(x,t)(\beta_1 + \beta_2 t)dt + \int_0^1 K_2(x,t)(\beta_1 + \beta_2 t)dt,
\end{aligned}
\tag{5.27}
$$

For the purpose of simplicity, let's assume $K_1(x,t) = 1$ and $K_2(x,t) = 0$, the equation reduced to the Volterra IDE

$$
\begin{aligned}
\textstyle\sum_{i=0}^{3p} a_i \Big[a(x)h_i(x) + b(x)\mathrm{P}_{1,i}(x) + c(x)\mathrm{P}_{\frac{3}{2},i}(x) + d(x)\mathrm{P}_{2,i}(x) - \\
\mathrm{P}_{3,i}(x)\Big] = f(x) - \{b(x)\beta_2 + c(x)D^{\alpha}(\beta_1 + \beta_2 x) + d(x)(\beta_1 + \beta_2 x)\}.
\end{aligned}
\tag{5.28}
$$

This is the matrix system $aH = F$ that results from discretizing the equation (5.28) by using collocation points.

Step 5: By solving this system of equations using Thomas algorithm, one can attain the values of unknown Haar coefficients $a_i's$. By putting the values of $a_i's$ in Eq. (5.24), an approximate solution is obtained.

Note: If the Kernal function involved in Eq. (5.20) is $K(x,t) \neq 1$, then the approximate solution is calculated by converting the integro-differential equations to corresponding differential equations and then applying the same procedure. The conversion is taken place via the Leibnitz rule.

5.4 Numerical Examples and Error Analysis

To demonstrate the presented computational scheme is suitable for the FrIDEs, the solutions to ten distinct problems have been analyzed, and a variety of errors have been calculated to examine the efficacy of the current scheme with the aid of the formulas that are mentioned below.

$$M_{cp} - error = \sqrt{\frac{1}{3N}\sum_{i=1}^{3p}\left|\xi_{ex}(x_m) - \xi_{ap}(x_m)\right|^2},$$

$$l_2 - error = \frac{\sqrt{\sum_{i=1}^{3p}\left|\xi_{ex}(x_m)-\xi_{ap}(x_m)\right|^2}}{\sum_{i=1}^{3p}|\xi_{ex}(x_m)|^2},\ E_{max} - error = \sqrt{\sum_{i=1}^{3p}\left|\xi_{ex}(x_m) - \xi_{ap}(x_m)\right|^2},$$

$$l_\infty - error = \max\left|\xi_{ex}(x_m) - \xi_{ap}(x_m)\right|, Absolute\ error = \left|\xi_{ex}(x_m) - \xi_{ap}(x_m)\right|$$

Example 5.1: Consider the VFrIDEs [292],

$$\begin{cases} D^{\alpha}\xi(x) = \int_0^x \xi(t)dt\,, \\ \xi(0) = 0. \end{cases} \qquad 0 < \alpha \leq 1. \tag{5.29}$$

The exact solution for $\alpha = 1$, is $\xi(x) = \sin(x)$ [292]. The approximated solution obtained by using the presented computational scheme for $\alpha = 1$ is $\xi(x) = \sum_{i=1}^{3p} P_{i,1}(x)$.

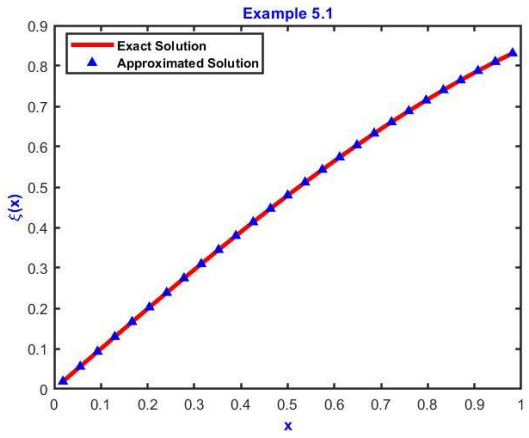

Figure 5.1: Visual analysis of exact solution and approximate solution for Example 5.1.

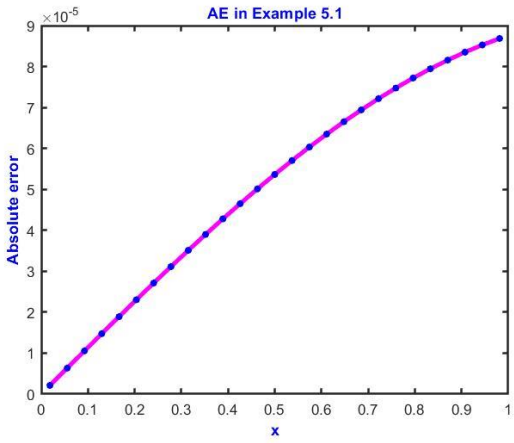

Figure 5.2: Graphical view of AE for Example 5.1.

The calculations of approximated solutions for different fractional values are presented in Table 5.1 and Figure 5.3. For $\alpha = 1$, the exact solution is compared with that of the approximate solution through Table 5.1 and Figure 5.1. Figure 5.1 shows that the presented scheme yields results that are in accordance with the exact solution. The absolute value of error for $\alpha = 1$ at various collocation points is illustrated in Table 5.1 and Figure 5.2.

Table 5.1: Computation of Approximated solution (AS) for different fractional values and Exact solution (ES) along with absolute error for Example 5.1.

x	AS at $\alpha = 0.7$	AS at $\alpha = 0.8$	AS at $\alpha = 0.9$	AS at $\alpha = 1$	ES at $\alpha = 1$ [292]	Absolute error
0.1	0.25959	0.20661	0.16356	0.12925	0.12927	1.4754E-05
0.2	0.35323	0.29525	0.24493	0.20227	0.20230	2.3041E-05
0.3	0.46905	0.41194	0.35835	0.30961	0.30964	3.5096E-05
0.4	0.56326	0.51318	0.46241	0.41312	0.41316	4.6499E-05
0.5	0.61603	0.57298	0.52659	0.47937	0.47943	5.3634E-05
0.6	0.68168	0.65167	0.61478	0.57371	0.57378	6.3486E-05
0.7	0.73231	0.71744	0.69281	0.66098	0.66105	7.2150E-05
0.8	0.76898	0.77050	0.76016	0.74010	0.74018	7.9460E-05
0.9	0.78610	0.79889	0.79890	0.78783	0.78791	8.3506E-05

For different values of dilation factor j, $l_2 - error$ and $l_\infty - error$ are calculated and presented in Table 5.2. Table 5.2 reveals that with increasing value of the dilation factor error decreases, which confirms the convergence of the presented computational scheme.

Table 5.2: Computation of multiple errors for Example 5.1.

j	1	2	3	4
$l_2 - error$	9.762149E-04	1.085714E-04	1.206476E-05	1.340544E-06
$l_\infty - error$	7.664870E-04	8.684871E-05	9.705164E-06	1.080312E-06

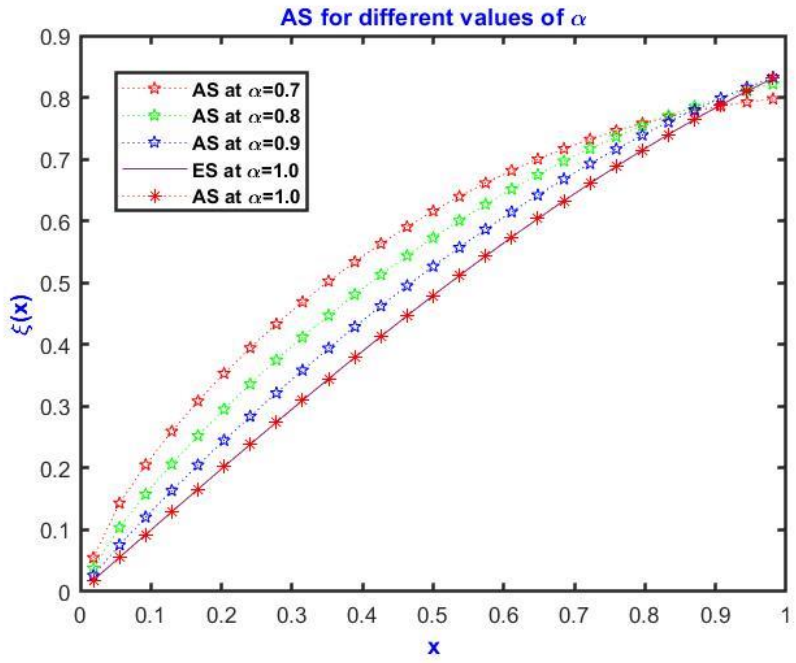

Figure 5.3: Graphical representation of AS and ES for different α at $j = 2$ for Example 5.1.

Example 5.2: Consider the VFrIDE [293],

$$\begin{cases} D^{\alpha}\xi(x) = f(x) + \int_0^x e^{(x-t)}\xi(t)dt\,, \\ \xi(0) = \xi'(0) = 0. \end{cases} \quad 1 \le \alpha < 2. \tag{5.30}$$

The function $f(x)$ is selected in a way that the exact solution for this equation for $\alpha = 1.2$ is $\xi(x) = x^3$ [293], and $f(x)$ is given by

$$f(x) = \frac{\Gamma(4)}{\Gamma(2.8)} x^{1.8} + 6 + 6x + 3x^2 + x^3 - 6e^x.$$

Table 5.3: Computation of Approximated solution (AS) for different fractional values and Exact solution (ES) along with absolute error for Example 5.2.

x	$\alpha = 1.3$	$\alpha = 1.5$	$\alpha = 1.7$	$\alpha = 1.9$	$\alpha = 1.2$	ES at $= 1.2$ [293]	Absolute error
0.05555	0.00012	0.00006	0.00003	0.00002	0.00017	0.00017	2.71E-20
0.16666	0.00341	0.00190	0.00110	0.00066	0.00462	0.00462	8.67E-19
0.27777	0.01650	0.00985	0.00599	0.00377	0.02143	0.02143	6.93E-18
0.38888	0.04684	0.02968	0.01898	0.01243	0.05881	0.05881	2.77E-17
0.50000	0.10210	0.06787	0.04528	0.03075	0.12500	0.12500	0.00E+00
0.61111	0.19015	0.13141	0.09087	0.06369	0.22822	0.22822	5.55E-17
0.72222	0.31900	0.22768	0.16235	0.11700	0.37671	0.37671	1.11E-16
0.83333	0.49672	0.36435	0.26678	0.19706	0.57870	0.57870	1.11E-16
0.94444	0.73145	0.54927	0.41164	0.310802	0.84242	0.84242	2.22E-16

The values for the approximated solution for different fractional values α are presented in Table 5.3. For $\alpha = 1.2$, the exact solution is compared with that of the approximate solution through Table 5.3 and Figure 5.4. Figure 5.4 shows that the presented scheme yields results that are in good agreement with the exact solution. The absolute value of error for $\alpha = 1.2$ at various collocation points is depicted in Table 5.3. For different values of dilation factor j, $l_\infty - error$ and $M_{cp} - error$ are calculated and presented in Table 5.4. The values of errors are compared with those already available in the literature [293]. Table 5.4 illustrates the results achieved by the proposed scheme are more promising than the existing results. The value of $l_\infty - error$ and $M_{cp} - error$ for $j = 1$ is 2.22045E-16 and 9.30092E-17 respectively.

Table 5.4: Computation of multiple errors for Example 5.2.

j	$l_\infty - error$	$l_\infty - error$ [293]	$M_{cp} - error$	$M_{cp} - error$ [293]
1	2.22045E-16	4.29043E-03	9.30092E-17	2.61915E-03
2	3.33067E-16	6.62737E-04	1.32085E-16	4.61688E-04
3	2.22045E-16	1.51488E-04	1.06737E-16	1.12962E-04
4	2.22045E-16	4.13522E-05	5.42902E-17	3.07077E-05

Figure 5.5 shows the graphical representation of the absolute value of error for $j = 2$ which is 10^{-16}.

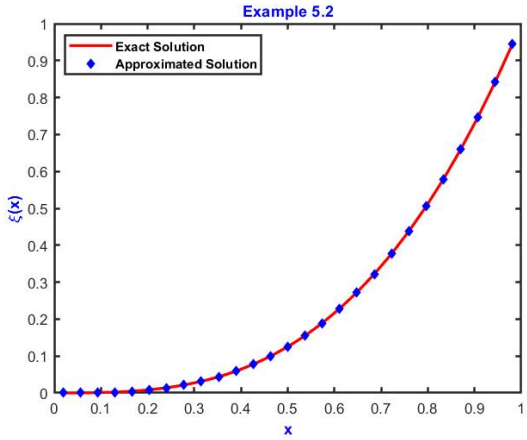

Figure 5.4: Visual analysis of exact solution and approximate solution for Example 5.2.

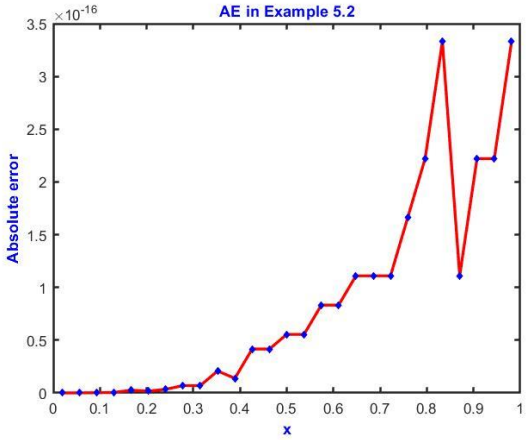

Figure 5.5: Graphical view of AE for Example 5.2.

Figure 5.6 represents the graphical representation of approximated solution for different fractional values α.

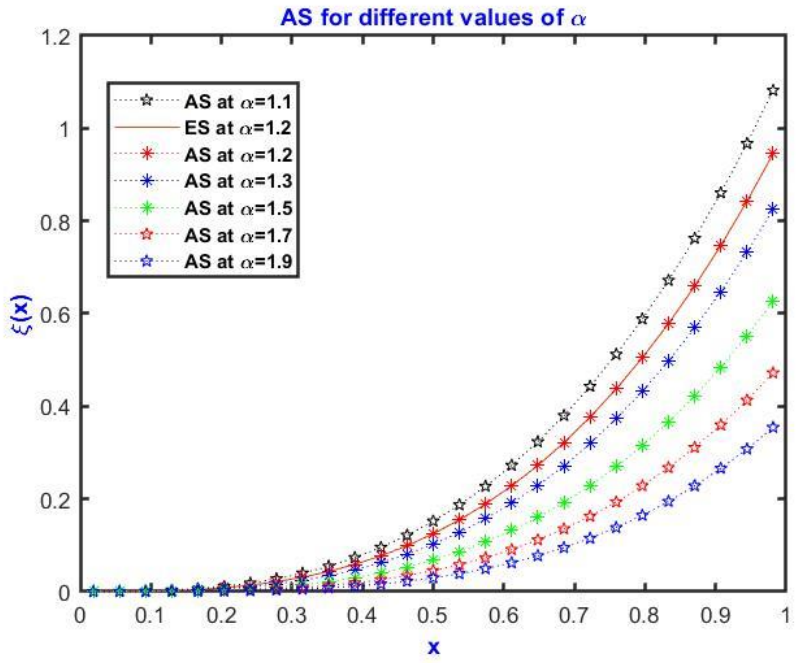

Figure 5.6: Graphical representation of AS and ES for different α at $j = 2$ for Example 5.2.

Example 5.3: Consider the singular VDE of fractional order [293],

$$\begin{cases} \xi''(x) + \dfrac{D^{\alpha}\xi(x)}{x} + \dfrac{1}{x-1}\xi(x) = f(x) + \displaystyle\int_0^x K(x,t)\xi(t)dt, & 0 < \alpha \leq 1. \\ \xi(0) = 0. \end{cases} \quad (5.31)$$

The value of the function $f(x)$ and kernel function $K(x,t)$ is selected in a way that the exact solution for this equation for $\alpha = 0.3$, is $\xi(x) = x^3(x-1)$ [293].

where $f(x) = \frac{\Gamma(5)}{\Gamma(4.7)}x^{2.7} - \frac{\Gamma(4)}{\Gamma(3.7)}x^{1.7} - 6x + 12x^2 + x^3 + \frac{x^5}{20} - \frac{x^6}{30}$ and $K(x,t) = x - t$.

For different fractional values, the approximated solution is calculated by using the proposed technique and presented in Table 5.5. Table 5.5 and Figure 5.7 present a comparison between both the results obtained and the exact solution at various levels of resolution. It is worth mentioning that the generated solution and the exact solution are approximately overlapped, which illustrates the high precision attained by the presented computational scheme for a small number of collocation points. The $l_{\infty} - error$ and $M_{cp} - error$ at $j = 4$ are 3.568987E-06 and 1.235782E-06 respectively, and these are lesser than the error reported in the case of the scale 2 Haar wavelet, which

is illustrated in Table 5.6. It is possible to make the important conclusion from Table 5.6 that, as the level of resolution j increases, the absolute error decreases, which indicates that the present solution eventually converges to the exact solution.

Table 5.5: Computation of Approximated solution (AS) for different fractional values and Exact solution (ES) along with absolute error for Example 5.3.

x	AS at $\alpha = 0.1$	AS at $\alpha = 0.5$	AS at $\alpha = 0.7$	AS at $\alpha = 0.9$	AS at $\alpha = 0.3$	ES at $\alpha = 0.3$ [293]	Absolute error
0.055	-0.00045	-0.00040	-0.00034	-0.00027	-0.00043	-0.00016	2.7E-04
0.166	-0.00469	-0.00417	-0.00365	-0.00297	-0.00450	-0.00385	6.4E-04
0.277	-0.01694	-0.01515	-0.01352	-0.01143	-0.01626	-0.01547	7.8E-04
0.388	-0.03835	-0.03412	-0.03056	-0.02616	-0.03667	-0.03594	7.3E-04
0.500	-0.06633	-0.05828	-0.05200	-0.04456	-0.06303	-0.06250	5.3E-04
0.611	-0.09450	-0.08131	-0.07172	-0.06088	-0.08893	-0.08875	1.7E-04
0.722	-0.11277	-0.09333	-0.08017	-0.06608	-0.10433	-0.10464	3.0E-04
0.833	-0.10731	-0.08083	-0.06419	-0.04749	-0.09550	-0.09645	9.4E-04
0.944	-0.06095	-0.02613	-0.00603	0.01244	-0.04500	-0.04680	1.7E-03

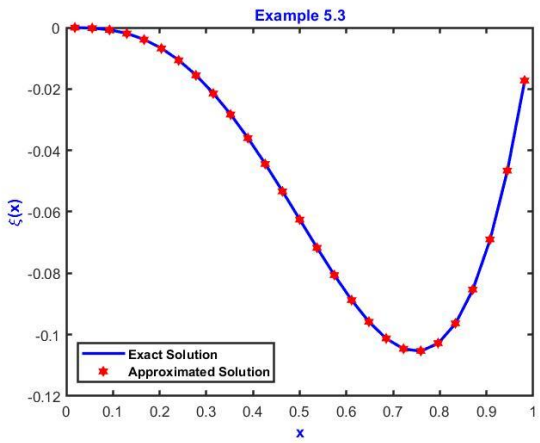

Figure 5.7: Visual analysis of exact solution and approximate solution for Example 5.3.

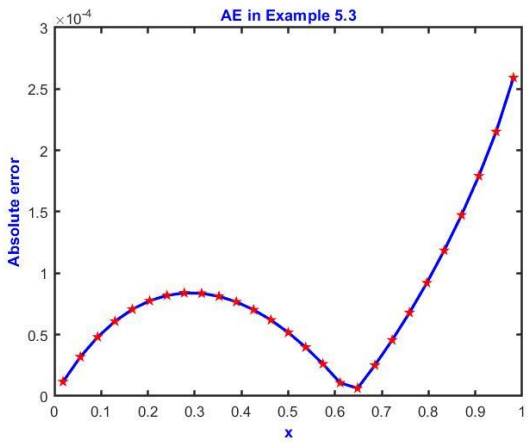

Figure 5.8: Graphical view of AE for Example 5.3.

Figure 5.8 represents the graph of the absolute value of error for dilation factor 2. The solution attained for different fractional values at various collocation points is presented graphically in Figure 5.9.

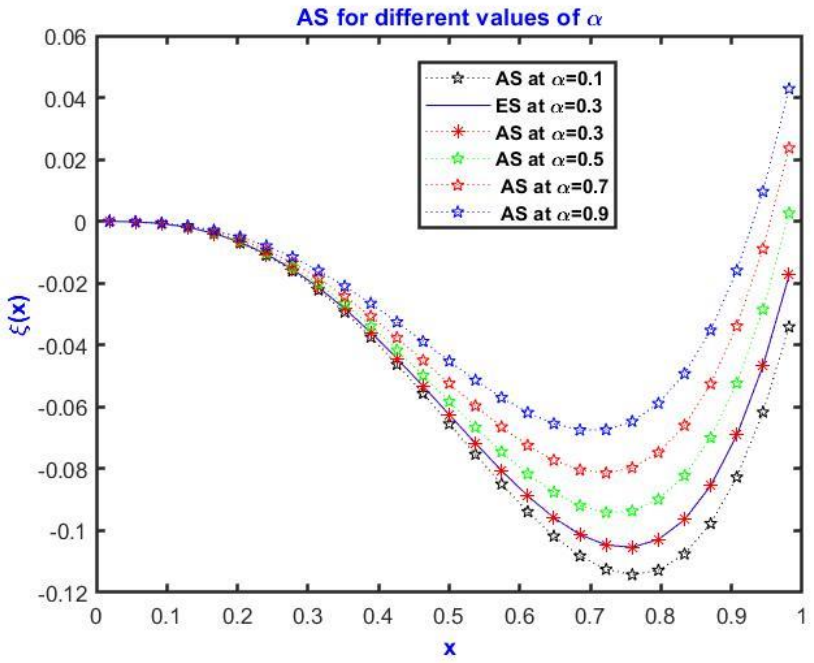

Figure 5.9: Graphical representation of AS and ES for different α at $j = 2$ for Example 5.3.

Table 5.6: Computation of multiple errors for Example 5.3.

j	$l_\infty - error$	$l_\infty - error$ [293]	$M_{cp} - error$	$M_{cp} - error$ [293]
1	1.798869E-03	2.64083E-03	8.294881E-04	1.56908E-03
2	2.592451E-04	1.67742E-03	9.860316E-05	7.18171E-04
3	3.125485E-05	9.12254E-04	1.110299E-05	3.28514E-04
4	3.568987E-06	3.68413E-04	1.235782E-06	1.26008E-04

Example 5.4: IDEs of non-integer order are used to simulate a variety of real-world scientific and engineering problems. The analysis of circuits represents only one of the numerous applications of this technology. As per Kirchhoff's second law, the net voltage drop throughout a closed loop is equal to the voltage impressed $E(x)$. (In its

most basic form, it is an example of energy conservation). Current flow in LCR circuits is defined by the following VIDE [293],

$$\begin{cases} D^{\alpha}\xi(x) = \frac{E(x)}{L} - \frac{R}{L}\xi(x) - \frac{1}{LC}\int_0^x \xi(t)dt, \\ \xi(0) = 0. \end{cases} \quad 0< \alpha \leq 1. \qquad (5.32)$$

where ξ represents the current, R stands for the resistance, C stands for the capacitance, and L stands for the inductance, by using $E(x) = 0.2m$, $R = 0.4ohms$, $C = 0.1$ and $L = 0.2$ and that $\xi(0)$ equals zero, then we have the exact solution for $\alpha = 1$ is $\xi(x) = \frac{1}{2}e^{-x}\sin(2x)$ [293].

Table 5.7: Computation of Approximated solution (AS) for different fractional values and Exact solution (ES) along with absolute error for Example 5.4.

x	AS at $\alpha =$ 0.5	AS at $\alpha = 0.6$	AS at $\alpha = 0.8$	AS at $\alpha = 0.9$	AS at $\alpha = 1.0$	ES at $\alpha = 1.0$ [293]	Absolute error
0.0555	0.1443	0.1173	0.0761	0.0613	0.0496	0.0524	2.79E-03
0.1666	0.2535	0.2331	0.1830	0.1585	0.1363	0.1384	2.11E-03
0.2777	0.2265	0.2339	0.2271	0.2143	0.1983	0.1997	1.42E-03
0.3888	0.2190	0.2276	0.2418	0.2421	0.2370	0.2378	7.69E-04
0.5000	0.1929	0.2079	0.2374	0.2486	0.2549	0.2551	2.03E-04
0.6111	0.1691	0.1840	0.2205	0.2392	0.2552	0.2550	2.45E-04
0.7222	0.1439	0.1582	0.1961	0.2187	0.2414	0.2409	5.64E-04
0.8333	0.1207	0.1329	0.1677	0.1910	0.2170	0.2163	7.54E-04
0.9444	0.0994	0.1091	0.1380	0.1594	0.1855	0.1846	8.27E-04

Table 5.8: Computation of multiple errors for Example 5.4.

j	$l_\infty - error$	$l_\infty - error$ [293]	$M_{cp} - error$	$M_{cp} - error$ [293]
1	2.7900638E-03	1.2743700E-02	1.3567107E-03	7.18780E-03
2	3.3219080E-04	3.5226000E-03	1.5088845E-04	1.78340E-03
3	3.7709821E-05	9.2736300E-04	1.6767122E-05	4.44804E-04
4	4.2192262E-06	2.3788900E-04	1.8630349E-06	1.11144E-04

By applying the algorithm, the solution obtained is presented for different fractional values in Table 5.7 and Figure 5.12. For $\alpha = 1$, the exact solution is compared with that of the approximate solution through Table 5.7 and Figure 5.10. Figure 5.10 shows that the presented scheme yields results that are in accordance with the exact solution. The absolute value of error for $\alpha = 1$ at various collocation points is depicted in Table 5.7 and Figure 5.11. For different values of dilation factor j, $l_\infty - error$ and $M_{cp} - error$ are calculated and presented in Table 5.8.

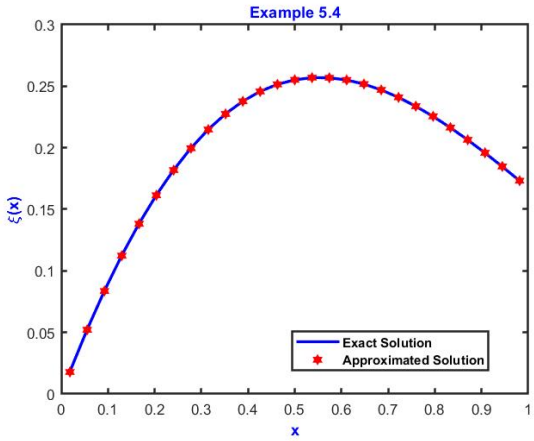

Figure 5.10: Visual analysis of exact solution and approximate solution for Example 5.4.

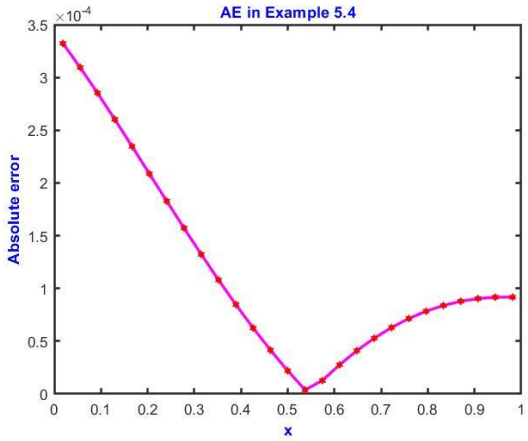

Figure 5.11: Graphical view of AE for Example 5.4.

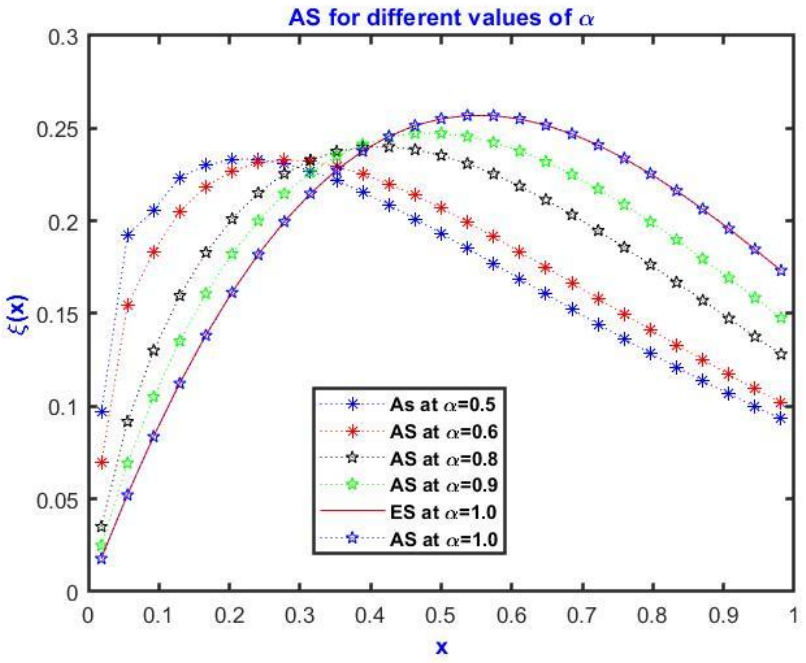

Figure 5.12: Graphical representation of AS and ES for different α at $j = 2$ for Example 5.4.

Table 5.8 determines that with the increasing value of the dilation factor error decreases, which ensures the convergence of the computational scheme. Additionally, the comparison of the proposed computational scheme with the existing results is shown in Table 5.8.

Example 5.5: Consider the VFIDE of fractional order [284],

$$\begin{cases} \xi''(x) + D^{\alpha}\xi(x) = f(x) + \int_0^1 K_1(x,t)\xi(t)dt - 2\int_0^x K_2(x,t)\,\xi(t)dt, \\ \xi(0) = \xi(1) = 0, \qquad 0 < \alpha \leq 1. \end{cases} \tag{5.33}$$

The exact solution for this equation for $\alpha = 1$ is $\xi(x) = \frac{1}{2}e^{-x}\sin(2x)$ [284]. By using the computational scheme, the approximated solution is calculated and presented in Table 5.9. Table 5.9 presents a comparison between both the results obtained and the exact solution at $j = 1$. The solution obtained is presented for different fractional values in Figure 5.13.

Table 5.9: Computation of Approximated solution and Exact solution for level of resolution 1 along with Absolute error for Example 5.5.

x	Approximated solution	Exact Solution [284]	Absolute error
0.055555556	-0.000442715	-0.000161942	2.807727364E-04
0.166666667	-0.004611224	-0.003858025	7.531989363E-04
0.277777778	-0.016819390	-0.015479729	1.339661203E-03
0.388888889	-0.038008048	-0.035941549	2.066499144E-03
0.500000000	-0.065390933	-0.062500000	2.890932794E-03
0.611111111	-0.092513259	-0.088753620	3.759639457E-03
0.722222222	-0.109252595	-0.104642966	4.609628587E-03
0.833333333	-0.101819630	-0.096450617	5.369012376E-03
0.944444444	-0.052758875	-0.046801174	5.957701162E-03

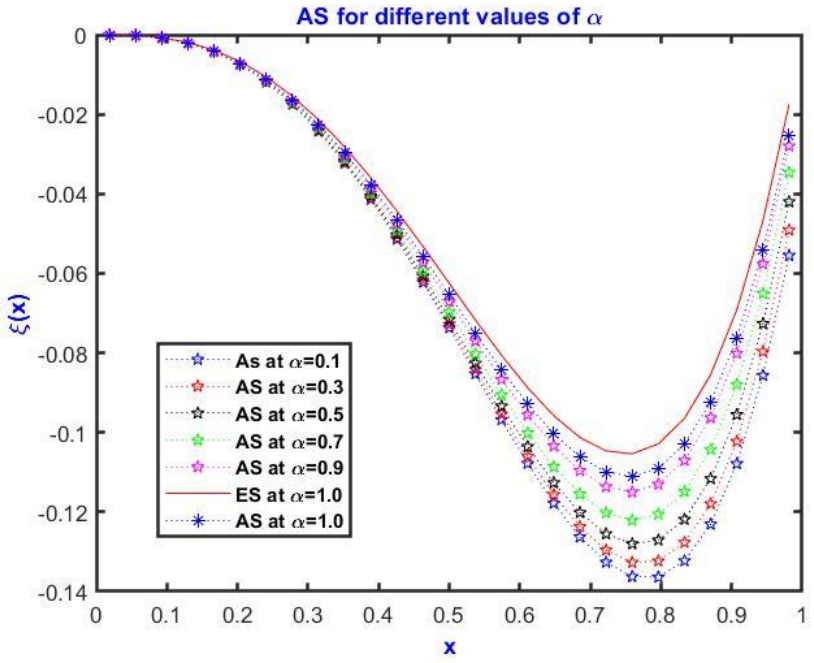

Figure 5.13: Graphical representation of AS and ES for different α at $j = 2$ for Example 5.5.

Table 5.10: Computation of Absolute value of error (AE) for different fractional values and comparison with existing methods for Example 5.5.

x	AE for $\alpha = 0.1$	AE for $\alpha = 0.1$ [284]	AE for $\alpha = 0.5$	AE for $\alpha = 0.5$ [284]	AE for $\alpha = 0.9$	AE for $\alpha = 0.9$ [284]
0.01	1.02E-05	-------	1.07E-05	------	1.14E-05	------
0.10	2.32E-04	3.39E-03	2.36E-04	1.94E-03	2.14E-04	1.18E-03
0.20	8.26E-04	6.46E-03	7.86E-04	3.60E-03	6.05E-04	2.17E-03
0.30	2.92E-03	8.64E-03	2.59E-03	4.55E-03	1.64E-03	2.77E-03
0.40	7.07E-03	9.36E-03	5.94E-03	4.41E-03	3.24E-03	2.81E-03
0.50	1.11E-02	8.22E-03	9.07E-03	3.01E-03	4.58E-03	2.20E-03
0.60	1.90E-02	5.28E-03	1.48E-02	5.42E-04	6.82E-03	1.01E-03
0.70	2.80E-02	1.17E-03	2.08E-02	2.39E-03	9.00E-03	4.70E-04
0.80	3.58E-02	2.71E-03	2.54E-02	4.66E-03	1.05E-02	1.72E-03
0.90	3.86E-02	4.61E-03	2.63E-02	4.60E-03	1.09E-02	1.94E-03

It is important to focus on that the generated solution and the exact solution are in accordance with each other, which explains the high precision attained by the presented computational scheme for a small number of collocation points. Figure 5.14 represents the graph of the absolute value of error for dilation factor 2. The solution attained for different fractional values at various collocation points is presented graphically in Figure 5.13. For different fractional values, the absolute error is calculated and presented in Table 5.10. The value of absolute error is also compared with existing methods as shown in Table 5.10.

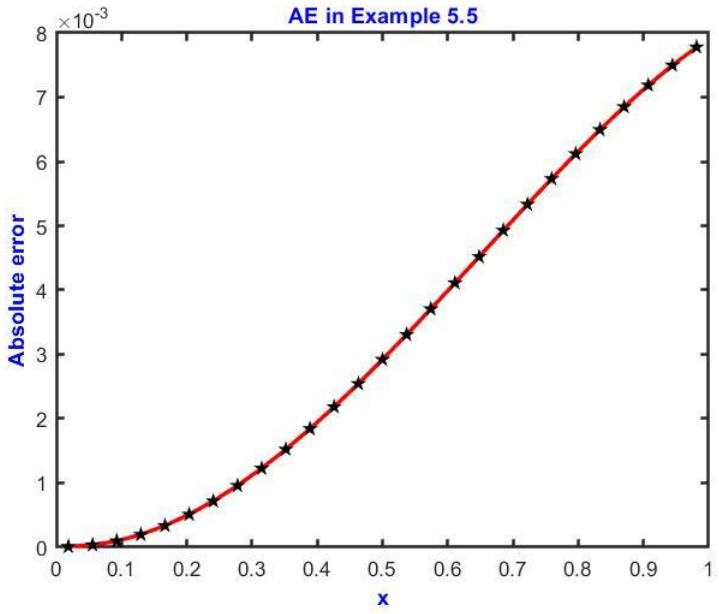

Figure 5.14: Graph for Absolute error for $j = 2$ for Example 5.5.

Example 5.6: Consider the FrVIDE [294],

$$\begin{cases} D^{0.8}\xi(x) = \int_0^x (x-t)\,[\xi(t)]^2 dt + f(x), \\ \xi(0) = 0. \end{cases} \quad 0 < \alpha \leq 1. \tag{5.34}$$

where $f(x) = \frac{1}{\Gamma(0.2)}\left(\frac{25}{3}x^{1.2} - 5x^{0.2}\right) - \frac{x^6}{30} + \frac{x^5}{10} - \frac{x^4}{12}$. The exact solution for this equation is $\xi(x) = x^2 - x$ [294].

In this example, we have considered the Volterra FrIDE with a difference kernel. The procedure for approximating the FrIDE under study involves several sequential steps, each with its unique scientific rationale. Initially, the Quasilinearization technique is utilized to address the nonlinearity present in the equation. Next, the Leibniz rule is employed to transform the integral equation into its corresponding differential equation, facilitating its analysis through the mathematical techniques of calculus. Subsequently, a truncated series of Haar functions is used to approximate the highest derivative involved in the differential equation. Finally, the process of integration is employed to compute the values of all the lower-order derivatives, providing a comprehensive understanding of the equation's behaviour as discussed in the presented algorithm.

Table 5.11: Computation of Exact solution and Approximated solution for level of resolution 1 along with Absolute error for Example 5.6.

x	Exact Solution [294]	Approximated Solution	Absolute Error
0.055555556	-0.052469136	-0.050411531	2.05760E-03
0.166666667	-0.138888889	-0.138418499	4.70390E-04
0.277777778	-0.200617284	-0.201185219	5.67935E-04
0.388888889	-0.237654321	-0.239138216	1.48390E-03
0.500000000	-0.250000000	-0.252326279	2.32628E-03
0.611111111	-0.237654321	-0.240769876	3.11556E-03
0.722222222	-0.200617284	-0.204478267	3.86098E-03
0.833333333	-0.138888889	-0.143456026	4.56714E-03
0.944444444	-0.052469136	-0.057705961	5.23682E-03

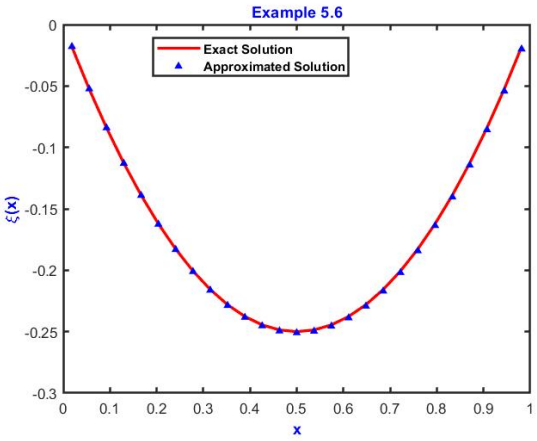

Figure 5.15: Visual analysis of exact solution and approximate solution for Example 5.6.

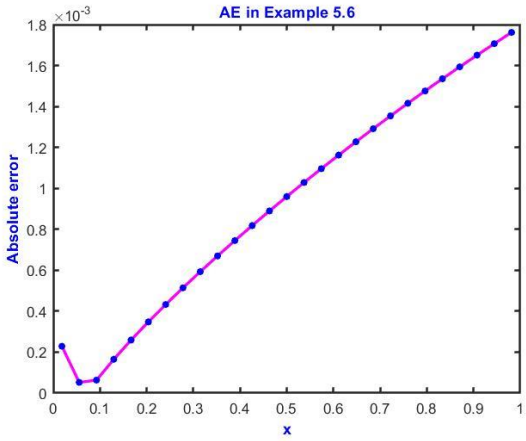

Figure 5.16: Graphical view of AE for Example 5.6.

Table 5.11 and Figure 5.15 illustrate a comparative analysis between the approximated solution obtained by implementing the proposed algorithm in Example 5.6 and the actual solution. The outcomes indicate that the proposed algorithm provides highly accurate approximations for various resolutions. The solution, which has been acquired through the experiment, is depicted in Figure 5.17 for various fractional values. Furthermore, a comparison with the previous method is also presented, and the results

demonstrate the superiority of the proposed method in addressing such types of problems. The values of different types of errors obtained through the proposed method are considerably lower than those obtained from the existing traditional Haar wavelet methods mentioned in the literature, as shown in Table 5.12. Additionally, it can be observed from Table 5.12 that increasing the dilation factor leads to a decrease in the error values, thus demonstrating the convergence of the proposed method. For $j = 2$, the absolute error value is 10^{-3}, which is graphically presented in Figure 5.16.

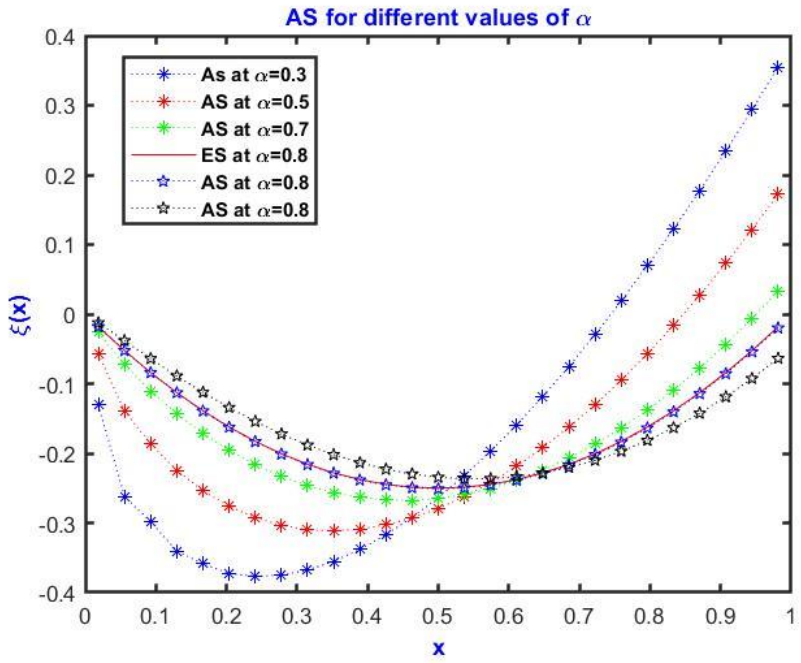

Figure 5.17: Graphical representation of AS and ES of Example 5.6 for different α at $j = 2$.

Table 5.12: Computation of different errors for Example 5.6 and comparison with existing results.

j	$l_2 - error$	$l_\infty - error$	$l_\infty - error$ [294]	$M_{cp} - error$	$M_{cp} - error$ [294]
1	5.859E-03	1.761E-03	1.5237E-02	1.069E-03	1.341E-02
2	5.859E-03	1.761E-03	3.8787E-03	1.069E-03	3.352E-03
3	1.722E-03	5.066E-04	9.7474E-04	3.144E-04	8.391E-04
4	4.769E-04	1.390E-04	2.4402E-04	8.707E-05	2.107E-04

Example 5.7: Consider the FrVIDE [294].

$$\begin{cases} D^{\alpha}\xi(x) = \int_0^x e^{-t}\,[\xi(t)]^2 dt + f(x), \\ \xi(0) = 0. \end{cases} \quad 0< \alpha \leq 1. \tag{5.35}$$

where $f(x)$ is chosen in such a way that the exact solution for $\alpha = 1$ for this equation is $\xi(x) = x^2$ [294].

Table 5.13: Computation of Exact solution and Approximated solution for level of resolution 1 for Example 5.7.

x	Exact Solution [294]	Approximated Solution	Absolute Error
0.055555556	0.003086420	0.006172856	3.08644E-03
0.166666667	0.027777778	0.030864541	3.08676E-03
0.277777778	0.077160494	0.080248823	3.08833E-03
0.388888889	0.151234568	0.154327215	3.09265E-03
0.500000000	0.250000000	0.253101533	3.10153E-03
0.611111111	0.373456790	0.376573676	3.11689E-03
0.722222222	0.521604938	0.524745494	3.14056E-03
0.833333333	0.694444444	0.697618717	3.17427E-03
0.944444444	0.891975309	0.895194912	3.21960E-03

In Example 5.7, we have solved a nonlinear FrVIDE having an exponential kernel. To assess the accuracy of our proposed algorithm, we conducted a comparative analysis between the approximated solution obtained from our method and the actual solution. The results of this analysis, shown in Table 5.13 and Figure 5.18, indicate that our proposed algorithm provides highly accurate approximations for various resolutions. We then tested the algorithm on various fractional values, and the resulting solution is presented in Figure 5.20. Furthermore, we compared the performance of our proposed algorithm with a traditional Haar wavelet method found in the literature, and our results show that our method outperforms the traditional method in addressing this type of problem. Specifically, the errors obtained through our method are considerably lower than those obtained using the traditional Haar wavelet method, as demonstrated in Table

5.14. We also found that increasing the dilation factor leads to a decrease in error values, indicating the convergence of our proposed method. When $j = 2$, the absolute error value is 10^{-4}, which is depicted graphically in Figure 5.19.

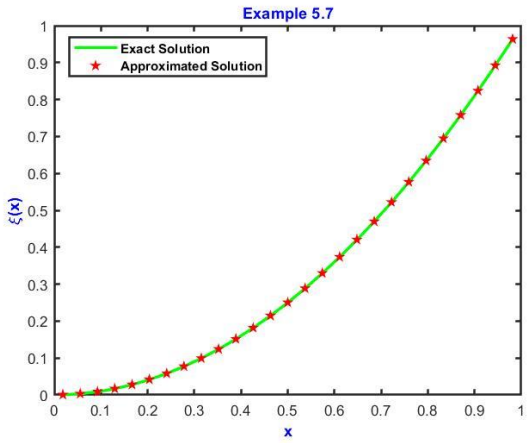

Figure 5.18: Visual analysis of exact solution and approximate solution for Example 5.7.

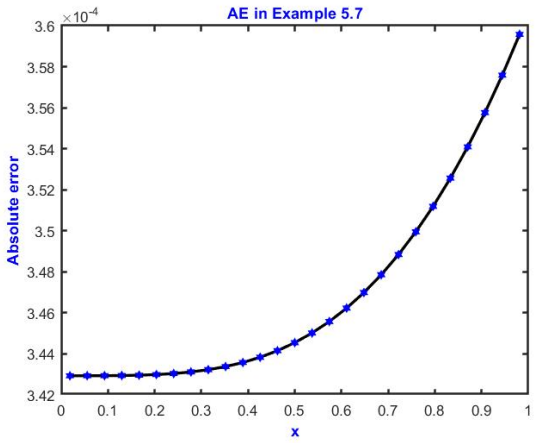

Figure 5.19: Graphical view of AE for Example 5.7.

Table 5.14: Computation of different errors for Example 5.7 and comparison with existing results.

j	$l_2 - error$	$l_\infty - error$	$l_\infty - error$ [294]	$M_{cp} - error$	$M_{cp} - error$ [294]
1	7.020E-03	3.219E-03	2.5848E-02	3.123E-03	1.9640E-02
2	7.763E-04	3.595E-04	6.8773E-03	3.469E-04	4.8303E-03
3	8.621E-05	4.002E-05	1.7982E-03	3.855E-05	1.2027E-03
4	9.578E-06	4.450E-06	4.6149E-04	4.283E-06	3.0044E-04

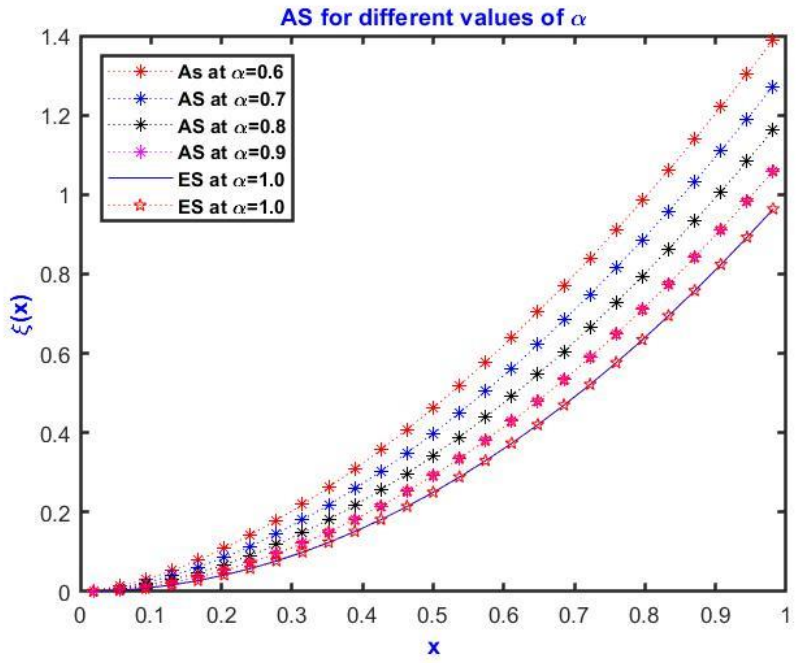

Figure 5.20: Graphical representation of AS and ES for Example 5.7 for different α at $j = 2$.

Example 5.8: Consider the FrFIDE [294],

$$\begin{cases} D^{1.7}\xi(x) = \int_0^1 (x+t)\xi(t)dt + \xi^2(x) + f(x), \\ \xi(0) = \xi'(0) = 0. \end{cases} \tag{5.36}$$

where $f(x)$ is selected in a manner that ensures the exact solution for this equation is $\xi(x) = x^2 + x^3$ [294].

Example 5.8 solved a nonlinear FrFIDE. The method is tested by comparing the approximated solution to the actual solution. Table 5.15 and Figure 5.21 illustrate that this method yields accurate approximations for various resolutions. This method outperforms a Haar wavelet method from the literature in solving this type of problem. Table 5.16 demonstrates that this approach yields lesser errors compared to the existing method. Figure 5.22 illustrates the absolute error value for $j = 2$.

Table 5.15: Computation of Exact solution and Approximated solution for level of resolution 1 along with absolute error for Example 5.8.

x	Exact Solution [294]	Approximated Solution	Absolute Error
0.055555556	0.003257888	0.003257888	0
0.166666667	0.032407407	0.032407407	0
0.277777778	0.098593964	0.098593964	0
0.388888889	0.210048011	0.210048011	0
0.500000000	0.375000000	0.375000000	5.55112E-17
0.611111111	0.601680384	0.601680384	1.11022E-16
0.722222222	0.898319616	0.898319616	1.11022E-16
0.833333333	1.273148148	1.273148148	2.22045E-16
0.944444444	1.734396433	1.734396433	2.22045E-16

Table 5.16: Computation of different errors and comparison with earliest techniques for Example 5.8.

j	$l_2 - error$	$l_\infty - error$	$l_\infty - error$ [294]	$M_{cp} - error$	$M_{cp} - error$ [294]
1	1.451E-16	2.220E-16	3.0259E-02	1.184E-16	1.9177E-02
2	3.120E-16	6.661E-16	8.3003E-03	2.563E-16	4.8215E-03
3	5.592E-16	1.332E-15	2.1792E-03	4.598E-16	1.2071E-03
4	7.297E-16	1.554E-15	5.5869E-04	6.000E-16	3.0188E-04

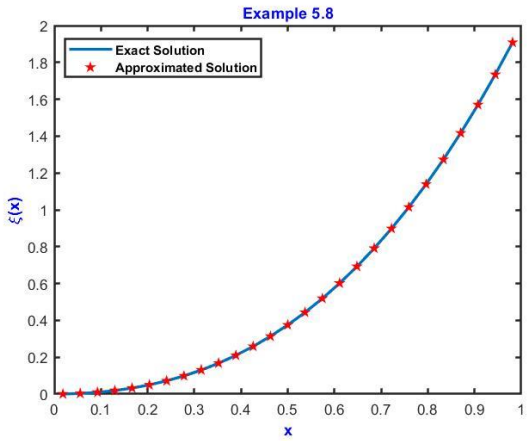

Figure 5.21: Visual analysis of exact solution and approximate solution for Example 5.8.

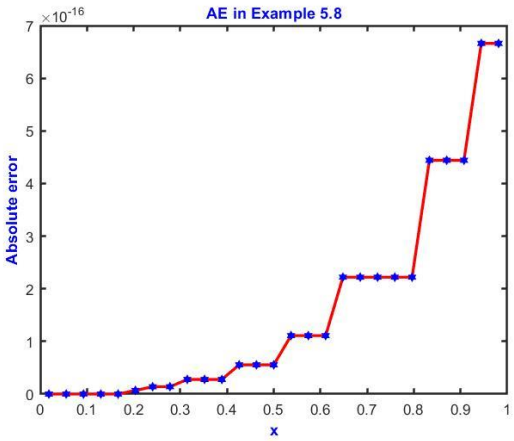

Figure 5.22: Graphical view of AE for Example 5.8.

Example 5.9: Consider the FrFIDE [294],

$$\begin{cases} D^{\sqrt{3}}\xi(x) = \int_0^1 x^2\, t\, [\xi(t)]^3 dt + f(x), \\ \xi(0) = \xi'(0) = 0. \end{cases} \tag{5.37}$$

where $f(x)$ is selected in a manner that ensures the exact solution for this equation is $\xi(x) = x^2$ [294]. Nonlinear FrFIDE having product kernel is solved in Example 5.9. Testing the procedure involves comparing the approximated solution to the true solution. The accurate approximations obtained using this method are shown in Table 5.17 and Figure 5.23 for a range of resolutions. The absolute error for $j = 2$ is 10^{-15} as shown in Figure 5.24.

Table 5.17: Computation of Exact solution and Approximated solution for level of resolution 2 along with Absolute error for Example 5.9.

x	Exact Solution [294]	Approximated Solution	Absolute Error
0.018518519	0.000342936	0.000342936	0
0.055555556	0.003086420	0.003086420	0
0.092592593	0.008573388	0.008573388	0
0.129629630	0.016803841	0.016803841	0
0.166666667	0.027777778	0.027777778	0
0.203703704	0.041495199	0.041495199	0
0.240740741	0.057956104	0.057956104	0
0.277777778	0.077160494	0.077160494	0
0.314814815	0.099108368	0.099108368	1.38778E-17
0.351851852	0.123799726	0.123799726	1.38778E-17
0.388888889	0.151234568	0.151234568	2.77556E-17
0.425925926	0.181412894	0.181412894	2.77556E-17
0.462962963	0.214334705	0.214334705	5.55112E-17
0.500000000	0.250000000	0.250000000	5.55112E-17
0.537037037	0.288408779	0.288408779	5.55112E-17
0.574074074	0.329561043	0.329561043	1.11022E-16
0.611111111	0.373456790	0.373456790	1.66533E-16
0.648148148	0.420096022	0.420096022	1.66533E-16
0.685185185	0.469478738	0.469478738	2.22045E-16
0.722222222	0.521604938	0.521604938	3.33067E-16
0.759259259	0.576474623	0.576474623	3.33067E-16
0.796296296	0.634087791	0.634087791	4.44089E-16
0.833333333	0.694444444	0.694444444	5.55112E-16
0.870370370	0.757544582	0.757544582	5.55112E-16
0.907407407	0.823388203	0.823388203	6.66134E-16
0.944444444	0.891975309	0.891975309	8.88178E-16
0.981481481	0.963305898	0.963305898	9.99201E-16

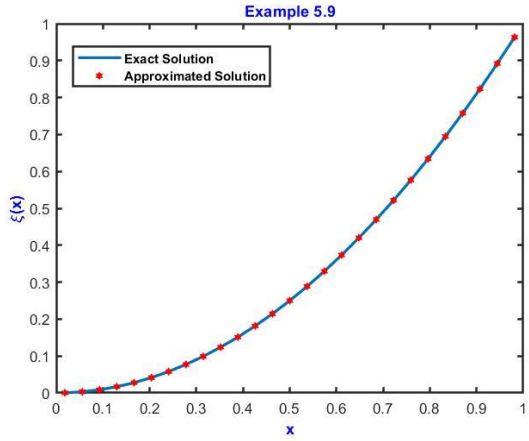

Figure 5.23: Visual analysis of exact solution and approximate solution for Example 5.9.

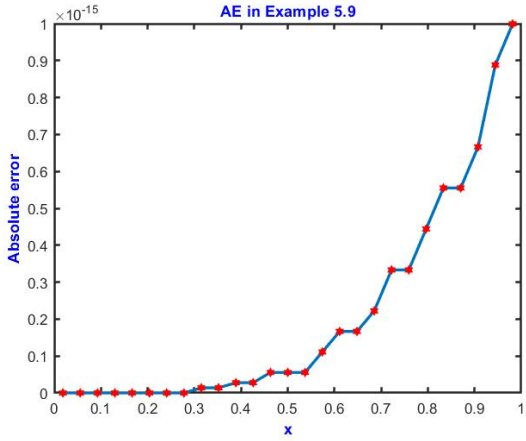

Figure 5.24: Graphical view of AE for Example 5.9.

Example 5.10: Consider the FrFIDE [295],

$$\begin{cases} D^{0.5}\xi(x) = \dfrac{1}{\Gamma(0.5)}\left(\dfrac{8}{3}x^{1.5} - 2x^{0.5}\right) - \displaystyle\int_0^1 x\, t\, [\xi(t)]^4 dt - \dfrac{x}{1260}, \\ \xi(0) = 0. \end{cases} \tag{5.38}$$

where $f(x)$ is selected in a manner that ensures the exact solution for this equation is $\xi(x) = x^2 - x$ [295]. Table 5.18 and Figure 5.25 illustrate a comparative analysis between the approximated solution obtained by implementing the proposed algorithm to Example 5.10 and the actual solution. The outcomes indicate that the proposed algorithm provides highly accurate approximations for various resolutions. The solution, which has been acquired through the experiment, is depicted in Figure 5.27 for various fractional values. Furthermore, a comparison with the previous method is also presented in Table 5.19, and the results demonstrate the superiority of the proposed method in addressing such types of problems. For $j = 2$, the absolute error value is 10^{-4}, which is graphically presented in Figure 5.26.

Table 5.18: Computation of Exact solution and Approximated solution for level of resolution 2 along with Absolute error for Example 5.10.

x	Exact Solution [295]	Approximated Solution	Absolute Error
0.018518519	-0.018175583	-0.018064826	1.10757E-04
0.055555556	-0.052469136	-0.052593734	1.24598E-04
0.092592593	-0.084019204	-0.084179050	1.59845E-04
0.129629630	-0.112825789	-0.113033973	2.08185E-04
0.166666667	-0.138888889	-0.139126014	2.37126E-04
0.203703704	-0.162208505	-0.162466625	2.58120E-04
0.240740741	-0.182784636	-0.183056216	2.71580E-04
0.277777778	-0.200617284	-0.200896380	2.79096E-04
0.314814815	-0.215706447	-0.215987928	2.81481E-04
0.351851852	-0.228052126	-0.228331513	2.79387E-04
0.388888889	-0.237654321	-0.237927614	2.73293E-04
0.425925926	-0.244513032	-0.244776611	2.63580E-04
0.462962963	-0.248628258	-0.248878809	2.50551E-04
0.500000000	-0.250000000	-0.250234456	2.34456E-04
0.537037037	-0.248628258	-0.248843764	2.15506E-04
0.574074074	-0.244513032	-0.244706909	1.93877E-04
0.611111111	-0.237654321	-0.237824043	1.69722E-04
0.648148148	-0.228052126	-0.228195300	1.43174E-04
0.685185185	-0.215706447	-0.215820796	1.14349E-04
0.722222222	-0.200617284	-0.200700634	8.33502E-05
0.759259259	-0.182784636	-0.182834906	5.02697E-05
0.796296296	-0.162208505	-0.162223695	1.51898E-05
0.833333333	-0.138888889	-0.138867074	2.18147E-05
0.870370370	-0.112825789	-0.112765112	6.06764E-05
0.907407407	-0.084019204	-0.083917871	1.01333E-04
0.944444444	-0.052469136	-0.052325407	1.43729E-04
0.981481481	-0.018175583	-0.017987772	1.87811E-04

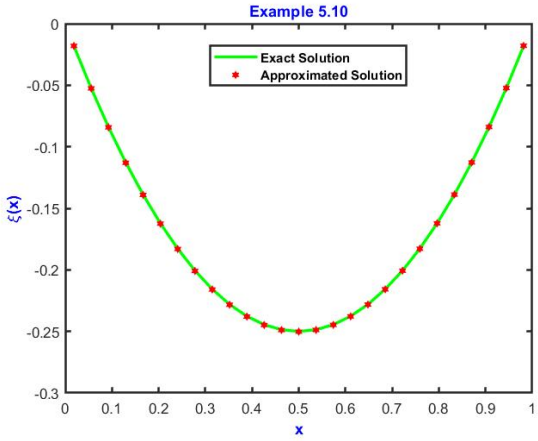

Figure 5.25: Visual analysis of exact solution and approximate solution for Example 5.10.

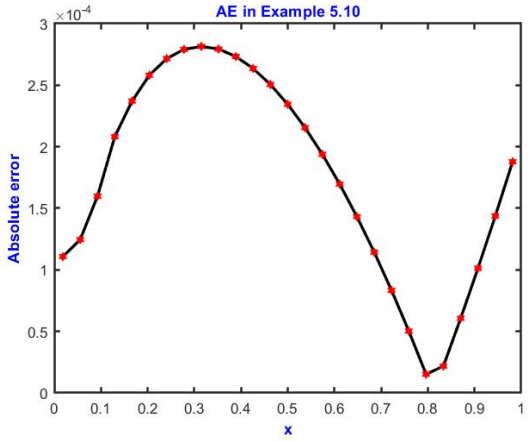

Figure 5.26: Graphical view of AE for Example 5.10.

Table 5.19: Computation of different errors and comparison with earliest methods for Example 5.10.

j	$l_2 - error$	$l_2 - error$ [295]	$l_\infty - error$	$M_{cp} - error$
2	1.062940E-03	9.01E-04 (N=5)	2.814812E-04	1.940655E-04
3	2.561450E-03	6.54E-04 (N=6)	9.839994E-04	4.676546E-04

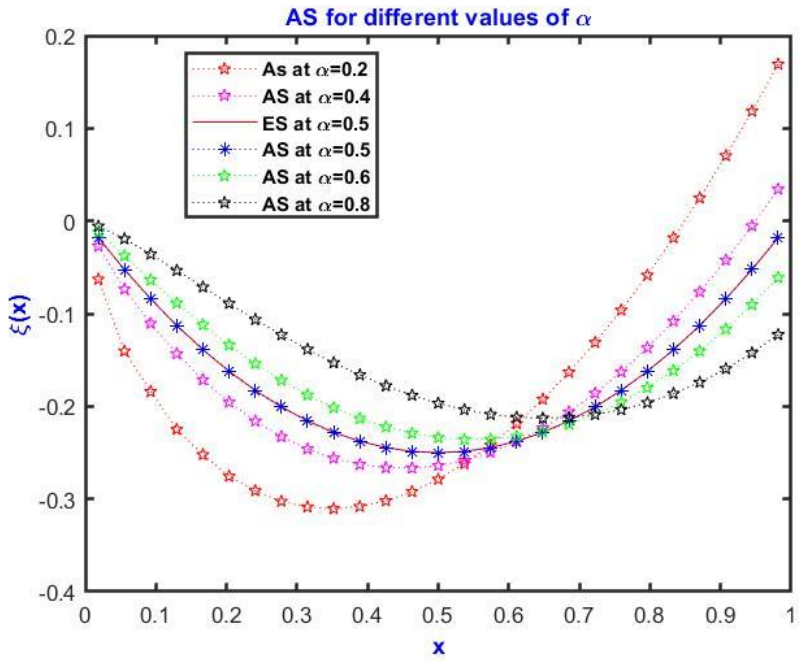

Figure 5.27: Graphical representation of AS and ES for Example 5.10 for different α at $j = 2$.

5.5 Conclusion

On FrIDEs of Volterra type, Fredholm type, and mixed Volterra-Fredholm type, the scale 3 Haar wavelet computational scheme in combination with Caputo derivative has been implemented. Numerous examples are presented to illustrate the convergence of the method. The absolute error, $l_2 - error$ and $l_\infty - error$ are provided in tables for numerical examples. Additionally, a comparison of the exact solution to the approximate solution is provided in figures and tables for different collocation points. The tables demonstrate that an increase in the value of 'j' leads to a reduction in both $l_2 - error$ and $l_\infty - error$, leading us to the conclusion that this method can produce accurate and appropriate results. The MATLAB software is used for all of the computational calculations that are performed.

Chapter 6.

Conclusions and Future Scope

6.1 Conclusions

Integral equations and integro-differential equations are frequently employed to model physical problems. However, obtaining analytical solutions for these equations can be very challenging, especially when the equations are nonlinear, have variable coefficients, or involve a large number of variables (i.e., are higher dimensional). Consequently, sophisticated numerical techniques are necessary to address this challenge. Researchers are actively working on improving existing methods and developing new hybrid methods to create strong solvers for these types of functional equations. In the literature, dyadic wavelets with dilatation factors that are powers of 2 are commonly used.

The primary focus of this thesis is to develop and investigate the implementation of a new numerical method based on non-dyadic Haar (Scale 3) wavelets, where the dilatation factor is a power of 3. This novel method is applied to compute the numerical solutions of a variety of important problems, including higher-order linear and nonlinear integro-differential equations having initial as well as boundary constraints, integral equations, fractional integro-differential equations, Lane-Emden and Emden-Fowler type equations. In this thesis, the Haar Scale 3 is combined with established numerical methods like the Collocation method, Quasilinearization technique, and Thomas algorithm to solve various types of linear and nonlinear, higher-order, and fractional integral and integro-differential equations. The convergence criteria for these numerical techniques are determined, and a novel Haar Scale 3 (non-dyadic) wavelet-based approach is introduced, which demonstrates superior efficiency compared to the traditional Haar Scale 2 dyadic wavelet-based method.

In conclusion, the use of Scale 3 Haar wavelets for the solution of integral and integro-differential equations is an innovative approach that has shown great potential in solving a wide range of mathematical problems. This research has highlighted the efficiency and effectiveness of this method, which provides accurate solutions with a

fast convergence rate. The research has provided a comprehensive overview of the theoretical background of Haar wavelets and their properties. It has also discussed the properties of IEs and IDEs and their solutions. Moreover, the research has demonstrated how Scale 3 Haar wavelets can be used to solve these equations. The research has presented numerical examples to demonstrate the effectiveness of Scale 3 Haar wavelets in solving integral and integro-differential equations. These examples have shown that the method is highly accurate and can produce solutions with a fast convergence rate. Moreover, the numerical results have shown that the method can be used to solve integral and integro-differential equations with different boundary conditions and coefficients. The research has also compared the results obtained using Scale 3 Haar wavelets with those obtained using alternative numerical methods described in the existing literature. The comparison has shown that the Scale 3 Haar wavelet method surpasses these methods in terms of both accuracy and efficiency. Moreover, the research has highlighted the advantage of using this method in solving high-dimensional problems. The study began by introducing the concept of wavelets and the Haar wavelet in particular. The basic properties of Haar wavelets were discussed, including their orthogonality, compact support, and their ability to approximate functions with discontinuities. The scale 3 Haar wavelet was then introduced, and its properties were discussed in detail. The study then moved on to discuss the use of wavelets for the solution of IEs and IDEs. The advantages of using wavelets over other numerical methods, such as finite differences and finite elements, were discussed, including their ability to handle irregular geometries and their superior convergence rates. Several numerical illustrations were provided to showcase the efficacy of the wavelet method in resolving IEs and IDEs. The examples included both linear and nonlinear problems and demonstrated the ability of the wavelet method to provide highly accurate solutions with relatively few wavelet coefficients. Finally, the study presented a novel approach for solving various integral and integro-differential equations using the wavelet method.

The use of Scale 3 Haar wavelets for the solution of IEs and IDEs is a powerful and efficient technique. The wavelet method offers several advantages over other numerical methods, including its ability to handle irregular geometries and its superior

convergence rates. The numerical examples presented in this study demonstrate the effectiveness of the wavelet method for solving a wide range of IEs and IDEs, including those with nonlocal boundary conditions. Potential future investigations may involve extending the application of the wavelet method to different categories of functional equations or exploring the utilization of alternative wavelet types for solving a variety of integral and integro-differential equations.

Although the main results of the proposed techniques have been presented in the previous chapters, we will now offer a concise overview of the benefits associated with these methods, which include:

- Scale 3 Haar wavelets provide a high level of accuracy in numerical solutions compared to other wavelet methods and numerical methods.
- The implementation of Scale 3 Haar wavelets is straightforward and relatively easy compared to other wavelet methods, making it more accessible to researchers and practitioners.
- Scale 3 Haar wavelets provide better resolution compared to other wavelet methods, which makes it possible to achieve a more precise solution for a given problem.
- Scale 3 Haar wavelets can be utilized in diverse problem domains, encompassing linear as well as nonlinear boundary value problems, fractional differential equations, time-dependent partial differential equations, and nonlinear systems of fractional partial differential equations.
- The use of Scale 3 Haar wavelets leads to reduced computational time compared to other numerical methods, such as finite difference or finite element methods.
- The convergence rate of Scale 3 Haar wavelets is better compared to other numerical methods, leading to faster convergence to the exact solution of a given problem.
- Scale 3 Haar wavelets can be adapted to handle problems with variable coefficients, nonuniform grids, and other complexities that are difficult to handle with other numerical methods.

- The use of Scale 3 Haar wavelets requires less memory compared to other numerical methods, making it possible to solve larger problems without running into memory limitations.
- The proposed method's effectiveness and precision are evident from the figures displayed in various chapters which illustrate the comparison between the outcomes obtained using Scale-3 Haar wavelets and the exact solutions available in the literature are shown to be closely aligned, even when using only a small number of collocation points. The degree of exactness achieved by the proposed method is up to 10^{-16}, and the accuracy of the results can be enhanced by augmenting the number of collocation points. This degree of accuracy is indicative of the method's ability to accurately solve a range of problems, including those with complex nonlinearities, variable coefficients, and higher dimensions. The success of the proposed method is also attributed to the suitability of Scale-3 Haar wavelets for handling such problems, as they offer superior resolution, convergence rates, and memory efficiency compared to other wavelet methods and numerical techniques. Overall, the proposed method has demonstrated significant potential for solving a range of physical problems with a high level of accuracy and efficiency.
- In conclusion, the Haar Scale 3 (non-dyadic) wavelet-based approach offers a more refined solution, characterized by its theoretical robustness, accuracy, straightforward implementation on computer systems, and minimal computational requirements. This method outperforms other classical wavelet methods in providing a more precise solution. The proposed technique is highly compatible with the computer environment, as a single program can serve as a subprogram for all the considered problems. This characteristic highlights the method's enhanced compatibility with programming in a computer environment. Overall, the Haar scale 3 wavelet-based method presents a promising approach for solving a range of complex physical problems with a high level of accuracy and efficiency.
- Due to their flexible characteristics, the extension of Haar Scale 3 wavelets to higher-dimensional and higher-order IDEs involving delay terms, delay differential equations, and fractional models can be easily achieved. This feature

makes Haar scale 3 wavelets a versatile tool for solving a range of complex physical problems with varying degrees of complexity and dimensions. As a result, the proposed method based on Haar scale 3 wavelets offers a powerful and effective solution to an extensive array of physical problems, including those with nonlinearities, variable coefficients, and higher dimensions.

- One of the primary limitations of the Non-dyadic Haar wavelet family is its discontinuity at partition points. This characteristic makes the derivative approach unsuitable for the initial stage. As a result, integration procedures are necessary to calculate the weight coefficients of the wavelets. Additionally, the computational time rises as the resolution level increases, posing another limitation to the use of Haar wavelets.

6.2 Future Scope

The Haar scale 3 wavelet method has shown promising results in the solution of differential, integral, and integro-differential equations. Its use is not limited to linear problems, and it has shown the potential to handle nonlinear equations as well. From the research conducted in this thesis, various potential research ideas can be inferred that could be explored in the future. The following are some of the key areas that could be the focus of upcoming research studies:

- The future scope for the Haar scale 3 wavelet method is vast. One potential application is in the field of data compression, where wavelet transforms are extensively used. The Haar scale 3 wavelet method can be further explored for its efficiency and effectiveness in data compression applications.
- In this thesis, the primary tools employed for the proposed numerical methods were Haar Scale 3 wavelets, in conjunction with established techniques such as the Collocation method, Quasilinearization method, and Gauss elimination. However, a multitude of other wavelets with diverse structures and characteristics are available in the literature, such as “Laguerre, Daubechies, Hermite, Bessel, Shannon, Bernoulli, Chebyshev, ultraspherical, Legendre, Gabor Spline, Gegenbauer, and CAS wavelets”. Conducting a comparative study to evaluate the efficiency and accuracy of a numerical technique based on

a specific wavelet would be both valuable and captivating, stimulating further inspiration and exploration.

- In the application of the Non-dyadic Haar wavelet collocation method, nonlinear problems are transformed into linear ones through the use of the Quasilinearization formula, as described in the thesis. It is possible to further investigate the use of this proposed technique with other available methods for handling nonlinear equations, such as the Broyden technique and the Generalized Newton-Rapson method.
- Furthermore, the Haar scale 3 wavelet method can be extended to deal with more complex and higher-dimensional problems. It is worth exploring its applicability in solving problems arising in the fields of engineering, physics, and finance.
- Finally, the Haar scale 3 wavelet method can be combined with other numerical techniques such as finite difference, finite element, and boundary element methods to improve the efficiency and accuracy of the solution of mathematical models. Its use in conjunction with machine learning algorithms can also be explored to develop new hybrid methods for solving mathematical models.

References

[1] R. Rajagopal, “Integral Equations and their Applications,” 2007. [Online]. Available: http://library.witpress.comwww.witpress.comWITPRESS

[2] M. Rehman, *Integral equations and their applications*. 2007. doi: 10.5860/choice.45-4442.

[3] M. A. Al-Jawary and L. C. Wrobel, “Radial integration boundary integral and integro-differential equation methods for two-dimensional heat conduction problems with variable coefficients,” *Eng Anal Bound Elem*, vol. 36, no. 5, pp. 685–695, May 2012, doi: 10.1016/j.enganabound.2011.11.019.

[4] V. Capasso, “Asymptotic Stability for an lntegrodifferential Reaction-Diffusion System *,” *J Math Anal Appl*, vol. 103, pp. 575–588, 1984.

[5] G. A. Hufford, “An Integral Equation Approach to the Problem of Wave Propagation over an irregular surface,” *Q Appl Math*, vol. 9, no. 4, pp. 391–404, 1952.

[6] E. G. Ladopoulos, “Non-linear multidimensional singular integral equations in two-dimensional #uid mechanics,” *Int J Non Linear Mech*, vol. 35, pp. 701–708, 2000.

[7] D. S. Weile, G. Pisharody, N. W. Chen, B. Shanker, and E. Michielssen, “A novel scheme for the solution of the time-domain integral equations of electromagnetics,” *IEEE Trans Antennas Propag*, vol. 52, no. 1, pp. 283–295, Jan. 2004, doi: 10.1109/TAP.2003.822450.

[8] L. A. Pipes, “Applications of Integral Equations to the Solution of Nonlinear Electric Circuit Problems,” *Transactions of the American Institute of Electrical Engineers, Part I: Communication and Electronics*, vol. 72, no. 4, pp. 445–450, 1953.

[9] V. S. Melezhik, I. V Puzynin, T. P. Puzynina, and L. N. Somov, “Numerical Solution of a System of lntegrodifferential Equations Arising from the Quantum

Mechanical Three-Body Problem with Coulomb Interaction," *J Comput Phys*, vol. 54, pp. 221–236, 1984.

[10] V. Vijayakumar *et al.*, "A Note on Approximate Controllability of Fractional Semilinear Integrodifferential Control Systems via Resolvent Operators," *Fractal and Fractional*, vol. 6, no. 2, Feb. 2022, doi: 10.3390/fractalfract6020073.

[11] J. Paulsen, "Risk theory in a stochastic economic environment," *Stoch Process Their Appl*, vol. 46, pp. 327–361, 1993.

[12] Ş. Yüzbaşı and M. Sezer, "An exponential approach for the system of nonlinear delay integro-differential equations describing biological species living together," *Neural Comput Appl*, vol. 27, no. 3, pp. 769–779, Apr. 2016, doi: 10.1007/s00521-015-1895-y.

[13] M. Rahman, Z. Jackiewicz, and B. D. Welfert, "Stochastic approximations of perturbed Fredholm Volterra integro-differential equation arising in mathematical neurosciences," *Appl Math Comput*, vol. 186, no. 2, pp. 1173–1182, Mar. 2007, doi: 10.1016/j.amc.2006.07.137.

[14] H. Brunner and N. Yan, "Finite element methods for optimal control problems governed by integral equations and integro-differential equations," *Numer Math (Heidelb)*, vol. 101, no. 1, pp. 1–27, Jul. 2005, doi: 10.1007/s00211-005-0608-3.

[15] J. Zhao and R. M. Corless, "Compact Finite Difference Method for Integro-Differential Equations."

[16] A. B. Iskakov, S. Descombes, and E. Dormy, "An integro-differential formulation for magnetic induction in bounded domains: Boundary element-finite volume method," *J Comput Phys*, vol. 197, no. 2, pp. 540–554, Jul. 2004, doi: 10.1016/j.jcp.2003.12.008.

[17] A. M. Wazwaz, "The combined Laplace transform-Adomian decomposition method for handling nonlinear Volterra integro-differential equations," *Appl*

Math Comput, vol. 216, no. 4, pp. 1304–1309, Apr. 2010, doi: 10.1016/j.amc.2010.02.023.

[18] J. Thorwe and S. Bhalekar, "Solving Partial Integro-Differential Equations Using Laplace Transform Method," *American Journal of Computational and Applied Mathematics*, vol. 2, no. 3, pp. 101–104, Aug. 2012, doi: 10.5923/j.ajcam.20120203.06.

[19] R. Singh and A. M. Wazwaz, "Numerical solutions of fourth-order Volterra integro-differential equations by the Green's function and decomposition method," *Mathematical Sciences*, vol. 10, no. 4, pp. 159–166, Dec. 2016, doi: 10.1007/s40096-016-0190-0.

[20] J. Saberi-Nadjafi and A. Ghorbani, "He's homotopy perturbation method: An effective tool for solving nonlinear integral and integro-differential equations," *Computers and Mathematics with Applications*, vol. 58, no. 11–12, pp. 2379–2390, Dec. 2009, doi: 10.1016/j.camwa.2009.03.032.

[21] A.-M. Wazwaz, *Linear and Nonlinear Integral Equations Methods and Applications*. Springer, 2011.

[22] R. Kumar, "Construction of Non-Dyadic Wavelets Family and their Integral for Multiscale Approximation of Unknown Function," *Journal of Emerging Technologies and Innovative Research*, vol. 5, no. 12, 2018, [Online]. Available: www.jetir.org

[23] R. Kalaba, "On Nonlinear Differential Equations, the Maximum Operation, and Monotone Convergence," *Indiana University Mathematics Journal*, vol. 8, no. 4, 1959, doi: 10.1512/iumj.1959.8.58037.

[24] T. D'Hondt, "Quasilinearization and nonlinear boundary value problems," *Bulletin de la Classe des sciences*, vol. 63, no. 1. pp. 22–33, 1977. doi: 10.3406/barb.1977.58179.

[25] A. Haar, "Zur Theorie der orthogonalen Funktionensysteme - Erste Mitteilung," *Math Ann*, vol. 69, no. 3, 1910, doi: 10.1007/BF01456326.

[26] S. G. Mallat, “Multiresolution approximations and wavelet orthonormal bases of L2(R),” in *Transactions of the American Mathematical Society*, vol. 315, 1989, pp. 69–87. doi: 10.1090/s0002-9947-1989-1008470-5.

[27] Y. Meyer, “Orthonormal Wavelets,” 1989. doi: 10.1007/978-3-642-97177-8_2.

[28] I. Daubechies, “Orthonormal bases of compactly supported wavelets,” *Commun Pure Appl Math*, vol. 41, no. 7, pp. 909–996, 1988, doi: 10.1002/cpa.3160410705.

[29] I. Daubechies and C. Heil, “Ten Lectures on Wavelets,” *Computers in Physics*, vol. 6, no. 6, 1992, doi: 10.1063/1.4823127.

[30] C. F. Chen and C. H. Hsiao, “Haar wavelet method for solving lumped and distributed-parameter systems,” *IEE Proceedings: Control Theory and Applications*, vol. 144, no. 1, pp. 87–93, 1997, doi: 10.1049/ip-cta:19970702.

[31] Ü. Lepik, “Application of wavelet transform techniques to vibration studies,” *Proceedings of the Estonian Academy of Sciences. Physics. Mathematics*, vol. 50, no. 3, p. 155, 2001, doi: 10.3176/phys.math.2001.3.05.

[32] Ü. Lepik and E. Tamme, “Application of the Haar Wavelets for Solution of Linear Integral Equations,” *Dynamical Systems and Applications*, no. July, pp. 494–507, 2004.

[33] K. Maleknejad and F. Mirzaee, “Using rationalized Haar wavelet for solving linear integral equations,” *Appl Math Comput*, vol. 160, no. 2, pp. 579–587, Jan. 2005, doi: 10.1016/j.amc.2003.11.036.

[34] Ü. Lepik, “Numerical solution of differential equations using Haar wavelets,” *Math Comput Simul*, vol. 68, no. 2, pp. 127–143, 2005, doi: 10.1016/j.matcom.2004.10.005.

[35] Ü. Lepik, “Haar wavelet method for nonlinear integro-differential equations,” *Appl Math Comput*, vol. 176, no. 1, pp. 324–333, May 2006, doi: 10.1016/j.amc.2005.09.021.

[36] Y. Ordokhani, “Solution of nonlinear Volterra-Fredholm-Hammerstein integral equations via rationalized Haar functions,” *Appl Math Comput*, vol. 180, no. 2, pp. 436–443, Sep. 2006, doi: 10.1016/j.amc.2005.12.034.

[37] Ü. Lepik, “Numerical solution of evolution equations by the Haar wavelet method,” *Appl Math Comput*, vol. 185, no. 1, pp. 695–704, 2007, doi: 10.1016/j.amc.2006.07.077.

[38] Ü. Lepik and E. Tamme, “Solution of nonlinear Fredholm integral equations via the Haar wavelet method,” *Proceedings of the Estonian Academy of Sciences: Physics, Mathematics*, vol. 56, no. 1, pp. 17–27, 2007, doi: 10.3176/phys.math.2007.1.02.

[39] E. Babolian and A. Shahsavaran, “Numerical solution of nonlinear Fredholm and Volterra integral equations of the second kind using Haar wavelets and collocation method,” 2007. [Online]. Available: www.SID.ir

[40] Ü. Lepik, “Application of the Haar wavelet transform to solving integral and differential equations,” *Proceedings of the Estonian Academy of Sciences: Physics, Mathematics*, vol. 56, no. 1, pp. 28–46, 2007, doi: 10.3176/phys.math.2007.1.03.

[41] M. H. Reihani and Z. Abadi, “Rationalized Haar functions method for solving Fredholm and Volterra integral equations,” *J Comput Appl Math*, vol. 200, no. 1, pp. 12–20, Mar. 2007, doi: 10.1016/j.cam.2005.12.026.

[42] P. Chang and P. Piau, “Haar Wavelet Matrices Designation in Numerical Solution of Ordinary Differential Equations,” *Int J Appl Math (Sofia)*, vol. 38, no. 3, pp. 164–169, 2008.

[43] Ü. Lepik, “Solving integral and differential equations by the aid of non-uniform Haar wavelets,” *Appl Math Comput*, vol. 198, no. 1, pp. 326–332, Apr. 2008, doi: 10.1016/j.amc.2007.08.036.

[44] E. Babolian and A. Shahsavaran, “Numerical solution of nonlinear Fredholm integral equations of the second kind using Haar wavelets,” *J Comput Appl Math*, vol. 225, no. 1, pp. 87–95, 2009, doi: 10.1016/j.cam.2008.07.003.

[45] Ü. Lepik, “Solving fractional integral equations by the Haar wavelet method,” *International Journal of Mathematics and Computation*, vol. 214, no. 2, pp. 468–478, 2009, doi: 10.1016/j.amc.2009.04.015.

[46] G. Hariharan and K. Kannan, “Haar wavelet method for solving some nonlinear Parabolic equations,” *J Math Chem*, vol. 48, no. 4, pp. 1044–1061, 2010, doi: 10.1007/s10910-010-9724-0.

[47] Siraj-ul-Islam, I. Aziz, and F. Haq, “A comparative study of numerical integration based on Haar wavelets and hybrid functions,” *Computers and Mathematics with Applications*, vol. 59, no. 6, pp. 2026–2036, Mar. 2010, doi: 10.1016/j.camwa.2009.12.005.

[48] Dr. G. Hariharan, “Solving Finite Length Beam Equation by the Haar Wavelet Method,” *Int J Comput Appl*, vol. 9, no. 1, pp. 27–34, 2010, doi: 10.5120/1349-1819.

[49] Siraj-ul-Islam, I. Aziz, and B. Šarler, “The numerical solution of second-order boundary-value problems by collocation method with the Haar wavelets,” *Math Comput Model*, vol. 52, no. 9–10, pp. 1577–1590, 2010, doi: 10.1016/j.mcm.2010.06.023.

[50] I. Hussain, A. Ali, A. Wali Khan University Mardan, and K. Pakhtunkhwa, “A Haar Wavelets Based Numerical Method for Third-order Boundary and Initial Value Problems,” *World Appl Sci J*, vol. 13, no. 10, pp. 2244–2251, 2011, [Online]. Available: https://www.researchgate.net/publication/304657142

[51] F. i-Haq and A. Ali, “Numerical solution of fourth order boundary-value problems using HAAR wavelets,” *Applied Mathematical Sciences*, vol. 5, no. 61–64, pp. 3131–3146, 2011.

[52] E. Babolian, S. Bazm, and P. Lima, “Numerical solution of nonlinear two-dimensional integral equations using rationalized Haar functions,” *Commun Nonlinear Sci Numer Simul*, vol. 16, no. 3, pp. 1164–1175, Mar. 2011, doi: 10.1016/j.cnsns.2010.05.029.

[53] S. M. Hashemiparast, M. Sabzevari, and H. Fallahgoul, “Improving the Solution of Nonlinear Volterra Integral Equations Using Rationalized Haar s-Functions,” 2011.

[54] H. Saeedi, N. Mollahasani, M. Moghadam, and G. Chuev, “An operational haar wavelet method for solving fractional volterra integral equations,” *International Journal of Applied Mathematics and Computer Science*, vol. 21, no. 3, pp. 535–547, Sep. 2011, doi: 10.2478/v10006-011-0042-x.

[55] A. Shahsavaran, “Haar Wavelet Method to Solve Volterra Integral Equations with Weakly Singular Kernel by Collocation Method,” 2011. [Online]. Available: https://www.researchgate.net/publication/267828810

[56] Ü. Lepik, “Solving PDEs with the aid of two-dimensional Haar wavelets,” *Computers and Mathematics with Applications*, vol. 61, no. 7, pp. 1873–1879, 2011, doi: 10.1016/j.camwa.2011.02.016.

[57] Ü. Lepik, “Exploring vibrations of cracked beams by theHaar wavelet method,” *Estonian Journal of Engineering*, vol. 18, no. 1, pp. 58–75, 2012, doi: 10.3176/eng.2012.1.05.

[58] V. Mishra, H. Kaur, and R. C. Mittal, “Haar wavelet algorithm for solving certain Differential , Integral and Integro-differential equations,” *Int. J. of Appl. Math and Mech*, vol. 8, no. 6, pp. 69–82, 2012, [Online]. Available: https://www.researchgate.net/publication/259644321

[59] N. Berwal, D. Panchal, and C. . L. . Parihar, “Solution of Wave-Like Equation Based on Haar Wavelet,” *LE Mathematiche*, vol. 67, no. II, pp. 157–167, 2012, doi: 10.4418/2012.67.2.12.

[60] S. Ziari, R. Ezzati, and S. Abbasbandy, “Numerical Solution of Linear Fuzzy Fredholm Integral Equations of the Second Kind Using Fuzzy Haar Wavelet,” 2012.

[61] M. A. Dehghan and M. J. Birgani, “Application of a new version of Haar wavelet for solving linear integral equations,” pp. 223–226, 2012, [Online]. Available: www.SID.ir

[62] I. Aziz and Siraj-Ul-Islam, “New algorithms for the numerical solution of nonlinear Fredholm and Volterra integral equations using Haar wavelets,” *J Comput Appl Math*, vol. 239, no. 1, pp. 333–345, 2013, doi: 10.1016/j.cam.2012.08.031.

[63] H. Kaur, V. Mishra, and R. C. Mittal, “Numerical Solution of a Laminar Viscous Flow Boundary Layer Equation Using Uniform Haar Wavelet Quasi-linearization Method,” *World Acad Sci Eng Technol*, vol. 79, no. 5, pp. 1682–1687, 2013, doi: 10.5281/zenodo.1087368.

[64] N. Berwal, D. Panchal, and C. l. Parihar, “Numerical solution of series L-C-R Equations Based on Haar Wavelet,” *Italian Journal of Pure and Applied Mathematics*, vol. 13, no. 30, pp. 157–166, 2013.

[65] G. Hariharan, “Wavelet method for a class of fractional Klein-Gordon equations,” *J Comput Nonlinear Dyn*, vol. 8, no. 2, pp. 1–6, 2013, doi: 10.1115/1.4006837.

[66] H. Kaur, R. C. Mittal, and V. Mishra, “A Collocation Approach with Uniform Haar Wavelets to Solve Volterra Population Model for Population Growth of a Species,” 2013.

[67] H. Saeedi, “Application Of Haar Wavelets In Solving Nonlinear Fractional Fredholm Integro-Differential Equations,” *Journal of Mahani Mathematical Research Center*, vol. 2, no. 1, pp. 15–28, 2013, [Online]. Available: https://jmmrc.uk.ac.ir/article_526.html

[68] Siraj-ul-Islam, I. Aziz, and M. Fayyaz, “A new approach for numerical solution of integro-differential equations via Haar wavelets,” *Int J Comput Math*, vol. 90, no. 9, pp. 1971–1989, Sep. 2013, doi: 10.1080/00207160.2013.770481.

[69] M. Fayyaz and M. Azram, “New algorithm for numerical solution of non-linear integro-differential equations of third order using Haar wavelets,” *Sci.Int.(Lahore)*, vol. 25, no. 1, pp. 1–6, 2013.

[70] I. Aziz, Siraj-Ul-Islam, and F. Khan, “A new method based on Haar wavelet for the numerical solution of two-dimensional nonlinear integral equations,” *J Comput Appl Math*, vol. 272, pp. 70–80, Dec. 2014, doi: 10.1016/j.cam.2014.04.027.

[71] Siraj-Ul-Islam, I. Aziz, and A. S. Al-Fhaid, “An improved method based on Haar wavelets for numerical solution of nonlinear integral and integro-differential equations of first and higher orders,” *J Comput Appl Math*, vol. 260, pp. 449–469, 2014, doi: 10.1016/j.cam.2013.10.024.

[72] U. Saeed and M. ur Rehman, “Assessment of Haar Wavelet-Quasilinearization Technique in Heat Convection-Radiation Equations,” *Applied Computational Intelligence and Soft Computing*, vol. 2014, no. 1, pp. 1–5, 2014, doi: 10.1155/2014/454231.

[73] S. Arora, Y. Singh Brar, and S. Kumar, “Haar Wavelet Matrices for the Numerical Solutions of Differential Equations,” *Int J Comput Appl*, vol. 97, no. 18, pp. 33–36, 2014, doi: 10.5120/17108-7759.

[74] R. C. Mittal, H. Kaur, and V. Mishra, “Haar wavelet-based numerical investigation of coupled viscous Burgers’ equation,” *Int J Comput Math*, vol. 92, no. 8, pp. 1643–1659, 2015, doi: 10.1080/00207160.2014.957688.

[75] S. C. Shiralashetti, R. A. Mundewadi, S. C. Shiralashetti, R. A. Mundewadi, and A. B. Deshi, “An Efficient Haar Wavelet Collocation Method for the Solution of Integral and Integro-differential Equations arising in Fluid Dynamics,” pp. 79–

83, 2014, [Online]. Available: https://www.researchgate.net/publication/318912297

[76] H. A. Zedan and E. Alaidarous, “Haar wavelet method for the system of integral equations,” *Abstract and Applied Analysis*, vol. 2014, 2014, doi: 10.1155/2014/418909.

[77] S. S. Ray, “Two reliable approaches involving Haar wavelet method and Optimal Homotopy Asymptotic method for the solution of fractional Fisher type equation,” *J Phys Conf Ser*, vol. 574, no. 1, 2014, doi: 10.1088/1742-6596/574/1/012131.

[78] M. Kumar and S. Pandit, “An efficient algorithm based on Haar wavelets for numerical simulation of Fokker-Planck equations with constants and variable coefficients,” *Int J Numer Methods Heat Fluid Flow*, vol. 25, no. 1, pp. 41–56, 2015, doi: 10.1108/HFF-03-2014-0084.

[79] M. Erfanian, M. Gachpazan, and H. Beiglo, “Rationalized Haar wavelet bases to approximate solution of nonlinear Fredholm integral equations with error analysis,” *Appl Math Comput*, vol. 265, pp. 304–312, Jun. 2015, doi: 10.1016/j.amc.2015.05.010.

[80] S. C. Shiralashetti and A. B. Deshi, “An efficient Haar wavelet collocation method for the numerical solution of multi-term fractional differential equations,” *Nonlinear Dyn*, vol. 83, no. 1–2, pp. 293–303, 2016, doi: 10.1007/s11071-015-2326-4.

[81] Oruç, F. Bulut, and A. Esen, “A Haar wavelet-finite difference hybrid method for the numerical solution of the modified burgers’ equation,” *J Math Chem*, vol. 53, no. 7, pp. 1592–1607, 2015, doi: 10.1007/s10910-015-0507-5.

[82] M. Fallahpour, M. Khodabin, and K. Maleknejad, “Approximation solution of two-dimensional linear stochastic Volterra integral equation by applying the Haar wavelet,” May 2015, [Online]. Available: http://arxiv.org/abs/1505.04855

[83] S. C. Shiralashetti, A. B. Deshi, and P. B. Mutalik Desai, “Haar wavelet collocation method for the numerical solution of singular initial value problems,” *Ain Shams Engineering Journal*, vol. 7, no. 2, pp. 663–670, 2016, doi: 10.1016/j.asej.2015.06.006.

[84] S. C. Shiralashetti, M. H. Kantli, and A. B. Deshi, “Haar wavelet based numerical solution of nonlinear differential equations arising in fluid dynamics,” *Int J Comput Mater Sci Eng*, vol. 5, no. 2, Jun. 2016, doi: 10.1142/S204768411650010X.

[85] I. Singh and S. Kumar, “Haar wavelet method for some nonlinear Volterra integral equations of the first kind,” *J Comput Appl Math*, vol. 292, pp. 541–552, 2016, doi: 10.1016/j.cam.2015.07.022.

[86] M. Erfanian, M. Gachpazan, and H. Beiglo, “A new sequential approach for solving the integro-differential equation via Haar wavelet bases,” *Computational Mathematics and Mathematical Physics*, vol. 57, no. 2, pp. 297–305, Feb. 2017, doi: 10.1134/S096554251702004X.

[87] N. A. Khan, A. Shaikh, and M. Ayaz, “Accurate numerical approximation of nonlinear fourth order Emden-Fowler type equations: A Haar based wavelet-collocation approach,” *Waves, Wavelets and Fractals*, vol. 3, no. 1, pp. 75–83, 2017, doi: 10.1515/wwfaa-2017-0007.

[88] F. A. Shah and R. Abass, “An operational Haar wavelet collocation method for solving singularly perturbed boundary-value problems,” *SeMA Journal*, vol. 74, no. 4, pp. 457–474, 2017, doi: 10.1007/s40324-016-0094-9.

[89] S. Arbabi, A. Nazari, and M. T. Darvishi, “A two-dimensional Haar wavelets method for solving systems of PDEs,” *Appl Math Comput*, vol. 292, pp. 33–46, 2017, doi: 10.1016/j.amc.2016.07.032.

[90] I. Aziz, Siraj-ul-Islam, and M. Asif, “Haar wavelet collocation method for three-dimensional elliptic partial differential equations,” *Computers and Mathematics*

with Applications, vol. 73, no. 9, pp. 2023–2034, 2017, doi: 10.1016/j.camwa.2017.02.034.

[91] I. Singh and S. Kumar, "Haar Wavelet Methods for Numerical Solutions of Harry Dym (HD), BBM Burger's and 2D Diffusion Equations," *Bulletin of the Brazilian Mathematical Society*, vol. 49, no. 2, pp. 313–338, 2018, doi: 10.1007/s00574-017-0055-7.

[92] Z. Avazzadeh and M. Heydari, "Haar wavelet method for solving nonlinear age-structured population models," *International Journal of Biomathematics*, vol. 10, no. 8, pp. 1–21, 2017, doi: 10.1142/S1793524517501145.

[93] U. Saeed, "Haar wavelet operational matrix method for system of fractional nonlinear differential equations," *Int J Wavelets Multiresolut Inf Process*, vol. 15, no. 5, pp. 1–16, 2017, doi: 10.1142/S0219691317500436.

[94] B. Prakash, A. Setia, and D. Alapatt, "Numerical solution of nonlinear fractional SEIR epidemic model by using Haar wavelets," *J Comput Sci*, vol. 22, pp. 109–118, 2017, doi: 10.1016/j.jocs.2017.09.001.

[95] R. Jiwari, V. Kumar, R. Karan, and A. S. Alshomrani, "Haar wavelet quasilinearization approach for MHD Falkner-Skan flow over permeable wall via Lie group method," *Int J Numer Methods Heat Fluid Flow*, vol. 27, no. 6, pp. 1332–1350, 2017, doi: 10.1108/HFF-04-2016-0145.

[96] S. C. Shiralashetti, L. M. Angadi, M. H. Kantli, and A. B. Deshi, "Numerical solution of parabolic partial differential equations using adaptive gird Haar wavelet collocation method," *Asian-European Journal of Mathematics*, vol. 10, no. 2, 2017, doi: 10.1142/S1793557117500267.

[97] R. C. Mittal and S. Pandit, "Sensitivity analysis of shock wave Burgers' equation via a novel algorithm based on scale-3 Haar wavelets," *Int J Comput Math*, vol. 95, no. 3, pp. 601–625, 2018, doi: 10.1080/00207160.2017.1293820.

[98] S. Foadian, R. Pourgholi, S. H. Tabasi, and J. Damirchi, "The inverse solution of the coupled nonlinear reaction–diffusion equations by the Haar wavelets," *Int*

J Comput Math, vol. 96, no. 1, pp. 105–125, 2019, doi: 10.1080/00207160.2017.1417593.

[99] A. Babaaghaie and K. Maleknejad, "Numerical solutions of nonlinear two-dimensional partial Volterra integro-differential equations by Haar wavelet," *J Comput Appl Math*, vol. 317, pp. 643–651, Jun. 2017, doi: 10.1016/j.cam.2016.12.012.

[100] S. C. Shiralashetti, R. A. Mundewadi, S. S. Naregal, and B. Veeresh, "Haar Wavelet Collocation Method for the Numerical Solution of Nonlinear Volterra-Fredholm-Hammerstein Integral Equations," 2017. [Online]. Available: http://www.ripublication.com

[101] E. Fathizadeh, R. Ezzati, and K. Maleknejad, "Hybrid Rational Haar Wavelet and Block Pulse Functions Method for Solving Population Growth Model and Abel Integral Equations," *Math Probl Eng*, vol. 2017, 2017, doi: 10.1155/2017/2465158.

[102] M. Kirs, K. Karjust, I. Aziz, E. Õunapuu, and E. Tungel, "Funktsionaalgradientmaterjalist tala vabavõnkumised: Haari lainikute meetodi evalveerimine," *Proceedings of the Estonian Academy of Sciences*, vol. 67, no. 1, pp. 1–9, Mar. 2018, doi: 10.3176/proc.2017.4.01.

[103] R. Singh, H. Garg, and V. Guleria, "Haar wavelet collocation method for Lane–Emden equations with Dirichlet, Neumann and Neumann–Robin boundary conditions," *J Comput Appl Math*, vol. 346, pp. 150–161, 2019, doi: 10.1016/j.cam.2018.07.004.

[104] R. Singh, H. Gargyand, and A. Garg, "Haar wavelet quasilinearization technique for doubly singular boundary value problems," no. 1, pp. 1–20, 2017, [Online]. Available: http://arxiv.org/abs/1711.10682

[105] M. Ahsan, Siraj-ul-Islam, and I. Hussain, "Haar wavelets multi-resolution collocation analysis of unsteady inverse heat problems," *Inverse Probl Sci Eng*, vol. 27, no. 11, pp. 1498–1520, 2019, doi: 10.1080/17415977.2018.1481405.

[106] A. K. Verma and D. Tiwari, “Higher resolution methods based on quasilinearization and Haar wavelets on Lane-Emden equations,” *Int J Wavelets Multiresolut Inf Process*, vol. 17, no. 3, May 2019, doi: 10.1142/S021969131950005X.

[107] J. Majak, M. Pohlak, K. Karjust, M. Eerme, J. Kurnitski, and B. S. Shvartsman, “New higher order Haar wavelet method: Application to FGM structures,” *Compos Struct*, vol. 201, pp. 72–78, 2018, doi: 10.1016/j.compstruct.2018.06.013.

[108] S. Haq, A. Ghafoor, M. Hussain, and S. Arifeen, “Numerical solutions of two dimensional Sobolev and generalized Benjamin–Bona–Mahony–Burgers equations via Haar wavelets,” *Computers and Mathematics with Applications*, vol. 77, no. 2, pp. 565–575, 2019, doi: 10.1016/j.camwa.2018.09.058.

[109] R. C. Mittal and S. Pandit, “Quasilinearized Scale-3 Haar wavelets-based algorithm for numerical simulation of fractional dynamical systems,” *Engineering Computations (Swansea, Wales)*, vol. 35, no. 5, pp. 1907–1931, 2018, doi: 10.1108/EC-09-2017-0347.

[110] M. Erfanian and A. Mansoori, “Solving the nonlinear integro-differential equation in complex plane with rationalized Haar wavelet,” *Math Comput Simul*, vol. 165, pp. 223–237, Nov. 2019, doi: 10.1016/j.matcom.2019.03.006.

[111] Ö. Oruç, A. Esen, and F. Bulut, “A haar wavelet approximation for two-dimensional time fractional reaction–subdiffusion equation,” *Eng Comput*, vol. 35, no. 1, pp. 75–86, Jan. 2019, doi: 10.1007/s00366-018-0584-8.

[112] M. Ahsan, I. Ahmad, M. Ahmad, and I. Hussian, “A numerical Haar wavelet-finite difference hybrid method for linear and non-linear Schrödinger equation,” *Math Comput Simul*, vol. 165, no. January, pp. 13–25, 2019, doi: 10.1016/j.matcom.2019.02.011.

[113] S. Saleem, I. Aziz, and M. Z. Hussain, “A simple algorithm for numerical solution of nonlinear parabolic partial differential equations,” *Eng Comput*, vol. 36, no. 4, pp. 1763–1775, 2020, doi: 10.1007/s00366-019-00796-z.

[114] A. Kaushik, G. Gupta, M. Sharma, and V. Gupta, “A Wavelet Based Rationalized Approach for the Numerical Solution of Differential and Integral Equations,” *Differ Equ Dyn Syst*, vol. 27, no. 1–3, pp. 181–202, 2019, doi: 10.1007/s12591-017-0393-3.

[115] V. Mehandiratta, M. Mehra, and G. Leugering, “An approach based on Haar wavelet for the approximation of fractional calculus with application to initial and boundary value problems,” *Math Methods Appl Sci*, vol. 44, no. 4, pp. 3195–3213, 2021, doi: 10.1002/mma.6800.

[116] I. Awana and F. A.Shah, “An efficient Haar wavelet collocation method for solving Pennes Bioheat Transfer Model,” *Acta Universitatis Apulensis*, vol. 2019, no. 60, pp. 75–89, 2019, doi: 10.17114/j.aua.2019.60.06.

[117] R. Singh, J. Shahni, H. Garg, and A. Garg, “Haar wavelet collocation approach for Lane-Emden equations arising in mathematical physics and astrophysics,” *Eur Phys J Plus*, vol. 134, no. 11, 2019, doi: 10.1140/epjp/i2019-12889-1.

[118] A. Mohammadi, N. Aghazadeh, and S. Rezapour, “Haar wavelet collocation method for solving singular and nonlinear fractional time-dependent Emden–Fowler equations with initial and boundary conditions,” *Mathematical Sciences*, vol. 13, no. 3, pp. 255–265, 2019, doi: 10.1007/s40096-019-00295-8.

[119] M. Fallahpour, M. Khodabin, and K. Maleknejad, “Theoretical Error Analysis of Solution for Two-Dimensional Stochastic Volterra Integral Equations by Haar Wavelet,” *Int J Appl Comput Math*, vol. 5, no. 6, Dec. 2019, doi: 10.1007/s40819-019-0739-3.

[120] S. C. Shiralashetti and L. Lamani, “Haar Wavelet Based Numerical Method for the Solution of Multidimensional Stochastic Integral Equations,” 2019. [Online]. Available: http://www.ripublication.com

[121] M. Erfanian and H. Zeidabadi, “Solving of nonlinear Fredholm integro-differential equation in a complex plane with rationalized Haar wavelet bases,” *Asian-European Journal of Mathematics*, vol. 12, no. 4, Aug. 2019, doi: 10.1142/S1793557119500554.

[122] R. C. Mittal and S. Pandit, “New Scale-3 Haar Wavelets Algorithm for Numerical Simulation of Second Order Ordinary Differential Equations,” *Proceedings of the National Academy of Sciences India Section A - Physical Sciences*, vol. 89, no. 4, pp. 799–808, 2019, doi: 10.1007/s40010-018-0538-y.

[123] R. Amin, K. Shah, M. Asif, I. Khan, and F. Ullah, “An efficient algorithm for numerical solution of fractional integro-differential equations via Haar wavelet,” *J Comput Appl Math*, vol. 381, Jan. 2020, doi: 10.1016/j.cam.2020.113028.

[124] M. Montazer, R. Ezzati, and M. Fallahpour, “Numerical Solution of Linear Volterra Integral Equations using Non-Uniform Haar Wavelets,” *Kragujevac Journal of Mathematics*, vol. 47, no. 4, pp. 599–612, 2023, [Online]. Available: https://www.researchgate.net/publication/347357949

[125] R. Amin, Ş. Yüzbaşi, L. Gao, M. Asif, and I. Khan, “Algorithm for the Numerical Solutions of Volterra Population Growth Model with Fractional Order via Haar Wavelet,” *Contemporary Mathematics*, pp. 102–111, Mar. 2020, doi: 10.37256/cm.00056.102-111.

[126] K. S. Jong, H. C. Choi, K. J. Jang, and S. A. Pak, “A new approach for solving one-dimensional fractional boundary value problems via Haar wavelet collocation method,” *Applied Numerical Mathematics*, vol. 160, pp. 313–330, 2021, doi: 10.1016/j.apnum.2020.10.019.

[127] R. Amin, K. Shah, M. Asif, and I. Khan, “Efficient numerical technique for solution of delay Volterra-Fredholm integral equations using Haar wavelet,” *Heliyon*, vol. 6, no. 10, p. e05108, 2020, doi: 10.1016/j.heliyon.2020.e05108.

[128] R. Amin, S. Nazir, and I. García-Magariño, “Efficient sustainable algorithm for numerical solution of nonlinear delay Fredholm-Volterra integral equations via

Haar wavelet for dense sensor networks in emerging telecommunications," *Transactions on Emerging Telecommunications Technologies*, vol. 33, no. 2, Feb. 2022, doi: 10.1002/ett.3877.

[129] T. Abdeljawad, R. Amin, K. Shah, Q. Al-Mdallal, and F. Jarad, "Efficient sustainable algorithm for numerical solutions of systems of fractional order differential equations by Haar wavelet collocation method," *Alexandria Engineering Journal*, vol. 59, no. 4, pp. 2391–2400, 2020, doi: 10.1016/j.aej.2020.02.035.

[130] N. Pervaiz and I. Aziz, "Haar wavelet approximation for the solution of cubic nonlinear Schrodinger equations," *Physica A: Statistical Mechanics and its Applications*, vol. 545, May 2020, doi: 10.1016/j.physa.2019.123738.

[131] A. Kumar, M. S. Hashmi, A. Q. Ansari, and S. Arzykulov, "Haar wavelet based algorithm for solution of second order electromagnetic problems in time and space domains," *J Electromagn Waves Appl*, vol. 34, no. 3, pp. 362–374, Feb. 2020, doi: 10.1080/09205071.2020.1713225.

[132] S. C. Shiralashetti, S. I. Hanaji, and S. S. Naregal, "Haar wavelet based numerical method for the solution of non-linear partial differential equation," in *AIP Conference Proceedings*, American Institute of Physics Inc., Jul. 2020. doi: 10.1063/5.0014599.

[133] S. Foadian, R. Pourgholi, S. H. Tabasi, and H. Zeidabadi, "Solving an inverse problem for a generalized time-delayed burgers-fisher equation by haar wavelet method," *Journal of Applied Analysis and Computation*, vol. 10, no. 2, pp. 391–410, 2020, doi: 10.11948/20170028.

[134] K. Shah, Z. A. Khan, A. Ali, R. Amin, H. Khan, and A. Khan, "Haar wavelet collocation approach for the solution of fractional order COVID-19 model using Caputo derivative," *Alexandria Engineering Journal*, vol. 59, no. 5, pp. 3221–3231, 2020, doi: 10.1016/j.aej.2020.08.028.

[135] G. Ahmadnezhad, N. Aghazadeh, and S. Rezapour, “Haar wavelet iteration method for solving time fractional Fisher’s equation,” *Computational Methods for Differential Equations*, vol. 8, no. 3, pp. 505–522, 2020, doi: 10.22034/cmde.2020.31527.1475.

[136] R. Singh, V. Guleria, and M. Singh, “Haar wavelet quasilinearization method for numerical solution of Emden–Fowler type equations,” *Math Comput Simul*, vol. 174, pp. 123–133, Aug. 2020, doi: 10.1016/j.matcom.2020.02.004.

[137] M. Montazer, R. Ezzati, M. Khodabin, and M. Fallahpour, “Non-uniform Haar wavelets method for solving linear stochastic ito-volterra Integral equations,” *U.P.B. Sci. Bull., Series A: Applied Mathematics and Physics ·*, vol. 82, no. 3, 2020, [Online]. Available: https://www.researchgate.net/publication/344710703

[138] H. Wu, R. Amin, A. Khan, S. Nazir, and S. Ahmad, “Solution of the Systems of Delay Integral Equations in Heterogeneous Data Communication through Haar Wavelet Collocation Approach,” *Complexity*, vol. 2021, 2021, doi: 10.1155/2021/5805433.

[139] X. Wen and J. Huang, “A Haar wavelet method for linear and nonlinear stochastic Itô–Volterra integral equation driven by a fractional Brownian motion,” *Stoch Anal Appl*, vol. 39, no. 5, pp. 926–943, 2021, doi: 10.1080/07362994.2020.1858873.

[140] W. Swaidan and H. S. Ali, “A Computational Method for Nonlinear Fredholm Integro-Differential Equations Using Haar Wavelet Collocation Points,” in *Journal of Physics: Conference Series*, IOP Publishing Ltd, Mar. 2021. doi: 10.1088/1742-6596/1804/1/012032.

[141] A. A. Khajehnasiri, R. Ezzati, and M. Afshar Kermani, “Solving systems of fractional two-dimensional nonlinear partial Volterra integral equations by using Haar wavelets,” *Journal of Applied Analysis*, 2021, doi: 10.1515/jaa-2021-2050.

[142] M. M. Alqarni *et al.*, "Solution of third order linear and nonlinear boundary value problems of integro-differential equations using Haar Wavelet method," *Results Phys*, vol. 25, no. January, p. 104176, 2021, doi: 10.1016/j.rinp.2021.104176.

[143] I. Ahmad, R. Amin, T. Abdeljawad, and K. Shah, "A Numerical Method for Fractional Pantograph Delay Integro-Differential Equations on Haar Wavelet," *Int J Appl Comput Math*, vol. 7, no. 2, Apr. 2021, doi: 10.1007/s40819-021-00963-1.

[144] R. Amin *et al.*, "A Computational Algorithm for the Numerical Solution of Nonlinear fractional integral Equations," *Fractals*, vol. 30, no. 1, pp. 1–8, 2022, doi: 10.1142/S0218348X22400308.

[145] M. Ahsan, I. Hussain, and M. Ahmad, "A finite-difference and Haar wavelets hybrid collocation technique for non-linear inverse Cauchy problems," *Applied Mathematics in Science and Engineering*, vol. 30, no. 1, pp. 121–140, 2022, doi: 10.1080/17415977.2022.2026350.

[146] M. Mehrparvar, J. Majak, K. Karjust, and M. Arda, "Free vibration analysis of tapered Timoshenko beam with higher order Haar wavelet method," *Proceedings of the Estonian Academy of Sciences*, vol. 71, no. 1, pp. 77–83, 2022, doi: 10.3176/proc.2022.1.07.

[147] R. Amin, K. Shah, H. Ahmad, A. H. Ganie, A. H. Abdel-Aty, and T. Botmart, "Haar wavelet method for solution of variable order linear fractional integro-differential equations," *AIMS Mathematics*, vol. 7, no. 4, pp. 5431–5443, 2022, doi: 10.3934/math.2022301.

[148] H. R. Marasi and M. H. Derakhshan, "Haar wavelet collocation method for variable order fractional integro-differential equations with stability analysis," *Computational and Applied Mathematics*, vol. 41, no. 3, pp. 1–19, 2022, doi: 10.1007/s40314-022-01792-8.

[149] S. C. Shiralashetti and L. Lamani, "Numerical solution of stochastic ordinary differential equations using HAAR wavelet collocation method," *Journal of*

Interdisciplinary Mathematics, vol. 25, no. 2, pp. 195–211, 2022, doi: 10.1080/09720502.2021.1874085.

[150] R. Amin, H. Alrabaiah, I. Mahariq, and A. Zeb, "Theoretical and Computational results for Mixed type Volterra-fredholm Fractional Integral Equations," *Fractals*, vol. 30, no. 1, Feb. 2022, doi: 10.1142/S0218348X22400357.

[151] J. Reunsumrit, K. Shah, A. Khan, R. Amin, I. Ahmad, and T. Sitthiwirattham, "Extension of Haar Wavelet Techniques for Mittag-Leffler type Fractional Fredholm Integro-Differential Equations," *Fractals*, vol. 31, no. 2, 2023, doi: 10.1142/S0218348X23400388.

[152] A. Darweesh, K. Al-Khaled, and O. A. Al-Yaqeen, "Haar wavelets method for solving class of coupled systems of linear fractional Fredholm integro-differential equations," *Heliyon*, vol. 9, no. 9, Sep. 2023, doi: 10.1016/j.heliyon.2023.e19717.

[153] M. Ahsan *et al.*, "A high-order reliable and efficient Haar wavelet collocation method for nonlinear problems with two point-integral boundary conditions," *Alexandria Engineering Journal*, vol. 71, pp. 185–200, May 2023, doi: 10.1016/j.aej.2023.03.011.

[154] A. M. Wazwaz, *A first course in integral equations, second edition*. 2015. doi: 10.1142/9570.

[155] A.-M. Wazwaz, "Applications of Integral Equations," *A First Course in Integral Equations*, pp. 249–282, 2015, doi: 10.1142/9789814675130_0009.

[156] A. Avudainayagam and C. Vani, "Wavelet-Galerkin method for integro-differential equations," *Applied Numerical Mathematics*, vol. 32, no. 3, pp. 247–254, 2000, doi: 10.1016/S0168-9274(99)00026-4.

[157] A. M. Wazwaz, "A reliable algorithm for solving boundary value problems for higher-order integro-differential equations," *Appl Math Comput*, vol. 118, no. 2–3, pp. 327–342, 2001, doi: 10.1016/S0096-3003(99)00225-8.

[158] A. Karamete and M. Sezer, “A Taylor collocation method for the solution of linear integro-differential equations,” *Int J Comput Math*, vol. 79, no. 9, pp. 987–1000, 2002, doi: 10.1080/00207160212116.

[159] S. M. El-Sayed and M. R. Abdel-Aziz, “A comparison of Adomian’s decomposition method and wavelet-Galerkin method for solving integro-differential equations,” *Appl Math Comput*, vol. 136, no. 1, 2003, doi: 10.1016/S0096-3003(02)00024-3.

[160] M. T. Rashed, “Numerical solution of functional differential, integral and integro-differential equations,” *Appl Math Comput*, vol. 156, no. 2, pp. 485–492, Sep. 2004, doi: 10.1016/j.amc.2003.08.021.

[161] A. Arikoglu and I. Ozkol, “Solution of boundary value problems for integro-differential equations by using differential transform method,” *Appl Math Comput*, vol. 168, no. 2, pp. 1145–1158, Sep. 2005, doi: 10.1016/j.amc.2004.10.009.

[162] H. Danfu and S. Xufeng, “Numerical solution of integro-differential equations by using CAS wavelet operational matrix of integration,” *Appl Math Comput*, vol. 194, no. 2, pp. 460–466, Dec. 2007, doi: 10.1016/j.amc.2007.04.048.

[163] A. Saadatmandi and M. Dehghan, “A Legendre collocation method for fractional integro-differential equations,” *JVC/Journal of Vibration and Control*, vol. 17, no. 13, pp. 2050–2058, Nov. 2011, doi: 10.1177/1077546310395977.

[164] J. Manafianheris, “Solving the Integro-Differential Equations Using the Modified Laplace Adomian Decomposition Method,” *Journal of Mathematical Extension*, vol. 6, no. 1, 2012.

[165] S. Yeganeh, Y. Ordokhani, A. Saadatmandi, S. Yeganeh, Y. Ordokhani, and A. Saadatmandi, “A sinc-collocation method for second-order boundary value problems of nonlinear integro-differential equation,” *Journal of Information and Computing Science*, vol. 7, no. 2, pp. 151–160, 2012, [Online]. Available: https://www.researchgate.net/publication/281994145

[166] B. S. H. Kashkaria and M. I. Syam, “Evolutionary computational intelligence in solving a class of nonlinear Volterra–Fredholm integro-differential equations,” *J Comput Appl Math*, vol. 311, 2017, doi: 10.1016/j.cam.2016.07.027.

[167] N. Rohaninasab, K. Maleknejad, and R. Ezzati, “Numerical solution of high-order Volterra–Fredholm integro-differential equations by using Legendre collocation method,” *Appl Math Comput*, vol. 328, 2018, doi: 10.1016/j.amc.2018.01.032.

[168] J. Chen, M. He, and Y. Huang, “A fast multiscale Galerkin method for solving second order linear Fredholm integro-differential equation with Dirichlet boundary conditions,” *J Comput Appl Math*, vol. 364, 2020, doi: 10.1016/j.cam.2019.112352.

[169] M. Faheem, A. Raza, and A. Khan, “Wavelet collocation methods for solving neutral delay differential equations,” *International Journal of Nonlinear Sciences and Numerical Simulation*, vol. 23, no. 7–8, 2022, doi: 10.1515/ijnsns-2020-0103.

[170] M. Faheem, A. Raza, and A. Khan, “Collocation methods based on Gegenbauer and Bernoulli wavelets for solving neutral delay differential equations,” *Math Comput Simul*, vol. 180, 2021, doi: 10.1016/j.matcom.2020.08.018.

[171] M. Faheem, A. Khan, and A. Raza, “A high resolution Hermite wavelet technique for solving space–time-fractional partial differential equations,” *Math Comput Simul*, vol. 194, 2022, doi: 10.1016/j.matcom.2021.12.012.

[172] G. Arora, R. Kumar, and H. Kaur, “A novel wavelet based hybrid method for finding the solutions of higher order boundary value problems,” *Ain Shams Engineering Journal*, vol. 9, no. 4, pp. 3015–3031, Dec. 2018, doi: 10.1016/j.asej.2017.12.006.

[173] A.-M. Wazwaz, “A reliable algorithm for solving boundary value problems for higher-order integro-differential equations,” *Appl Math Comput*, vol. 118, no. 2001, pp. 327–342, 2001, [Online]. Available: www.elsevier.com/locate/amc

[174] Ravikiran Mundewadi, “A Study of Wavelet Theory and its Applications to solve Integral and Integro-differential Equations,” Karnatak University, Karnatak, 2017.

[175] S. A. Mohamed, N. A. Mohamed, and S. I. Abo-Hashem, “A novel differential-integral quadrature method for the solution of nonlinear integro-differential equations,” *Math Methods Appl Sci*, vol. 44, no. 18, 2021, doi: 10.1002/mma.7667.

[176] Ş. Yüzbaşi, N. Şahn, and M. Sezer, “Bessel polynomial solutions of high-order linear Volterra integro-differential equations,” *Computers and Mathematics with Applications*, vol. 62, no. 4, pp. 1940–1956, Aug. 2011, doi: 10.1016/j.camwa.2011.06.038.

[177] R. Amin, K. Shah, M. Awais, I. Mahariq, K. S. Nisar, and W. Sumelka, “Existence and Solution of Third-Order Integro-Differential Equations Via Haar Wavelet Method,” *Fractals*, 2023, doi: 10.1142/S0218348X23400376.

[178] Gegele O A and Evans O P, “Numerical Solution of Higher Order Linear Fredholm-Integro-Differential Equations,” *American Journal of Engineering Research (AJER)*, vol. 03, pp. 243–247, 2014, [Online]. Available: www.ajer.org

[179] X. Shang and D. Han, “Application of the variational iteration method for solving nth-order integro-differential equations,” *J Comput Appl Math*, vol. 234, no. 5, 2010, doi: 10.1016/j.cam.2010.02.020.

[180] R. Kumar and S. Bakhtawar, “Non-dyadic Haar Wavelet Algorithm for the Approximated Solution of Higher order Integro-Differential Equations,” *International Journal of Mathematical, Engineering and Management Sciences*, vol. 8, no. 4, pp. 787–803, Jul. 2023, doi: 10.33889/IJMEMS.2023.8.4.045.

[181] R. Amin, I. Mahariq, K. Shah, M. Awais, and F. Elsayed, “Numerical solution of the second order linear and nonlinear integro-differential equations using Haar wavelet method,” *Arab J Basic Appl Sci*, vol. 28, no. 1, pp. 11–19, 2021, doi: 10.1080/25765299.2020.1863561.

[182] Siraj-Ul-Islam, I. Aziz, and A. S. Al-Fhaid, “An improved method based on Haar wavelets for numerical solution of nonlinear integral and integro-differential equations of first and higher orders,” *J Comput Appl Math*, vol. 260, pp. 449–469, 2014, doi: 10.1016/j.cam.2013.10.024.

[183] K. Maleknejad, B. Basirat, and E. Hashemizadeh, “Hybrid Legendre polynomials and Block-Pulse functions approach for nonlinear VolterraFredholm integro-differential equations,” *Computers and Mathematics with Applications*, vol. 61, no. 9, pp. 2821–2828, May 2011, doi: 10.1016/j.camwa.2011.03.055.

[184] E. Babolian, Z. Masouri, and S. Hatamzadeh-Varmazyar, “Numerical solution of nonlinear Volterra-Fredholm integro-differential equations via direct method using triangular functions,” *Computers and Mathematics with Applications*, vol. 58, no. 2, 2009, doi: 10.1016/j.camwa.2009.03.087.

[185] A. D. (Andreĭ D. Polı̂anin and A. V. (Aleksandr V. Manzhirov, *Handbook of integral equations*. CRC Press, 1998.

[186] A.-M. Wazwaz, *A First Course in Integral Equations*. 2015.

[187] K. Maleknejad, M. Tavassoli Kajani, and Y. Mahmoudi, “Numerical solution of linear Fredholm and volterra integral equation of the second kind by using Legendre wavelets,” *Kybernetes*, vol. 32, no. 9–10, pp. 1530–1539, 2003, doi: 10.1108/03684920310493413.

[188] K. Maleknejad and Y. Mahmoudi, “Numerical solution of linear Fredholm integral equation by using hybrid Taylor and Block-Pulse functions,” *Appl Math Comput*, vol. 149, no. 3, pp. 799–806, Feb. 2004, doi: 10.1016/S0096-3003(03)00180-2.

[189] K. Maleknejad, M. Shahrezaee, and H. Khatami, “Numerical solution of integral equations system of the second kind by Block-Pulse functions,” *Appl Math Comput*, vol. 166, no. 1, pp. 15–24, Jul. 2005, doi: 10.1016/j.amc.2004.04.118.

[190] K. Maleknejad and F. Mirzaee, “Using rationalized Haar wavelet for solving linear integral equations,” *Appl Math Comput*, vol. 160, no. 2, pp. 579–587, Jan. 2005, doi: 10.1016/j.amc.2003.11.036.

[191] Y. Mahmoudi, “Wavelet Galerkin method for numerical solution of nonlinear integral equation,” *Appl Math Comput*, vol. 167, no. 2, pp. 1119–1129, Aug. 2005, doi: 10.1016/j.amc.2004.08.004.

[192] A. Akyüz-Daşcioğlu and H. Çerdik Yaslan, “An approximation method for the solution of nonlinear integral equations,” *Appl Math Comput*, vol. 174, no. 1, pp. 619–629, Mar. 2006, doi: 10.1016/j.amc.2005.04.108.

[193] S. A. Yousefi, “Numerical solution of Abel’s integral equation by using Legendre wavelets,” *Appl Math Comput*, vol. 175, no. 1, pp. 574–580, Apr. 2006, doi: 10.1016/j.amc.2005.07.032.

[194] K. Maleknejad, S. Sohrabi, and Y. Rostami, “Numerical solution of nonlinear Volterra integral equations of the second kind by using Chebyshev polynomials,” *Appl Math Comput*, vol. 188, no. 1, pp. 123–128, May 2007, doi: 10.1016/j.amc.2006.09.099.

[195] K. Maleknejad, H. Almasieh, and M. Roodaki, “Triangular functions (TF) method for the solution of nonlinear Volterra-Fredholm integral equations,” *Communications in Nonlinear Science and Numerical Simulation*, vol. 15, no. 11. pp. 3293–3298, Nov. 2010. doi: 10.1016/j.cnsns.2009.12.015.

[196] A. Mohsen and M. El-Gamel, “On the numerical solution of linear and nonlinear volterra integral and integro-differential equations,” *Appl Math Comput*, vol. 217, no. 7, pp. 3330–3337, Dec. 2010, doi: 10.1016/j.amc.2010.08.065.

[197] K. Maleknejad, E. Hashemizadeh, and R. Ezzati, “A new approach to the numerical solution of Volterra integral equations by using Bernstein’s approximation,” *Commun Nonlinear Sci Numer Simul*, vol. 16, no. 2, pp. 647–655, Feb. 2011, doi: 10.1016/j.cnsns.2010.05.006.

[198] S. Sohrabi, “Comparison Chebyshev wavelets method with BPFs method for solving Abel’s integral equation,” *Ain Shams Engineering Journal*, vol. 2, no. 3–4, pp. 249–254, 2011, doi: 10.1016/j.asej.2011.10.002.

[199] A. Shahsavaran, “Numerical Solution of Nonlinear Fredholm-Volterra Integtral Equations via Piecewise Constant Function by Collocation Method,” *American Journal of Computational Mathematics*, vol. 01, no. 02, pp. 134–138, 2011, doi: 10.4236/ajcm.2011.12014.

[200] K. Maleknejad and E. Najafi, “Numerical solution of nonlinear volterra integral equations using the idea of quasilinearization,” *Commun Nonlinear Sci Numer Simul*, vol. 16, no. 1, pp. 93–100, Jan. 2011, doi: 10.1016/j.cnsns.2010.04.002.

[201] I. Aziz, Siraj-Ul-Islam, and W. Khan, “Quadrature rules for numerical integration based on Haar wavelets and hybrid functions,” *Computers and Mathematics with Applications*, vol. 61, no. 9, pp. 2770–2781, May 2011, doi: 10.1016/j.camwa.2011.03.043.

[202] E.-B. Lin and Y. Al-Jarrah, “A Wavelet Based Method for the Solution of Fredholm Integral Equations,” *American Journal of Computational Mathematics*, vol. 02, no. 02, pp. 114–117, 2012, doi: 10.4236/ajcm.2012.22015.

[203] Z. Chen and W. Jiang, “An approximate solution for a mixed linear Volterra-Fredholm integral equation,” *Appl Math Lett*, vol. 25, no. 8, pp. 1131–1134, Aug. 2012, doi: 10.1016/j.aml.2012.02.019.

[204] A. Setia, “Numerical solution of various cases of Cauchy type singular integral equation,” *Appl Math Comput*, vol. 230, pp. 200–207, Mar. 2014, doi: 10.1016/j.amc.2013.12.114.

[205] S. Bazm, “Bernoulli polynomials for the numerical solution of some classes of linear and nonlinear integral equations,” *J Comput Appl Math*, vol. 275, pp. 44–60, 2015, doi: 10.1016/j.cam.2014.07.018.

[206] I. Singh and S. Kumar, “Haar wavelet method for some nonlinear Volterra integral equations of the first kind,” *J Comput Appl Math*, vol. 292, pp. 541–552, Jan. 2016, doi: 10.1016/j.cam.2015.07.022.

[207] Y. H. Youssri and R. M. Hafez, “Chebyshev collocation treatment of Volterra–Fredholm integral equation with error analysis,” *Arabian Journal of Mathematics*, vol. 9, no. 2, pp. 471–480, Aug. 2020, doi: 10.1007/s40065-019-0243-y.

[208] S. Hatamzadeh-Varmazyar and Z. Masouri, “Numerical Solution of Second Kind Volterra and Fredholm Integral Equations Based on a Direct Method Via Triangular Functions,” 2019. [Online]. Available: http://ijim.srbiau.ac.ir/

[209] S. Amiri, M. Hajipour, and D. Baleanu, “A spectral collocation method with piecewise trigonometric basis functions for nonlinear Volterra–Fredholm integral equations,” *Appl Math Comput*, vol. 370, Apr. 2020, doi: 10.1016/j.amc.2019.124915.

[210] F. Usta, “Numerical analysis of fractional Volterra integral equations via Bernstein approximation method,” *J Comput Appl Math*, vol. 384, Mar. 2021, doi: 10.1016/j.cam.2020.113198.

[211] D. Barrera, M. Barton, I. Chiarella, and S. Remogna, “On numerical solution of Fredholm and Hammerstein integral equations via Nyström method and Gaussian quadrature rules for splines,” *Applied Numerical Mathematics*, vol. 174, no. 2022, pp. 71–88, 2022.

[212] R. Farnoosh and M. Ebrahimi, “Monte Carlo method for solving Fredholm integral equations of the second kind,” *Appl Math Comput*, vol. 195, no. 1, pp. 309–315, Jan. 2008, doi: 10.1016/j.amc.2007.04.097.

[213] J. Saberi-Nadjafi and M. Heidari, “Solving linear integral equations of the second kind with repeated modified trapezoid quadrature method,” *Appl Math Comput*, vol. 189, no. 1, pp. 980–985, Jun. 2007, doi: 10.1016/j.amc.2006.11.165.

[214] R. A. Mundewadi and B. A. Mundewadi, “Hermite Wavelet Collocation Method for the Numerical Solution of Integral and Integro - Differential Equations,” *International Journal of Mathematics Trends and Technology*, vol. 53, no. 3, pp. 215–231, Jan. 2018, doi: 10.14445/22315373/IJMTT-V53P527.

[215] M. Erfanian, M. Gachpazan, and H. Beiglo, “Rationalized Haar wavelet bases to approximate solution of nonlinear Fredholm integral equations with error analysis,” *Appl Math Comput*, vol. 265, pp. 304–312, Jun. 2015, doi: 10.1016/j.amc.2015.05.010.

[216] I. Aziz and Siraj-Ul-Islam, “New algorithms for the numerical solution of nonlinear Fredholm and Volterra integral equations using Haar wavelets,” *J Comput Appl Math*, vol. 239, no. 1, pp. 333–345, Feb. 2013, doi: 10.1016/j.cam.2012.08.031.

[217] F. Mirzaee and A. A. Hoseini, “Numerical solution of nonlinear Volterra-Fredholm integral equations using hybrid of block-pulse functions and Taylor series,” *Alexandria Engineering Journal*, vol. 52, no. 3, pp. 551–555, 2013, doi: 10.1016/j.aej.2013.02.004.

[218] E. Babolian and A. Shahsavaran, “Numerical solution of nonlinear Fredholm integral equations of the second kind using Haar wavelets,” *J Comput Appl Math*, vol. 225, no. 1, pp. 87–95, Mar. 2009, doi: 10.1016/j.cam.2008.07.003.

[219] K. Maleknejad and M. Yousefi, “Numerical solution of the integral equation of the second kind by using wavelet bases of Hermite cubic splines,” *Appl Math Comput*, vol. 183, no. 1, pp. 134–141, Dec. 2006, doi: 10.1016/j.amc.2006.05.104.

[220] P. E. Bedient and H. T. Davis, “Introduction to Nonlinear Differential and Integral Equations.,” *The American Mathematical Monthly*, vol. 71, no. 9, 1964, doi: 10.2307/2311950.

[221] K. Parand and S. Hashemi, “RBF-DQ method for solving non-linear differential equations of Lane-Emden type,” *Ain Shams Engineering Journal*, vol. 9, no. 4, pp. 615–629, Dec. 2018, doi: 10.1016/j.asej.2016.03.010.

[222] M. Dehghan and F. Shakeri, “Approximate solution of a differential equation arising in astrophysics using the variational iteration method,” *New Astronomy*, vol. 13, no. 1, pp. 53–59, Jan. 2008, doi: 10.1016/j.newast.2007.06.012.

[223] R. P. Agarwal and D. O’Regan, “Second order initial value problems of Lane-Emden type,” *Appl Math Lett*, vol. 20, no. 12, pp. 1198–1205, Dec. 2007, doi: 10.1016/j.aml.2006.11.014.

[224] O. W. Richardson, “The Emission of Electricity from Hot Bodies.,” *Journal of the Röntgen Society*, vol. 18, no. 72, 1922, doi: 10.1259/jrs.1922.0041.

[225] H. J. Lane, “On the theoretical temperature of the Sun, under the hypothesis of a gaseous mass maintaining its volume by its internal heat, and depending on the laws of gases as known to terrestrial experiment,” *Am J Sci*, vol. s2-50, no. 148, 1870, doi: 10.2475/ajs.s2-50.148.57.

[226] St. M., “Gaskugeln - Anwendungen der mechanischen Wärmetheorie auf kosmologische und meteorologische Probleme von Dr. R. Emden, Priv.-Doz. f. Phys. u. Met. a. d. kgl. techn. Hochsch. in München. Mit 24 Figuren, 12 Diagrammen und 5 Tafeln. VI+498 S. 8°. Leipzig u. Berlin, B. G. Teubner, 1907. Preis M. 13-,” *Monatshefte für Mathematik und Physik*, vol. 19, no. 1, 1908, doi: 10.1007/BF01736734.

[227] A. H. Hadian-Rasanan, D. Rahmati, S. Gorgin, and K. Parand, “A single layer fractional orthogonal neural network for solving various types of Lane–Emden equation,” *New Astronomy*, vol. 75, Feb. 2020, doi: 10.1016/j.newast.2019.101307.

[228] P. Roul, H. Madduri, and R. Agarwal, “A fast-converging recursive approach for Lane–Emden type initial value problems arising in astrophysics,” *J Comput Appl Math*, vol. 359, pp. 182–195, Oct. 2019, doi: 10.1016/j.cam.2019.03.037.

[229] H. Singh, “An efficient computational method for the approximate solution of nonlinear Lane-Emden type equations arising in astrophysics,” *Astrophys Space Sci*, vol. 363, no. 4, 2018, doi: 10.1007/s10509-018-3286-1.

[230] R. C. Duggan and A. M. Goodman, “Pointwise bounds for a nonlinear heat conduction model of the human head,” *Bull Math Biol*, vol. 48, no. 2, 1986, doi: 10.1007/BF02460025.

[231] S. H. Lin, “Oxygen Difbion in a Spherical Cell with Nonlinear Oxygen Uptake Kinetics,” 1976.

[232] A.-M. Wazwaz, “A new method for solving singular initial value problems in the second-order ordinary differential equations,” *Appl Math Comput*, pp. 45–57, 2002, [Online]. Available: www.elsevier.com/locate/amc

[233] N. Caglar and H. Caglar, “B-spline solution of singular boundary value problems,” *Appl Math Comput*, vol. 182, no. 2, pp. 1509–1513, Nov. 2006, doi: 10.1016/j.amc.2006.05.035.

[234] S. A. Yousefi, “Legendre wavelets method for solving differential equations of Lane-Emden type,” *Appl Math Comput*, vol. 181, no. 2, pp. 1417–1422, Oct. 2006, doi: 10.1016/j.amc.2006.02.031.

[235] V. Suat Ertürk, “differential Transformation Method for Solving Differential Equations of Lane-Emden type,” *Mathematical and Computational Applications*, vol. 12, no. 3, pp. 135–139, 2007.

[236] J. I. Ramos, “Series approach to the Lane-Emden equation and comparison with the homotopy perturbation method,” *Chaos Solitons Fractals*, vol. 38, no. 2, pp. 400–408, 2008, doi: 10.1016/j.chaos.2006.11.018.

[237] K. Parand, M. Shahini, and M. Dehghan, “Rational Legendre pseudospectral approach for solving nonlinear differential equations of Lane-Emden type,” *J Comput Phys*, vol. 228, no. 23, pp. 8830–8840, Dec. 2009, doi: 10.1016/j.jcp.2009.08.029.

[238] S. Karimi Vanani and A. Aminataei, “On the numerical solution of differential equations of Lane-Emden type,” *Computers and Mathematics with Applications*, vol. 59, no. 8, pp. 2815–2820, Apr. 2010, doi: 10.1016/j.camwa.2010.01.052.

[239] K. Parand, M. Dehghan, A. R. Rezaei, and S. M. Ghaderi, “An approximation algorithm for the solution of the nonlinear Lane-Emden type equations arising in astrophysics using Hermite functions collocation method,” *Comput Phys Commun*, vol. 181, no. 6, pp. 1096–1108, Jun. 2010, doi: 10.1016/j.cpc.2010.02.018.

[240] S. Iqbal and A. Javed, “Application of optimal homotopy asymptotic method for the analytic solution of singular Lane-Emden type equation,” *Appl Math Comput*, vol. 217, no. 19, pp. 7753–7761, Jun. 2011, doi: 10.1016/j.amc.2011.02.083.

[241] A. M. Wazwaz, R. Rach, and J. S. Duan, “A study on the systems of the Volterra integral forms of the Lane-Emden equations by the Adomian decomposition method,” *Math Methods Appl Sci*, vol. 37, no. 1, pp. 10–19, Jan. 2014, doi: 10.1002/mma.2776.

[242] A. Taghavi and S. Pearce, “A solution to the Lane-Emden equation in the theory of stellar structure utilizing the Tau method,” *Math Methods Appl Sci*, vol. 36, no. 10, pp. 1240–1247, Jul. 2013, doi: 10.1002/mma.2676.

[243] Ş. YüzbaşI and M. Sezer, “An improved Bessel collocation method with a residual error function to solve a class of Lane-Emden differential equations,” *Math Comput Model*, vol. 57, no. 5–6, pp. 1298–1311, Mar. 2013, doi: 10.1016/j.mcm.2012.10.032.

[244] A. M. Wazwaz and S. A. Khuri, “The variational iteration method for solving the Volterra integro-differential forms of the Lane-Emden and the Emden-Fowler problems with initial and boundary value conditions,” *Open Engineering*, vol. 5, no. 1, pp. 31–41, Jan. 2015, doi: 10.1515/eng-2015-0006.

[245] S. Asadpour, H. Hosseinzadeh, A. Yazdani, S.; Asadpour, and H.; Hosseinzadeh, "Numerical Solution of the Lane-Emden Equations with Moving Least Squares Method," *Applications and Applied Mathematics: An International Journal (AAM),* vol. 14, no. 2, pp. 762–776, 2019.

[246] P. Kumar Sahu, "Numerical Solution for Volterra Integro-differential forms of Lane-Emden Equations of First and Second kind using Legendre Multi-Wavelets," *Electronic Journal of Differential Equations,* vol. 2015, no. 28, pp. 1–11, 2015.

[247] S. Balaji, "A New Bernoulli Wavelet Operational Matrix of Derivative Method for the Solution of Nonlinear Singular Lane-Emden Type Equations Arising in Astrophysics," *J Comput Nonlinear Dyn,* vol. 11, no. 5, Sep. 2016, doi: 10.1115/1.4032386.

[248] P. K. Sahu and S. Saha Ray, "Chebyshev wavelet method for numerical solutions of integro-differential form of Lane-Emden type differential equations," *Int J Wavelets Multiresolut Inf Process,* vol. 15, no. 2, Mar. 2017, doi: 10.1142/S0219691317500151.

[249] R. Singh, J. Shahni, H. Garg, and A. Garg, "Haar wavelet collocation approach for Lane-Emden equations arising in mathematical physics and astrophysics," *Eur Phys J Plus,* vol. 134, no. 11, Nov. 2019, doi: 10.1140/epjp/i2019-12889-1.

[250] Z. Sabir, H. A. Wahab, M. Umar, M. G. Sakar, and M. A. Z. Raja, "Novel design of Morlet wavelet neural network for solving second order Lane–Emden equation," *Math Comput Simul,* vol. 172, pp. 1–14, Jun. 2020, doi: 10.1016/j.matcom.2020.01.005.

[251] S. Gümgüm, "Taylor wavelet solution of linear and nonlinear Lane-Emden equations," *Applied Numerical Mathematics,* vol. 158, pp. 44–53, Dec. 2020, doi: 10.1016/j.apnum.2020.07.019.

[252] A. M. Wazwaz, *Linear and Nonlinear Integral Equations Methods and Applications*. Springer, 2011.

[253] A. K. Verma and D. Tiwari, “Higher resolution methods based on quasilinearization and Haar wavelets on Lane-Emden equations,” *Int J Wavelets Multiresolut Inf Process*, vol. 17, no. 3, May 2019, doi: 10.1142/S021969131950005X.

[254] M. M. Chawla, R. Subramanian, and H. L. Sathi, “A fourth order method for a singular two-point boundary value problem,” *BIT*, vol. 28, no. 1, 1988, doi: 10.1007/BF01934697.

[255] R. Singh, H. Garg, and V. Guleria, “Haar wavelet collocation method for Lane–Emden equations with Dirichlet, Neumann and Neumann–Robin boundary conditions,” *J Comput Appl Math*, vol. 346, pp. 150–161, Jan. 2019, doi: 10.1016/j.cam.2018.07.004.

[256] A. S. V. Ravi Kanth and K. Aruna, “He’s variational iteration method for treating nonlinear singular boundary value problems,” *Computers and Mathematics with Applications*, vol. 60, no. 3, pp. 821–829, Aug. 2010, doi: 10.1016/j.camwa.2010.05.029.

[257] R. Singh and J. Kumar, “An efficient numerical technique for the solution of nonlinear singular boundary value problems,” *Comput Phys Commun*, vol. 185, no. 4, 2014, doi: 10.1016/j.cpc.2014.01.002.

[258] H. Aminikhah and S. Moradian, “Numerical Solution of Singular Lane-Emden Equation,” *ISRN Mathematical Physics*, vol. 2013, pp. 1–9, Aug. 2013, doi: 10.1155/2013/507145.

[259] M. Cui and F. Geng, “Solving singular two-point boundary value problem in reproducing kernel space,” *J Comput Appl Math*, vol. 205, no. 1, 2007, doi: 10.1016/j.cam.2006.04.037.

[260] W. Yulan, T. Chaolu, and P. Jing, “New algorithm for second-order boundary value problems of integro-differential equation,” *Journal of Computational and Applied Mathematics*, vol. 229, no. 1. pp. 1–6, Jul. 01, 2009. doi: 10.1016/j.cam.2008.10.007.

[261] J. Lu, “Variational iteration method for solving two-point boundary value problems,” *J Comput Appl Math*, vol. 207, no. 1, 2007, doi: 10.1016/j.cam.2006.07.014.

[262] A. M. Wazwaz, “Solving two emden-fowler type equations of third order by the variational iteration method,” *Applied Mathematics and Information Sciences*, vol. 9, no. 5, pp. 2429–2436, 2015, doi: 10.12785/amis/090526.

[263] S. B. Yuste and J. Quintana-Murillo, “A finite difference method with non-uniform timesteps for fractional diffusion equations,” *Comput Phys Commun*, vol. 183, no. 12, pp. 2594–2600, Dec. 2012, doi: 10.1016/j.cpc.2012.07.011.

[264] M. Raberto, E. Scalas, and F. Mainardi, “Waiting-times and returns in high-frequency ÿnancial data: an empirical study,” 2002. [Online]. Available: www.elsevier.com/locate/physa

[265] R. Gorenflo, F. Mainardi, E. Scalas, and M. Raberto, “Fractional Calculus and Continuous-Time Finance III: the Diffusion Limit,” 2001.

[266] “2014 Reaction Front in an A + B → C Reaction-Subdiffusion Process”.

[267] K. Maleknejad, E. Hashemizadeh, and B. Basirat, “Computational method based on Bernstein operational matrices for nonlinear Volterra-Fredholm-Hammerstein integral equations,” *Commun Nonlinear Sci Numer Simul*, vol. 17, no. 1, pp. 52–61, Jan. 2012, doi: 10.1016/j.cnsns.2011.04.023.

[268] R. N. Bracewell and A. C. Riddle, “Inversion of Fan-beam scans in Radio Astronomy,” *Astrophys J*, vol. 150, pp. 427–434, 1967.

[269] M. Ali Akbar *et al.*, “Soliton solutions to the Boussinesq equation through sine-Gordon method and Kudryashov method,” *Results Phys*, vol. 25, Jun. 2021, doi: 10.1016/j.rinp.2021.104228.

[270] L. Akinyemi *et al.*, “Nonlinear dispersion in parabolic law medium and its optical solitons,” *Results Phys*, vol. 26, Jul. 2021, doi: 10.1016/j.rinp.2021.104411.

[271] D. Baleanu, A. Jajarmi, and M. Hajipour, “On the nonlinear dynamical systems within the generalized fractional derivatives with Mittag–Leffler kernel,” *Nonlinear Dyn*, vol. 94, no. 1, pp. 397–414, Oct. 2018, doi: 10.1007/s11071-018-4367-y.

[272] R. P. Kanwal and K. C. Liu, “A Taylor expansion approach for solving integral equations,” *Int J Math Educ Sci Technol*, vol. 20, no. 3, pp. 411–414, May 1989, doi: 10.1080/0020739890200310.

[273] A. Atangana, A. Akgül, and K. M. Owolabi, “Analysis of fractal fractional differential equations,” *Alexandria Engineering Journal*, vol. 59, no. 3, pp. 1117–1134, Jun. 2020, doi: 10.1016/j.aej.2020.01.005.

[274] A. Atangana and A. Akgül, “Can transfer function and Bode diagram be obtained from Sumudu transform,” *Alexandria Engineering Journal*, vol. 59, no. 4, pp. 1971–1984, Aug. 2020, doi: 10.1016/j.aej.2019.12.028.

[275] A. E. Abouelregal and H. Ahmad, “Thermodynamic modeling of viscoelastic thin rotating microbeam based on non-Fourier heat conduction,” *Appl Math Model*, vol. 91, pp. 973–988, Mar. 2021, doi: 10.1016/j.apm.2020.10.006.

[276] D. Baleanu, A. Jajarmi, J. H. Asad, and T. Blaszczyk, “The motion of a bead sliding on a wire in fractional sense,” *Acta Phys Pol A*, vol. 131, no. 6, pp. 1561–1564, Jun. 2017, doi: 10.12693/APhysPolA.131.1561.

[277] F. C. Meral, T. J. Royston, and R. Magin, “Fractional calculus in viscoelasticity: An experimental study,” *Commun Nonlinear Sci Numer Simul*, vol. 15, no. 4, pp. 939–945, Apr. 2010, doi: 10.1016/j.cnsns.2009.05.004.

[278] R. C. Koeller, “Applications of Fractional Calculus to the Theory of Viscoelasticity,” 1984. [Online]. Available: http://asme.org/terms

[279] S. Momani and M. Aslam Noor, “Numerical methods for fourth-order fractional integro-differential equations,” *Appl Math Comput*, vol. 182, no. 1, pp. 754–760, Nov. 2006, doi: 10.1016/j.amc.2006.04.041.

[280] E. A. Rawashdeh, “Numerical solution of fractional integro-differential equations by collocation method,” *Appl Math Comput*, vol. 176, no. 1, pp. 1–6, May 2006, doi: 10.1016/j.amc.2005.09.059.

[281] A. Arikoglu and I. Ozkol, “Solution of fractional integro-differential equations by using fractional differential transform method,” *Chaos Solitons Fractals*, vol. 40, no. 2, pp. 521–529, Apr. 2009, doi: 10.1016/j.chaos.2007.08.001.

[282] H. Saeedi, M. M. Moghadam, N. Mollahasani, and G. N. Chuev, “A CAS wavelet method for solving nonlinear Fredholm integro-differential equations of fractional order,” *Communications in Nonlinear Science and Numerical Simulation*, vol. 16, no. 3. pp. 1154–1163, Mar. 2011. doi: 10.1016/j.cnsns.2010.05.036.

[283] Z. Meng, L. Wang, H. Li, and W. Zhang, “Legendre wavelets method for solving fractional integro-differential equations,” *Int J Comput Math*, vol. 92, no. 6, pp. 1275–1291, Jun. 2015, doi: 10.1080/00207160.2014.932909.

[284] S. Alkan and V. Fuat Hatipoglu, “Approximate solutions of Volterra-Fredholm integro-differential equations of fractional order.”

[285] L. Zhu and Q. Fan, “Solving fractional nonlinear Fredholm integro-differential equations by the second kind Chebyshev wavelet,” *Commun Nonlinear Sci Numer Simul*, vol. 17, no. 6, pp. 2333–2341, Jun. 2012, doi: 10.1016/j.cnsns.2011.10.014.

[286] J. R. Loh, C. Phang, and A. Isah, “New Operational Matrix via Genocchi Polynomials for Solving Fredholm-Volterra Fractional Integro-Differential Equations,” *Advances in Mathematical Physics*, vol. 2017, 2017, doi: 10.1155/2017/3821870.

[287] D. Xu, W. Qiu, and J. Guo, “A compact finite difference scheme for the fourth-order time-fractional integro-differential equation with a weakly singular kernel,” *Numer Methods Partial Differ Equ*, vol. 36, no. 2, pp. 439–458, Mar. 2020, doi: 10.1002/num.22436.

[288] E. Keshavarz and Y. Ordokhani, “A fast numerical algorithm based on the Taylor wavelets for solving the fractional integro-differential equations with weakly singular kernels,” *Math Methods Appl Sci*, vol. 42, no. 13, pp. 4427–4443, Sep. 2019, doi: 10.1002/mma.5663.

[289] S. Behera and S. S. Ray, “A wavelet-based novel technique for linear and nonlinear fractional Volterra–Fredholm integro-differential equations,” *Computational and Applied Mathematics*, vol. 41, no. 2, Mar. 2022, doi: 10.1007/s40314-022-01772-y.

[290] R. C. Mittal and S. Pandit, “Sensitivity analysis of shock wave Burgers’ equation via a novel algorithm based on scale-3 Haar wavelets,” *Int J Comput Math*, vol. 95, no. 3, pp. 601–625, Mar. 2018, doi: 10.1080/00207160.2017.1293820.

[291] C. K. Chui and J. A. Lian, “Construction of compactly supported symmetric and antisymmetric orthonormal wavelets with scale = 3,” *Appl Comput Harmon Anal*, vol. 2, no. 1, 1995, doi: 10.1006/acha.1995.1003.

[292] O. A. Arqub and B. Maayah, “Fitted fractional reproducing kernel algorithm for the numerical solutions of ABC – Fractional Volterra integro-differential equations,” *Chaos Solitons Fractals*, vol. 126, pp. 394–402, Sep. 2019, doi: 10.1016/j.chaos.2019.07.023.

[293] R. Amin, K. Shah, M. Asif, I. Khan, and F. Ullah, “An efficient algorithm for numerical solution of fractional integro-differential equations via Haar wavelet,” *J Comput Appl Math*, vol. 381, Jan. 2020, doi: 10.1016/j.cam.2020.113028.

[294] R. Amin, H. Ahmad, K. Shah, M. Bilal Hafeez, and W. Sumelka, “Theoretical and computational analysis of nonlinear fractional integro-differential equations via collocation method,” *Chaos Solitons Fractals*, vol. 151, Oct. 2021, doi: 10.1016/j.chaos.2021.111252.

[295] H. Bin Jebreen and I. Dassios, “On the Wavelet Collocation Method for Solving Fractional Fredholm Integro-Differential Equations,” *Mathematics*, vol. 10, no. 8, Apr. 2022, doi: 10.3390/math10081272.

List Of Published and Communicated Papers from the Thesis

1. An improved algorithm based on Haar Scale 3 Wavelets for the numerical solution of integro-differential equations. This paper has been published in Scopus indexed Journal: Mathematics in Engineering, Science and Aerospace (MESA), with **SJR 0.187**

Citation:

Kumar, R., & Bakhtawar, S. (2022). An improved algorithm based on Haar scale 3 wavelets for the numerical solution of integro-differential equations. *Mathematics in Engineering, Science & Aerospace (MESA)*, Vol. 13, no. 2 pp.617-633.

View online:

http://nonlinearstudies.com/index.php/mesa/article/view/2978

Published by Cambridge Scientific Publisher

2. Non-dyadic Haar Wavelet Algorithm for the Approximated Solution of Higher order Integro-Differential Equations. This paper has been published in Scopus and ESCI indexed Journal: *International Journal of Mathematical Engineering and Management sciences (IJMEMS)*, with **SJR 0.334.**

View online: https://doi.org/10.33889/IJMEMS.2023.8.4.045.

Citation:

Kumar, R., & Bakhtawar, S. (2023). Non-dyadic Haar Wavelet Algorithm for the Approximated Solution of Higher order Integro-Differential Equations. *International Journal of Mathematical, Engineering and Management Sciences*, *8*(4), 787-803.

3. Ratesh Kumar and Sabiha Bakhtawar. Approximation of Volterra and Fredholm Integral Equations by utilizing Non-dyadic Haar Wavelets. This paper has been published in Scopus indexed journal: *Palestine Journal of Mathematics*, with **SJR 0.175.**

Citation: Kumar, R., & Bakhtawar, S. (2023) Approximation of Volterra and Fredholm Integral Equations by utilizing Non-dyadic Haar wavelets. *Palestine Journal of Mathematics, 12*, 106-118.

4. Ratesh Kumar and Sabiha Bakhtawar. Haar Wavelet Collocation Algorithm for the Numerical Solution of Volterra Integro-differential form of Emden-Fowler Type Equations. This Paper has been communicated in the *journal of Contemporary Mathematics*.

5. Ratesh Kumar and Sabiha Bakhtawar. Application of Haar Scale 3 Wavelets for the Numerical Solution of Volterra Integro-differential form of the LaneEmden Equations Arising in Astrophysics. This paper has been communicated in the *Journal of Computational and Applied Mathematics.*

6. Ratesh Kumar and Sabiha Bakhtawar. Numerical Solution of Volterra Integrodifferential Equations of Fractional order Via Scale 3 Haar Wavelet Computational Scheme. This paper has been communicated in the *Journal of Chaos. Solitons and Fractals.*

International Conferences Attended

1. An international conference "5th International Conference on Mathematical Techniques in Engineering Applications (ICMTEA2021)" jointly organised by Graphic Era Deemed to be University and Graphic Era Hill University Dehradun, Uttarakhand, INDIA on December 3-4, 2021 was attended and a paper titled "A Novel Algorithm Based on Haar Scale 3 Wavelets for the Numerical Solution of Integral and Integro-Differential Equations" was presented (Details of the paper attached).

2. An international conference "International Conference on Mathematical Analysis and Applications" organised by Baba Ghulam Shah Badshah University, Rajouri, Jammu & Kashmir, India on March 30-31, 2022 was attended and a paper titled "Approximation of Fredholm and Volterra Integral and Integro-differential Equations by utilizing Non-Dyadic Haar Wavelet" was presented.

3. An international conference "International Conference on Computational Methods in Sciences and Engineering (CMSE-2022)" Organized by Department of Mathematics, Birla Institute of Technology and Science-Pilani, Hyderabad Campus, Telangana, India on April 22-24, 2022 was attended and a paper titled "Novel Technique for Approximating the Solutions of Linear and Nonlinear Integral and Integro-DifferentialEquations based on Non-Dyadic Haar Wavelet" was presented.

4. An international conference "International Conference on Dynamical System and Numerical Methods (ICDSNM-22)" Organized by Department of Mathematics, Jamia Millia Islamia, New Delhi, India on May 20-21, 2022 was attended and a paper titled "Haar Wavelet Collocation Approach for the Solution of Linear and Nonlinear Integral Equations" was presented.

5. An international conference "1st International Conference on Mathematical Methods and Techniques in Engineering and Sciences (ICMMTES2022)" jointly organised by Graphic Era Deemed to be University and Graphic Era Hill University Dehradun, Uttarakhand, India on December 9-10, 2022 was attended and a paper titled "Non-dyadic Haar wavelet Method for the Numerical Solution of Higher-Order Integrodifferential Equations" was presented.

6. An international conference "International Conference on Fractional Calculus: Theory, Applications and Numerics (ICFCTAN)" Organized by Department of

Mathematics, National Institute of Technology, Puducherry, Karaikal, India on January 27-29, 2023 was attended and a paper titled “Non-dyadic Haar Wavelet Collocation Algorithm for the Numerical Solution of Volterra Integrodifferential form of Emden-Fowler Type Equations” was presented.

7. An international conference “4th International Conference on Recent Advances in Fundamental and Applied Sciences (RAFAS 2023)” organized by School of Chemical Engineering and Physical Sciences, Lovely Professional University, Punjab, India on March 24-25, 2023 was attended and a paper titled “Numerical Solution of Volterra Integrodifferential Equations of Fractional order Via Scale 3 Haar Wavelet Computational Scheme” was presented.